Defluoridation Studies using Calcium based compounds

This thesis is submitted as a partial fulfilment of the PhD programme in Engineering by

POONAM MONDAL
ID: 2012RCH9053

Under the supervision of
DR. SUJA GEORGE
Head and Associate Professor

DEPARTMENT OF CHEMICAL ENGINEERING

MALAVIYA NATIONAL INSTITUTE OF TECHNOLOGY JAIPUR

JAIPUR-302017

September, 2016

DECLARATION

I hereby certify that the work which is presented in the thesis entitled **"Defluoridation Studies using Calcium based compounds"** in partial fulfilment of the requirements for the award of Doctor of Philosophy, in the Department of Chemical Engineering, Malaviya National Institute of Technology, Jaipur, is an authentic record of my own work unless otherwise referenced or acknowledged. The thesis was completed under the supervision of Dr. Suja George, Associate Professor, Department of Chemical Engineering, Malaviya National Institute of Technology, Jaipur. The results presented in this thesis have not been submitted in part or full, to any other University or Institute for award of any degree. The content of the thesis has been checked using online software 'Turnitin'.

Poonam Mondal
2012RCH9053
Department of Chemical Engineering
MNIT, Jaipur

CERTIFICATE

This is to certify that the work reported in this thesis entitled **"Defluoridation Studies using Calcium based compounds"** has been carried out by Ms. Poonam Mondal and submitted to Malaviya National Institute of Technology, Jaipur for the award of Doctor of Philosophy. It is a bonafide record of research work carried out by her under my supervision. The thesis work has reached the requisite standard, fulfilling the requirements for the degree of Doctor of Philosophy. The thesis embodies the original work done by her and has not been carried out earlier to the best of my knowledge and belief.

Dr. Suja George
Associate Professor
Department of Chemical Engineering
MNIT, Jaipur

Acknowledgement

Undertaking this Ph.D. has been an amazing and truly life-changing experience for me and it would not have been possible without the support and guidance that I received from many people.

First and foremost, I thank the Almighty who directed me through each step, lighted my path and blessed my efforts.

I wish to express my earnest gratitude towards my supervisor Dr. Suja George who not only guided me in research but acted as a mother and friend at times. Her patience and support rescued me from despair on countless occasions. It is her who taught me that to achieve success, you have to embrace the prospect of failure. The joy and enthusiasm she has for her research was contagious and motivational for me.

Besides my supervisor, I would like to thank my Department Research Evaluation Committee (DREC): Dr. S.K Jana, Dr. P. Pandit and Dr. V. Saharan for their insightful comments, and also for the hard question which incented me to widen my research from various perspectives. I am particularly indebted to Dr. V. Saharan for his support on countless occasions with several instruments used for experiments and for his valuable suggestions in writing this thesis. I will forever be grateful to Prof A. B Gupta for being a special invitee in my DREC and enlightening me with his expertise in this area. My sincere gratitude goes to Prof S.P. Chaurasia and Dr. R.K. Vyas for giving me access to the research facilities in their laboratory whenever needed. I would like to express my sincere thanks to Dr. U. K. Arun Kumar for his insights in thesis writing and boosting my morale at all times. I am also hugely appreciative towards, rest of the faculty members of my department (Dr. A. Gupta, Dr. K. Singh, Dr. M. Vashishtha, Dr. M. Agarwal, Dr. D. Datta, Dr. S. Upadhaya, Dr. R.K Dohare, Dr. Subbaramaiah V and Mr. Shiv Om Meena), without their precious support it would not be possible to conduct this research.

The financial support from Malaviya National Institute of Technology, Jaipur is gratefully acknowledged. I would like to thank Prof. I.K Bhat, Director, MNIT, Jaipur for his ever-supportive gesture towards research activities in the Institute.

I am very thankful to the LINC (Learning in community) programme, a partnership between MNIT Jaipur and University of Illinois, USA under which the field visits to villages having high fluoride concentration in groundwater were arranged and water samples were collected. It also helped me in realizing the impact of fluorosis on a community level and learning the current technologies offered by Government and NGOs.

Special mention goes to the technical staff of Materials Research Centre, MNIT, Jaipur; especially Mr. Reja and Mr. Ramesh who selflessly helped in the characterization studies. I also acknowledge the analytical services of Central Salt & Marine Chemicals Research

Institute for surface area measurements of samples. I extend my appreciation to the technical assistants, Mr. R. Sharma, Mr. R. Goswami and Mr. S. N. Reddy Y and office staff Mrs. Babita for supporting and cheering me in this journey.

A good support system is essential for surviving and staying sane during uncertain times in Ph.D. For that, I thank my faithful friends and research mates Mr. Prakash Kumar Singh and Mr. Shivendu who were always concerned about me and gave me an unconditional support. I would like to convey the warmest appreciation to Mr. Dhiraj Mehta, my fellow research mate and best friend who helped me through tough times and kept my zeal for research lighted. I am also grateful to Dr. Richa Soni for helping me with suggestions regarding editing of this thesis and Mr Vikas Sharma, Ph.D. scholar, IIT Mandi for being a constant support throughout the past four years. I greatly appreciate the support of my best friends Rajvir and Simran; my sister Diksha and brother in law Amit ; my hostel mates (Vatsala, Tanuja and Niketa) who always believed in me and supported me. I would also like to thank my extended family Mr Vinod Mehta and Mrs Vandana Mehta for their love and compassion.

Most importantly, none of this would have been possible without the love and patience of my family. I wish to express my admiration to my brother Abhishek and mother Mrs. Kabita Mondal for their thoughtful care and concerns for me. However, I am forever grateful to my father, Mr. PP Mondal for showing me the value of education through his immense encouragement throughout my life.

(Poonam Mondal)

Dedicated to my FAMILY

List of Publications

Publications in Journals

1. Poonam Mondal and Suja George, A review on adsorbents used for defluoridation of drinking water. *Reviews in Environmental Science and Bio/Technology*, 2015, 14:195-210.

2. Poonam Mondal and Suja George, Removal of Fluoride from Drinking Water Using Novel Adsorbent Magnesia-Hydroxyapatite. *Water, Air, & Soil Pollution*, 2015, 226(8): 1-15.

3. Poonam Mondal, Suja George, Dhiraj Mehta, Defluoridation studies with synthesized Magnesium incorporated Hydroxyapatite and parameter optimization using Response Surface methodology, *Desalination and water treatment*, 2016, 1-20, doi: 0.1080/19443994.2016.1167628.

4. Dhiraj Mehta, Poonam Mondal, Suja George. Utilization of marble waste powder as a novel adsorbent for removal of fluoride ions from aqueous solution, *Journal of Environmental Chemical Engineering* , 2016, 4:932-942.

5. Dhiraj Mehta, Poonam Mondal, Suja George, Virendra Saharan. Synthesis of Hydroxyapatite Nanorods for application in water defluoridation and optimization of process variables: Advantage of ultrasonication with precipitation method over conventional method, *Ultrasonics Sonochemistry,* 2016 (Communicated).

6. Poonam Mondal**,** Suja George and Dhiraj Mehta. Use of Calcite for Defluoridation of Drinking Water in Acidic medium. *Research Journal of Chemical Sciences*, 2014, 4(6):62-65

7. Dhiraj Mehta, Suja George, Poonam Mondal. Synthesis of Hydroxyapatite by Chemical Precipitation Technique and Study of Its Biodegradability. *International Journal of Research in Advent Technology*, 2014, 2(4): 159–161.

Publications in Conferences

1. Poonam Mondal and Suja George, Assessment of Defluoridation of Drinking Water Using Novel Adsorbent Nano-Crystalline Magnesium Amended Hydroxyapatite (M-HAP), *AIChE Spring Meeting & 11th Global Congress on Process Safety,18th Topical Conference on Refinery Processing by AIChE* at Austin, USA , 2015, 198.

2. Poonam Mondal, Suja George and Dhiraj Mehta, Synthesis of Calcia-Magnesia Adsorbent (CMA) and Utilizing It for Defluoridation of Drinking Water, *International Conference in Exploring Basic & Applied Sciences for Next Generation Frontiers* by Elsevier at Jalandhar, 2014, 204-206 [ISBN:978-93-5107-313-0].

3. Dhiraj Mehta, Poonam Mondal, Suja George, Synthesis of Biomaterial Hydroxyapatite and Effect of Calcination on Its Structure, *International Conference in Exploring Basic & Applied Sciences for Next Generation Frontiers* by Elsevier at Jalandhar, 2014, 207-209 [ISBN:978- 93-5107-313-0].

4. Poonam Mondal and Suja George, Fluoride Removal by Using Calcium aluminum – Magnesium Powder as Adsorbent, *International Conference on Materials for the Future, Innovative Materials, Processes, Products and Applications* by Bonfire at Thrissur, 2013, 562-564 [ISBN 978-93-82338-83-3].

5. Poonam Mondal, A.B. Gupta, Savitha, Suja George, Effect on Activated Alumina Fluoride Removal Capacity in Presence of Chloride, *International Conference on Materials for the Future, Innovative Materials, Processes, Products and Applications* by Bonfire at Thrissur, 2013, 598-600 [ISBN 978-93-82338-83-3].

6. Poonam Mondal, Suja George ,Biosorbents : An Alternative Method of Fluoride Removal, *All India Seminar on Pollution Prevention Through Development of Bio-Based Material and Energy* by MNIT at Jaipur , 2013, 20-21 .

7. Poonam Mondal, Suja George, A.B. Gupta, Overview of Activated Alumina Defluoridation Process, *National Conference on Water Quality Management* by MNIT Jaipur at Jaipur, 2012, 22-25.

Abstract

Safe drinking water can be said to be the elixir for human life but in the current scenario millions of people around the globe are not fortunate enough to access it due to presence of various contaminants. Fluoride is one such contaminant which when present in excess (>1 mg/L) in drinking water can cause severe health effects like fluorosis. India is among the many countries where millions of people are vulnerable to fluorosis. The consumption of high amount of water in warm climatic conditions of India along with the increased incidence of malnutrition has aggravated the issue.

High end technologies such as reverse osmosis are not viable options for rural populations and therefore, treatment of potable water with appropriate adaptation to a novel, yet simple and efficient defluoridation methodology has become the necessity. Since, adsorption technology is the most preferred method of defluoridation in developing countries, this study is focused on reducing fluoride in drinking water below the permissible limit by using adsorbents. Aluminum based adsorbents have the highest affinity towards fluoride, but recent reports have suggested high amount of residual aluminum in treated water making it unsafe for consumption. In this study, calcium based adsorbents were explored for defluoridation due to their good affinity for fluoride ions. Moreover, calcium compounds are available in abundance and are biocompatible in all forms with the human body. For improving the defluoridation capacity of adsorbents, calcium compounds were amended with magnesium in this study. Both calcium and magnesium have high permissible limit (75 mg/L and 30 mg/L respectively) for their presence in drinking water, therefore even if some of these ions leach into treated water up to a safe limit it will not pose a threat to health. The adsorbents used for exploring the defluoridation potential are Activated Calcite (ACal), Calcia-Magnesia Adsorbent (CMA), Dicalcium phosphate ($CaHPO_4$), Dolomite [$CaMg(CO_3)_2$] and Hydroxyapatite [$Ca_{10}(PO_4)_6(OH)_2$].

The adsorbents were selected and characterized using FTIR, XRD, SEM, TEM/EDX, XPS, BET, particle size distribution and TGA-DTA techniques. The characterization studies helped in identifying the more promising adsorbent with which further experiments were conducted. Batch defluoridation studies were performed varying crucial process parameters such as pH, contact time, dosage and interfering ions. To get an insight of the mechanism of the process, adsorption isotherms and kinetic models were studied. A regeneration method was also developed for reuse of the adsorbent.

In this study we have made a novel approach to synthesize and utilize the biomaterial *magnesium incorporated hydroxyapatite* as an adsorbent for fluoride mitigation in drinking water. Among the adsorbents studied, magnesium incorporated hydroxyapatite was selected for further experiments on the basis of its novelty, adsorption capacity,

independence from effect of solution pH, negligible effect of interfering ions, ability for regeneration and water quality after adsorption. The process parameters for magnesium incorporated hydroxyapatite were optimized by RSM approach using Central composite design. The optimum values for experimental parameters were found to be at pH 7, 303 K temperature, 10 mg/L fluoride concentration, 180 min contact period with a dose of 10 g/L.

Experimental data obtained for batch studies are not pertinent to practical treatment systems. Removal of contaminants can be achieved most effectively via column studies since the adsorbent capacity can be utilized efficiently leading to better quality of treated water. For column studies the adsorbent magnesium incorporated hydroxyapatite was converted into pellets using extrusion-spheronization procedure. Column adsorption studies with the pelletized adsorbent were conducted by varying the operational parameters (shape of pellets, particle size, bed height, flow rate, feed fluoride concentration) for evaluating practical feasibility of the process. The experimental data were matched with the theoretical data obtained from simulation carried out in MATLAB software. The column adsorption capacity was observed to be 1.46 mg/g at feed fluoride concentration of 10 mg/L, flow rate of 1 L/h and bed height of 30 cm. It was noticed that for 30 cm bed height, 22.1 bed volumes can be processed and the adsorbent exhaustion rate for the same was 6.15 g/L.

Thereafter, field water samples were collected from fluoride prone areas and physico-chemical parameters such as pH, EC, TDS, salinity, alkalinity, total hardness, turbidity, Cl^-, Ca^{2+}, Mg^{2+} and F^- were examined before and after treatment adsorption. It was found that all the water quality parameters were under the permissible limit prescribed by WHO and BIS. Finally, a domestic defluoridation unit was designed with which approximately 348 L of water can be treated with 3 kg of magnesium incorporated hydroxyapatite adsorbent.

Contents

List of Figures

List of Tables

Nomenclature

List of Abbreviations

pH_{PZC} pH at point of zero charge

AA Activated alumina

AER Adsorbent exhaustion rate

APHA American Public Health Association

BET Brunauer, Emmett and Teller

BIS Bureau of Indian Standards

BV Bed volume

CCD Central composite design

CDTA 1, 2-diaminocyclohexane tetra acetic acid

EBCT Empty bed contact time

EC Electrical conductivity

EDX Energy dispersive X-ray analysis

FTIR Fourier transform infrared spectroscopy

JCPDS Joint Committee on Powder Diffraction Standards

PAZ Primary adsorption zone

RSM Response surface methodology

SEM Scanning electron microscopy

SSE Sum of errors squared

TDS Total dissolved solids

TEM Transmission electron microscopy

TGA-DTA Thermogravimetric analysis-Differential thermal analysis

TISAB Total ionic strength adjustment buffer

UNICEF United Nations Children's Emergency Fund

WHO World Health Organization

XPS X-ray photoelectron spectroscopy

XRD X-ray powder diffraction

List of Mathematical symbols

ε Polanyi potential

A_T Temkin isotherm binding constant

B_T Temkin constant related to the heat of adsorption

C_0 Initial fluoride concentration

C_b Fluoride concentration at breakpoint

C_e Equilibrium fluoride concentration

C_{EX} Fluoride concentration at exhaustion point

E_d Mean adsorption energy

H_{UNB} Height of unused bed

k_1 Pseudo first order rate constant

k_2 Pseudo second order rate constant

K_A Adsorption rate constant

K_f Freundlich adsorption capacity

k_i Intraparticle diffusion rate constant

k_Y Yoon - Nelson rate constant

k_{th} Thomas rate constant

N_0 Adsorption potential

Q_0 Langmuir adsorption capacity

q_b Adsorption capacity at breakthrough

q_d Dubinin–Radushkevich constant

q_e Adsorption capacity at equilibrium

q_t Adsorption capacity at time t

q_{EX} Adsorption capacity at exhaustion point

R_L Separation factor

t_b Breakthrough time

t_f Time for formation of primary adsorption zone

t_x Time to establish PAZ

t_z Time for movement of primary adsorption zone down the column

t_{EX} Exhaustion time

V_b Throughput volume at breakpoint

V_{EX} Throughput volume at exhaustion

Z_0 Critical bed depth

$\%S$ Percentage saturation in column

χ^2 Chi square

δ Length of the adsorption zone

ΔG° Standard free energy change

ΔH° Standard enthalpy change

ΔS° Standard entropy change

b Langmuir constant related to energy

F Flow rate

f Fractional capacity

M Adsorbent mass

R Universal gas constant

T Temperature

u Linear flow velocity

V Volume of solution

Z Bed height

CHAPTER 1

Chapter 1

Introduction

"Water is life" is an old saying, yet millions of people in our planet are deprived of safe drinking water. The situation persists and it will continue to persist unless seriously dealt with at all levels of community. People around the globe living in rural and remote areas do not have access to safe drinking water; so they either fetch it from distant places or drink unsafe water. The time lost fetching water robs entire communities of their future and drinking the unsafe water slowly eradicates the community itself. It is estimated that 750 million people around the world lack access to safe water. Among them, 82 % of those who lack access to improved water live in rural areas, while just 18 % reside in urban areas [1].

Fluorine is the 13^{th} most abundant element on earth crust and the most electronegative in nature. It exists as a diatomic molecule with a remarkably low dissociation-energy (38 kcal/mole) due to which it is highly reactive and has a strong tendency to acquire a negative charge which in solution forms F^- (fluoride) ions. Fluoride is one the many contaminants present in drinking water that has caused adverse effects on health of people. As stated by WHO and UNICEF "The most important contaminants from a public health perspective are faecal pathogens and the elements arsenic and **fluoride**, which can occur naturally, especially in groundwater" [1]. In the past two decades, several technologies for defluoridation of potable water has been developed. Many of them have resulted in failure and not considered as a feasible solution. Therefore, appropriate defluoridation method is needed to be applied for a sustainable solution.

This chapter presents an introduction to the occurrence of fluoride ions, severity of presence of excess fluoride in drinking water and various technologies to reduce it. The role of calcium in water sources w.r.t fluoride, in human body w.r.t fluorosis and its role as an adsorbent for defluoridation is also highlighted in this chapter. Further, outline of the research work conducted and a glimpse into the organization of the thesis is also given.

1.1 Occurrence of Fluoride

The occurrence of high fluoride content in ground water has now become one of the most important health associated geo-environmental topic of concern in many countries of the world and being the only perennial source of water in rural areas, the situation is alarming. A schematic diagram showing possible sources of fluoride in the environment is given in Figure 1.1. As seen from the Figure, fluoride is commonly associated with volcanic activity and gases originating from fumaroles. Fluoride ions can also be found in effluents discharged from semiconductor and fertilizer industries. However, maximum fluoride comes as natural input from the minerals and rocks which have fluoride in their composition [2]. Water with high fluoride concentration is found mostly in calcium-deficient groundwater in many basement aquifers like granite and gneiss, geothermal waters and in some sedimentary basins [3]. Fluoride occurs mainly as fluorspar (CaF_2) in sedimentary rocks and as cryolite (Na_2AlF_6) in igneous rocks. Fluoride is an essential constituent in minerals like topaz, fluorite, fluorapatite, cryolite, phosphorite, theorapatite, etc. [4]. As these fluoride minerals are almost insoluble in water, fluoride is found only in groundwater when conditions favor their dissolution or high fluoride containing effluents are discharged to the water bodies from industries [5].

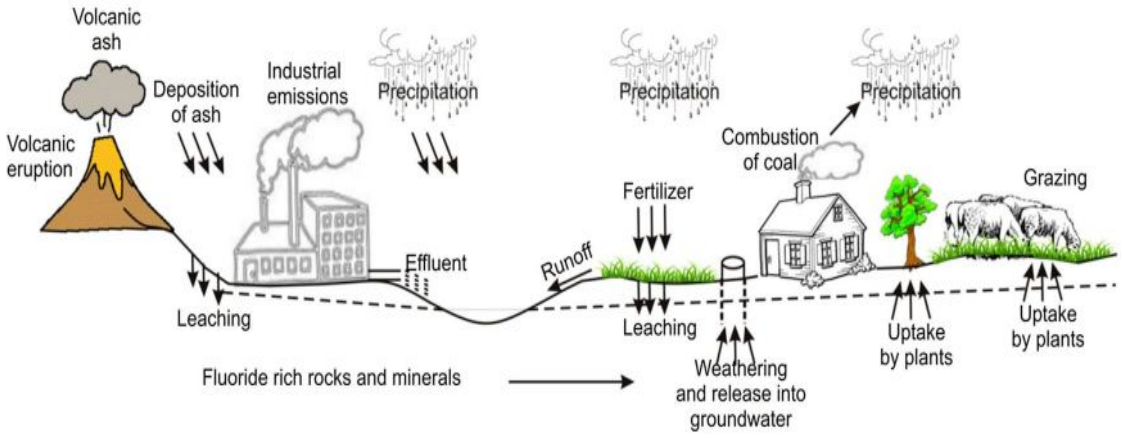

Figure 1.1: Schematic diagram showing sources of fluoride in environment [2]

Presence of fluoride is a global issue and Figure 1.2 presents the international status of prevalence of fluoride. Countries which are affected most are China, India, Sri Lanka, Mexico, western USA, Argentina and many African countries [6]. Some countries conduct fluoride removal by water treatment while in some high-fluoride water resources are consumed without any treatment (mostly developing countries). Due to this, huge populations in several parts of developing countries suffer the ill effects of chronic endemic

fluorosis. It is estimated that about 200 million people throughout the world are consuming water with fluoride concentration greater than the WHO (World Health Organization) prescribed limit. In India, fluorosis is distributed in nearly 20 states and about 66 million people are using groundwater having excessive fluoride content [7]. The worst affected states in the country are Rajasthan, Andhra Pradesh, and Gujarat [2, 8, 9, 10]. In these states 70-100 % districts are affected with high fluoride content. Figure 1.3 illustrates about percentage extent of fluoride level in different states of India. In the states of Bihar, Tamilnadu, Uttar Pradesh, Uttarakhand, Sikkim, Assam, Chattisgarh, Jharkhand, Harayana, Karnataka, Maharashtra, Madhya Pradesh and Punjab 40 to 70 % districts are affected while in Jammu & Kashmir, West Bengal, Orissa and Kerala less than 40 % districts are affected. In rest of the states prevalence of fluorosis is not known [11].

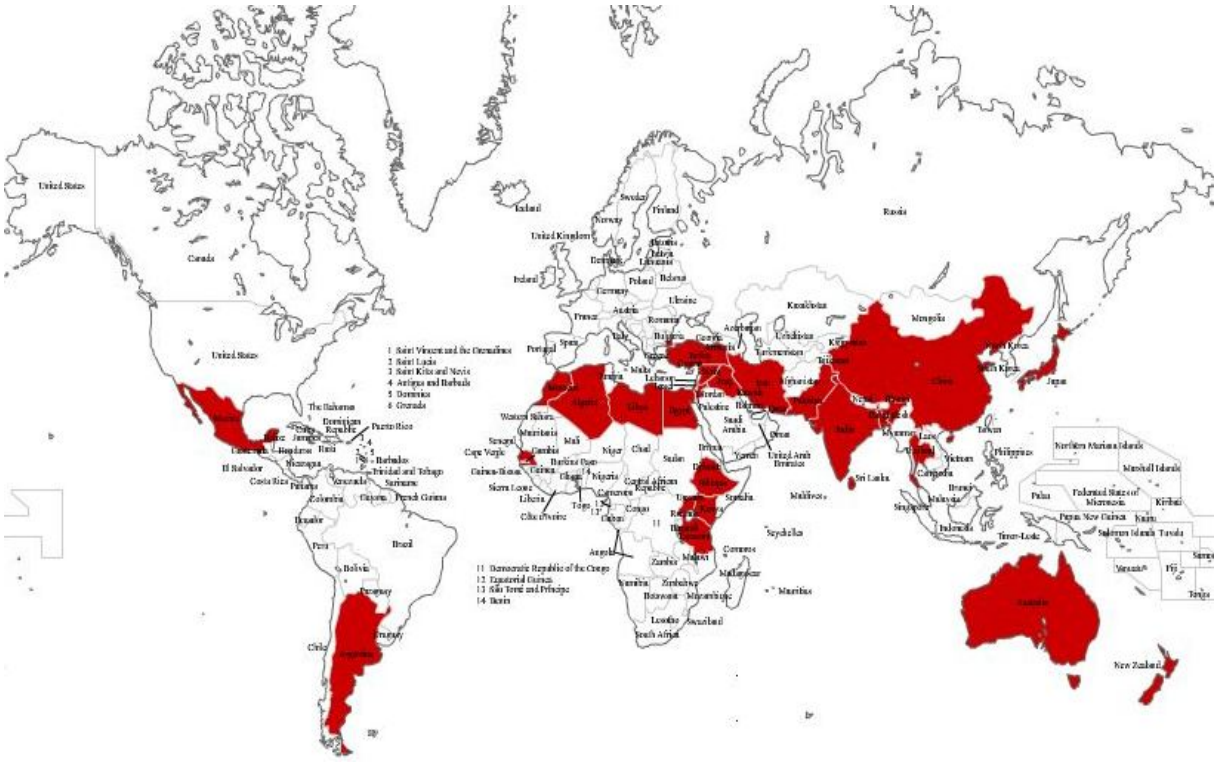

Figure 1.2: Prevalence of Fluorosis worldwide [11]

Due to the warm climate in India, the consumption of water is quite high and along with the increased incidence of malnutrition, a direct comparison of the Indian experience with fluorosis can be made. Figure 1.4 explains the hydrogeochemical basis of endemic fluorosis in India. Presence of fluoride ions is more in regions with arid conditions like the state of Rajasthan where severe cases of fluorosis are encountered. High fluoride groundwaters are also found in areas where sodium and bicarbonate waters dominate. However, it is solubility of mineral which controls the accumulation of fluoride in groundwater [2]. So, in

places where calcium content in groundwaters is high, concentration of fluoride is limited by saturation with the calcium fluoride (mineral fluorite). As described by Handa [8] evaporation is a significant factor causing high concentration of fluoride in groundwater. Because of high rate of evaporation, the Ca^{2+} ions present in groundwater precipitate out in form of calcium carbonate which mitigates amount of calcium, and as a result, the solubility control of calcium fluoride on fluoride enrichment in the water becomes weak.

Therefore, the concentration of fluoride in groundwater can be attributed to geological, chemical and physical characteristics of the aquifer, porosity of the rocks, the temperature, the action of co-existing chemical elements, depth of the water source and intensity of weathering [12].

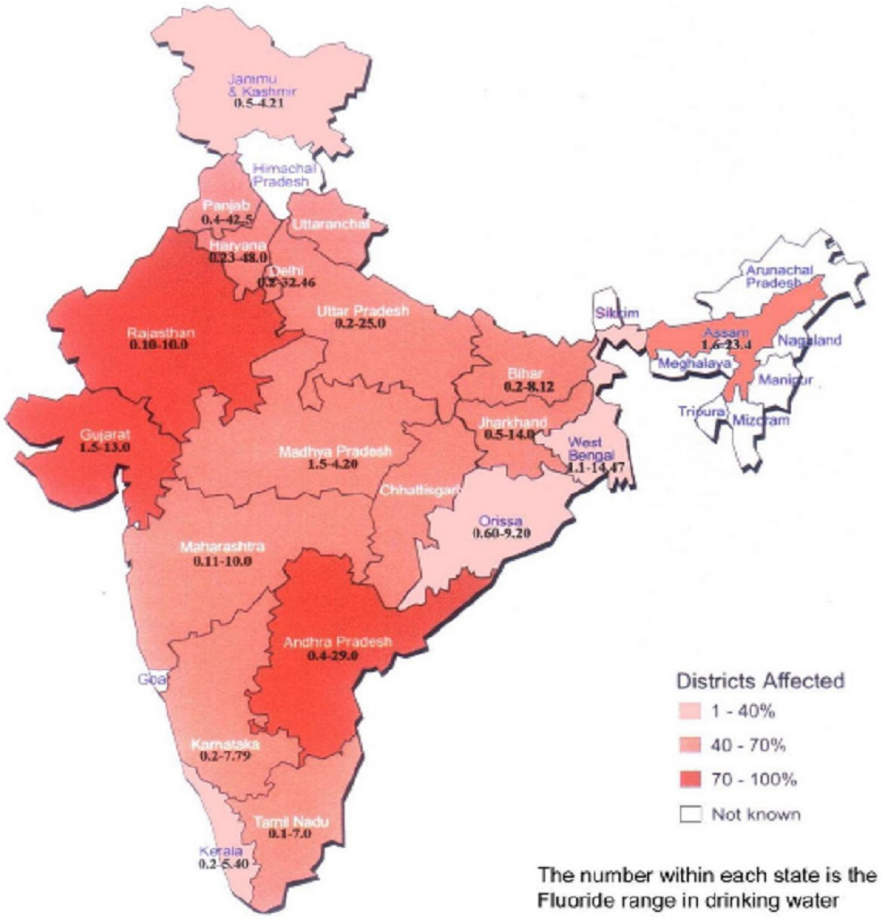

Figure 1.3: Prevalence of Fluorosis in India [10]

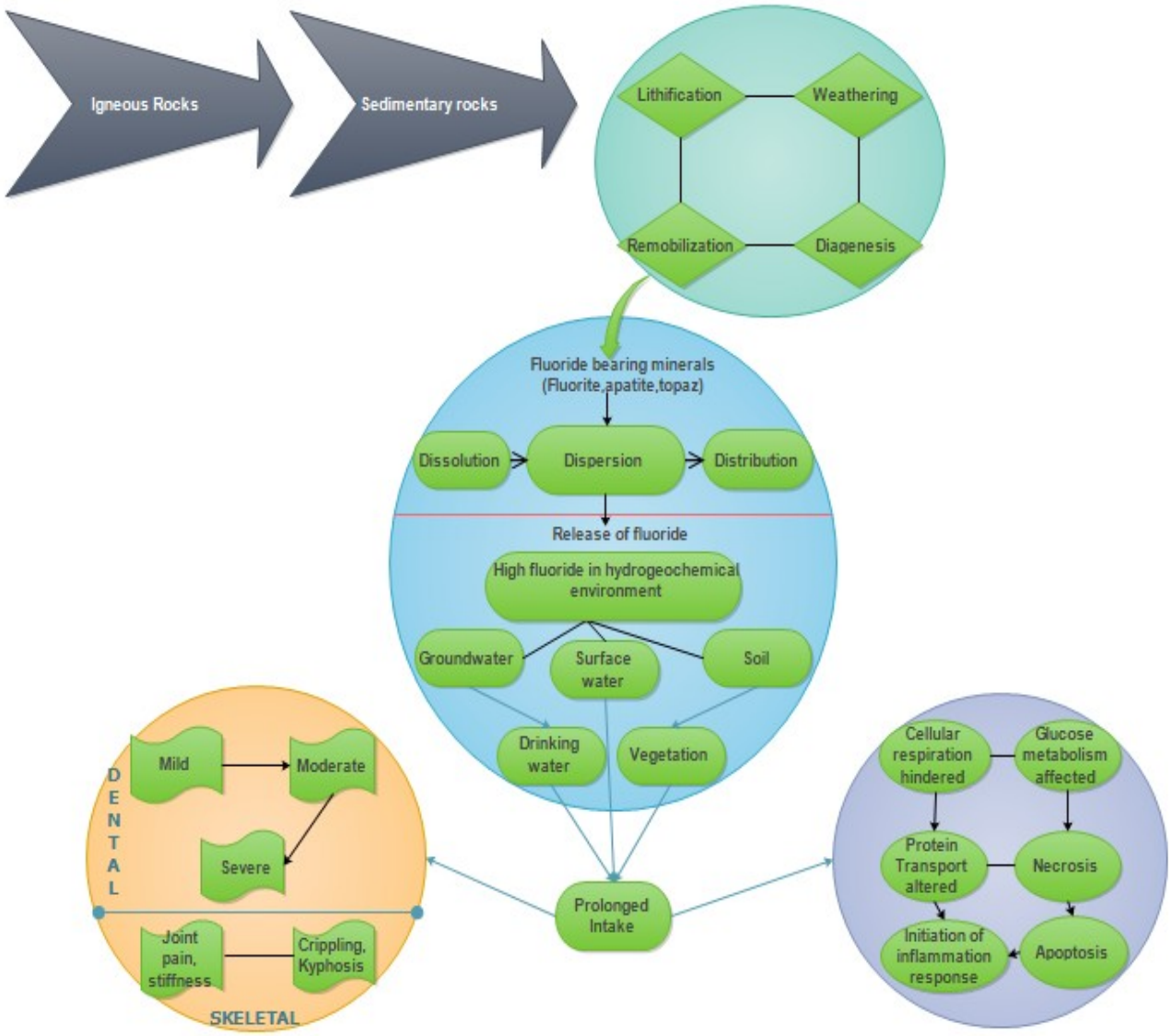

Figure 1.4: Endemic fluorosis in India: Hydrogeochemical basis

1.2 Health Issues due to excess fluoride intake

Fluoride is such an element which needs to maintain a balance in the environment so that it just acts as a beneficial additive and not a detrimental contaminant. Intake of water with less than 0.5 mg/L of fluoride may cause dental caries while water having fluoride concentration higher than the permissible limit may lead to skeletal or dental fluorosis or both. The permissible limit of fluoride in drinking water as determined by the WHO is 1.5 mg/L. Many countries have also adopted this guideline value as a standard for limiting fluoride in drinking water, although due to geological reasons some choose to differ. The

maximum permissible limit of fluoride in drinking water in India is 1.0 mg/L as determined by the Bureau of Indian Standards (BIS;IS:10500) [13]. Some of the hazardous effects due to consumption of excess fluoride in human body are illustrated in Figure 1.5.

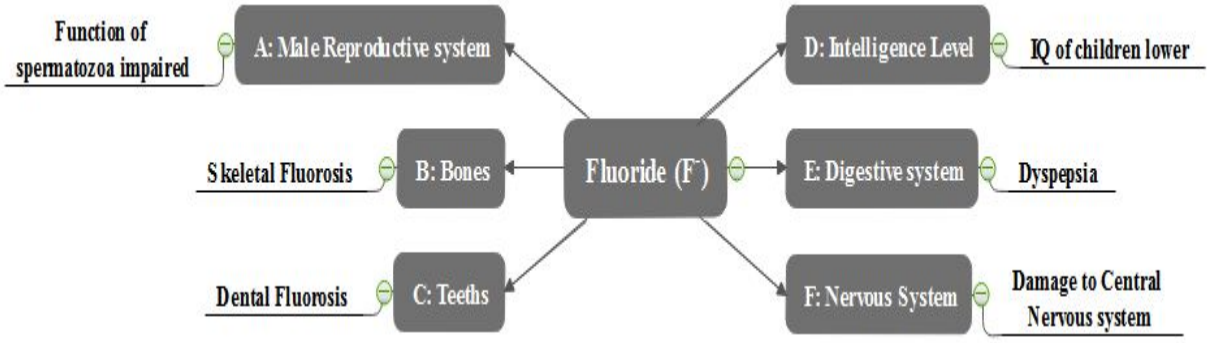

Figure 1.5: Effects of excess fluoride in human body (A: [14], B: [15], C:[16], D: [17], E: [18], F: [19])

1.2.1 Fluorosis

Majority of the ingested fluoride is rapidly absorbed via gastrointestinal tract and lungs. The absorbed fluoride is transported through blood and is either excreted through the renal system or gets accumulated in the calcified tissues. Cations such as calcium, magnesium and aluminum if present in elevated concentration can form insoluble complexes with fluoride and decrease gastrointestinal fluoride absorption [20]. As per literature reports, adults and children above the age of three readily excrete about 90 % of the ingested fluoride. However, children below 3 years excrete only about 50 % of the fluoride ingested and approximately 90 % of the fluoride which is retained in the body are deposited in the skeleton and teeth which further leads to skeletal and dental fluorosis respectively [21].

1.2.1.1 Dental Fluorosis

The most vital caries preventive means in dentistry is by using fluoride. However, high exposure to fluoride through numerous ways is most probable cause for an upsurge in the occurrence of mild to severe forms of dental fluorosis in many countries. Dental fluorosis is caused by the consumption of fluoridated water for a long-term especially during tooth development [16, 20].

An incomplete removal of amelogenin proteins (required for enamel development) under influence of fluoride during tooth development leads to dental fluorosis. The enamel is composed of hydroxyapatite crystals [$Ca_{10}(PO_4)_6(OH)_2$] and if high levels of fluoride

ions is present during enamel formation, a significant amount of hydroxyapatite is converted to fluoroapatite. The reaction releases OH^- ions from hydroxyapatite and changes the pH which could cause amelogenins to aggregate and prevent the diffusion of the protein out of the maturing enamel. Bronckers et al. [22] proposed a molecular mechanism for dental fluorosis, presented in Figure 1.6. In the Figure, **"A"** represents early stage of tooth development in non-fluorotic conditions and **"B"** in fluorotic conditions. "A1" is enlarged into "A2" to show crystal formation at the molecular level. The thread like structures shown are amelogenins which then form nanospheres (1) which adhere to the surfaces of growing crystals and increase crystal growth in length (2). The crystal growth generates protons (H^+) which is neutralized as amelogenins binds to them (3). The boxed area in "B1" is magnified into "B2" where fluoride ions disrupts the process by accelerating the crystal growth in thickness which leads to generation of more protons. Amelogenins fail to neutralize such large amount of protons and detach from the crystal surface due to acidic conditions. Thus, control over crystal growth in length is lost and fluoride ions may further alter the ameloblast cell functions leading to dental fluorosis.

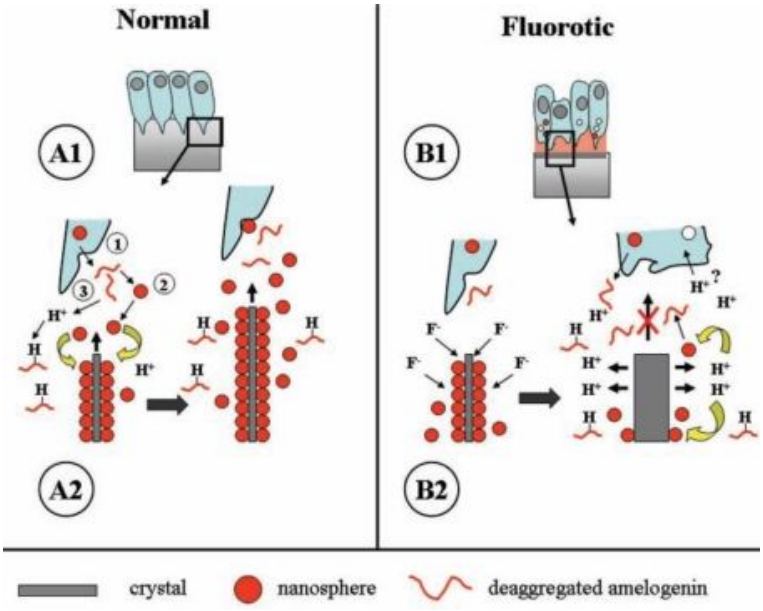

Figure 1.6: Mechanism of dental fluorosis (Comparison between normal and fluorotic conditions is shown) [22]

Aoba and Fejerskov [16] reported that fluoride intake in low concentrations over a long duration may result in various degrees of enamel porosity. Dental fluorosis can be identified initially by opaque white patches on teeth. In advanced stages, teeth show marked hypoplasia, attrition and pitting with brown or black staining (Figure 1.7a). Dental fluorosis can be recognized easily and is a sensitive health pointer of excess fluoride exposure.

Therefore, it can be used for consistent monitoring of health complications related to environmental fluoride contamination.

1.2.1.2 Skeletal Fluorosis

Bone comprises of 50 - 70% mineral and the mineral content of bone is mostly hydroxyapatite, with minute concentrations of carbonate, magnesium, and acid phosphate. Fluoride plays an important role in mineralization of bones and thus makes the skeletal system stable. When fluoride is present at low concentrations it helps to reduce the solubility of apatite crystals and makes the structural system of bone stable [16].

On the other hand, endemic skeletal fluorosis is a chronic metabolic bone and joint ailment instigated by consumption of high concentrations of fluoride either through water or seldom from foods of endemic regions. As bones are largely composed of calcium compounds, particularly hydroxyapatite, the reaction of Ca^{2+} ions and F^- forms CaF_2. Being an insoluble salt, CaF_2 is eliminated by the body, which also leaches out some of the calcium that would be part of the bone matrix [20]. A large number of people in developing countries are calcium deficient and due to excess fluoride intake more calcium ions are leached out from the body [23]. Consumption of fluoride increases bone mineral density, however it decreases the tensile strength and bones become brittle. Skeletal Fluorosis can cause pain and stiffness in joints [24] as well as deformities such as crippling, kyphosis, and genu varum [15].

Whitford [20] stated that incorporation of fluoride in bones is directly proportional to age of the person which makes older people more susceptible to the disease. Excess fluoride ions affect the bone cells (both osteoblasts and osteoclasts) and appear in form of skeletal manifestations such as crippling- deformities, osteoporosis, and osteosclerosis [25]. In the advanced stages of this disease, the bones and joints become extremely weak and locomotion becomes troublesome (Figure 1.7b). The vertebrae in the spine practically fuse together in such a way that the patient is left crippled which is the final stage of skeletal fluorosis. Skeletal fluorosis is augmented by a variety of factors such as climatic conditions related to water consumption, additional sources of fluoride consumption, exposure to other materials that may modify the absorption of fluoride into the body, nutritional status and diet of the person.

The manifestations of skeletal and dental fluorosis is given in form of pictures in Figure 1.7.

(a) Dental fluorosis (Different stages)[26, 27] (b) Skeletal fluorosis (Crippling stage)

Figure 1.7: Pictorial representations of Dental and Skeletal Fluorosis

1.2.2 Other implications

Apart from dental and skeletal fluorosis, excessive fluoride intake may cause other complex health issues. Even at molecular level fluoride renders various toxicological affects as listed in Figure 1.8. Barbier et al. [25] affirmed that necrosis is a primary mechanism of cell death when relatively high fluoride concentrations are present and apoptosis is induced by fluoride which in turn elevates oxidative stress-induced lipid peroxidation. Trivedi et al. [28] observed glucose intolerance and abnormalities in insulin production while studying fluoride toxicity. Inflammatory responses were noticed on high fluoride exposure by Lund et al. [29]. They reported increase in the number of neutrophils and total cells while there was a decrease in cell viability. Lack of production of reactive oxygen species during fluoride-induced apoptosis and the generation of superoxide anions are supposed to increase on fluoride exposure causing oxidative stress [30]. Fluoride is proclaimed to inhibit the activity of antioxidant enzymes like superoxide dismutase, glutathione peroxidase and catalase. For this reason, oxidative stress is recognized in many soft tissues of people living in endemic fluorosis areas. In addition, the interference with protein synthesis and secretion was reported as an effect of fluoride exposure [25].

These facts clearly show the severity of health issues caused by fluoride ions. There is no established treatment for fluorosis and it is often an irreversible condition, therefore prevention remains the only solution. Therefore, drinking water with permissible fluoride concentration is the only way to keep the disease in check.

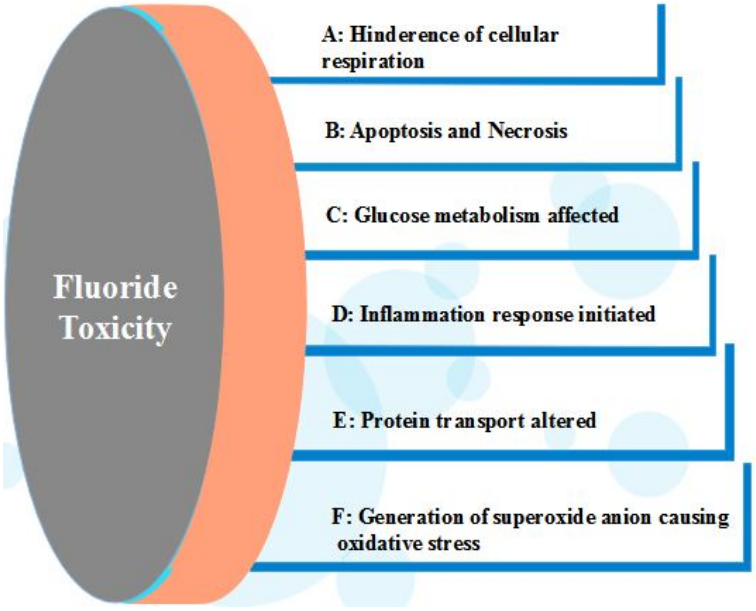

Figure 1.8: Toxic effects of fluoride in body at molecular level (A: [31], B: [25], C: [28], D: [29], E: [25], F: [30]

1.3 Techniques for Fluoride removal

Various techniques widely used for defluoridation of water on basis of the mechanisms involved are membrane filtration, electrocoagulation, ion exchange resins, coagulation-precipitation and adsorption. The objective of using all these technologies in fluoride removal is to treat the contaminated water and to bring down fluoride concentration to acceptable limits. A brief description about each technology is given in the following section along with their advantages and limitations.

1.3.1 Membrane filtration

Reverse osmosis (RO) technology is a pressure driven membrane process through which fluoride removal is achieved. Various other molecules and ions are also removed alongwith fluoride. The residue from the feed water along with excluded impurities is discharged as concentrated waste stream. The efficacy of the method and the quantity of permeate produced depends on factors like water quality, size and charge of chemical ions, membrane properties, as well as system operating pressure, temperature and flowrate [32]. Nanofiltration is another membrane filtration process which have also been utilized for fluoride removal in recent years [33]. It is a relatively low-pressure process compared to RO and removes primarily higher concentration of dissolved solids. Membranes used

in nanofiltration have slightly larger pores than the membranes used in RO and offer less resistance to passage of solvent and solutes.

Problems faced during operation of RO include membrane scaling, fouling, as well as high consumption of energy and high capital costs. RO membranes may also act as media for microbiological growth [34]. Chemicals like calcium, magnesium, and silica may cause scaling and decrease efficiency of membrane. Failure of membrane will allow contaminants to pass on to the treated water. Moreover, a reverse osmosis unit produces large quantity of reject water, therefore cannot be applied in regions where availability of water is already an issue (arid areas). This technique is not viable for water having high salinity and TDS. Both reverse osmosis and nanofiltration technologies are expensive making them undesirable for low income communities and rural areas.

1.3.2 Electrocoagulation

In electrocoagulation, a potential is applied using an external power source which leads to oxidation of the anode and reductive deposition of elemental metals. Aluminum electrodes are generally used for fluoride removal using electrocoagulation process. If aluminum electrodes are used, Al^{3+} ions will undergo further spontaneous reactions to form corresponding hydroxides and polyhydroxides which have strong affinity for dispersed particles as well as counter ions to cause coagulation [35, 36]. Due to usage of aluminum electrodes and dissolution of cathode, residual aluminum was found in the treated water creating major health issues. Therefore, Vasudevan et al. [37] used magnesium and Mg-Al-Zn alloy as the anode material for the removal of fluoride by electrocoagulation.

The electrochemical reduction of water in the cathode also instigates the formation of hydrogen bubbles leading to a soft turbulence in the system that bond with the contaminant decreasing their relative specific weight. Thus, flocculation process is enhanced [38]. The important factors in this process include type of electrode, solution pH, electricity applied and the time period. Some researchers have suggested electrocoagulation process as an alternative to the conventional coagulation [39, 40]. Understanding the electrocoagulation process requires detailed knowledge of the electrolytic reactions occurring and mechanism of defluoridation involved.

Moreover, electrocoagulation process is not cost effective as it consumes electricity. Electrode corrosion, formation and disposal of sludge are the other problems associated with this technique. Sometimes an impermeable oxide layer is observed to be formed on the cathode electrode, further creating an interference with the process efficiency. Timely replacement of the anodes used is paramount and a minimum conductivity is necessary

for the applied current to pass [36], which means in water with extremely low TDS, conductivity has to be introduced. All this requires skilled labour which is not viable for rural areas and adds to the process expenses.

1.3.3 Ion exchange resins

Strongly basic anion-exchange resin containing quaternary ammonium functional groups are used for water defluoridation purpose. Ion exchange resins are said to remove 90 to 95 % of the fluoride from contaminated water. Fluoride removal via ion exchange resins takes place as per the following reaction:

$$Matrix - NR_3^+Cl^- + F^- \rightarrow Matrix - NR_3^+F^- + Cl^- \tag{1.3.1}$$

As evident from the equation, the fluoride ions get exchanged for the chloride ions. This causes an increase in concentration of chloride ions in the treated solution. Often pH adjustments are needed post-treatment as the treated water has low pH. Large amount of regenerant is required for regeneration of the resins. In addition, sludge loaded with fluoride needs to be treated separately before disposal. The complex nature of the resins and their susceptibility towards contamination makes the process less desirable. Also, this process is not cost effective and presence of competing ions such as sulfate, phosphate, bicarbonate may offer ionic competition, thus reducing the efficiency of the resins used for defluoridation [34]. This is because the ion exchange resins tend to prefer counter ions which are of greater valency, higher concentration and ions of smaller hydrated equivalent volume. The anion exchange resins have a order of selectivity for anions which makes the defluoridation process troublesome. The order is as follows: citrate > sulfate > oxalate > iodide > nitrate > chromate > bromide > thiocynate > chloride > acetate > fluoride [41]. Examples of ion exchange resins used for fluoride removal are Indion FR 10 [42, 43], modified Amb200CT resin [44] and modified Amberlite XAD-4™ resin [45]. Meenakshi and Viswanathan [42] suggested that cationic type resins were more selective for fluoride removal than the anion exchange resins. But the fluoride uptake capacity and selectivity of the cationic type resins is dependent on the type of the metal ion in the resin. Therefore, researchers have modified the cationic resins by loading different metal ions [42, 43, 44].

Ion exchange resins are expensive, contamination prone and complex making them less preferable for defluoridation of water for low income communities.

1.3.4 Coagulation-Precipitation

Precipitation processes are generally based on the addition of certain chemicals which subsequently forms some fluoride compounds in aqueous solution. Examples of these processes are alum and lime addition, aluminum sulfate addition and addition of poly aluminum chloride. The addition of lime causes the fluoride to precipitate as insoluble metal fluoride and raises the pH value of the water up to 11–12 due to release of hydroxyl ions as shown in Eq. 1.3.2.

$$Ca(OH)_2 + 2F^- \rightarrow CaF_2 + 2OH^- \tag{1.3.2}$$

However, precipitation processes are controlled by the solubility of a forming salt. In lime based defluoridation processes solubility of calcium hydroxide is low hindering the removal of fluoride completely and settling characteristics of the precipitate are poor as well [34].

The Nalgonda process developed by NEERI (India) was one of the most used defluoridation method in India, especially at community level. It was a two-step process where predetermined amounts of alum and lime were added. In this method, precipitation occurred by lime dosing. The reaction caused formation of insoluble aluminum hydroxide followed by formation of alumino-fluoro complexes. For domestic purpose, bucket defluoridation system based on Nalgonda process was used for a daily routine, where one bucket of water is treated for one day's water supply of about 20 L. The residual fluoride in the treated water was between 1 and 1.5 mg/L. This technique was then introduced in many countries including Kenya, Senegal and Tanzania [5]. Dahi et al. [46] has described the operation of the Nalgonda process in the Tanzanian village of Ngurdoto.

The major limitations encountered with this technique is low treatment efficiency of approximately 70% and need of very large dosage of aluminum sulfate were needed (about 700-1200 mg/L) [34]. This method is discontinued due to leaching of aluminum ions into water, much higher than the permissible limit of 0.2 mg/L and posing health threats [47]. Generation of unwanted precipitate and its disposal is also a disadvantage of this technique.

1.3.5 Adsorption

Many methods have been developed over the past years for mitigating excess fluoride from drinking water, among them adsorption appears to be an effective, environmental friendly and economical technique [48, 5]. Adsorption process is a surface phenomenon involving uptake of fluoride ions on the active sites of the adsorbent. The process of fluoride adsorption onto an adsorbent generally takes three major steps, described as follows [5, 48]

and shown in Figure 1.9:

- At first, F^- ions diffuses or transports to the external surface of the adsorbent from bulk solution across the boundary layer which is surrounding the adsorbent (external mass transfer);
- Thereafter, the adsorption of fluoride ions on to particle surface occurs;
- Lastly, the adsorbed F^- ions probably exchange with the structural elements present inside the adsorbent particles (depending on the chemistry of adsorbent material), or the adsorbed fluoride ions are transferred to the internal surfaces for porous materials (intraparticle diffusion).

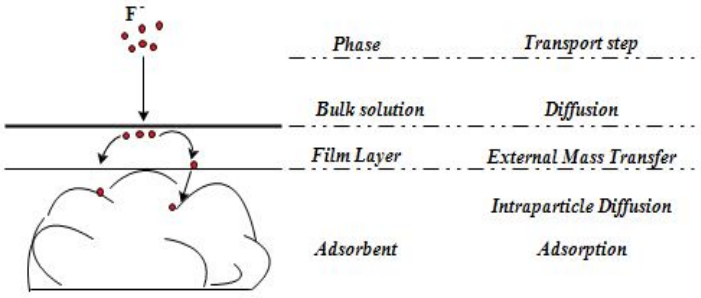

Figure 1.9: Process of fluoride adsorption

The fluoride adsorption phenomenon involves the passage of fluoridated water through a contact bed where fluoride is removed by ion exchange or surface chemical reaction. Defluoridation by adsorption method holds a strong potential in fluoride removal due to its key process features such as removal even at low fluoride concentrations, high removal capacities, economic viability and ability to reuse the adsorbent (regeneration). Due to these features researchers have always continued to explore further possibilities with adsorbents and attempts are been made to make the process more efficient. For estimation of practical application of an adsorbent consideration of fluoride uptake capacity, pH of solution, contact time needed for fluoride removal, adsorption capacity in presence of interfering anions are essential. All research papers do not report on these factors and therefore it is quite difficult to readily compare all the adsorbents [5]. Even if a wide range of adsorbents are being studied for fluoride removal, among them only a few adsorbents are able to bring the residual fluoride concentration in the range of 1.0 – 1.5 mg/L which is required for drinking water [49]. Activated alumina (AA) is the most commonly used adsorbent for

defluoridation of water and voluntary organizations funded by UNICEF or other agencies propagated it in many villages. Sarita Sansthan, Udaipur, Rajasthan (India) has publicized the activated alumina defluoridation technique with the practical assistance of UNICEF via providing a bucket (20 L capacity approximately) fitted with a microfilter at the bottom containing 5 kg of activated alumina [50]. However, the process had a narrow pH range (5 – 6), high TDS, low integrity and suffered from ionic competition from groundwater. Presence of residual alumimum in water treated with AA is also reported [47].

Some limitations faced while using adsorbents are pH dependence of the process; decrease in removal efficiency in presence of interfering ions like sulfate, phosphate, bicarbonate and necessity of regeneration [34]. However, these limitations can be overcomed if the adsorbent is selective in nature, the adsorption process is not pH dependent and a suitable regenerant is identified for its reuse.

Various types of adsorbents are developed in the past years and can be classified as aluminum based, calcium based, metal based adsorbents and natural adsorbents. Among these adsorbents, calcium based adsorbents are gaining interest among researchers due to their lower cost and electropositive nature. The literature regarding these adsorbents along with crucial process parameters for adsorption is reviewed in the next chapter (Literature Review).

1.4 Role of calcium

Calcium is the fifth most abundant element on the earth crust and is an essential part of bones and teeth. The role of calcium in controlling the effect of fluorosis and defluoridation of water is detailed in the following sections:

1.4.1 Role of calcium in water sources with respect to fluoride

Fluoride content in groundwater sources are limited by fluorite (CaF_2) solubility. In this context, Hem et al. [51] stated that in the presence of 40 mg/L calcium, fluoride should be limited to 3.1 mg/L and hence, the absence of calcium in water sources allows higher fluoride concentrations to be stable. In places where sodium ions are more and can be exchanged for calcium ions, fluoride concentrations may be high [6]. A negative correlation between calcium and fluoride content and a positive correlation between fluoride and bicarbonate content in groundwaters with high fluoride concentration is affirmed by Handa [8]. Even in the state of Rajasthan, regions with low fluoride concentration (< 1.5 mg L^{-1}) are associated with carbonate rocks and these regions have higher calcium which may have

inhibited an excess of fluoride ions [6].

1.4.2 Role of calcium in human body with respect to fluorosis

Presence of calcium in the form of calcium carbonate or calcium phosphate may decrease the fluoride adsorption in human body by 50 %. It was observed that regions where water hardness (due to high amount of calcium and magnesium) are high, incidents of fluorosis is much lower. Chandra et al. [52] reported that the community Fluorosis Index in Rajasthan was lower in areas where calcium intake was higher. Fluorosis once developed is irreversible and nutrition plays an important role in the onset of the disease. Edmunds and Smedley [6] recognized that dietary deficiencies in calcium and vitamin C are important augmenting factors. Radiological studies conducted by Mithal et al. [53] showed decreased bone density in people having lower dietary intake of calcium and suggested an important role of calcium intake in determining the skeletal changes in endemic fluorosis.

It is hypothesized that women are more prone to fluorosis during the period of pregnancy and lactation because of deficiency of calcium. Adequate intake of calcium is crucial for attainment of peak bone mass and prevention of osteoporosis [54]. A substantial section of population has less than average daily calcium intake and calcium deficiency coupled with secondary hyperparathyroidism has been found very common [55]. Calcium supplementations mainly include calcium tablets and dairy products. The human body can eliminate excess calcium in body but prolonged deficiency of calcium has adverse effects [56]. Böhmer et al. [56] reported that water rich in calcium may serve as an effective alternative to calcium supplementation from milk and dairy products because of their comparable or possibly even better bioavailability of calcium. Calcium intake through milk source also pose issues such as lactose intolerance in people. This means if calcium based adsorbents are used for defluoridation and some calcium ions leach into water, this will serve as a calcium supplementation to calcium deficient people. Since, mostly calcium deficient population are the improvised people, this alternative is best suited to their needs.

1.4.3 Role of calcium as adsorbent for defluoridation

Calcium ions have a good affinity for the electronegative fluoride ions and are biocompatible with the human body in all forms, due to which calcium based adsorbents hold the potential to be effective in defluoridation of potable water. The calcium containing tissues (bones and teeth) in body attract the fluoride ions, likewise calcium materials can remove fluoride ions effectively. Some calcium based materials which are used widely include calcite materials (limestone) where reduction in fluoride levels occurs via

precipitation; bone char which is being used for a very long time and calcium apatite materials which has given a new dimension to the field of defluoridation [48, 57, 58]. Some other materials are quicklime, calcium chloride, calcium sulfate, bleaching powder and plaster of paris [5, 48, 59].

A comprehensive literature review on calcium based materials is presented in the next chapter (Literature review).

1.5 Objectives of Research

Excess intake of fluoride causes several health problems including dental fluorosis, skeletal fluorosis, deformed RBCs, neurological as well as gastrointestinal disorders. Due to highly electropositive nature of aluminum compounds, they are chiefly used for defluoridation which is responsible for introduction of residual aluminum and alumino-fluoro compounds in water resulting in further toxicity. Since, calcium compounds has a good affinity for fluoride ions and possess a higher permissible limit (75 - 200 mg/L) in drinking water compared to aluminum (0.2 mg/L), calcium based compounds may be utilized as adsorbents for mitigating the fluoride level in water to the permissible limit. Previous studies for fluoride mitigation via adsorption process revealed that implementation of adsorption method are restricted chiefly because of the narrow pH range, presence of residual toxic ions, high total dissolved salts (TDS) in treated water and lack of regeneration of adsorbent. Therefore, in the present study, the crucial points are to develop a novel adsorbent which can overcome shortcomings pointed above. Keeping these issues in mind and after identifying the grey areas in research, the following objectives were formulated:

- To study different calcium based adsorbents and selecting a novel adsorbent suitable for keeping the fluoride level of drinking water within permissible limit and conducting characterization studies.
- To conduct batch studies varying different parameters for optimization of the adsorption process and to study equilibrium adsorption isotherms and adsorption kinetics.
- To carry out column studies to observe the actual potential of the adsorption process. It will be useful for predicting the breakthrough performances, estimation of number of usable cycles as well as to optimize defluoridation unit design parameters.
- To perform regeneration studies for estimating maximum capacity of adsorbent and reusing the adsorbent.

- Studies on defluoridation using water samples from fluorosis prone areas are to be conducted for field studies.

1.6 Outline of the work conducted

An outline of the research work conducted is given in form of flow chart in Figure 1.10.

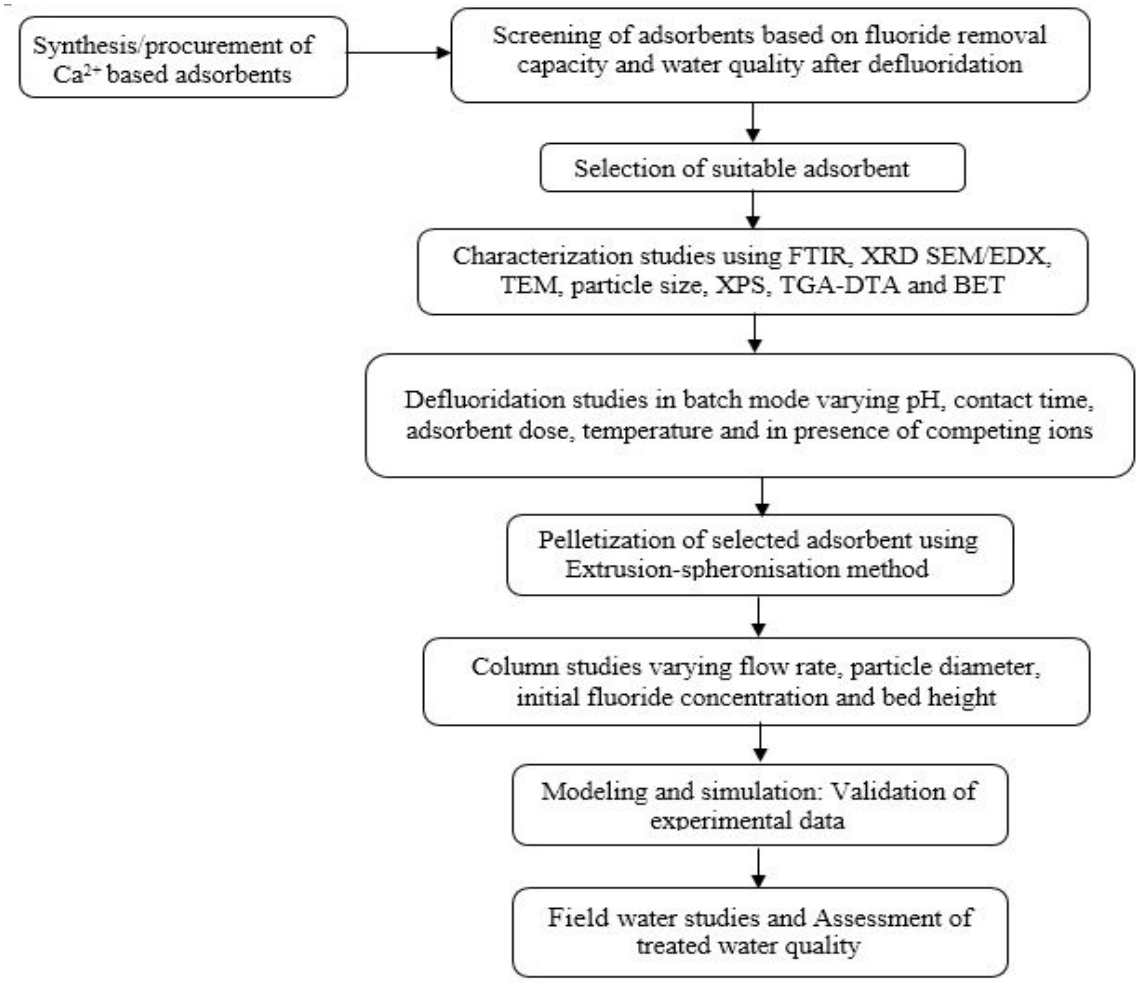

Figure 1.10: Outline of the Research Work

In the first part of this study, calcium based compounds were procured or synthesized in the laboratory and screening of adsorbents were carried out based on their fluoride removal capability and water quality after adsorption. After this, suitable adsorbent were selected and characterized using FTIR, XRD, SEM, TEM/EDX, XPS, BET, particle size distribution and TGA-DTA techniques. The characterization studies also helped in identifying the more promising adsorbent with which further experiments were conducted. In the second part of the study, batch defluoridation studies were performed varying crucial process parameters

such as pH, contact time, dosage and interfering ions. To get an insight of the mechanism of the process, adsorption isotherms and kinetic models were studied. A regeneration method was also developed for reuse of the adsorbent.

After batch experiments, an adsorbent was chosen for pelletization via extrusion-spheronization method. The third part of this study comprised of column adsorption tests with the pelletized adsorbent, varying the operational parameters for evaluating practical feasibility of the process. The experimental data were matched with the theoretical data obtained from simulation carried out in MATLAB software. In the fourth part of this study, field water samples were collected from fluoride prone areas and physico-chemical parameters were examined before and after adsorption.

1.7 Organisation of the thesis

The entire thesis is divided into seven chapters. The highlight of each chapter is presented as follows:

Chapter 1 provides an introduction to the problem addressed and outline of the work conducted.

Chapter 2 presents a review on adsorption based defluoridation processes using various types of adsorbents and major parameters affecting defluoridation process.

Chapter 3 recounts the materials, chemical reagents, solutions used for experimental studies and the methodologies adopted to attain the objectives of the study.

Chapter 4 illustrates characterization of adsorbents using various techniques.

Chapter 5 elaborates defluoridation studies with various calcium compounds in batch mode.

Chapter 6 focused on exploring the practical feasibility of the fluoride adsorption process through column mode.

Chapter 7 includes studies with field water samples and assessment of treated water quality using both batch and column experiments.

Conclusion comprises of all the major findings in the study.

Recommendations for future work gives a glimpse into the future possibilities for further research.

1.8 Summary of the Chapter

The subtle balance of fluoride needed for human body is very crucial defining the thin boundary between a beneficial element to a contaminant. In many parts of the world including India, fluoride in drinking water is responsible for notable public health issues. Fluoride concentration higher than the permissible limit (1.0 mg/L) may lead to skeletal or dental fluorosis or both and many other implications as well. The severe impact of consumption of excess fluoride on human health has raised concerns for development of reliable materials for defluoridation of drinking water. Among the existing technologies for water defluoridation, adsorption technique was chosen for abatement of fluoride because of its key features such as high removal capacity, ease of handling and ability to reuse the adsorbent. Considering the role of calcium in human body, its affinity towards fluoride ions and biocompatibility; it was selected as the chief material for defluoridation in the present study. The next chapter gives an overview of the various adsorbents used for defluoridation along with some crucial process parameters which control the adsorption process.

CHAPTER 2

Chapter 2

Literature Review

2.1 Introduction

The profound literature on defluoridation via adsorption gives a detailed insight on the wide range of adsorbents adopted and compares the probability of fluoride removal using them. This chapter presents a review on the various types of adsorbents such as aluminum based, calcium based, metal based adsorbents and natural adsorbents. These adsorbents are listed in Table 2.2 along with their defluoridation capabilities and various process parameters. Following the literature reports, crucial adsorption process parameters are outlined in this chapter for better understanding of the phenomenon.

The most prominently used method for fluoride removal based on adsorption which is also found in large municipal treatment systems is activated alumina [49, 60]. Some more advanced defluoridation technologies include reverse osmosis and electrocoagulation. However, these technologies are expensive as well as technically complex, making them infeasible for low income rural communities [12]. Considering these facts, precipitation and adsorption processes are technologically and economically viable water treatment options. The Nalgonda method developed in India was based on precipitation technique and was found to be economically effective for defluoridation [12, 61]. Research in the past two decades revealed the presence of residual aluminum in treated water due to usage of aluminum salts. This technique was therefore discontinued which otherwise may have led to neurological disorders due to residual aluminum consumption via this water.

Fluoride is deliberated as one of the major contaminants in eco-toxicological studies. Fluoride ions are responsible for alterations in the functional mechanisms of liver, kidney, digestive system, respiratory system, excretory system, central nervous system and reproductive system, destruction of many enzymes [25]. An elaborate view of action of fluoride ions in several cellular processes and its toxicological implications is presented

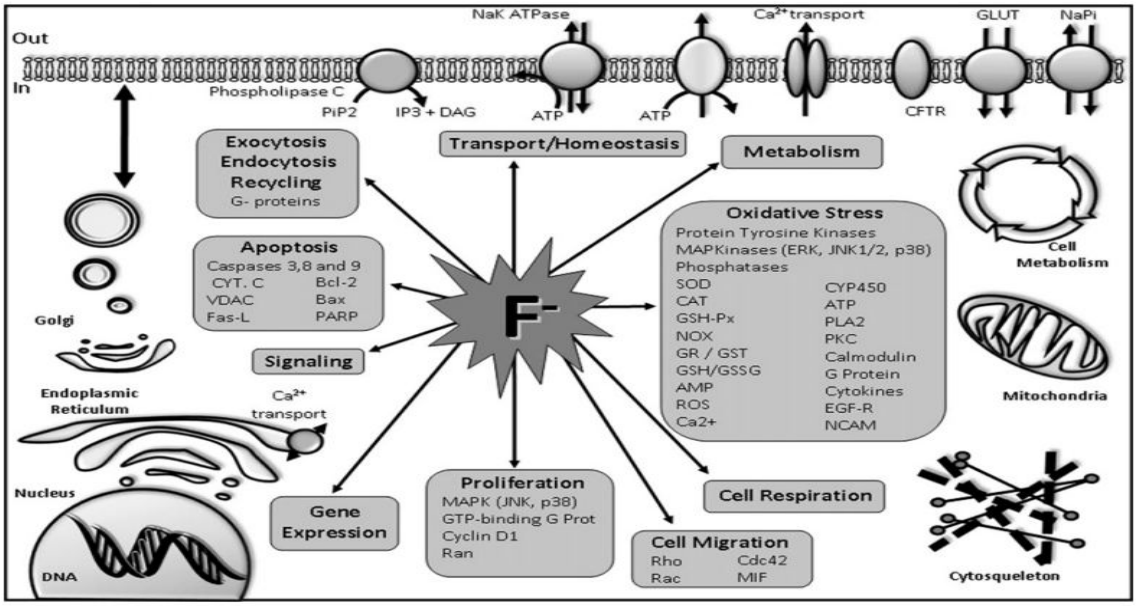

Figure 2.1: Biological consequence of fluoride (F^-) exposure on mammalian cells [25]

in Figure 2.1. Fluorosis is endemic in India and many people residing in rural areas of have no choice but to consume water containing even 44 mg/L of fluoride [62]. The consumption of such high levels of fluoride causes calcium from bones to leach out resulting in bone, teeth and muscle damage, paralysis and pre-mature aging. It has been reported that calcium supplements have the potential to increase the serum calcium level and inhibit the absorption of fluoride ions in the gut as well as prevent fluorosis [21]. Therefore, usage of calcium based adsorbents for defluoridation of drinking water will provide the benefit of improving the calcium concentration levels in the body as people with a calcium deficient diet are more vulnerable to fluorosis. Factors such as social, geographical, environmental and economic should be taken into account while choosing a relevant method for removal of excess fluoride ions from drinking water. The prevalent adsorbents studied by researchers in order to mitigate fluoride are described in the following section.

2.2 Various kinds of adsorbents used in defluoridation studies

2.2.1 Aluminum based adsorbents

Being the most electropositive element, aluminum and aluminum based adsorbents are the first choice for water defluoridation. Aluminum salts, alumina balls and other aluminum based adsorbents are widely used for defluoridation of drinking water because of the high

affinity between aluminum and fluoride ions resulting in very high adsorption capacity. Alumina (chemically aluminum oxide) is considered to be the most effective adsorbent for defluoridation of water. Goswami and Purkait [63] developed acidic alumina as adsorbent for water defluoridation and found it to be highly pH dependent with 94 % fluoride removal efficiency at pH value of 4.4 and temperature 25 ± 2 ºC. Adsorption equilibrium isotherms were fitted with Langmuir isotherm model indicating a maximum capacity of 8.4 mg/g of adsorbent. Further thermodynamic studies carried out proved the process feasibility and endothermic nature with activation energy values estimated at 95.13 kJ/mol. A study conducted for fluoride removal on alumina with alkoxide origin reported the defluoridation capacity decreased from 3.14 to 0.59 mg/g as the adsorbent dose increased from 0.5 to 8 g/L at neutral pH and 30 ± 2 ºC [64]. As activated alumina (AA) adsorbent has tremendous surface area and is highly porous, therefore the AA impregnated with alum (AAIA) was studied to increase its sorption capacity for fluoride removal [49]. AIAA was found to remove 99 % of fluoride at optimum pH 6.5, temperature 25 ± 2 ºC with contact time of 3 h, and adsorbent dosage of 8 g/L while treating 20 mg/L of fluoride. Energy dispersive X-ray analysis (EDX) depicted that the process of fluoride uptake is due to surface precipitation process. A modified immobilized activated alumina (MIAA) was prepared using alum through the sol gel process which gave 1.35 times better performance than unmodified immobilized alumina and the removal rate was also comparatively faster [65] . When compared to activated charcoal which gave an adsorption capacity of 0.45 mg/g, MIAA had an adsorption capacity of 0.76 mg/g for same initial fluoride concentration at 20 ± 2 ºC.

Other modified forms of AA used for fluoride removal include modification by using different metals such as magnesia, manganese oxide, manganese dioxide, cerium and titanium. Magnesia amended activated alumina (MAAA) was synthesized by Maliyekkal et al. [66] by calcining magnesium hydroxide impregnated alumina. The sorption behavior was principally due to the formation of $Mg(OH)_2$ when magnesia reacted with water. As magnesium hydroxide was formed, the fluoride ions present in the contaminated water replaced the hydroxyl ions of brucite crystal lattice without disturbing the crystal structure of the compound. The maximum sorption capacity of fluoride estimated using Sips equation was found to be approximately 10.12 mg/g. Further, manganese dioxide was coated onto activated alumina surface (MCAA) for fluoride removal by Tripathy and Raichur [67]. The coated adsorbent MCAA adsorbed more fluoride than uncoated (AA) one for a wider pH range. Fluoride concentration reduced to 0.2 mg/L (98 %) when initial concentration of fluoride in water was 10 mg/L. Maliyekkal et al. [68] synthesized manganese-oxide-coated alumina (MOCA) and found the maximum fluoride uptake capacity for MOCA and AA to be 2.85 and 1.08 mg/g respectively.

An attempt has been made by Liu et al. [69] for combining aluminum and cerium and preparing aluminum – cerium (Al – Ce) hybrid adsorbent through co-precipitation method. A synergistic interaction between aluminum and cerium compounds occurred in the hybrid adsorbent, which was found to be advantageous for fluoride removal. The adsorbent had sorption capacity of 27.5 mg/g at equilibrium fluoride concentration of 1.0 mg/L, neutral pH and 25 ± 2 ºC temperature. Polysaccharides like chitosan have also been used to prepare adsorbent for defluoridation and to increase their capacity for fluoride uptake they are coupled with aluminum ions. An adsorbent was synthesized by a group of researchers based on titanium–aluminum metal oxide via precipitation method supported through beads using chitosan and the fluoride removal capacity was observed to be 2.22 mg/g [70]. In recent years, usage of metal oxides at a nanoscale has been found very promising for the fluoride removal. Working in this direction, Kumar et al. [71], synthesized nano-alumina and noticed an adsorption capacity of 14 mg/g.

Among the various aluminum based adsorbents such as AAIA, MIAA, MAAA, Manganese dioxide coated alumina, MOCA, titanium–aluminum metal oxide, nano alumina and Al – Ce hybrid adsorbent compared in this section, alum impregnated AA showed best removal capacity of 40.68 mg/g with an initial fluoride concentration of 1 to 35 mg/L [49]. This is due to the fact that available surface sites for fluoride adsorption increased after impregnation of alum on AA and affinity of the amorphous precipitate of aluminum hydroxide on AA in AIAA greatly favored the adsorption phenomenon. However, due to high residual aluminum in treated water, usage of alumina and aluminum based adsorbent is not desirable. The presence of residual aluminum in treated water is further elaborated in section 2.4.3.

The permissible limit of aluminum in drinking water is extemely low i.e 0.2 mg/L as per WHO and BIS (IS:10500) [13, 72]. Exposure to different forms of aluminum viz total Al, total dissolved Al, monomeric organic Al, monomeric inorganic Al, polymeric Al, AlOH, fluoroaluminates, $AlSO_4$ in drinking water is responsible for instigating Alzheimer's disease [73]. Along with Alzheimer's disease, aluminum plays significant role in amyotrophic lateral sclerosis (ALS), Parkinson's disease, and Guam dementia complex [74].

In view of the drastic effects which may arise through intake of water treated with aluminum based adsorbents, search for a substitute adsorbent is apparent.

2.2.2 Calcium based adsorbents

Calcium has good affinity for fluoride anions, and therefore calcium based adsorbents are also being used for fluoride adsorption in aqueous systems. Low cost of calcium based compounds and its biocompatibility with the human body is another reason for their increasing usage for fluoride removal processes.

Fan et al. [48] studied some low cost adsorbents and revealed that their adsorption capacities follow the order: hydroxyapatite > fluorspar > quartz activated using ferric ions > calcite > quartz. For initial fluoride concentrations ranging from 0.000025 to 0.0634 mg/L, removal capacity of hydroxyapatite and fluorspar was 90 and 25 % respectively. Calcined paper sludge which contain mainly cellulose fibers and inorganic fillers together with coating materials such as calcite, kaolinite, and talc was investigated by Wajima and Rakovan [75]. They prepared the adsorbent using sludge fired at temperatures between 200 and 1000 °C for 6 h producing amorphous phase below 800 °C and crystalline phases above 800 °C temperature in the order of kaolinite < calcite < talc and gehlenite at 1000 °C. The soluble components present in calcined paper sludge dissolved and the main process responsible for fluoride sequestration and removal is the formation of fluorite by reaction between labile calcium and fluoride in solution.

Low cost of calcium based compounds are of great interest especially for rural areas. Bhagat [76] studied a method for removal of fluoride in rural areas by using acid enhanced limestone defluoridation (AELD). However, this method increased the calcium hardness in drinking water from the initial value of 0.72 mg/L to the range of 69–115 mg/L. Calcium however is not harmful to human health rather it is essential for proper growth and development. Moreover, this technique also used citric acid to decrease the concentrations of phosphate, nitrate and sulfate in the groundwater, which is an advantage of this defluoridation method since other coexisting ions in groundwater would not affect the adsorption process. Defluoridation of water using quicklime was conducted and found that the adsorption process is chemisorption combined with precipitation [59]. Removal efficiency was found to be maximum when the initial fluoride concentration was high (50 mg/L). The maximum fluoride sorption capacity of activated quick lime was found to be at 16.67 mg/g. This removal technique may be applicable to treat industrial effluents with high fluoride concentrations, but cannot be used for domestic purpose as it cannot bring fluoride concentration within permissible limit, and rather increases the pH of the treated water. Synthesis of calcium containing charcoals by incorporating calcium chloride into wood and thereafter carbonizing at different temperatures of 500, 650 and 900 °C was done to prepare a porous adsorbent [77]. Charcoal prepared at 650 °C showed optimum fluoride adsorption capacity of 19.05 mg/L.

Since, aluminum has the highest affinity for fluoride ions; calcium based adsorbents impregnated or doped with aluminium, aluminum oxide or aluminate were being developed to increase the defluoridation capacity. Aluminum hydroxide impregnated limestone (AILS) was prepared by Jain and Jayaram [78] for defluoridation. The highest adsorption capacity shown by limestone was 43.10 mg/g; while in case of AlLS sorbent it increased to 84.03 mg/g. FTIR analysis of the AILS adsorbent indicated physical adsorption of fluoride. Another calcium–aluminum adsorbent is calcium aluminate (CA), a highly porous material prepared by using combustion method [79]. It showed high fluoride uptake with 85 % removal for initial concentration of 8.9 mg/L using an adsorbent dose of 3 g/L. Eggshell (calcium carbonate), a waste natural material was converted to Eggshell Composite (EC) by mixing with aluminum sulfate [80]. The adsorption capacity of EC was 37 mg/g due to a synergistic effect between calcium and aluminum in the composite.

Hydroxyapatite is widely studied as the main constituent of teeth and bone, which has attracted the attention due to its special apatite structure as hydroxyl ions can be replaced by fluoride ions in its crystal structure. Jimenez-Reyes and SolacheRios [81] explored hydroxyapatite the calcium-containing constituent of bone matrix ($Ca_{10}(PO_4)_6(OH)_2$) as a potential adsorbent for defluoridation as it can be synthetically prepared. The sorption capacity of fluoride ions by Hydroxyapatite (HAP) was reported as 4.7 mg/g. Nano sized synthetic hydroxyapatite with various particle sizes were prepared and comparison of their defluoridation ability with bulk hydroxyapatite material obtained by conventional solid-state reaction was done [82]. It was noted that hydroxyapatite with smaller particle sizes exhibited better performances with higher adsorption efficiency. The maximum Langmuir sorption capacity of different sized hydroxyapatites ranged between 0.295 and 0.489 mg/g. Nano-hydroxyapatite (n-HAp) was also synthesized by Pandi and Viswanathan [83] and it was incorporated with gelatin biocomposite. They found a fluoride uptake capacity of 4.16 mg/g with the mechanism for fluoride removal governed by electrostatic attraction and ion-exchange. Further, the removal efficiency of fluoride by glass derived hydroxyapatite (G-HAP) was investigated by Liang et al. [84]. The effects of size and quantity of particles, pH value and adsorption time on adsorption performance were studied. The adsorption percentage (%) was between 86.7 and 96.6 when the fluoride concentration was varied from 5 to 10 g/L. The results depicted that the G-HAP could more effectively immobilize fluoride in solution than nano sized Hydroxyapatite. Cationic surfactant modification of HAP powder was done and the removal capacity increased from 2.63 mg/g to 9.36 mg/g for a fluoride concentration of 10g/L and 50 mg dosage [85]. The calcium hydroxyapatite present in lamb and chicken bones were utilized by some researchers and a removal efficiency of 99.4 % and 99.8 % respectively was noted [86]. Al-HAP nanoparticles were synthesized

through co-precipitation method by Nie et al. [87]. Al-HAP possessed higher defluoridation capacity of 32.57 mg/g than unmodified hydroxyapatite (16.38 mg/g) when treated with 50 mg/L of fluoride solution with a dosage of 0.05 g at pH 7. Adsorption phenomenon showed that the – OH ions on surface of Al-HAP were the adsorption sites. Significant research has been carried out with hydroxyapatite which shows its suitability for defluoridation process. However, few constraints noticed while using it as an adsorbent were the limited pH range, ionic competition with interfering ions and lack of continuous column studies.

It can clearly be observed that among the adsorbents discussed in this section, the higher removal capacity was achieved only with those adsorbents where aluminum or its salts are used either modified or impregnated (EC, CA, AILS, Al - HAP). Aluminum hydroxide impregnated limestone [78] exhibited the maximum sorption capacity for fluoride i.e 84.04 mg/g. The high electro-positivity of aluminum led to this high removal capability. Any experimental studies on information for leaching of the toxic aluminum ions into water from the adsorbent was not provided. Though calcium adsorbents have comparatively lower capacity than aluminum, but even if leached into treated water they have an added advantage of causing no adverse health effects. Another interesting fact noted by Jha et al. [88] while working on fluoride concentration along with other physico-chemical parameters in groundwater samples in India was the negative relationship of presence of fluoride with calcium and magnesium. This confirms that if calcium and magnesium can be used together in some stable adsorbent form, it can effectively reduce the fluoride concentration through adsorption and precipitation in the aqueous medium.

2.2.3 Carbon based adsorbents

Activated carbon (AC) has high surface area available for adsorption which makes it suitable for fluoride removal. $KMnO_4$ modified activated carbons were prepared by one-step steam pyrolysis of rice straw at different temperatures (550, 650, 750 °C) had defluoridation capacity of 15.9 mg/g and lower temperatures favored fluoride adsorption at an optimum pH of 2 [89]. Carbonaceous material from pyrolysis of sewage sludge used, for defluoridation of water had an adsorption capacity of 2.84 mg/g using 0.075 g of carbonaceous material for an initial fluoride concentration of 5 g/L [90].

Allotropes of carbon of varying grades of graphite was used as an adsorbent for fluoride removal and the sorption capacity of fluoride was reported as 3.13 mg/g [91]. Lignite is a lower rank of coal having high affinity for the fluoride anion. Pekar [92] found that fluoride uptake decreased with increasing fluoride concentration but still remained above 90 % and even after leaching only minor part (13 %) goes into water. The sorption mechanism

remains effective also at low fluoride concentrations which is still above health risk limit (1.5 mg/L) [72].

In order to make adsorbents more efficient and novel, hybrid adsorbents were designed by Sivasankar et al. [93] who synthesized cerium dispersed in carbon (CeDC) by carbonization of ammonium cerium sulfate impregnated starch. CeDC is a hybrid adsorbent and showed fluoride sorption of 29.1 mg/g. Uptake capacity of CeDC decreased as fluoride concentrations increased from 2 to 8.3 mg/L and the defluoridation potential of CeDC was dependent on the temperature. Carbon slurry is a waste from fertilizer industry and can act as a cheaper alternative adsorbent. Adsorption of fluoride on waste carbon slurry was investigated by Gupta et al. [94]. Maximum adsorption capacity of 4.861 mg/g was observed at an initial fluoride concentration of 15 mg/L with an adsorbent dose of 1.0 g/L. Carbon fibers and nanofibers were used by some investigators with sizes that are at the nanoscale level. A micronanohierarchal web was developed by Gupta et al. [95] that constituted activated carbon fibers and carbon nanofibers, incorporated with aluminum for fluoride removal from wastewater. Li et al. [96] prepared a new kind of carbon material utilizing catalytic decomposition of xylene using ferrocene as catalyst and called as ACNT (aligned carbon nanotubes). They exhibit high defluoridation capacity (4 mg/g) due to their surface defects, amorphous nature, inner cavities and inter nanotube spaces.

More studies are being carried out to modify the surface of carbon adsorbents to increase the fluoride removal rate. However, carbon based adsorbents are more appropriate for small scale and column studies are rarely reported which restricts its practical applicability.

2.2.4 Metal based adsorbents

Recent advances in adsorption technologies have led to usage of various metal oxides and hydroxides or combination of both for enhanced fluoride removal. Granular ferric hydroxide (GFH) was studied for fluoride removal from aqueous solutions by adsorption [97]. The adsorption capacity of GFH for fluoride was 7.0 mg/g at pH 6.0 – 7.0 and temperature 25 ± 2 ºC. Dou et al. [98] synthesized a granular zirconium-iron oxide by extrusion method that had a fluoride removal capacity of 9.80 mg/g for an equilibrium concentration of 10 mg/L at pH 7.0. Rao and Karthikeyan [99] used lanthanum oxide as adsorbent for fluoride removal. Batch studies indicate a removal of 90 % in 30 min from a 4 mg/L fluoride solution. Some rare metal oxides have proven to be very effective for water defluoridation. The efficiency of FeO(OH) in removing fluoride from aqueous environment was examined by Stoica et al. [100]. Its granular structure, high surface area and effective capacity of fluoride removal make this adsorbent a highly potential media to be used in

removing the fluoride from aqueous systems. The adsorption capacity of FeO(OH) for fluoride was 5 mg/g at fluoride concentration of 50 mg/L and 4.5 pH.

Tailor made hybrid composite materials of defined superior characteristics are being designed and synthesized now-a-days in the field of polymeric nano-adsorbents. Hybrid thorium phosphate syndicates the properties of thorium phosphate and cinnamamide with an adsorption capacity of 4.749 mg/g at pH 2 [101]. Dash et al. [102] synthesized Ce loaded mesoporous zirconium phosphate by a surfactant assisted route and the removal capacity possessed by this adsorbent was 20.5 mg/g. Mg – Fe – La trimetal composite displayed the maximum capacity of fluoride removal (112.17 mg/g) among the metal oxides and hydroxide adsorbents as listed in Table 2.2. Wang et al. [103] synthesized this adsorbent via co-precipitation method and the multivalent adsorbent removed fluoride ions from aqueous solution through the mechanism of adsorption/complexation and ion exchange interaction.

Although metal oxides and hydroxides show greater adsorption capacity, using such adsorbents for drinking water treatment purpose always pose a higher risk of leaching of these metallic elements into water causing detrimental and unaltered health effects.

2.2.5 Natural adsorbents

Most of the adsorbents for defluoridation used at present are synthetic chemicals and the scope of natural adsorbents has never been explored in a commercial scale. Our natural resources like plant parts, natural polymers, polysaccharides etc had also been studied for defluoridation capacity by various researchers. Studies of Chidambaram et al. [104] on fluoride removal by natural materials like red soil, charcoal, brick, fly-ash and serpentine revealed that red soil has good defluoridation capacity followed by brick, fly-ash, serpentine and charcoal. Bark of babool was used as an adsorbent and at 5 g/L of dosage, 5 mg/L fluoride concentration, the defluoridation capacity was 0.77 mg/g [105]. Natural materials modified or activated were used as adsorbents for defluoridation studies. Natural materials when coupled with some metal can further increase the fluoride uptake capacity. Kamble et al. [106] observed the usage of chitin, chitosan and 20 % – lanthanum incorporated chitosan as adsorbents for the removal of excess fluoride from drinking water. They found that 20 % La – chitosan showed higher fluoride removal capacity and affinity as compared to the untreated chitin and chitosan. Adsorption of fluoride on lanthanum modified chitosan was explained on basis of the ligand exchange mechanism between fluoride ion and hydroxide ion coordinated to lanthanum (III) ion immobilized on the chitosan. Fluoride removal using chitin/cellulose composite from aqueous solution was investigated [107] through batch adsorption studies and indicated that for optimum adsorbent dose at 3 g of chitin/cellulose

composite, maximum adsorption capacity was 83.75 mg/g at pH 6.5.

Natural materials apart from being safe if used in drinking water treatment have another advantage of being less expensive than chemicals used. Activated carbon prepared by the thermal process from *Phyllanthus emblica* was used by Veeraputhiran and Alagumuthu [108] as a low cost adsorbent for fluoride removal from water. The biosorbent showed enhanced removal of fluoride (82.1 %) at equilibrium for 3 mg/L initial fluoride concentration with an adsorbent dose of 0.75 g. Studies on the biosorbent using varying particle sizes revealed that the defluoridation efficiency of the sample with particle size 53 µm recorded highest defluoridation efficiency due to larger surface area. Defluoridation studies for *Cynodon dactylon* were carried out in 105 min, 83.77 % removal (2.01 mg/g capacity) was achieved for 3.0 mg/L fluoride concentration and 1.25 g adsorbent dosage at neutral pH [109]. Chakrabarty and Sarma [110] investigated adsorption capacity of neem charcoal from fluoride solutions. Ninety four percent of fluoride ions were removed from solution of 10 mg/L fluoride concentration and equilibrium was achieved in 180 min. Pumice stone is highly porous in nature which accounts for its high adsorption capacity. This property of pumice stone was used by Asgari et al. [111] for removing fluoride from water. Pumice stone was activated by surfactant, hexadecyltrimethyl ammonium. Optimum dosage for the surfactant modified pumice (SMP) was 0.5 g/L at pH 6, with initial fluoride concentration of 10 mg/L. The pumice stone exhibited a maximum sorption capacity of 41 mg/g.

Clay has been used around the world for many years containing clay minerals and organic matter or metal oxides. Red soil pots have been used for water treatment for many decades. Studies have revealed that the red soil pots have ability to remove fluoride. Gogoi and Baruah [112] observed kaolinite clay when activated with acid has good defluoridation capacity. With small particle size and at low pH the sorption capacity of the acid activated clay for fluoride ranged between 0.0450 and 0.0557 mg/g at different temperatures with a fluoride concentration of 3 mg/L. Montmorillonite has also been used as adsorbent for removal of fluoride [113]. Bentonite clay is another type of clay which mostly consists of montmorillonite. Bentonite clay was modified using lanthanum, magnesium and manganese, in order to increase its adsorption capacity for fluoride ions [114]. Ten percent La – bentonite showed higher fluoride uptake capacity for defluoridation of drinking water as compared to Mg – bentonite, Mn – bentonite and bare bentonite clay. Ten percent La – bentonite had a adsorption capacity of 4.24 mg/g and maximum loading capacity was found to be 1.4 mg/g at an adsorbent dose of 1.0 g/L and 5 mg/L fluoride concentration. Thakre et al. [115] studied bentonite clay modified with magnesium which showed significant fluoride removal in pH range of 3 to 10 and the adsorption capacity was found to be

2.26 mg/g at an initial fluoride concentration of 5.52 mg/L and dosage of 3 g/L. The higher capacity of magnesium – bentonite as compared to the bare bentonite is due to presence of magnesium which has high affinity for all halogens including fluoride. Since, clays are natural resources possessing adsorption properties, these can be used further by modifying its composition for capturing fluoride ions from water and make it safer for consumption. Among all the natural adsorbents discussed above, chitin/cellulose composite had the highest adsorption capacity of 83.75 mg/g of fluoride. Chitin and cellulose both are natural polysaccharides. Modification of chitin using cellulose and the crosslinking agent, glutaraldehyde may be the reason for its high adsorption capacity.

There is an apparent improvement in different organic and inorganic adsorbents with advancement of nanotechnology and characterization techniques. In view of all the adsorbents used for defluoridation it has been found that aluminum has the highest affinity for fluoride ions, which is the reason why most researchers focus on aluminum based compounds or amend aluminum with other metals. However, the permissible limit of aluminum in water is just 0.2 mg/L which is extremely low and leaching of Al^{3+} ions into water is reported by many researchers (detailed in section 2.4.3). Metal oxides/hydroxides, composite metals and rare earth oxide-based materials have displayed a very high potential for defluoridation as compared to other adsorbents. But these materials are very difficult to regenerate thus making them economically less feasible. Additionally, these metals can prove to be toxic to human body, if leached into water. Some chitosan derivatives and composites are used for the purpose of fluoride removal. But, the drawback lies in the fact that chitosan is a crystallized polymer, therefore adsorption takes place in the amorphous area of the crystals, restricting the adsorption capacity. Also, cross linked chitosan derivatives are insoluble in acidic and alkaline conditions and show reduced fluoride removal capacity as the amino functional groups involved in crosslinking are inaccessible for ion exchange mechanism with the fluoride ions [116]. Other natural adsorbents have the disadvantage of low efficiency and difficulty in reuse. Though a lot of studies are reported on carbon based adsorbents, however column studies has not been reported to establish a suitable carbon based adsorbent.

Calcium has a good affinity for fluoride anion and has been used widely in fluoride removal studies. Residual calcium ions do not add to any toxicity to treated water, rather it will be beneficial to health as Teotia et al. [117] stated that calcium-deficient diet increases the toxic effects of fluoride. Thus, considering these facts, calcium based adsorbents may be considered as the safe and efficient alternative.

2.3 Defluoridation process characteristics

The major process parameters affecting the defluoridation process are discussed in this section. These are surface area of adsorbent, equilibrium isotherms, kinetic studies, pH of water and presence of interfering ions. The defluoridation capacity of adsorbent, mechanism of adsorption and chemistry of the process is dependent on these parameters.

2.3.1 Surface area of adsorbent

The surface area of an adsorbent depends on its structure; the more pores it has, the greater the area and hence higher the adsorption capacity. Activated alumina (AA) is highly porous in nature having very high specific surface area. The specific surface area of adsorbents are determined by BET analysis through evaluation of materials by nitrogen multilayer adsorption measured as a function of relative pressure. BJH (Barrett-Joyner-Halenda) analysis is used to determine pore area and specific pore volume using adsorption and desorption techniques.

After impregnation of metal ions on AA, some studies indicate decrease in surface area and pore volume. Surface area of AA decreased from 242 to 203 m^2/g when impregnated with manganese dioxide (manganese dioxide coated activated alumina i.e MCAA) and pore volume decreased to 0.23 from 0.39 cm^3/g [67]. Similar trend of reduction in surface area was seen in case of MAAA (magnesia-amended AA) where the surface area declined to 193.5 from 242.07 m^2/g [66]. Goswami and Purkait [63] characterized the surface area of acidic alumina to be 144 m^2/g. Decrease in surface area indicates that diffusion of coated ions takes place into the pores of the AA surface. However, surface area of AIAA (alum impregnated AA) increased to 176 from 113 m^2/g after impregnation, signifying to the uniform coating of aluminum hydroxide on AA surface [49]. Alumina with alkoxide origin has surface area 100 m^2/g and pore volume 0.6 cm^3/g. Surface area of nano-alumina was estimated to be 151.7 m^2/g though it did not displayed a distinct porous arrangement [71]. Wang et al. [103] observed that calcination temperature has significant effect on the specific surface area and pore structure of the adsorbent. The surface area and pore volume of Mg – Fe – La trimetal composite increased from 142.55 to 178.55 m^2/g and 0.992 to 1.116 cm^3/g respectively when calcined to 400 °C. The surface area varied as the molar ratios of zirconium and cerium varied in cerium loaded mesoporous zirconium phosphate[102]. For Zr to Ce molar ratio of 1:0, the surface area was 228 m^2/g but when cerium was incorporated and the ratio became 2:1, it raised to 280 m^2/g. This may be due to background substitution of Ce^{4+} ions in the adsorbent.

Natural adsorbent pumice has a porous structure and a large surface area which was

processed and modified into surfactant modified pumice (SMP) [111]. The surface area and total pore volume of natural pumice were 13.77 m^2/g and 0.0052 cm^3/g respectively. When bentonite clay (surface area 46.56 m^2/g) was modified with lanthanum to increase its adsorption capacity the surface area decreased to 19.48 m^2/g due to incorporation of lanthanum in the pores of bentonite and heating of the clay during synthesis resulting in shrinking of pore size of bentonite clay [114]. The surface area (272 m^2/g) and pore volume (0.59 cm^3/g) of carbonaceous material obtained from pyrolysis of sewage sludge was comparable to AA[90]. The specific area of aligned carbon nanotubes (ACNT) and pore volume of ACNT was 74 m^2/g and 0.15 cm^3/g respectively [96]. A very high surface area of 323.83 m^2/g was observed in Ti – Al binary metal oxide and the pore volume was 0.35 cm^3/g showing mesoporous nature of the adsorbent [70]. The high surface area was attributed to well-dispersed metal oxides obtained after partial combustion of organic matter present. Specific surface area of calcium aluminate (CA) adsorbent was found to be 6.27 m^2/g. Islam and Patel [59] thermally activated quicklime to enhance its adsorbing capacity by increasing the porosity and surface area. The surface area of untreated quicklime was found to be 4.19 m^2/g while that of thermally treated sample increased to 11.75 m^2/g. Eggshell composite synthesized from eggshell membrane and aluminum sulfate possessed a surface area of 20 m^2/g [80]. Bioceramic hydroxyapatite has been used and modified in many ways for increasing the adsorption capability. Aluminum modified calcium hydroxyapatite (Al-HAP) had a surface area of 258.6 m^2/g, which was almost 4 times larger than that of unmodified-hydroxyapatite (75.7 m^2/g) [87]. Even the particle sizes of Al-HAP (5 – 15 nm in diameter and 20 – 50 nm in length) reduced significantly with the presence of aluminum in the structure. It was observed that compared to hydroxyapatite, Al - HAP was more dispersible and fluffy, resulting in high defluoridation capacity. Surface area of some other adsorbents are mentioned in Table 2.2.

It is assumed that the higher the surface area, higher will be the adsorption capacity of the material. In case of synthesized or modified adsorbents, the surface area may increase or decrease depending on the physical and chemical properties of the adsorbent material.

2.3.2 Equilibrium isotherms

To design an adsorption system it is very essential to predict adsorption capacity of an adsorbent and analysis of isotherm data is an interesting way for depicting it. Most of the adsorption processes (as presented in Table 2.2) fitted well with Langmuir isotherm. Langmuir isotherm model assumes monolayer coverage of adsorbate over a homogenous adsorbent surface and does not consider surface heterogeneity of the sorbent. It assumes

fluoride sorption will take place only at specific sorption sites within the sorbent. Some processes tend to follow Freundlich isotherm showing the heterogeneity of the adsorbent surface and multilayer adsorption process [85, 98, 99, 106, 107, 48, 81, 92, 84]. In some reports both Langmuir and Freundlich isotherms fitted the experimental data [82, 77, 100, 86, 78, 89, 110, 114]

At times, when the two parameter models Freundlich and Langmuir could not predict the experimental data well three parameters models like Sips and Toth are used [66]. Fluoride adsorption on Magnesia-amended activated alumina (MAAA) followed Sips and Toth isotherm model. Sips model is a combination of Langmuir and Freundlich models and Toth model is an improved version of Sips model. It assumes that, most sites have adsorption energy lower than the maximum adsorption energy. To distinguish between physical and chemical adsorption, the adsorption data can be further interpreted by Dubinin–Radushkevich isotherm [118]. The parameter called mean free energy of adsorption in this isotherm is useful for estimating the type of adsorption [119]. Daifullah et al. [89] reported that $KMnO_4$ modified activated carbon adsorbent has a mean free energy of adsorption of 10.46 kJ/mol which proposes the mechanism of adsorption to be ion exchange.

Thus, study of equilibrium isotherm help in determining the mechanism behind the adsorption process and predicting the favorability of the process.

2.3.3 Kinetic studies

The kinetics of any sorption process is a function of different parameters, such as the structural properties of adsorbent, nature and concentration of adsorbate, and adsorbent–adsorbate interactions. It was observed that some adsorbents reach the equilibrium state very fast. Nearly 95 % removal of fluoride was achieved for granular ferric hydroxide (GFH) within the first 10 min of contact time and only 3 – 4 % of additional removal occurred in the following 24 h [97]. Within 10 to 60 min, most of the fluoride is removed by Alum impregnated activated alumina (AIAA) and the maximum fluoride removal was reached at 3 h and thereafter remains constant. SMP stone reached equilibrium in 30 min [49]. Li et al. [96] and Maliyekkal et al. [66] studied defluoridation by Aligned carbon nanotube (ACNT) and Magnesia-amended activated alumina (MAAA) respectively and found that their adsorption rate is very fast in first 1 h and then it gradually reaches equilibrium in 3 h. It took considerable time to reach equilibrium for some adsorbents such as charcoal containing calcium (16 h), carbonaceous materials (18 h) and eggshell composite (24 h) [77, 90, 80]. Further, the adsorbed fluoride ions exchange with the

structural components inside adsorbent particles depending on the chemistry of adsorbent or fluoride ions adsorbed which get transferred to the internal pores and is known as intraparticle diffusion. Intraparticle diffusion is observed as the rate limiting step in many adsorption mechanisms and is mathematically stated by the Weber Morris equation [120].

Adsorption kinetics followed pseudo-second-order model for majority of the adsorbents studied as detailed in Table 2.2 which indicates that fluoride removal might be due to chemisorption process coupled with ion exchange mechanism [121]. The kinetic adsorption data is one of the most crucial parameter in the design of an adsorption system for industrial applications since it determines the adsorbate uptake rate and the time needed to attain equilibrium.

2.3.4 pH of water

The pH of the drinking water principally depends upon geological characteristic of soil and weather conditions. Hence, it is necessary to study the effect of pH on uptake of fluoride ions. Some adsorbents were observed to work well over a wide range of pH (3 – 12), some work best under acidic conditions while for some adsorbents neutral pH (7) give optimum results. At low pH (acidic) values, surface of the adsorbent has ample positive charge and attract fluoride ions through columbic forces of attraction, which led to a high adsorption rate while at higher pH (alkaline) values, surface of the adsorbent has more negative charges and hinder the movement of fluoride ions to the adsorbent surface by electrical repulsion.

The fluoride ions would have to overcome electrostatic forces as there would be a higher density of negative charge very close to the surface, hence greater electrostatic repulsion [122]. Lanthanum oxide and hydroxide, calcium aluminate, Ti – Al metal oxide, eggshell composite and graphite worked well over a wide range of pH [99, 79, 70, 80, 91]. Almost all the natural adsorbents studied such as surfactant modified pumice, chitin – cellulose composite, 20 % La – chitosan, *Cynodan dactylon*, *Phylanthus embilica* have optimum removal efficiency at neutral pH range [111, 107, 106, 109, 108]. Alum impregnated activated alumina, magnesia-amended activated alumina, manganese dioxide-coated activated alumina, manganese oxide-coated alumina, carbon slurry, cerium dispersed carbon, carbonaceous materials, all forms of hydroxyapatite studied, charcoal containing calcium compound, Mg – Fe – La trimetal composite and Al – Ce hybrid adsorbent also showed best adsorption capacity for neutral pH [49, 66, 67, 68, 94, 93, 90, 77, 103, 69]. These adsorbents showed least adsorption under acidic and alkaline conditions. The lower removal rate at acidic pH (3–5) may be due to the formation of weak hydrofluoric acid (HF). Acidic alumina, surfactant modified hydroxyapatite,

$KMnO_4$ modified activated carbon, FeO(OH), nano-hydroxyapatite in gelatin matrix, hybrid thorium phosphate composite and alkoxide origin alumina showed maximum fluoride removal capacity in acidic pH, since the surface of the adsorbent became highly protonated [63, 85, 89, 100, 83, 101, 64]. The high removal at acidic pH is due to a greater increase in the attractive force between positively charged surface and negatively charged fluoride ions.

It is evident that metallic adsorbents and all forms of hydroxyapatite gave optimum results for fluoride uptake capacity around neutral pH range (6 – 8) which is suitable for drinking water purpose. However, hydroxyapatite as an adsorbent is safer to use as there is no probability of leaching of toxic compounds at any pH, unlike the metal based adsorbents.

2.3.5 Presence of interfering anions

Groundwater contaminated with fluoride contains several other ions that can compete with fluoride during the adsorption process. The selective nature of the fluoride by the adsorbent depends on charge, polarizability, size and difference in electronegativity. Anions are of the same charge as fluoride ion, thus they create an environment of competition in the solution causing decrease in adsorption capacity of the adsorbent. Therefore, several studies were conducted to evaluate the interference of other ions that are mostly prevalent in drinking water and their effect on fluoride removal capacity. It was noted that some ions are more potent than others in decreasing the defluoridation capacity. Chloride and nitrate ions posed minimum threat to the removal efficiency of various adsorbents. On the other hand, bicarbonate, sulfate and phosphate ions when present affected the removal capacity severely. Maliyekkal et al. [66] reported that for an initial anion concentration of 200 mg/L fluoride removal capacity of magnesia-amended activated alumina (MAAA) was reduced by about 20 – 25 and 10 % for sulfate and bicarbonate respectively. In case of nano alumina, phosphate decreased the removal rate followed by carbonate ions [71].

The fluoride adsorption amount decreased quickly from 82.1 to 51.9 % with the increase of bicarbonate concentration 0 – 500 mg/L while using *Phyllanthus emblica* adsorbent [108]. At higher bicarbonate concentration (400 – 600 mg/L) decrease in fluoride removal efficiency has also been seen when Sakhare et al. [79] worked on calcium aluminate. While studying the effect of presence of co-ions Kamble et al. [106] found that bicarbonate and carbonate ions showed no removal of fluoride by lanthanum – chitosan adsorbent. Bicarbonate, arsenate, phosphate, humic acid competed with fluoride ions and reduced the removal efficiency considerably when fluoridated water was treated with granular zirconium iron oxide [98]. Other adsorbents such as nano-hydroxyapatite in gelatin matrix,

acidic alumina, alumina with alkoxide origin, bentonite clay, charcoal containing calcium compound, surfactant modified hydroxyapatite and *Cynodon dactylon* also showed negative trend of adsorption in presence of bicarbonate ions. The reduction in fluoride removal observed by the presence of co-existing anions was due to the competition from these ions for available adsorption sites or due to the change in pH or possibly a combination of both processes. Kamble et al. [114] observed that addition of carbonate and bicarbonate ions resulted in increased pH of the fluoride solution which may be another reason for lowering of adsorption capacity. A few adsorbents such as manganese oxide coated alumina and natural adsorbent bark of babool showed no effect in their respective adsorption capacities in presence of interfering anions [68, 105] which is of great practical utility.

Since, groundwater always consists of some co-existing ions, a certain degree of selectivity of the adsorbent towards fluoride ions is preferable so that the presence of other ions fluoride uptake capacity is not reduced significantly.

2.4 Some other important factors for practical feasibility of defluoridation process

The practical feasibility of the defluoridation process is depicted by the performance of the adsorbent in column mode, ability of adsorbent to desorb fluoride ions and regenerate for reusage. Another important factor regarding practical feasibility of the process is the stability of the adsorbent so that the treated water doesn't contain residual toxic ions.

2.4.1 Column studies

Column studies depict the actual feasibility of usage of adsorbent in field and are essential for industrial scale designing of the fixed bed adsorbent systems. Breakthrough curve that correspond to the column bed dimensions is a function of concentration of solute vs time and are used to study the adsorption behaviour in the column.

The breakthrough curves are obtained for fluoride ion adsorption for different bed depths of adsorbent. The breakthrough volume varies with change in bed depth. With increase in depth of bed, the axial dispersion phenomena decreases and thus reduction in diffusion of metabolic ions can be observed since the fluoride ions has not time long enough in order to diffuse into the whole of adsorbent. While studying carbon slurry adsorbent, 4.155 mg/g breakthrough capacity has been reported which is considerably lower than the batch adsorption capacity [94]. The capacity of the column tests of granular zirconium iron oxide were far lower (22.1 mg/g at pH 8.0) than the value calculated from

the Langmuir isotherm [97]. This reduction was accredited to comparatively less time of interaction between sorbent and adsorbate surface. On the contrary, Tor et al. [123] reported higher adsorption capacities of the columns than their respective batch capacities while using granular red mud (GRM) for the same initial fluoride concentration. The reason was attributed to the GRM pores that favoured enhanced solidstate diffusion in column mode as compared to batch tests. Flow rate is an important parameter for removal of fluoride ions from aqueous solution. Low flow rates lead to higher removal of solute due to increase in contact time with the adsorbent and vice versa. It is observed that in case of Ti – Al metal oxide at a lower flow rate of 2 mL/min fluoride removal was efficient which decreased with gradual occupancy of active sites of adsorbent [70]. Since, the rate of adsorption is influenced by intraparticulate diffusion process; Chidambaram et al. [104] had used column containing different thickness layers of red soil, brick, fly ash, charcoal and serpentine arranged as per the capacities of the adsorbents.

Breakthrough curves for lanthanum oxide for a dose of 30 g and for different flow rates of 20, 25 and 30 mL/min are revealed to be "S" shaped curves [99]. In breakthrough curves, the point of inflection denotes the formation of sorption zone and plateau indicates exhaustion. It was observed by Kamble et al. [64] that with an increase inflow rate of fluoride solution from 10, 15 to 20 cm^3/min the breakthrough capacity decreases from 100, 45 16 to 20 cm^3/g respectively and even after breakthrough at slower rate adsorption continued. If an early break through happens, it leads to quite low bed adsorption capacity. As inlet fluoride concentration increases, the driving force increases for the mass transfer which results in a decrease in adsorption length zone. Therefore, with increase in inlet concentration of fluoride sharper breakthrough curves are obtained. Considering the above stated factors it can be stated that study of continuous flow systems is very essential for practical applications.

2.4.2 Desorption of fluoride and regeneration studies

To develop an efficient adsorbent for defluoridation of drinking water it must be reused to make the process economical. Few researchers have considered this aspect of adsorbent studies. To study the regeneration of a particular adsorbent, the adsorbent is saturated with fluoride by keeping it in fluoride solution or shaking in fluoride solution. After the full saturation of adsorbent, it was subjected to regeneration using different regeneration media. It is also required that the adsorbent should be desorbed completely and pH plays a very important role in this. Many of the researchers found that after repeated use of the regenerated adsorbent, the adsorption capacity is decreased [49, 114]. Thakre et al. [70]

found that after the first and second reuse of Ti – Al binary metal oxide supported by beads using chitosan template showed decrease in fluoride removal efficiency by 13 and 28 % respectively, while third reuse showed decrease of 53 %. The reuse of the regenerated magnesium incorporated bentonite clay (MB) by Thakre et al. [115] showed decrease in the fluoride removal efficiency from 95.47 to 73 % at an initial fluoride concentration of 5.52 mg/L. This decrease in the fluoride removal efficiency after regeneration is due to the treatment of MB with highly alkaline pH 12 and 13 of regenerating media and MB was found to show lower fluoride removal at pH 11.

In case of alumina with alkoxide origin, Kamble et al. [64] used sulfuric acid for regeneration, however the regenerated alumina have less capacity compared to the fresh alumina. The adsorption capacity of regenerated alum impregnated activated alumina (AIAA) reduced from 92 to 84 % in first cycle itself due to removal of alum impregnation at alkaline pH. Maliyekkal et al. [66] noted that after the third cycle, approximately 20 % reduction in removal efficiency attributing to the gradual dissolution of magnesium from the magnesia-amended activated alumina (MAAA) surface. Acidic alumina regeneration showed that the capacity was reduced from 94 to 85 % with 15 mg/L of initial fluoride concentration as some of the pores of alumina was already occupied by fluoride particles due to improper desorption process. Pandi and Vishwanathan [83] was able to achieve 94 % desorption of fluoride and suggested 0.1 M NaOH for the regeneration of nano-hydroxyapatite in gelatin matrix.

Complete regeneration of adsorbents has not been achieved yet. Sakhare et al. [79] regenerated 84 % of calcium aluminate adsorbent. Rao and Karthikeyan [99] experienced some problems in downflow pattern of lanthanum oxide, like non-uniform flow, formation of lumps, piping in the bed and at the walls and elution of sorbent material along with the flow due to fine size (less than 5 micron) of adsorbent. So, they conducted upflow studies for the same at varying doses and flow rates and observed that for a flow rate of 20 mL/min, 100 % removal was obtained for initial 7 h and effluent concentration raised to 2.5 mg/L after a run of about 15 h and increased gradually till it reached 100 % exhaustion at about 60 h. Hence, the lanthanum oxide was regenerated several times with little capacity loss during cycles of regeneration.

Natural adsorbents are claimed to be inexpensive, but it is difficult to regenerate most of these adsorbents due to complexity in their structures. Considering this fact, it is observed that regeneration rate of natural adsorbents is extremely low. The adsorbent capacity of *Cynodon dactylon* as adsorbent lowered to 19 % in the third cycle only [109]. With initial fluoride concentration of 4 mg/L adsorption efficiency of the montmorillonite decreased from 65 to 58 % after the first regeneration [113].

Ninety percent of fluoride was desorbed at pH 10 in cerium loaded mesoporous zirconium [102]. The activity of the adsorbent was found to be 82 % in the first cycle and thereafter it decreases to 79.5 %, 77.5 %, 73 % and 38 % for second, third, fourth and fifth cycle respectively. Less than 8% desorption was achieved in hybrid thorium phosphate composite which clearly states the chemisorptive nature of the process and fluoride ions are held firmly to the adsorbent with comparatively stronger bonds [101]. It is evident from literature review that regeneration studies are seldom done by researchers. Also, it is always recommended to use a column setup for better extent of adsorption and desorption in continuous mode. Considering the economic perspective of the whole process, regeneration of adsorbent is an important factor.

2.4.3 Leaching of ions from adsorbents into treated water

Most of the adsorbents with high capacity for defluoridation of drinking water are metal based. Intake of water with heavy metal ions or toxic ions may cause severe health issues, many of which may manifest only after prolonged consumption. Therefore, presence of residual ions from adsorbents used for water treatment is a major area of concern but unfortunately rarely reported. Some of the elements used as adsorbent in water defluoridation are enlisted in Table 2.1 with their permissible concentrations in drinking water. The lower limit shows the desirable concentration and the upper limit indicates the permissible limit in absence of any alternative.

Table 2.1: Permissible concentration in drinking water for different elements

Element used as adsorbent	**Permissible concentration in drinking water (mg/L)** [13]
Iron	0.3 - 1.0
Manganese	0.1 - 0.3
Aluminum	0.03 - 0.2
Calcium	75 - 200
Magnesium	30 - 100
Chloride	250 - 1000
Lanthanum, Cerium, Titanium, Zirconium	-

Some researchers have reported leaching of aluminum from AA and other aluminum based adsorbents. Aluminum ions get solubilized from the surface of alumina in presence of high fluoride ions in water and variation in pH causes the dissolution of more aluminum ions into the treated water. Residual aluminum ranging from 2.01 to 6.86 mg/L was reported

in Nalgonda technique and 0.16 to 0.45 mg/L was reported from AA process [47] which was a commonly used household process in areas of endemic fluorosis mostly in rural areas. Aluminum (permissible limit 0.2 mg/L) is a very potent neurotoxin and associated with series of neurological diseases including amyotrophic lateral sclerosis, dementia associated with Parkinson's disease as well as Alzheimer's disease [124]. Many researchers have modified alumina by impregnating or coating with various metal oxides and increased the defluoridation capacity compared to unimpregnated alumina. However, aluminum leaching studies have not been done for these adsorbents.

Sometimes natural adsorbents such as clays and red soil may contain some metal oxides which may leach into water during the adsorption process. Even in case of clay based adsorbents (composed of aluminosilicate) claimed to be safe because of its natural origin there is a possibility of aluminum leaching since the adsorption process in aluminosilicate through ion exchange between fluoride and hydroxyl group from clay the lattice. At times when natural adsorbents are modified with metal ions such as lanthanum modified chitosan, lanthanum ions are found to be released (1.05 mg/L) into treated solution at alkaline pH and in presence of other anions [106]. Leaching of iron and zirconium ions were observed from granular zirconium ferric oxide adsorbent and reported to be less than 1.48 mg/L and 1.88 mg/L respectively.

In acidic and alkaline conditions significant leaching of calcium and aluminum was found from CA adsorbent into water [79]. Tchomgui-Kamga et al. [77] measured the amounts of dissolved calcium in solution after adsorption by charcoals containing calcium compounds ($CaCl_2$ compound) under various pH values. The amount of calcium ions leached was 3.3 mg/L for pH range of 3 – 8 which increased for pH values above 8 and reached to 4.31 mg/L at pH 10. However, the leached calcium concentration is in permissible limit. Also, calcium is not a toxic metal and even if consumed with drinking water will enrich our body system rather than causing any harm. The amount of dissolved chloride was also measured in the solution and noted between 5.3 and 7.6 mg/L which is less than the recommended value (200 mg/L) [72]. The concentration of calcium and aluminum ions in solution after the adsorption experiments by Al-HAP was measured and found to be 21.1 and 0.19 mg/L respectively [87]; although in the XRD analysis of Al-HAP, no peaks corresponding to aluminum element were found, which indicated Al (III) incorporation into hydroxyapatite. This indicates that if toxic metals are constituents of adsorbents used for water treatment, they can always leach into drinking water in due course of time.

It was observed that most of the elements listed in Table 2.1 have extremely low permissible limit above which they are toxic to human beings unlike calcium and magnesium which possess comparatively higher limits. There is no permissible limit

mentioned for lanthanum, titanium and cerium ions by the regulatory bodies since they are not supposed to be present in drinking water. Lanthanide metal ions and their complexes are reported to cause genotoxicity [125] and toxic effects of cerium and titanium are also described by researchers [126, 127, 128]. Therefore, incessant record of the treated water should be kept to avoid undesirable health implications.

Table 2.2: Comparison of different adsorbents considering various process parameters

Author, Year	**Adsorbent**	**Surface area (m^2/g)**	**Fluoride uptake Capacity**	**Initial F^- conc. (mg/L)**	**Equilibrium isotherm/ Thermodynamic nature**	**Kinetics**	**Interference of anions**	**pH**	**Temp. (±2˚C)**
Aluminum based Adsorbents									
Goswami and Purkait [63]	Acidic Alumina	144	8.4 mg/g	15	Langmuir, [b]Sp and [e]Endo	Pseudo 2nd order	CO_3^{2-}, HCO_3^-	4.4	25
Kamble et al. [64]	Alumina with alkoxide	100	2 mg/g	5	Langmuir, [b]Sp and [d]Exo	Pseudo 2nd order	SO_4^{2-}, CO_3^{2-}-, HCO_3^-	7	30
Tripathy et al. [49]	AIAA	176	40.68 mg/g	25	Langmuir	Not studied	Not studied	6.5	25
Maliyekkal et al.[66]	MAAA	193.5	10.12 mg/g	10	Sips and Toth	Pseudo 2nd order	SO_4^{2-}, PO_4^{3-}, Cl^-, NO_3^-	7	25
Tripathy and Raichur [67]	MCAA	203	1.22 mg/g	5	Langmuir	Pseudo 2nd order	SO_4^{2-}, HCO_3^-	5-7.5	30
Maliyekkal et al. [68]	MOCA	170.39	2.85 mg/g	5	Langmuir	Pseudo 2nd order	No effect	4-7	30
Liu et al. [69]	Al - Ce hybrid adsorbent	Not studied	27.5 mg/g	10	Not studied	Pseudo 2nd order	Not studied	6-7.5	25
Thakre et al. [70]	Ti - Al metal oxide	323.83	2.22 mg/g	5	Langmuir, [b]Sp and [d]Exo	Pseudo 2nd order	CO_3^{2-}, HCO_3^-, PO_4^{3-}	3-10	30

Table 2.2: Comparison of different adsorbents considering various process parameters

Author, Year	**Adsorbent**	**Surface area (m^2/g)**	**Fluoride uptake Capacity**	**Initial F^- conc. (mg/L)**	**Equilibrium isotherm/ Thermodynamic nature**	**Kinetics**	**Interference of anions**	**pH**	**Temp. (±2˚C)**
Rafique et al. [65]	MIAA	Not studied	0.76 mg/g	5	Langmuir	Not studied	Not studied	[a]NR	20
Calcium Based Adsorbents									
Fan et al. [48]	Hydroxyapatite, Fluorspar, Activated Quartz, Calcite,Quartz	Not studied	4.54 mg/g,1.79 mg/g, 1.16 mg/g, 0.39 mg/g, 0.19 mg/g	$3X10^{-5}$	Freundlich	Pseudo 2nd order	Not studied	6	[a]NR
Islam et al. [59]	Quicklime	11.75	16 mg/g	50	Langmuir,[b]Sp and [e]Endo	First order	PO_4^{3-}, SO_4^{2-}, NO_3^-	>12	25
Tchomgui-Kamga [77]	Charcoals containing calcium compounds	Not studied	19.05 mg/g	10	Langmuir and Freundlich	Pseudo 2nd order	HCO_3^-	7.4 to 7.7	25
Jain and Jayaram [78]	AILS	Not studied	84.03 mg/g	50	Langmuir and Freundlich	Pseudo 1st order	Not studied	8	30
Sakhare et al. [79]	Calcium aluminate	6.27	4.37 mg/g	8.9	Langmuir,[b]Sp and [e]Endo	Pseudo 1st order	HCO_3^-	3-11	25

Table 2.2: Comparison of different adsorbents considering various process parameters

Author, Year	**Adsorbent**	**Surface area (m^2/g)**	**Fluoride uptake Capacity**	**Initial F^- conc. (mg/L)**	**Equilibrium isotherm/ Thermodynamic nature**	**Kinetics**	**Interference of anions**	**pH**	**Temp. (±2˚C)**
Lunge et al. [80]	Eggshell composite	20	37 mg/g	5.6	Langmuir	Not studied	Not studied	3-9	30
Jiménez-Reyes and Solache-Ríos [81]	Hydroxyapatite	Not studied	4.7 mg/g	5	Freundlich	Pseudo 2^{nd} order	Not studied	5-7.3	25
Gao et al.[82]	Nano sized synthetic Hydroxyapatite	Not studied	0.489 mg/g	10	Langmuir & Freundlich, [c]Non–Sp & [e]Endo	Pseudo 2^{nd} order	Not studied	5-6	25
Liang et al. [84]	Glass derived HAP	Not studied	17.34 mg/g	100	Freundlich	Pseudo 2^{nd} order	Not studied	6.72	35
Nie et al. [87]	Al-HAP	258.6	32.57 mg/g	10	Langmuir, [e]Endo	Pseudo 2^{nd} order	CO_3^{2-}, PO_4^{3-}	5	25
Prabhu and Meenakshi [85]	Surfactant modified HAP	Not studied	9.39 mg/g	10	Freundlich,[b]Sp and [e]Endo	Pseudo 2^{nd} order	HCO_3^-	3	25
Pandi and Vishwanathan [83]	Nano-HAP in gelatin matrix	Not studied	4.15 mg/g	10	Langmuir, [b]Sp and [e]Endo	Pseudo 2^{nd} order	HCO_3^-	3	25

Table 2.2: Comparison of different adsorbents considering various process parameters

Author, Year	**Adsorbent**	**Surface area (m^2/g)**	**Fluoride uptake Capacity**	**Initial F^- conc. (mg/L)**	**Equilibrium isotherm/ Thermodynamic nature**	**Kinetics**	**Interference of anions**	**pH**	**Temp. (±2˚C)**
Ismail and AbdelKareem [86]	Lamb bone, chicken bone	Not studied	0.122 mg/g, 0.226 mg/g	10	Langmuir & Freundlich	Pseudo 2^{nd} order	No effect	7	25
Carbon Based Adsorbents									
Pekar et al. [92]	Lignite	3	0.71mg/g	20	Freundlich	Not studied	Not studied	2-8	25
Karthikeyan and Elango [91]	Graphite	818	0.16–3.13 mg/g	4	Freundlich, [c]Non- Sp & [e]Endo	First[st]order	Not studied	3-9	30
Daifullah et al. [89]	$KMnO_4$ modified activated carbons	122.9	15.9 mg/g	20	Langmuir Freundlich, [b]Sp and [d]Exo	Pseudo 2^{nd} order	Not studied	2	25-55
Mendoza et al. [90]	Carbonaceous material (from pyrolysis of sewage sludge)	272	2.84 mg/g	5	Langmuir Freundlich	Pseudo 2^{nd} order	Not studied	7.06	[a]NR
Sivasankar et al. [93]	CeDC	685	29.1 mg/g	2.8	Langmuir , [b]Sp and [e]Endo	Pseudo 2^{nd} order	PO_4^{3-}, HCO_3^-	7.75	25

Table 2.2: Comparison of different adsorbents considering various process parameters

Author, Year	**Adsorbent**	**Surface area (m^2/g)**	**Fluoride uptake Capacity**	**Initial F^- conc. (mg/L)**	**Equilibrium isotherm/ Thermodynamic nature**	**Kinetics**	**Interference of anions**	**pH**	**Temp. (±2˚C)**
Gupta et al. [94]	Carbon slurry	Not studied	4.861 mg/g	15	Langmuir , [b]Sp and [e]Endo	Pseudo 2nd order	Not studied	7.58	25
Natural adsorbents									
Mamilwar et al. [105]	Bark of babool	Not studied	0.77 mg/g	5	Langmuir	Pseudo 2nd order	No effect	6-8	30
Kamble et al. [106]	Chitin, chitosan, 20% La-chitosan	Not studied	3.1 mg/g	5	Freundlich	Pseudo 1st order	SO_4^{2-}, Cl^-, CO_3^{2-}, HCO_3^-	6.7	30
Jayapriya et al. [107]	Chitin/cellulose composite	Not studied	83.75 mg/g	Not mentioned	Freundlich	Pseudo 2nd order	Not studied	6.5	30
Veeraputhiran and Alagumuthu [108]	*Phyllanthus emblica*	Not studied	3.28 mg/g	3	Not studied	Not studied	HCO_3^-, SO_4^{2-}	7	30
Alagumuthu et al. [109]	*Cynodon dactylon*	Not studied	2.01 mg/g	3	Redlich – Peterson and Langmuir, [b]Sp and [e]Endo	Pseudo 2nd order	HCO_3^-, SO_4^{2-}	7	30

Table 2.2: Comparison of different adsorbents considering various process parameters

Author, Year	**Adsorbent**	**Surface area (m^2/g)**	**Fluoride uptake Capacity**	**Initial F^- conc. (mg/L)**	**Equilibrium isotherm/ Thermodynamic nature**	**Kinetics**	**Interference of anions**	**pH**	**Temp. (±2˚C)**
Chakrabarty and Sarma [110]	Neem charcoal	Not studied	18.8 mg/g	10	Langmuir and Freundlich	Pseudo 1st and 2ndorder	Not studied	5	30
Tor [113]	Montmorillonite	18.5	0.263 mg/g	20	Freundlich, Redlich-Peterson	Not studied	Not studied	6	25
Thakre et al. [115]	MB 10%	Not studied	2.26 mg/g	5	Langmuir, [b]Sp and [e]Endo	Pseudo 1st order	HCO_3^-	3-11	30
Kamble et al. [114]	La-bentonite	19.48	4.24 mg/g	5	Langmuir and Freundlich	Pseudo 1st order	$HCO_3^-$and CO_3^{2-}	5	30
Metal Based Adsorbents									
Kumar et al. [97]	GFH	250–300	7.0 mg/g	20	Langmuir, [b]Sp and [e]Endo	Pseudo 1st order	PO_4^{3-}, CO_3^{2-},SO_4^{2-}	4.0-8.0	25
Dou et al. [98]	Granular zirconium-iron Oxide	95.5	9.80 mg/g	10	Freundlich	Pseudo 2nd order	PO_4^{3-}, HCO_3^-, arsenate, humic acid	7.0	25

Table 2.2: Comparison of different adsorbents considering various process parameters

Author, Year	**Adsorbent**	**Surface area (m^2/g)**	**Fluoride uptake Capacity**	**Initial F^- conc. (mg/L)**	**Equilibrium isotherm/ Thermodynamic nature**	**Kinetics**	**Interference of anions**	**pH**	**Temp. (±2˚C)**
Islam et al. [101]	Hybrid Thorium phosphate composite	101.2	4.749 mg/g	5	Langmuir, [b]Sp and [d]Exo	First[st] order	HCO_3^-, SO_4^{2-}, NO_3^-,Cl^-	2	25
Dash et al. [102]	Cerium loaded mesoporous Zirconium phosphate	228	20.5 mg/g	50	Langmuir, [b]Sp and [e]Endo	Pseudo 2[nd] order	Not studied	6	Room Temp.
Rao and Karthikeyan [99]	Lanthanum oxide	Not studied	2.50 mg/g	4	Freundlich	Pseudo 2[nd] order	SO_4^{2-},CO_3^{2-}	3.0 -9.5	26–30
Stoica et al. [100]	FeO(OH)	Not studied	5 mg/g	50	Langmuir and Freundlich	Not studied	Not studied	4.5	aNR
Wang et al.[103]	Mg–Fe–La trimetal composite	178.55	112.17 mg/g	50	Langmuir, [b]Sp and [d]Exo	Pseudo 2[nd] order	Not studied	7	25

[a]NR: Not reported ;[b]SP: Spontaneous ;[c]Non-Sp: Non- Spontaneous; [d]Exo: exothermic; [e]Endo: endothermic

2.5 Research gaps

A thorough literature survey was done for understanding the defluoridation process, precisely different kind of adsorbents and crucial process parameters involved. The issues pertaining to the process are summarized below :

- It is clear that further research is required to develop cost effective adsorbent materials to mitigate fluoride from water, especially for the communities that do not have access to safe drinking water.
- Though calcium adsorbents have comparatively lower capacity than aluminum, but even if leached into treated water they have an added advantage of causing no adverse health effects. Also, calcium compounds are comparatively cheaper than aluminum compounds. Another interesting fact noted by Jha et al. [88] while working on fluoride concentration along with other physico-chemical parameters in groundwater samples in India was the negative relationship of presence of fluoride with calcium and magnesium. This confirms that if calcium and magnesium can be used together in some stable adsorbent form, it can effectively reduce the fluoride concentration in the aqueous medium.
- Feasibility of using any adsorbent can be properly predicted only after continuous studies. Many advanced adsorbents have been developed in the past few years but column studies are rarely reported.
- To predict the adsorption behaviour in column for comparison with experimental studies, chemical modeling and simulation techniques are required.
- Assessment of water quality parameters such as pH, total hardness and alkalinity after treatment with adsorbent is essential for evaluating its application for drinking water purpose. In literature only some reports show these evaluation after the adsorption process.
- Not all adsorbents reported in literature can be regenerated. Many adsorbents can be regenerated only to a small percent which reduces its applicability and viability for practical usage of the adsorbent
- However, it is essential to ponder on some key features such as chemical and physical stability, unwanted leaching of ions into treated water. Furthermore, it is necessary to confirm the use of the adsorbent materials reported in the literature

through adsorption and desorption cycles, column studies before these materials are implemented for defluoridation systems to meet the drinking water regulations.

CHAPTER 3

Chapter 3

Materials and Methods

This chapter describes the materials, chemical reagents, solutions used for experimental studies and the methodologies adopted to attain the objectives of the study. It includes synthesis of adsorbents, the characterization techniques used and methods of application of adsorbents in fluoride removal. The entire work of this thesis is done in Department of Chemical Engineering, Malaviya National Institute of Technology, Jaipur. Characterization of adsorbents were carried out at Materials Research Center, MNIT , Jaipur and the BET analysis were done at Central Salt & Marine Chemicals Research Institute, Bhavnagar. Various calcium compounds were used to test their defluoridation potential via batch studies. The adsorbent was then converted into pellets in order to evaluate its applicability in column studies and the experimental results were verified with modeling and simulation.

3.1 Reagents and standard solution preparation

All chemicals used in the present study were of Analytical grade and were obtained from Merck India Ltd, Mumbai, India. Glasswares and plasticwares used were of Borosil and Tarsons make respectively. Deionized water (Mili-Q Milipore with electrical conductivity of 0.055 μS/cm) and double distilled water were used for all purposes to avoid any issue related to ionic contamination. All the weight estimations were done with Kern ABS 220-4N analytical balance. The micropipettes used in this study were of Thermo Scientific make. A stock solution of fluoride was prepared by dissolving 2.21 g of sodium fluoride in 1 L of double distilled water, and working solutions were obtained by appropriate dilutions from the stock solution. For studies pertaining the presence of interfering ions, standard stock solutions of 1000 mg/L were prepared corresponding to each ion. Total ionic strength adjustment buffer (TISAB) was prepared by using 58 g of sodium chloride, 4 g of 1, 2-diaminocyclohexane tetra acetic acid (CDTA), 57 mL of glacial acetic acid and diluting the

mixture to 500 ml. For adjusting the pH of the buffer to 5.0 to 5.5, 5 M NaOH solution is used. This solution was kept in a water bath for cooling. Thereafter, the solution was transferred to a one litre volumetric flask and made upto the mark using deionized water.

3.2 Calcium based adsorbents

Calcium has good affinity for fluoride ions, and therefore calcium based adsorbents are potential materials for fluoride adsorption in aqueous systems. Calcium compounds are readily available and are biocompatible in all forms with the human body. This is another reason for their usage in fluoride removal processes. The following calcium based adsorbents i.e Activated Calcite, Calcia-Magnesia adsorbent, Dicalcium phosphate and hydroxyapatite were either procured or synthesized for defluoridation studies.

3.2.1 Activated Calcite

Calcite ($CaCO_3$) is the most stable polymorph of calcium carbonate. Calcite used in this study was obtained from Chanda Minerals, Alwar, Rajasthan, India and chemical composition of calcite is given in Table 3.1. It was washed several times with double distilled water, air dried and then sieved to 53 to 63 micron size.

Glacial acetic acid at different concentrations (0.01 M, 0.025 M, 0.05 M, 0.075 M and 0.10 M) was used for activating calcite. Glacial acetic acid is a weak acid and one of the edible acids, so it will not add any unwanted contaminant or unpleasant odour to the treated water. In this study, the effect of calcite dosage, contact time and pre-acid treatment of fluoride water on the removal efficiency was studied. pH of water before and after treatment was also noted.

Table 3.1: Chemical composition of Calcite

Compound present	**Percentage (%)**
$CaCO_3$	90 - 97
MgO	1.5 - 2.5
Silica	1 - 3.5

3.2.2 Synthesis of Calcia-Magnesia Adsorbent (CMA)

Calcia-Magnesia adsorbent was synthesized and studied for defluoridation of drinking water. Calcium hydroxide and magnesium hydroxide powders (100 g each) were taken in 1:1 ratio and dissolved in 1 L double distilled water to prepare the CMA adsorbent. The

colloidal mixture thus obtained was shaken in an orbital shaker (Remi CIS24BL) for 3 h at 250 rpm at a temperature of 25 ± 0.5˚C. The mixture was then filtered by a vacuum-filtration assembly and the paste thus obtained after filtration was dried in a hot air oven (Chino instruments) at 110 ± 0.2 ˚C for about 10 h. The dried product was powdered and the powder was sieved uniformly to 63 to 74 micron. The prepared CMA adsorbent was kept in a muffle furnace (Optics technology) at 900 ºC for 25 h and thereafter used for batch defluoridation experiments.

3.2.3 Dolomite [$CaMg(CO_3)_2$]

Dolomite is a double carbonate, having an alternating structural arrangement of calcium and magnesium ions. Since magnesium and calcium possess good affinity for fluoride ions, this adsorbent was studied for defluoridation. Dolomite was used as procured without any modifications.

3.2.4 Dicalcium phosphate ($CaHPO_4$)

Dicalcium phosphate is a calcium compound mainly used as a dietary supplement in various food products. Owing to this fact its fluoride removal capacity in drinking water was studied. Dicalcium phosphate was procured from Merck, Pvt Ltd., India and used without any modifications.

3.2.5 Hydroxyapatite

Hydroxyapatite (HAP) is a calcium phosphate based bioceramic, having the chemical formula $Ca_5(PO_4)_3(OH)$ with the Ca/P ratio being 1.67 and is being used in the medical field widely [129]. The HAP structure can be represented as two subsystems: first, the calcium channels in which the –OH groups are arranged and second the main framework of calcium phosphate. Fluoride ions can be substituted in place of hydroxide ions in the hydroxyapatite structure to form fluorapatite which is more thermodynamically stable than HAP itself [130].

Different forms of Hydroxyapatite was studied for estimating their defluoridation capacity in drinking water:

- Modification of natural hydroxyapatite
- Synthesis of pure hydroxyapatite
- Synthesis of Magnesium incorporated hydroxyapatite

3.2.5.1 Modification of natural Hydroxyapatite

Hydroxyapatite (HAP) is the chief inorganic chemical constituent of animal bones and teeth. Bovine bones are most natural sources for preparation of HAP. Hydroxyapatite of animal origin (aHAP) was procured in powdered form from Clarion Pharmaceuticals Ltd., New Delhi, India, and its chemical composition is given in Table 3.2. aHAP was modified using magnesium hydroxide [$Mg(OH)_2$] powder and thus magnesia-hydroxyapatite (Mg-HAP) was prepared for defluoridation studies. Magnesium hydroxide and aHAP powders were sieved separately to 63 to 74 micron size and mixed in 1:1 ratio. The product thus obtained was kept in a muffle furnace for calcination at 800 °C for 3 h. It was then sieved to 63 to 74 micron size again for getting uniform particle size and used in the batch experiments.

Table 3.2: Chemical composition of Hydroxyapatite of animal origin

Composition	**Percentage present (%)**
Calcium	22.80
Phosphorus	10.15
Moisture	1.96
Ash content	61.58
Other	3.51

3.2.5.2 Synthesis of pure-Hydroxyapatite (pHAP) and Hydroxyapatite incorporated with magnesium (M-i-HAP)

Chemical precipitation method was employed for the synthesis process. Potassium phosphate dibasic (K_2HPO_4), calcium nitrate tetrahydrate ($Ca(NO_3)_2.4H_2O$) and magnesium nitrate hexahydrate ($Mg(NO)_3.6H_2O$) were used as source of phosphorous, calcium and magnesium respectively for synthesis of magnesium incorporated HAP (M-i-HAP). For synthesizing M-i-HAP, 0.19 M potassium phosphate was added drop-wise into an alkaline solution consisting of magnesium nitrate and calcium nitrate with varying Mg/Ca molar ratios. The solution was constantly stirred at 800 rpm at 80 - 85°C. The total concentration of magnesium and calcium in initial solution was 0.32 M. Ammonia solution (NH_4OH) was used to maintain the alkalinity of solution during the reaction time. The suspension subsequently obtained was kept for aging (24 h) at room temperature. Thereafter, it was centrifuged at 2500 rpm for 15 min and the pallet was dried in an oven at 110°C for 5 h. The targeted chemical composition correspond to 'n' values of 0, 1.5, 2 and 4 in the chemical formula of M-i-HAP [i.e $Ca_{(10-n)}Mg_n(PO_4)_6(OH)_2$] and denoted as pHAP (pure hydroxyapatite), M-i-HAPa, M-i-HAPb and M-i-HAPc respectively. Since

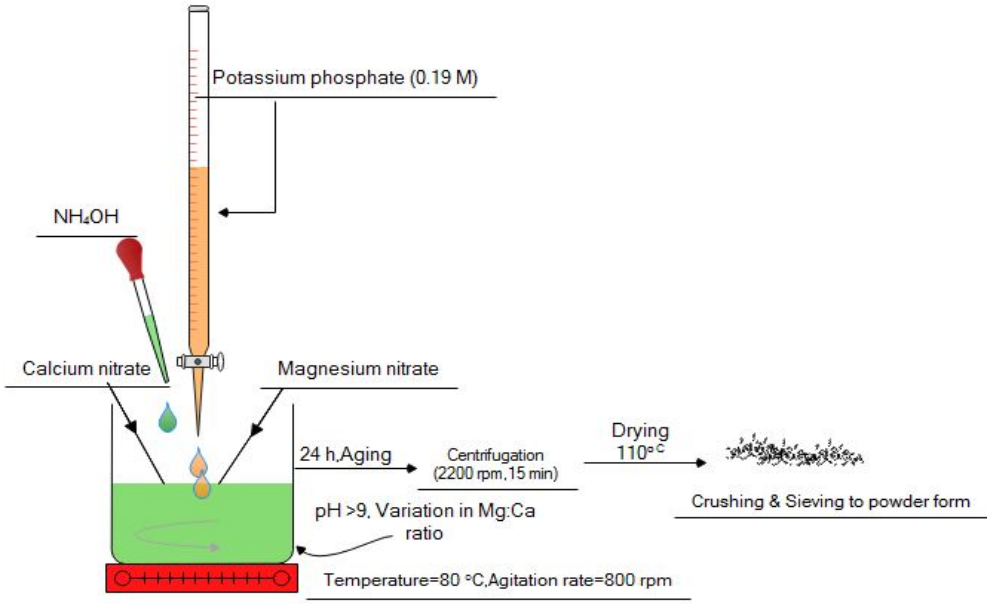

Figure 3.1: Synthesis procedure for M-i-HAP

this formula does not consider increase in phosphate ion incorporation or the lattice defects due to increase in magnesium concentration in hydroxyapatite; therefore, it may only be used as an approximation [131]. The step by step synthesis protocol is illustrated in Figure 3.1.

Reaction for synthesis of M-i-HAP is presented as follows:

$$(10-n)\{Ca(NO_3)_2\} + n\{Mg(NO_3)_2\} + 6K_2HPO_4 + 8NH_4OH \rightarrow$$
$$Ca_{(10-n)}Mg_n(PO_4)_6(OH)_2 + 12KNO_3 + 8NH_4NO_3 + 6H_2O$$

3.2.6 Preparation of pellets for column studies

For facilitating engineering applications, it is essential to formulate adsorbents in powder form into pellets of suitable size. Wet-mass extrusion and spheronization is an established technique of producing spherical shaped pellets [132]. The Extrusion-Spheronization process includes four steps, explained as follows [133] and also shown in Figure 3.2:

- **Combination**: It is the first step of the process in which the wet mass of adsorbent was mixed with the chosen binder. There is an urge to attain homogeneous distribution of the liquid phase so that a wet mass of uniform consistency is obtained. The objective of this step was to generate a properly mixed material.

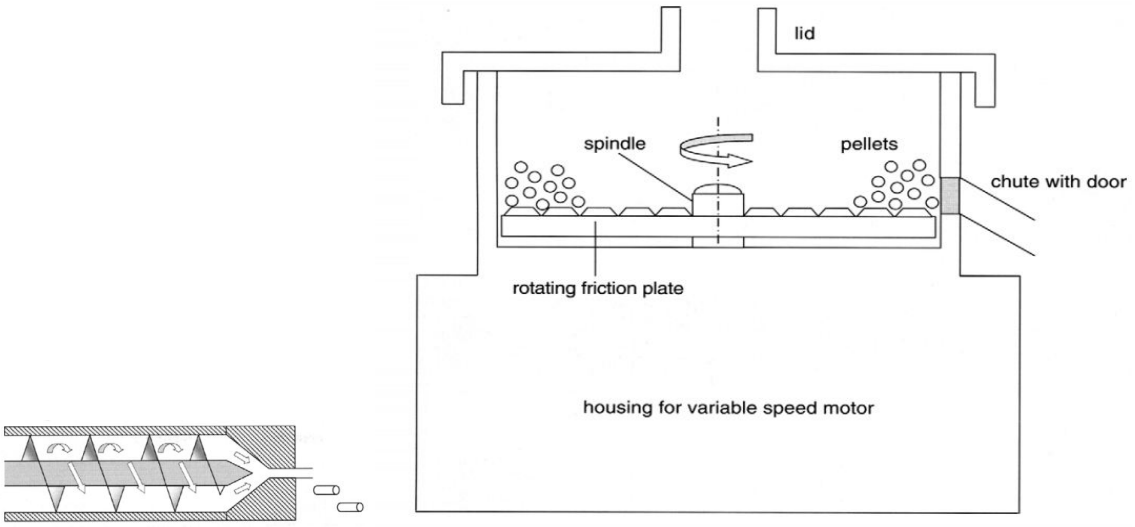

(a) Extrusion (b) Spheronization

Figure 3.2: Extrusion and Spheronization [133]

- **Extrusion**: Combination step is followed by extrusion step where the wet mass generated was compacted to a density approaching its saturation density and expelling entrapped air. Therefore, the material is needed to be held at a high pressure for some time for yielding a dense product. The extruding pressure is generated by the auger or ram. In this process, the material was given a cylindrical shape by forcing it through a multi-holed circular dies (Figure 3.2a).

- **Spheronisation** : The cylindrical extrudates were cut manually into smaller rods and further given a spherical form by the action of a horizontal rotating friction plate. Figure 3.2(b) shows a spheroniser, with a friction plate rotating at predetermined speed so that extrudates form into pellets.

- **Drying**: The pellets obtained were then dried for 4 h at appropriate temperature in a hot air oven.

The synthesized magnesium incorporated hydroxyapatite powder (section 3.2.5.2) was used for preparation of pellets. Polyvinyl alcohol (PVA) was dissolved in double distilled water at 10 wt% concentration possessing a viscosity of 25-32 cps at 90 ± 2 °C in a water bath and thereafter cross-linked with propanedioic acid (5 wt % of PVA) at 95 ± 2 °C for 5 h. The M-i-HAP adsorbent in powdered form and cross-linked PVA acquired as a binder were mixed thoroughly and granulated to cylinder-shaped granules of various diameters (2 mm to 3 mm) using an extruder (PRISM make). The extruder speed was kept 60 rpm. Some of the cylindrical granules thus obtained were dried at 70 ± 2 °C temperature for

4 h and broken up manually into small bars of 0.5 - 1 mm in length. The rest of the extruded material was fed into a spheroniser (PRISM make) for making spherical shaped pellets by the action of a horizontal rotating friction plate. The extrudates collide with the plate, the walls and neighboring particles, as a result the pellet edges are rounded off and their structure changes from rounded rods to dumb-bells to ellipsoids to spheres [133]. The spherodizer was fitted with a chequered plate of 2.25 mm pitch, operated at a speed of 750 to 850 rpm and compressed air was provided at the rate of 2 kg/cm^2 pressure for 2-3 min. The spherical pellets were then dried at 70 ± 2 °C for 4 h before being used in column studies. Zhao et al. [134] reported that exposure to temperature as high as 130 °C can destroy PVA structure, therefore, 70°C was chosen as drying temperature for pellets. A schematic diagram of the whole process is illustrated in Figure 3.3.

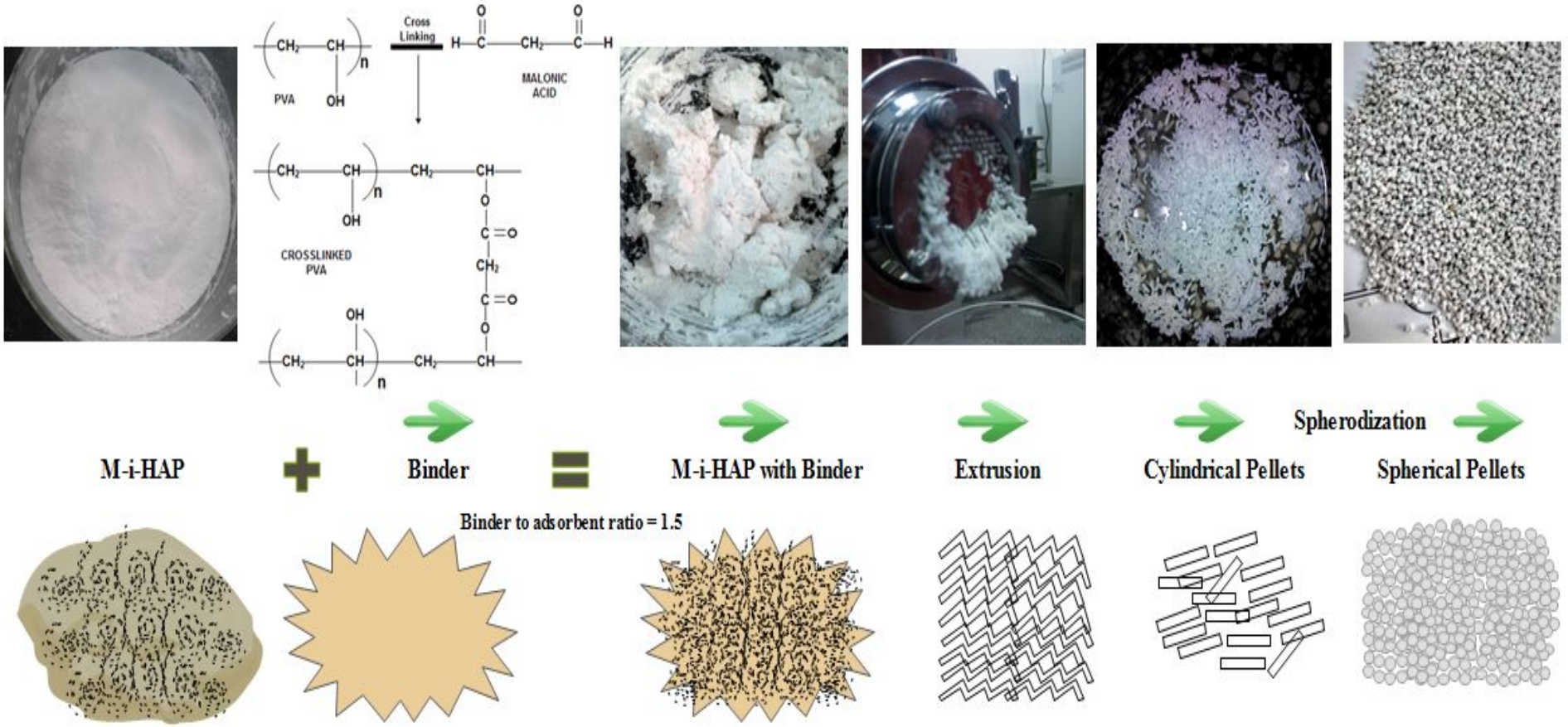

Figure 3.3: Process of pellet preparation for M-i-HAP adsorbent

3.3 Characterization techniques

The synthesized adsorbents were characterized for evaluating the functional groups, bonding patterns, crystallinity, structure, surface morphology, surface area, elemental composition, particle size distribution and thermal behavior.

3.3.1 FTIR study

The bonding patterns and functional groups in the adsorbents were characterized using a PerkinElmer Fourier transform infrared spectrophotometer (FTIR) (UTR TWO) in the range of 450 – 4000 cm^{-1} with a resolution of 4 cm^{-1}. The adsorbent was mixed with KBr in the ratio of 1:50 in order to remove the scattering effects due to large crystals. The mixture was crushed using agate mortar and pestle and mixed powder was kept on a standard sample holder. Thereafter, a translucent pellet was obtained by using a KBr press (Model M-15, Technosearch Instruments) by applying 5 ton pressure for 2 min. The instrument was switched on and a background scan was taken before placing the pellet. The pellet was then placed in the pellet holder and graphic representation of the spectra was taken using standard software provided with the instrument.

3.3.2 X-Ray Diffraction study

X-ray diffraction patterns were recorded on PANanalytical X'pert powder X-ray diffractometer (Cu Kα = 1.5406 Å radiation source) operating at 40 kV and 30 mA. The samples were scanned for 2θ range from 10º to 80º with step size of 0.15º and scan step time of 3 s. Identification of phases in the samples were carried out by comparing the diffraction data with standards of Joint Committee on Powder Diffraction Standards (JCPDS) using PANalytical X'Pert HighScore software. Scherer equation given below was used to calculate the mean crystallite size:

$$D_p = \frac{0.94\lambda}{\beta_{1/2} cos\theta} \tag{3.3.1}$$

Where D_p = Average Crystallite size, β = Line broadening in radians. θ = Bragg angle. λ = X-ray wavelength.

3.3.3 Scanning Electron microscopy (SEM)

The surface morphology and microstructure of the adsorbents were visualized by means of scanning electron microscopy (Nova Nano SEM 450). All the samples were coated with

thin film of platinum using JEOL/JFC1600 Auto fine coater (30 to 90 seconds as needed at current of 50 mA at vacuum) to reduce charging of the sample so that conductivity of sample can be increased.

3.3.4 Transmission electron microscopy (TEM)/Energy dispersive X-ray analysis (EDX)

The crystallographic structure of adsorbents were determined with transmission electron microscope (Technai G2T20). For TEM analysis, samples were prepared by ultrasonic vibration method. A small amount of sample was suspended in methanol solution and subjected to ultrasonic vibrations in an ultrasonic cleaner (Buehler Ultramet) for 30 min for dispersion of the powder homogeneously. Once the adsorbent particles were thoroughly dispersed, a tiny droplet of the suspension was dropped onto a copper TEM grid with a micropipette. Thereafter, the TEM grid was mounted into the microscope and the sample was analyzed.

Simultaneously, for analyzing the elemental compositions of the sample, Energy dispersive X-ray analysis (EDX) was used (Xflash 6TI30 Bruker).

3.3.5 XPS

Magnesium incorporated hydroxyapatite powdered adsorbent samples were analyzed before fluoride adsorption, after fluoride adsorption and after regeneration using X-ray photoelectron spectroscopy (XPS;Omicron nanotechnology) with Mg Kα X-ray source (1253.6 eV of photons) to determine the Ca, O, Mg, F and P contents on the adsorbent surface.

3.3.6 Thermal behavior

The thermogravimetric analysis (TGA) and differential thermal analysis (DTA) of Magnesium-incorporated hydroxyapatite were carried out in a Perkin Elmer Simultaneous Thermal Analyzer (STA) 6000. The thermal analysis was performed by continuous heating of the samples from ambient temperature to 900 ºC with a heating rate of 10 ºC per min in nitrogen atmosphere for studying the weight loss and thermal behavior. The results obtained were analysed with the help of Pyris series software provided with the instrument.

3.3.7 Particle size distribution

The particle size distribution of Magnesium-incorporated hydroxyapatite was characterized using Malvern Zetasizer Nano ZSP. A small pinch of adsorbent powder was dispersed in the solvent media (methanol) and sonicated for 30 min in an ultrasonic cleaner (Buehler Ultramet). It was then taken in a quartz cuvette for analysis.

3.3.8 Surface area analysis

The surface area and pore size distribution of the adsorbent were calculated from the corresponding nitrogen adsorption-desorption isotherm at 77.57 K using a Micrometrics ASAP analyzer 2010. The specific surface area was calculated using the BET isotherms, and the pore size distribution was determined by using the density functional theory (DFT). Surface area analysis was carried out for pHAP, M-i-HAPa powder and M-i-HAPa pellets.

3.4 Fluoride removal

3.4.1 Batch experiments

A series of experiments were conducted in 250 ml Teflon containers (Tarsons make) at ambient temperature by adding a known adsorbent dosage in 100 ml fluoride solution of known concentration. The Teflon containers were capped in order to avoid any change of concentration due to evaporation. The defluoridation process was carried out in an orbital shaker (Remi CIS24BL) at a constant shaking speed. Studies were carried out at varying shaking speeds for determining the optimum speed for point of maximum adsorption. In the batch adsorption process, effect of varying parameters such as pH, initial fluoride concentration, contact time, adsorbent dosage, temperature and presence of interfering ions were observed. Except for pH studies, all the studies were conducted at their natural pH and no pH adjustments were made. Effect of each parameter on fluoride removal capacity was observed by keeping other parameters constant.

After performing fluoride adsorption equilibrium experiments, the samples were filtered using Whatman filter paper no. 42 and analyzed for the presence of residual fluoride. All the experiments were carried out in triplicates and the mean values were reported in the study.

3.4.1.1 Effect of adsorbent dose

Fluoride adsorption capacities of adsorbents at different doses were investigated by using 100 mL of fluoride solution with known initial concentration. The solutions were kept for definite time intervals by keeping the pH, initial fluoride concentration and temperature constant. These studies determined the optimum dose of adsorbent required to bring the residual fluoride concentration in treated solutions less than the permissible limit (1.0 mg/L).

3.4.1.2 Effect of contact time

The effect of contact time on the fluoride removal capacity by the adsorbents was determined by keeping initial fluoride concentration, dosage, temperature and pH constant.

3.4.1.3 Effect of pH

The pH of the aqueous solution plays an important role in controlling the fluoride adsorption at the adsorbent – water interface. Therefore, adsorption experiments were carried out at pH 3 to 11 keeping the contact time, initial fluoride concentration, pH, temperature and adsorbent dosage constant.

3.4.1.4 Effect of initial fluoride concentration

In order to evaluate the effect of initial fluoride concentration on fluoride removal capacity, experiments were performed with different initial concentrations of fluoride ions ranging from 2 - 20 mg/L for Mg-HAP and M-i-HAPa. For CMA adsorbent, experiments were carried out with initial fluoride concentration of 2 to 14 mg/L. All the other parameters such as contact time, adsorbent dose, pH, temperature were kept constant.

3.4.1.5 Effect of temperature

Effect of temperature was monitored for M-i-HAPa powder adsorbent at 303, 313 and 333 K and the thermodynamic parameters were calculated. Optimum adsorbent dose was taken with a constant pH, initial fluoride concentration and pH. Thermodynamic parameters related to adsorption process are standard free energy change (ΔG^o), standard enthalpy change (ΔH^o) and standard entropy change (ΔS^o).

The standard Gibbs free energy (kJ/mol) can be computed using the following equation:

$$\Delta G^{o} = RT\, lnK_e \tag{3.4.1}$$

The equilibrium constant (K_e) can be expressed in terms of enthalpy change (kJ/mol) and entropy change (kJ mol^{-1} K^{-1}) as a function of temperature:

$$ln\, K_e = \frac{-\Delta H^{o}}{RT} + \frac{\Delta S^{o}}{R} \tag{3.4.2}$$

$$\text{and } K_e = \frac{C_{ae}}{C_e}$$

where C_{ae} and C_e indicate the equilibrium fluoride concentration (mg/L) on adsorbent and in the solution, respectively; R is the universal gas constant (8.314 J/mol)

3.4.1.6 Effect of presence of interfering ions

Drinking water usually contains other ions such as chloride, sulfate, nitrate, phosphate, and bicarbonate, which may compete with fluoride during the adsorption process. Hence, it is necessary to study the effect of coexisting ions on the removal of fluoride. The most common ions found in groundwater are chloride, sulfate, and bicarbonate [135, 136]. Some other prominent ions are phosphate and nitrate. Batch adsorption studies were performed at varying initial concentrations of Cl^{-}, SO_4^{2-}, NO_3^{-}, PO_4^{3-}, and HCO_3^{-} in the range of 100, 200, and 300 mg/L by keeping other parameters such as adsorbent dosage, initial fluoride concentration, temperature, contact time and pH constant. The concentration of interfering ion solutions were obtained by appropriate dilution from the stock solutions prepared (section 3.1).

3.4.2 Column experiments

An adsorption-regeneration column setup was fabricated as presented in Figure 3.4. The entire setup was made of stainless steel (SS304), the column was made of acrylic and connections were made of acrylic make. The column length was 50 cm and internal diameter was 5 cm. Feed solution was pumped from a stainless steel tank of 20 L across the packed column with a magnetic drive pump (Promivac make) and the flow rate was controlled through a flow meter (Eureka make). For regeneration experiments, the regenerant solution was pumped from another tank (Alkali tank) in upflow mode. The Tank

1 in Figure 3.4 was employed for storing the overflow solution and Tank 2 was used for collecting the treated water.

Before the experiments were started, double distilled water (stored in a 20 L tank) was run through the column for 2 h so that an equilibrium is established between the magnesium incorporated hydroxyapatite pellets and water. Fluoride solution with known initial concentration was fed from the top of the column with different bed heights at a predetermined flow rate continuously. Treated water samples were collected from bottom of the column at definite time intervals. This procedure was pursued until the fluoride concentration in the outflow matched the inflow fluoride concentration, i.e., C_e/C_0 is approximately equal to unity. The column experiments were performed at room temperature (about 30 ºC) and no adjustments regarding pH was done. The results acquired were plotted in terms of C_e/C_0 vs time to obtain the breakthrough curve.

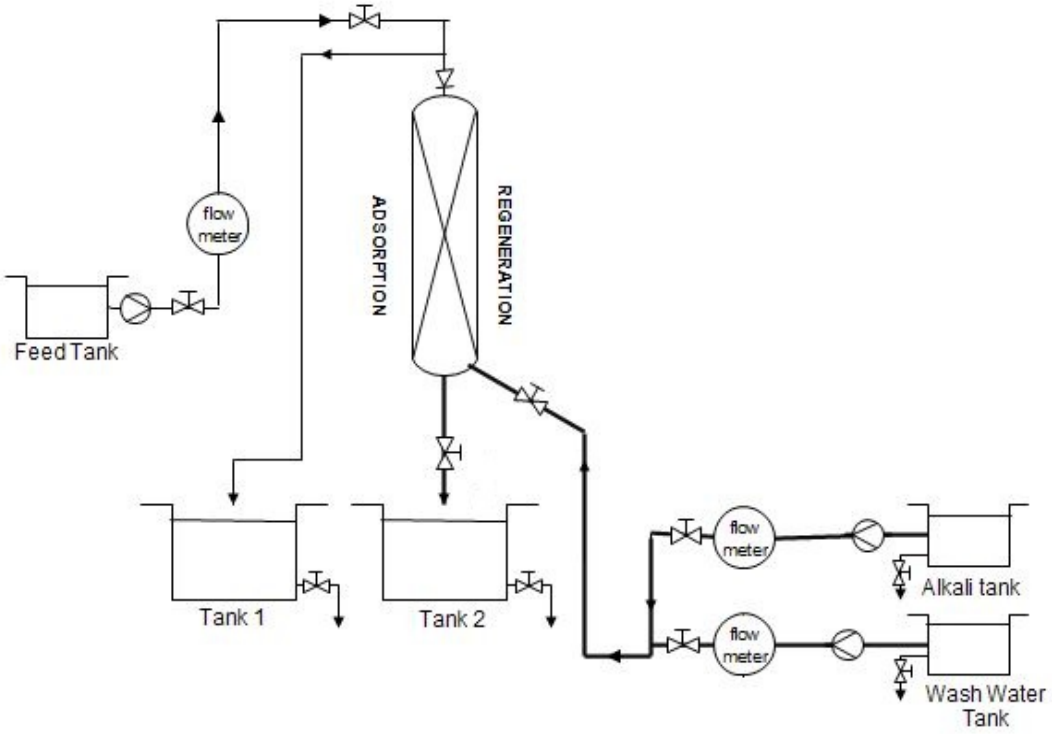

Figure 3.4: Adsorption-Regeneration Column Setup

In a continuous adsorption system, the adsorbent pellets present closest to feed water saturates first and initially maximum adsorption takes place there. The adsorption zone then moves as time lapses and then reaches towards the bed exit. The residual solute concentration at the outlet becomes equal to the inlet solute concentration when the adsorption zone has completely travelled the column. The total quantity of fluoride

adsorbed (q_b) is determined by the area under the breakthrough curve for a known fluoride feed concentration from the following equation :

$$q_b = \int_0^{t_b} \frac{C_0 - C_t}{M} dt \tag{3.4.3}$$

where $C_0$and C_t fluoride concentrations (mg/L) at inlet and outlet respectively; M is the adsorbent mass (g) and t_b is the time (L) at breakthrough point. The breakthrough point was considered at residual fluoride concentration of 1.0 mg/L (the permissible limit for fluoride in water).

Adsorption capacity (q_{EX}) at exhaustion point of M-i-HAPa pellet adsorbent was calculated from the following equation:

$$q_{EX} = \int_0^{t_{EX}} \frac{C_0 - C_t}{M} dt \tag{3.4.4}$$

where t_{EX} (h) is the exhaustion time when the column is saturated.

The empty bed contact time (EBCT) is determined by the relation between bed height (Z; cm) of adsorbent used and the volumetric flow rate (F;L/h) as written below:

$$EBCT = \frac{Z}{F} \tag{3.4.5}$$

3.4.2.1 Effect of shape of pellets

Two types of pellets were obtained – cylindrical shaped (obtained after extrusion step) and spherical shaped (obtained after spheronization step). Defluoridation capability of both these pellets were tested through column studies at constant flow rate, bed height and fluoride feed solution. The cylindrical bar shaped pellets were of 0.5 - 1.0 mm in length and the spherical pellets were 1 - 1.5 mm in diameter. Both types of pellets were extruded by fitting a 2 mm sieve in the extruder.

3.4.2.2 Effect of particle size of spherical pellets

The particle size of pellets was controlled through the sieve size used in the extruder, the pitch size of chequered plate in spherodizer and final sieving of particles. Accordingly, the pellets formed were classified into three groups i.e < 1 mm, 1-1.5 mm and 1.5-2 mm.

3.4.2.3 Effect of bed height

The experiments were carried out at constant feed concentration (10 mg/L), flow rate (1 L/h i.e 16 mL/min) with three different bed height viz. 5 cm, 10 cm and 30 cm. The weight of the adsorbent corresponding to 5, 10 and 30 cm bed heights were 14, 27 and 80 g.

3.4.2.4 Effect of flow rate

The adsorption column was operated by varying flow rates (16, 25 and 33 mL/min i.e 1, 1.5 and 2 L/h) till no further fluoride removal was observed. The inlet fluoride concentration and bed height were kept constant at 10 mg/L and 30 cm respectively.

3.4.2.5 Effect of fluoride concentration

Concentration of fluoride ions in the feed water will determine the breakthrough concentration. The column was run at two different fluoride concentrations: 5 mg/L and 10 mg/L with a constant flow rate of 1 L/h and bed height of 30 cm.

3.4.3 Desorption and Regeneration experiments

The ease with which fluoride ions can be eluted from the adsorbent, determines its reusability. To increase the efficacy of the process, it is imperative that the adsorbent used should be regenerated. Desorption and regeneration experiments were carried out for M-i-HAPa powder in batch mode and M-i-HAPa pellets in continuous mode.

3.4.3.1 Batch mode

Fluoride adsorption was carried out with a 100 mL solution containing 10.0 mg/L of fluoride and 10 g/L M-i-HAPa powder adsorbent at pH 7.0 for 180 min at a mixing rate of 200 rpm. The treated solution was filtered and the adsorbent was retained as residue left on the filter paper and residual fluoride concentration in the filtrate was measured. Various eluents such as sodium hydroxide, sulfuric acid, hydrochloric acid, and potassium hydroxide were tested as potential regenerating agents. The retained adsorbent was stirred

for 90 min in 100 mL of regenerant solution and the residual solution was measured for presence of fluoride ions. The regeneration experiment was conducted by repeating this process till the fluoride adsorbed on the adsorbent was desorbed to the utmost level possible. The reusability of regenerated adsorbent M-i-HAPa was evaluated by determining the number of cycles the same adsorbent can be used and loss of its capacity to remove fluoride with successive cycles.

3.4.3.2 Continuous mode

During column studies, when the residual fluoride concentration in outlet became almost constant and equal to the inlet concentration, it was assumed that the adsorbent pores were loaded with fluoride ions and the M-i-HAPa pellets were considered to be fully exhausted. The desorption experiments in column studies were carried out using the upflow mode instead of the downflow mode because a better and faster regeneraion rate was observed via this mode due to good contact between the exhausted bed and regenerant solution.

The exhausted column was regenerated using the eluent solution identified in batch mode with a flow rate of 1 L/h in upflow mode until maximum amount of the adsorbed fluoride was recovered. The adsorbent bed was restored by washing with double distilled water for approximately 4 h in the aforesaid upflow mode with the same flow rate until the pH of the water collected from outlet was neutral (7.0 ± 0.1). The bed was then reused and its performance was assessed.

3.4.4 Analysis of treated water samples

The residual fluoride concentration was analyzed using an ion selective electrode (Orion Versa Star 93). Calibrations were done using fluoride standards and the electrode slope was -58.16 mv/decade at 25 ± 0.5°C. Standard fluoride solutions with fluoride concentrations ranging from 0.5 to 10 mg/L were prepared from standard stock solution of 1000 mg/L. For de-complexation of complexes and avoiding interference with the electrode performance, TISAB-II solution was added in 1:1 proportion to 10 mL sample solution. The solution was mixed with the help of built-in stirrer with the ion meter, until a constant reading was displayed. Calibrations were also checked in between sample measurements to ensure the accuracy of readings obtained. The same ion meter coupled with pH electrode (Orion ROSS combination pH electrode) was used to measure the pH of the solution. The pH electrode was calibrated using 4.01, 7.0 and 10.01 buffer solutions (Orion^{TM} pH Buffer) and the electrode slope was 98 %. The pH values were adjusted using 0.01 M NaOH and 0.01 M HCl. The point of zero charge (pH_{PZC}) of the adsorbent was determined by the solid

addition method using 0.15 g of adsorbent with 0.01 M NaCl as a background electrolyte, whose initial pH values (2 to 12) were adjusted accordingly. The solutions were kept for shaking for 48 h and pH after this duration was noted. A graph was plotted between initial pH and final pH after 48 h for determining the pH_{pzc} value.

Fluoride adsorption capacity and removal efficiency (RE) of the adsorbents in the batch mode were calculated using the following equations:

$$q_e = \frac{(C_0 - C_e)V}{w} \tag{3.4.6}$$

$$RE\,(\%) = \frac{(C_0 - C_e)}{C_0} X\,100 \tag{3.4.7}$$

where q_e represents adsorption capacity (mg/g) at equilibrium; C_0 and C_e are the initial and equilibrium concentration (mg/L) of fluoride in solution respectively; w is weight of adsorbent (g) and V corresponds to the volume of solution used in litres.

Total dissolved solids (TDS) and electrical conductivity analysis of treated water was performed using conductivity electrode of ion meter, while turbidity present in the aqueous solution was measured with a turbidity meter (NT4000, Spectra Lab). The calcium concentration, magnesium concentration, total hardness, total alkalinity, and phosphorus concentration of solution were calculated by APHA standard procedures [137].

3.4.5 Kinetic modeling for batch studies

In adsorption process, the rate of reaction is of prime importance and one of the most important factors that decides the design of adsorption equipment. For interpretation of the experimental data accurately, it is necessary to determine the steps in adsorption process which govern the overall rate of sorption. The rate limiting step is also of great importance from the application point of view. The kinetics of adsorption was studied to explain the fluoride uptake mechanism in the adsorbents. Fluoride ions are transported through film and pores to the solid-solution interface and surface reaction mechanism of the fluoride ions with the surface of adsorbent regulate the rate. Application of the kinetic model depends on the initial and final fluoride concentrations at various time intervals. Kinetic models are beneficial for designing and optimization of the process. To investigate the mechanism of fluoride adsorption by adsorbent materials, three kinetic models (Pseudo first order, Pseudo second order, Intraparticle diffusion) were studied.

3.4.5.1 Pseudo first order kinetic model (Lagergren's rate equation)

Pseudo first order kinetic model is one of the most common sorption rate equations used for adsorption of a solute from a liquid solution [59, 64, 66, 78, 87, 91, 138]. This model assumes that the rate of change of solute uptake with time is directly proportional to the difference in saturation concentration and the amount of solid uptake with time. In cases where the adsorption process is preceded by diffusion through a boundary, pseudo first order kinetics is followed. In simple words, the overall rate of adsorption is directly proportional to the driving force (i.e. $q_e - q_t$). Therefore, the pseudo first order kinetic equation can be expressed as:

$$\frac{dq_e}{dt} = k_1 (q_e - q_t) \tag{3.4.8}$$

where q_e is the equilibrium adsorption capacity (mg/g), q_t (mg/g) is the adsorption capacity at time t (min), k_1 (min^{-1}) is the pseudo first order rate constant for the kinetic model.

Integrating the Eq 3.4.8 and applying boundary conditions, t = 0 and q_t = 0 to t = t and $q_t = q_t$, the equation is given as follows:

$$log (q_e - q_t) = log\, q_e - \frac{k_1 t}{2.303} \tag{3.4.9}$$

3.4.5.2 Pseudo second order kinetic model

Adsorption process where chemisorption is the rate control the pseudo second order model is followed. The rate expression for pseudo second order kinetic model states that the driving force, (i.e $q_e - q_t$), is proportional to the available fraction of active sites [138] and can be given as follows:

$$\frac{dq_e}{dt} = k_2 (q_e - q_t)^2 \tag{3.4.10}$$

where k_2 (g mg^{-1} min^{-1}) is the pseudo second order rate constant for the kinetic model.

Integrating the above equation and applying boundary conditions, t = 0 and q_t = 0 to t = t and $q_t = q_t$,the equation can be expressed as follows:

$$\frac{t}{q_t} = \frac{1}{k_2 q_e^2} + \frac{1}{q_e} \tag{3.4.11}$$

The pseudo second order kinetic model has been applied to the adsorption of various metal ions, dyes and organic substances from aqueous solutions [66, 69, 84, 121, 139, 140, 86].

3.4.5.3 Intraparticle diffusion

Fluoride ions may be transported from the bulk solution into the adsorbent solid phase via an intra-particle diffusion process, which is observed to be the rate-limiting step in several batch adsorption processes. The adsorption process is combination of several mechanisms (bulk diffusion, external diffusion, surface or pore diffusion) where an important part is played by intraparticle diffusion. In order to test the contribution of intraparticle diffusion on the adsorption process, the rate constant was obtained by using the following equation [120]:

$$q_t = k_i t^{0.5} + I \tag{3.4.12}$$

where 'k_i' is the intraparticle diffusion rate constant (mg $min^{1/2}$/g) , 'I' is the intraparticle diffusion constant i.e. intercept of the line and is directly proportional to the thickness of boundary layer. The mathematical dependency of solid concentration on square root of time ($t^{0.5}$) has been derived by contemplating the adsorption mechanism to be governed by diffusion in the sorbent (as spherical particles) and convective diffusion in the solution [141].

3.4.6 Adsorption isotherms

Adsorption of fluoride onto the adsorbent material involves the establishment of equilibrium between the fluoride adsorbed on the adsorbent surface and the concentration of fluoride ions in solution. The variation of extent of adsorption with concentration of solute is represented by adsorption isotherms. The isotherm provides an idea about effectiveness of the adsorbent in removing fluoride ion from water and determines the maximum amount of fluoride adsorbed by the prepared adsorbent. Isotherms can also be used to determine

the comparative performance of different adsorbents. Experimental isotherm data for M-i-HAPa adsorbent was collected at different temperatures to fit in Langmuir, Freundlich, Tempkin and Dubinin-Raduskevich adsorption isotherms. However, isotherm data for Mg-HAP was collected only at 25 $\pm$ 0.5 ℃.

3.4.6.1 Langmuir isotherm model

The Langmuir isotherm model presumes monolayer surface assimilation (the adsorbed layer is one molecule in thickness), where surface assimilation can only happen at a finite (fixed) count of certain localized sites, that are indistinguishable and equivalent, with no lateral contact and steric hindrance between the adsorbed molecules, even on neighbouring sites. Langmuir isotherm relates to homogeneous surface assimilation in which every molecule own constant enthalpies and sorption activation energy (all sites own equal chemical attraction for the adsorbate), with no transmigration of the adsorbate in the plane of the surface. Langmuir isotherm model is expressed as follows:

$$\frac{C_e}{q_e} = \frac{1}{bQ_0} + \frac{C_e}{Q_0} \tag{3.4.13}$$

where b is the Langmuir constant related to energy (L/g), Q_0 is the maximum adsorption capacity (mg/g). Langmuir isotherm is also evaluated by a separation factor R_L, which determines the feasibility of the isotherm and is determined by the following equation:

$$R_L = \frac{1}{1 + bC_0} \tag{3.4.14}$$

3.4.6.2 Freundlich

Freundlich isotherm predicts a multilayer form of adsorption and provides detailed idea about effectiveness of the adsorbent and maximum amount of adsorbate that will get adsorbed by an adsorbent. This isotherm model assumes that the adsorption occurs on heterogeneous surfaces having varied adsorption energies. Therefore, the sum adsorbed is the abridgment of adsorption on all sites, the strongest binding sites are engaged first, until surface assimilation energy are exponentially reduced upon the achievement of surface assimilation procedure. The slope ranging between 0 to 1 is a quantification of surface assimilation strength or surface heterogeneity, fetching more heterogeneity as its value gets nearer to zero.

$$log\, q_e = log\, K_f + \frac{1}{n} log\, C_e \tag{3.4.15}$$

where K_f is the Freundlich adsorption capacity (mg/g) and n is the heterogeneity factor. 1/n is the indicator of the intensity of the reaction and predicts the favorability of the adsorbent-adsorbate system.

3.4.6.3 Temkin isotherm model

The Temkin isotherm contains a factor (A_T) that explicitly considers adsorbate–adsorbent interactions. By ignoring the extremely low and high value of concentration, it assumes that the heat of adsorption of all molecules in the layer would decrease linearly rather than logarithmic with coverage. As inferred in the equation [142], its derivation is categorized by a homogeneous division of binding energies (up to highest binding energy).

$$q_T = B_T ln A_T + B_T ln C_e \tag{3.4.16}$$

where B_T is the constant related to the heat of adsorption and A_T(L/min) is the Temkin isotherm binding constant.

3.4.6.4 The Dubinin-Radushkevich isotherm model

The Dubinin-Radushkevich isotherm assumes the multilayer character of adsorption and involves van der Waals forces [118, 142]. Depending on the activation energies, this isotherm model gives an estimate about the type of adsorption.

$$ln\, q_e = ln\, q_d - B\varepsilon^2 \tag{3.4.17}$$

$$\text{where } \varepsilon = RT\, ln\left(1 + \frac{1}{C_e}\right)$$

where q_d is the Dubinin–Radushkevich constant attributing to the theoretical maximum adsorption capacity and B is the constant of adsorption energy related to the mean adsorption energy (E_d) where it is transferred to the surface of the solid from infinity in the solution. ε is the Polanyi potential, R represents the gas constant (8.314 J/mol/K) and

T is the temperature (K). The constant 'B' can be correlated with mean adsorption energy [143], and can be calculated as:

$$E_d = \frac{1}{\sqrt{2B}} \tag{3.4.18}$$

The mean adsorption energy obtained from this isotherm may give an insight regarding the nature of adsorption process (chemical or physical). The magnitude of E_d is useful for estimating the type of adsorption and if values of E_d obtained are less than 8 kJ/mol, the adsorption process is considered to be physical in nature; values in between 8 to 16 kJ/mol indicate chemical adsorption [89].

3.4.7 Modeling of breakthrough profile in column studies

Breakthrough curves are obtained for estimating the performance of continuous mode adsorption processes. The shape of the curve as well as the point at which breakthrough is attained are very crucial for column operation and designing. In order to find the best model describing the adsorption kinetics in column , three models were employed: Hutchins Bed Depth Service Time (BDST) model, Thomas model and Yoon-Nelson model.

3.4.7.1 Hutchins Bed Depth Service Time (BDST) model

The Bed Depth Service Time model developed by Hutchins is a modified form of Bohart-Adams model [144] used to compare the adsorption capacity for continuous adsorption processes. The BDST model is deduced on the assumptions that intraparticular diffusion and external mass resistance are negligible. Moreover, the kinetics is assumed to be governed by surface chemical reaction between the fluoride ions in the solution and the adsorbent which is unused. This model proves to be beneficial for comparison of the column performance operating under distinct process parameters. The constants of this model may be useful for scaling up the adsorption process for some other flow rates and inlet fluoride concentrations without conducting any further experiments. It is important to determine the column performance for any bed height, provided data for some bed heights are known. In simple words, it states that the bed height and column service time have a linear relationship. The mathematical expression can be written as follows:

$$t_b = \frac{N_0}{uC_0}Z - \frac{1}{K_A C_0} ln\left(\frac{C_0}{C_b} - 1\right) \tag{3.4.19}$$

Critical bed depth equation is expressed in the following form:

$$Z_0 = \frac{u}{K_A N_0} ln\left(\frac{C_0}{C_b} - 1\right) \tag{3.4.20}$$

where 'C_0' and 'C_b' are initial and breakpoint fluoride concentration respectively, 'K_A' is the adsorption rate constant (L/mgh), 'N_0' denotes the adsorption potential (mg/L), 'u' is the linear flow velocity (cm/h) 'Z' is the bed depth (cm) , 'Z_0 ' is the critical bed depth and 't_b' is the service time to breakthrough in h.

3.4.7.2 Thomas model

Thomas proposed a model [145] for elucidating the column adsorption performance. This model is deduced by assuming Langmuir kinetics of adsorption–desorption where the axial dispersion is absent and the rate driving force follows the second-order reversible reaction kinetics. The model computes the maximum solid phase concentration of the solute on the adsorbent and the adsorption rate constant for a continuous mode adsorption system [146].

Mathematically the Thomas model can be expressed as follows :

$$ln\left(\frac{C_0}{C_e} - 1\right) = k_{th} q_0 \frac{M}{F} - k_{th} C_0 t \tag{3.4.21}$$

where 'k_{th}' is the Thomas rate constant (L/mg h), 'q_0' represents the equilibrium adsorbate uptake (mg/g), 'F' is the flow rate (L/h) and 'M' is the amount of M-i-HAPa pellets (adsorbent) in the column (g).

3.4.7.3 Yoon-Nelson model

The Yoon- Nelson model is deduced on the assumption that the rate of decrease in the probability of adsorption for each adsorbate molecule is proportional to the probability of adsorbate adsorption and the probability of adsorbate breakthrough on the adsorbent [147]. The linearised form of this model can be written as follows:

$$ln\left(\frac{C_e}{C_0 - C_e}\right) = k_Y t - \tau k_Y \tag{3.4.22}$$

where 'k_Y' represents the Yoon - Nelson rate constant (h^{-1}) and 'τ' is the time required for 50% adsorbate breakthrough (h^{-1}).

3.5 Mathematical modeling

Response surface technology (RSM) is a statistical experimental design, which was used for studying the factors influencing the adsorption process in batch mode and interaction between those factors was explored. An adsorption simulator "ADSORB" was developed in MATLAB software to study fluoride adsorption in a column system and obtain breakthrough curves by varying process parameters.

3.5.1 Response Surface Methodology (RSM)

Limitations of a classical experimental method can be eliminated by optimizing all the factors affecting together by statistical experimental design such as response surface methodology (RSM) [148]. RSM is mainly used for modeling of process parameters and to evaluate the relative importance of factors influencing the process even in the presence of complex interaction [149]. This methodology is widely used in chemical and environmental engineering, particularly to optimize adsorption process [150, 151]. By utilizing RSM, response over an entire space may be examined along with locating the region where the response value reaches optimum. The intent of this study was application of RSM coupled with Central composite design (CCD) as a statistic tool for optimization of fluoride adsorption on Magnesium-incorporated hydroxyapatite through batch studies.

The objective of using RSM was:

(a) For fitting a linear regression model to some initial data points in the search space (via repetitions of the simulation model);

(b) For fitting a nonlinear quadratic regression equation to this new area of the search space and thereafter determining the optimum of this equation.

3.5.1.1 Design of Experiments

Design Expert Version 9.0.4.1,Trial version (Stat Ease, USA) was used for regression and graphical analysis of the data obtained. The response was studied with a standard RSM design called central composite design (CCD). CCD for some independent variables was applied for designing experiments where the variance of predicted response (Y) at some points of independent variables (X) is only a function of the distance from the point to the center of design. The basis of experimental design matrix was decided

upon the effect of various process parameters that affect the defluoridation process. The defluoridation capacity of the adsorbent is principally affected by adsorbent dose, pH, time and temperature for a constant initial fluoride concentration. The optimization of fluoride removal was carried out by four chosen independent process variables viz. adsorbent dose (2 - 18 g/L), pH (3 - 11), contact time (15 - 345 min) and temperature (303 - 323 K) and the response was observed in terms of fluoride removal (%) and adsorption capacity (mg/g). Other crucial adsorption process parameters such as agitation speed (200 rpm) and initial fluoride concentration (10 mg/L) were kept constant. Range of parameters and the levels used for the experiments are given in Table 3.3 where A denotes adsorbent dose, B denotes pH of the solution, C denotes contact time and D symbolises the temperature.

Table 3.3: The parameters and levels for CCD

S.No	Parameter	Name	Level				
			-α	-1	0	+1	+α
1	Adsorbent dose (g/L)	A	6	2	10	18	14
2	pH	B	5	3	7	11	9
3	Contact time (min)	C	97.5	15	180	345	262.5
4	Temperature (K)	D	308	303	313	318	323

After the predecided range of parameter values are defined, they are coded to lie at different points: ±1 for the factorial points, 0 for the center points and ±α for the axial points.

This method was selected since it is appropriate for fitting a quadratic surface and it helps to optimize the effective parameters with a minimum number of experiments, and also to analyze the interaction between the parameters [152]. CCD consists of a 2^n factorial runs with 2n axial runs and n_c center runs (six replicates) which indicated that thirty experiments were required as per the following equation:

$$N = 2^n + 2n + n_c = 2^4 + 2X4 + 6 = 30 \tag{3.5.1}$$

where 'N' is requisite number of experiments and 'n' is the number of parameters (here n = 4). The center points help in predicting the experimental error and data reproducibility. These thirty experiments were performed as per the design mentioned in Table 3.3. The independent parameters are coded to -1 and 1 where they represent low and high levels respectively. Axial points in a CCD are located at (±α, 0, 0), (0, ±α, 0) and (0, 0, ±α), where the distance of axial point from center is denoted by 'α'. In this study the value of α

was fixed at 0.5. The optimum values of the chosen parameters were acquired by solving the regression equation and by examining the response surface plots [32]. An empirical model was developed for correlating the response to the adsorption process and is based on a second order quadratic model for fluoride removal using M-i-HAPa as given by Eq. 3.5.2:

$$Y = b_0 + \sum_{i=1}^{n} b_i X_i + \sum_{i=1}^{n} b_{ii} X_i^2 + \sum_{i=1}^{n} \sum_{j>1}^{n} b_{ij} X_i Y_j \tag{3.5.2}$$

where Y is the response of input parameters, X_i, X_i^2 and X_iX_j are the square and interaction terms of parameters, respectively whereas b_0, b_i, b_{ii} and b_{ij} are the unknown regression coefficients.

3.5.2 Modeling and simulation of adsorption column using MATLAB

The computational technique of mathematical modeling and simulation is significant for its theoretical approach as it requires only the various process parameters characteristic of the process, working conditions and provides almost accurate solutions predicting the performance of the system. In this study, the objective was to develop a simulator for depicting fluoride adsorption from aqueous solution in a column system and to obtain the breakthrough curves with varying parameters. For this purpose, an adsorption simulator named as "ADSORB" was developed in MATLAB. The method followed to obtain the model equations and solutions was by linearizing the differential equations describing the system by implicit finite difference method and simultaneously solving it by Gauss Jordan matrix elimination method to obtain the breakthrough curves.

3.5.2.1 Theoretical Model

A set of convective diffusion equations coupled with source terms due to adsorption and diffusion inside the adsorbent particles were used to describe the dynamics adsorption bed. From the bulk interstitial phase the molecules were transported onto the particle surface through axial convection and Fickian diffusion (film diffusion). The molecules may diffuse through solid diffusion or pore diffusion or both ways inside the particle. Model of the fixed bed column is shown in Figure 3.5.

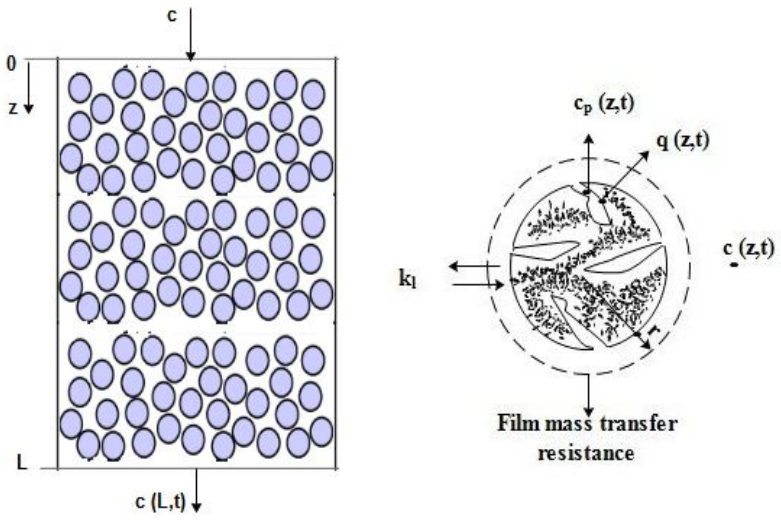

Figure 3.5: Model of the fixed bed column

For formulation of a model which may predict adsorption dynamics in a column system involving external film diffusion followed by internal diffusion, some assumptions were made which are as follows:

- The concentration of adsorbable component is small. Hence, the velocity of fluid is considered to be constant throughout the column.
- Adsorption equilibrium isotherm is a temperature dependent function and represented by the Langmuir equilibrium constant 'b', given by the equation $b = b_0 exp\frac{-\Delta H(T_0/T_s)}{R_g T_0}$, where T_s is the temperature of particle surface, R_g is the gas constant, T_0 is the inlet temperature, b_0 is the Langmuir constant corresponding to T_0 and $\triangle H$ is the standard enthalpy change.
- Axially dispersed plug flow pattern is assumed since constant axial dispersion coefficient is considered.
- Mass transfer resistance includes the external fluid film resistance, macropore diffusional resistance and resistance to heat transfer, all three characterized by coefficient assumed to be constants.
- Similar transfer effects were assumed for both mass and heat transfer between the particle and the fluid and the transfer coefficients are related by the equation $h = k_l \rho_l c_{pl}$

Based on the assumptions above, the basic equations for the mass and thermal balances and transfer rates are as follows:

External field Mass transfer

The equations describing the phenomena of adsorption through diffusion liquid – solid at the interface is described by the following equations:

$$\frac{\partial c}{\partial t} = D_L \frac{\partial^2 c}{\partial z^2} - u\frac{\partial c}{\partial z} - \left(\frac{1-\varepsilon}{\varepsilon}\right)\frac{3k_l}{R}[c(z,t) - c_{p/r=R}] \tag{3.5.3}$$

Boundary conditions for field mass balance :

$$\text{At column inlet, z = } 0^+,\ D_L \frac{\partial c}{\partial z}_{/z=0} = -u[-c_{/z=0^+} - c_{/z=0^-}]$$

$$\text{At column outlet, z = L },\ \frac{\partial c}{\partial z}_{/z=L} = 0$$

Particle field mass balance

The equations describing the phenomena of adsorption through the solid adsorbent particles is described by the following equations:

$$\frac{\partial q}{\partial t} + \varepsilon_p \frac{\partial c_p}{\partial t} = \varepsilon_p D_p \left[\frac{\partial^2 c_p}{\partial r^2} + \frac{2}{r}\frac{\partial c_p}{\partial r}\right] \tag{3.5.4}$$

where c_p is the concentration at particle surface. The function ∂q defines the solid phase adsorbate concentration averaged over the adsorbent particle, and the equilibrium relationship for the process is given by

$$q = \frac{q_0}{\lambda_0}\frac{bc_p}{(1+bc_p)} \tag{3.5.5}$$

$$\lambda_0 = \frac{b_0 c_0}{1 + b_0 c_0} \tag{3.5.6}$$

Boundary conditions for field mass balance:

$$\text{At center},\ \frac{\partial c_p}{\partial r}_{/r=0} = 0$$

$$\text{At the surface},\ \varepsilon_p D_p \left(\frac{\partial c_p}{\partial r}\right)_{r=R} = k_g[c(z,t) - c_{p/r=0}]$$

External field heat balance

The external field heat balance is given by:

$$\frac{\partial T}{\partial t} = \frac{K_L}{\rho_g c_{pg}} \frac{\partial^2 T}{\partial z^2} - u\frac{\partial T}{\partial z} - \left(\frac{1-\varepsilon}{\varepsilon}\right)\frac{3K_g}{R}[c(z,t) - c_{p/r=0}] \tag{3.5.7}$$

Boundary conditions for field heat balance:

$$\text{At column inlet, z = } 0^+,\ K_L \frac{\partial T}{\partial t}_{/z=0^+} = -u\rho_g c_{pg}\left[T_{/z=0^-} - T_{/z=0^+}\right]$$

$$\text{At column outlet, z = L, } \frac{\partial T}{\partial z}_{/z=L} = 0$$

Particle heat balance

The particle heat balance equation is given by:

$$\rho_s c_{ps}\frac{\partial T_s}{\partial t} = \frac{3h}{R}[T - T_s] + \frac{(-\triangle H)3k_g}{R}[c(z,t) - c_{p/r=R}] \tag{3.5.8}$$

$$\text{Boundary conditions: } T_p(r,t) = T_s(t)$$

The temperature distribution in the particle is assumed to be constant. This is because in case of adsorption, the time constant of heat transfer in the particles is smaller than the time constant of intraparticle diffusion.

3.5.2.2 Numerical Solution

The system of liquid solid adsorption in a packed bed column can be defined in terms of various equations describing the mass transfer of adsorbate in the field and inside the adsorbent particle / pellet and the heat transfer in the field and inside the adsorbent pellet has to be solved simultaneously to obtain the concentration and temperature of the bed at different time interval and bed length. The dimensionless constants used are listed in the Appendix. The dimensionless equations and boundary conditions are given in Table 3.4.

Table 3.4: Dimensionless equations and boundary conditions

External field mass balance	$$\frac{\partial U}{\partial \tau} = \frac{1}{Pe_m} W \frac{\partial^2 U}{\partial x^2} - W \frac{\partial U}{\partial x} - \frac{3(1-\varepsilon)}{\varepsilon} \psi [U - U_{p/n=1}]$$
	At x=0 $\frac{\partial U}{\partial x_{/x=0}} = -Pe_m [U_{/x=0} - U_{/x=0}$ At x=1 $\frac{\partial U}{\partial x_{/x=1}} = 0$
Particle mass balance	$$\frac{\partial Q}{\partial \tau} + \varepsilon_p \frac{\partial U_p}{\partial \tau} = \varepsilon_p \left[\frac{\partial^2 U_p}{\partial \eta^2} + \frac{2}{\eta} \frac{\partial U_p}{\partial \eta} \right]$$
	At the center $U_p(\eta, 0) = 0, \frac{\partial U_{p/n=0}}{\partial \eta} = 0$ At the surface $\frac{\partial U_{p/n=1}}{\partial \eta} = \frac{\psi}{\varepsilon_p} \left[U - U_{p/n=1} \right]$
External field heat balance	$$\frac{\partial V}{\partial \tau} = \frac{1}{Pe_h} W \frac{\partial^2 V}{\partial x^2} - W \frac{\partial V}{\partial x} - \frac{3(1-\varepsilon)}{\varepsilon} [V - V_s]$$
	At column inlet x=0 $\frac{\partial V_{/x=0}}{\partial x} = -Pe_h [V - V_{x=0}]$ At column outlet x= 1 $\frac{\partial V_{/x=1}}{\partial x} = 0$
Particle heat balance	$$\frac{\partial V_s}{\partial \tau} = 3\psi\phi(V - V_s) + 3\psi\beta\phi \left[U - U_{p/\eta=1} \right]$$
	$$V_p(\eta, \tau) = V_s(\tau)$$

3.5.2.3 The grid

The partial differential equations are converted to dimensionless forms for mathematical expediency of the process. The equations describing the external field mass and temperature and particle mass and temperature balance is then written with respect to the

dimensionless–ordinate of time (τ) , the axial co-ordinate (x) along the column length and the radial coordinate (γ) along the particle radius (Figure 3.6). A set of 6 finite difference points were considered along the axial and radial coordinates , dividing the bed into 5 equal bed steps and particle radius of 5 equal increments. The points along the time, length and radial ordinates are designated by n, i and m resp. Thus, the future values in the grid were calculated by using the present values and simultaneously solve these equations by iterating the values till we reach convergence.

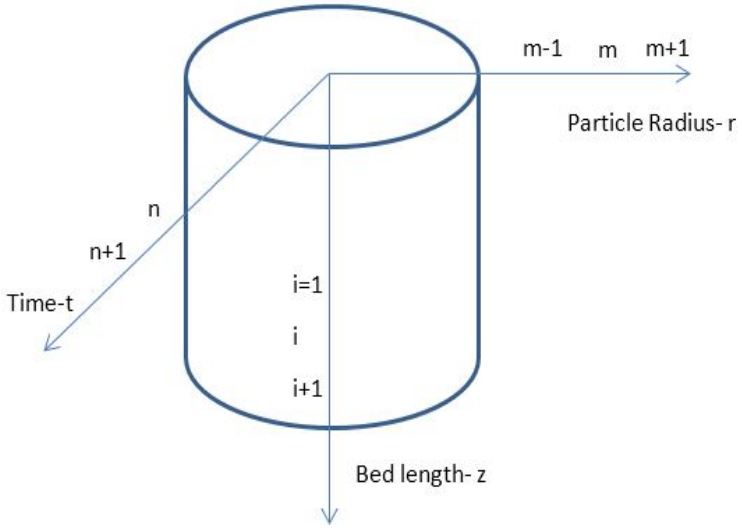

Figure 3.6: The 3D grid describing bed length – time – particle radius axis

3.5.2.4 Implicit finite difference numerical method

If we use the backward difference at time t^{n+1} and a second-order central difference for the space derivative at position xj, we get the recurrence equation:

$$\frac{u_j^{n+1} - u_j^n}{k} = \frac{u_{j+1}^{n+1} - 2u_j^{n+1} + u_{j-1}^{n+1}}{h^2} \tag{3.5.9}$$

The above expression is an implicit method for solving the one-dimensional heat equation.

We can u_j^{n+1} obtain from solving a system of linear equations:

$$(1 + 2ru_j^{n+1} - ru_{j-1}^{n+1} - ru_{j+1}^{n+1}) = u_n^j \tag{3.5.10}$$

The scheme is always numerically stable and convergent but usually more numerically intensive than the explicit method as it requires solving a system of numerical equations on each time step. The errors are linear over the time step and quadratic over the space step.

3.5.2.5 Linearized equations

Since these partial differential equations need to be linearized in order to find out a numerical solution, implicit finite difference approximation is applied to them in accordance with the appendix 1.0.

External field mass balance

The total number of equations is 6 along the bed length.

For bed step i = 0,

$$\begin{aligned} AU_{(n+1,i=1)} - (B+C)U_{(n+1,i=0)} + EU_{p_{n+1,i=1,m=5}} = \\ -D - AU_{(n,i=1)} + (B-C)U_{(n,i=0)} + EU_{p_{n,i=0,m=5}} \end{aligned}$$

For bed step i = 1,2,3,4,

$$\begin{aligned} (A/2-Z)U_{(n+1,i+1)} - (B1+C)U_{(n+1,i)} + (A/2+Z)U_{(n+1,i-1)} - EU_{p_{(n+1,i,m=5)}} = \\ (-A/2+Z)U_{(n,i+1)} + (B1-C)U_{(n,i)} - (A/2+Z)U_{(n,i-1)} + EU_{p_{(n,i,m=5)}} \end{aligned}$$

For bed step i = 5,

$$\begin{aligned} [(-A)/2+Z] - C + EU_{(n+1,i=5)} + [A/2+Z]U_{(n+1,i=4)} - EU_{p_{(n+1,i=5,m=5)}} = \\ [A/2+Z-E-C]U_{(n,i=5)} - (A/2+Z)U_{(n,i=4)} + EU_{p_{(n,i=5,m=5)}} \end{aligned}$$

Particle mass balance

The total number of equation obtained is 36.

For i = 0, 1, 2,3,4,5 and m = 1, 2, 3, 4

$$\begin{aligned} (1+1/m)GU_{p_{n+1,i,m+1}} + (-2G+H)U_{p_{n+1,i,m}} + (1-1/m)GU_{p_{n+1,i,m-1}} + IV_{s_{n+1.i.m=5}} = \\ -(1+1/m)GU_{p_{n,i,m+1}} + (2G+H)U_{p_{n,i,m}} + G(-1+1/m)U_{p_{n,i,m-1}} + IV_{s_{n,i,m=5}} \end{aligned}$$

For i = 0,1, 2,3,4,5 and m =0

$$(6G)U_{p_{n+1,i,m+1}} + (-6G+H)U_{p_{n+1,i,m}} + IV_{s_{n+1,i,m}} = (-6G)U_{p_{n,i,m+1}} + (6G+H)U_{p_{n,i,m}} + IV_{s_{n,i,m}}$$

For i = 0, 1, 2,3,4,5 and m = 5

$$[6JG/5]U_{n+2,i}+(-2G+H-6JG/5)U_5+(2G)U_{p_{n+1,i,m=4}})+IV_{s_{n+1,i,m=5}}=$$
$$[2G+H+6JG/5]U_5+(-2G)U_{p_{n,i,m=4}}+((-6JG)/5)U_{n,i})+IV_{s_{n,i,m=5}}$$

External field heat balance

The total number of equations obtained is 6

For bed step i = 0

$$A2V_{n+1,i=1}-(B+C)V_{n+1,i=0}-EV_{p_{n+1,i=0,m=5}}=-D-A2V_{n,i=1}+(B-C)V_{n,i=0}+EV_{p_{n,i=0,m=5}}$$

For bed step i = 1,2, 3, 4

$$(A2/2-Z)V_{(n+1,i+1)}-(-B2-C)V_{(n+1,i)}+(A2/2+Z)V_{(n+1,i-1)}-EV_{p_{(n+1,i,m=5)}}=$$
$$-(A2/2-Z)V_{p_{(n,i+1)}}+(B2-C)V_{(n,i)}+((-A2)/2-Z)V_{(n,i-1)}+EV_{p_{(n,i,m=5)}}$$

For bed step i = 5

$$(-(A2/2+Z)-C+E)V_{n+1,i=5}+(A2/2+Z)V_{n+1,i=4}-EV_{p_{n+1,i=5,m=5}}=$$
$$(A2/2+Z-E-C)V_{n,i=5}+(-A2/2-Z)V_{n,i=4}+EV_{p_{n,i=5,m=5}}$$

Particle heat balance

The number of equations obtained is 6

For i = 0,1, 2, 3, 4, 5

$$Y_AV_{p_{n+1,i,m=5}}+Y_BV_{n+1,i}+Y_CU_{n+1,i}-Y_CU_{p_{n+1,i,m=5}}=Y_DV_{p_{n,i,m=5}}-Y_BV_{ni}-Y_CU_{n,i}+Y_CU_{p_{n,i,m=5}}$$

The total number of equations from all these 4 sections is 54 and the total number of variables is 54. The LHS of these equations contains future values of variables and RHS contains the present values of the variables .Thus we calculate the future values by using the present values of the variables .Thus a 54*54 matrix is formed using the LHS of these equations .The RHS of these equations now serves as the 54*1 matrix, both these matrix will be simultaneously solved to find out the values of the 54 variables.

constants and variables

The constants A, B, C, D etc. are all listed in Appendix 2.0 , they are a combination of all the dimensionless constants grouped together to simplify the equations. The values of

all the constants except H and I are constant at all iterations but these two are dependent on the temp and concentration at that point in the grid. Cp is the adsorbate concentration in particulate phase and since it is assumed that the particle is spherical it is a ratio as given below:

$$C_p = \frac{(\int_r^R 4\pi r^2 C_p \partial r)}{(4/3)\pi R^3}$$

Since, $\eta = r/R$

Thus, $C_p = 3\int_1^0 \eta^2 C_p \partial\eta$ where $\eta = 0,1,2,3,4,5$

Thus $U_p = C_p/C_0$changing the above equation into $U_{pi} = 3\int_0^1 \eta^2 U_p(n=1,i=0,\eta)\partial\eta$

Applying the standard trapezoidal rule, the average concentration of adsorbate in the particulate phase is given by

$U_p0 = (3\eta/2)[(0*U_p(n,i,\eta=0)) + (2*\eta^2*U_p(n,i,\eta=1)) + (2*4\eta^2*U_p(n,i,\eta=2)) + (2*9\eta^2*U_p(n,i,\eta=3)) + (2*16\eta^2*U_p(n,i,\eta=4)) + (2*1*U_p(n,i,\eta=5))]$

The values of U_{p0},U_{p1},U_{p2},U_{p3},U_{p4},U_{p5} were calculated corresponding to bed step i = 0,1,2,3,4,5

The Langmuir constant b varies with the surface temperature of the adsorbent $b = b_0 \exp\left[\delta\left(\frac{T_0}{Ts} - 1\right)\right]$

$$\text{Thus, } Q_c = 1 + \left[\frac{(bQ_0C_0)}{(\lambda_0\varepsilon_p(1+bC_0U_p)^2}\right]$$

$$\text{and } Q_t = \frac{(-b\delta Q_0C_0\varepsilon_p)}{(\lambda_0\varepsilon_p V_s^2(1+bC_oU_p)^2)}$$

Thus it can be seen from the formula of Q_c and Q_t that both these variables are dependent on both time and bed length.

Thus $H = \frac{Q_c}{k}$ and $I = \frac{Q_t}{k}$ are the constants which change with changing grid points.

Gauss Jordan method

The Gauss-Jordan reduction method is an extension of the Gauss elimination method. It reduces a set of n equations from its canonical form of

Ax = c

to the diagonal set of the form

Ix=c

where I is the unit matrix. is identical to

x=c

that is, the solution vector is given by the c' vector.

The Gauss-Jordan reduction method applies the same series of elementary operations that are used by the Gauss elimination method. It applies these operations both below and above the diagonal in order to reduce all the off-diagonal elements of the matrix to zero. In addition, it converts the elements on the diagonal to unity.

The Gauss-Jordan reduction procedure applied to the (n) x (n + 1) augmented matrix can be given in a three-part mathematical formula for the initialization, normalization, and reduction steps as shown below:

Initialization formula:

$$a_{ij}^{(0)}) = a_{ij}\{j = 1,2....n\{i = 1,2....n\}\}$$

$$a_{ij}^{(0)} = c_i\{j = n+1\}$$

Normalization formula:

$$a^{(k)}kj = \frac{a_{kj}^{k-1}}{a_{kk}^{k-1}}\{j = n+1,n...k\{k = 1,2,....n\}\}; \qquad \{a_{kk}^{k-1}) \neq 0\}$$

Reduction formula:

$$a_{ij}^{k} = a_{ij}^{k-1} + a_{kj}^{k}a_{ik}^{k-1}\{j = n+1,n....k\{i = 1,2....n\{k = 1,2....n$$

$$i \neq k$$

The initialization formula places the elements of the coefficient matrix in columns 1 to n and the vector of constants in column (n + 1) of the augmented matrix. The normalization formula divides each row of the augmented matrix by its pivot element and makes this change permanent, thus causing the diagonal elements of the coefficient segment of the augmented matrix to become unity. Finally, the reduction formula reduces to zero the off-diagonal elements in each row and column in the coefficient segment of the augmented matrix, and converts column (n + 1) to the solution vector.

3.5.2.6 Working programme

Once the solution scheme was formulated for the theoretical model, the algorithms were adapted to draw a workable MATLAB programme, as it provides more ease and computational speed in obtaining the solution.

Stepwise algorithm is given as follows (also presented in Figure 3.7):

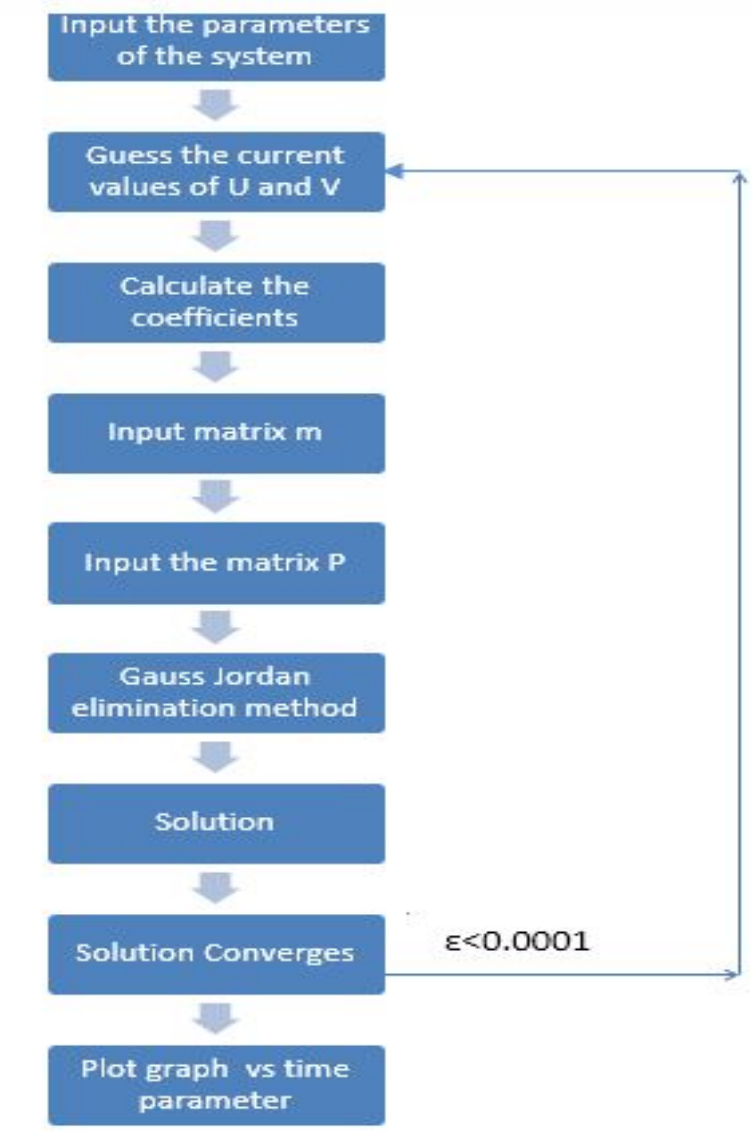

Figure 3.7: Algorithm for the programme "ADSORB"

1. The user will be asked to input the various parameters like Sherwood number, initial adsorbate concentration, peclet number etc.

2. The first guess values of the present variables were assumed as U(j) = Up(j) = 0 and V(j) = Vp(j) = 1.

3. The program will calculate the value the constant such as A, B, C, E, Z, A2, B2, B1, J, G, Ya, Yb, Yc, Yd and variable constant such as H and I.

4. The 54*54 matrix (say m) will be entered while simultaneously calculating the value of each row and column

5. The 54*1 matrix (say P) is entered by entering the RHS of the equations.

6. Matrix m and P are augmented and gauss Jordan elimination method is applied to them.

7. The values obtained are used as the new values for the present value and again the future values are obtained

8. The iterations will continue till the solution converges.

9. Once the final solution is obtained, it will be plotted against time dimensionless parameter.

3.6 Statistical techniques

3.6.1 Chi-squared Analysis

For identifying an appropriate isotherm model for fluoride adsorption on the adsorbent, Chi-squared analysis has been carried out. Chi-squared test statistic is the sum of the squares of the differences between the data obtained experimentally and data calculated from the model, with each squared difference divided by the corresponding data calculated from the model. The mathematical expression is given as follows:

$$\chi^2 = \sum \frac{(q_e - q_{calc})^2}{q_{calc}} \tag{3.6.1}$$

where q_{calc} is the equilibrium capacity obtained by calculating from the model (mg/g). If value of data obtained from the model are close to the data obtained experimentally,the value of χ^2 will be a small number, However, for a large difference between these values, χ^2 will be higher. Therefore, it is imperative to analyze the data set using the nonlinear chi squared test to confirm the best fit isotherm for the adsorption system.

3.6.2 Sum of squared errors

The kinetic models employed for fitting the adsorption data were assessed by calculating the sum of errors squared (SSE), alongwith the value of R^2 which can be represented as written below:

$$SSE = \sqrt{\sum \frac{(q_e - q_{calc})^2}{N_s}} \tag{3.6.2}$$

where N_s is the number of data points. A lower value of SSE is considered to be a better fit to adsorption data [138].

3.7 Summary of the Chapter

This chapter is a narrative of the materials used and methodology adopted for performing the experiments and the simulation studies. The details of reagents prepared and adsorbent synthesized or procured is given along with the list of characterization tools used in this study. The parameters varied for defluoridation in batch and column adsorption experiments are specified. The method of regeneration is also stated. The details of isotherm and kinetic models applied to the experimental data are mentioned. An explanation of mathematical modeling and simulation carried out in this study is also provided. Statistical analysis techniques such as Chi-squared test and SSE were also applied to the experimental data set. A low value of $\chi^2$and SSE indicates that experimental data provides a good quality fit to the value from the model. Therefore, data were analysed to confirm the best-fit isotherms for the fluoride adsorption system.

The next chapter marks the beginning of results and discussions.

CHAPTER 4

Chapter 4

Characterization of Adsorbents

Characterization of adsorbents is a very important part of this research work in order to identify the bonding patterns, functional groups, phase characteristics, crystallinity and minerological compositions. It will also help in getting an insight into the surface morphology, particle size, surface area, pore volume and thermal behaviour of the adsorbent studied.

The samples synthesized or amended were characterized while the samples used as procured were not characterized. This chapter describes the characterization of the following the calcium based adsorbents used :

- Calcia-Magnesia adsorbent
- Modified natural hydroxyapatite
- Magnesium incorporated hydroxyapatite (powder form)

4.1 Calcia-Magnesia Adsorbent (CMA)

The synthesized adsorbent CMA (section 3.2.2) was characterized using FTIR , XRD and SEM techniques and presented in the following subsections:

4.1.1 FTIR

Fourier Transform Infrared Spectroscopy (FTIR) study was carried out to identify the functional groups present in CMA adsorbent in the 4000 - 500 cm^{-1} range. The FTIR spectrum of CMA showed some characteristic bonding patterns present in the adsorbent (Figure 4.1). The peak at 3696.89 cm^{-1} and 3643.43 cm^{-1} represents -OH bonds present in $Mg(OH)_2$ and $Ca(OH)_2$ respectively. The peak seen at 1420.19 cm^{-1}represents bending of

O-H bond. The broad peaks below 1000 cm^{-1} are due to presence of Mg-OH bond. FTIR graph also showed the weak band at 442 cm^{-1}, which was attributed to Ca–O stretching.

4.1.2 XRD

XRD analysis is considered as one of the most important characterization techniques used in solid state chemistry and materials science. The X-ray diffraction (XRD) pattern of CMA (Figure 4.2) indicated the crystalline nature of the product as narrow and sharp peaks were obtained in the pattern. The adsorbent CMA was prepared from calcium and magnesium hydroxides, and therefore various peaks of these compounds were found to be matched as per the standard JCPDS database. These compounds with their respective card numbers are calcium [00-001-0737], magnesium hydroxide [00-001-1169], magnesium oxide [00-002-1207], calcium-magnesium [00-001-1070], calcium oxide hydrate [00-002-0968] and magnesium oxide hydrate [00-002-1092]. The adsorption and precipitation during defluoridation is attributed to the presence of calcium and magnesium compounds that form complex with the negatively charged fluoride ions.

The average crystallite size was calculated using Scherer equation (given in Eq. 3.3.1) to be 43.55 nm.

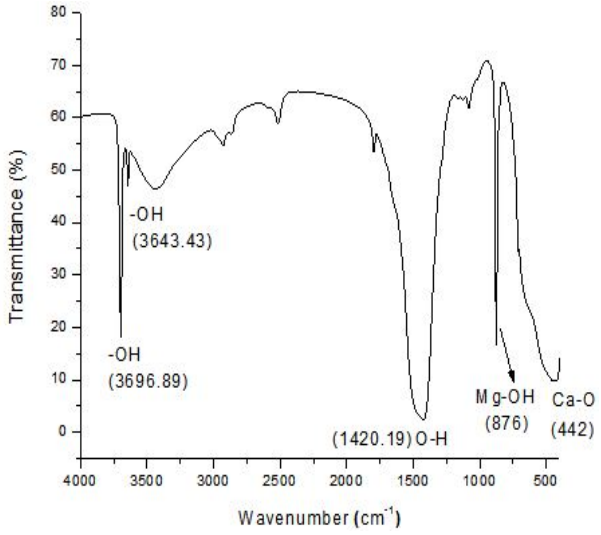

Figure 4.1: FTIR spectra for CMA adsorbent

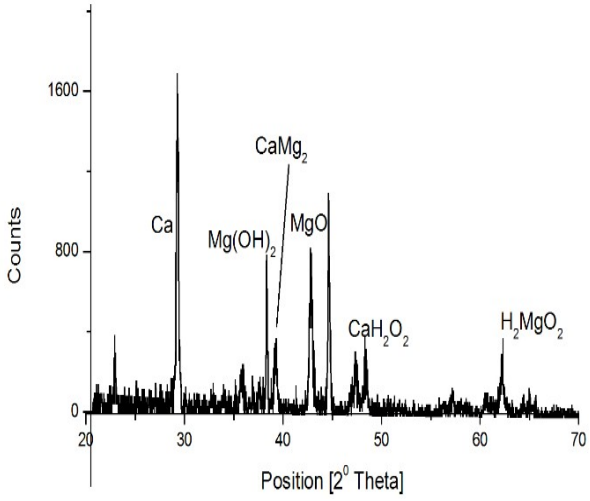

Figure 4.2: XRD pattern for CMA adsorbent

4.1.3 SEM

The surface morphology of CMA adsorbent was analyzed through SEM technique. The micrograph given in Figure 4.3a shows dense agglomerations of particles. The elemental image displaying regions with calcium (blue colored area) and magnesium (red colored area) element on the adsorbent surface is given in Figure 4.3b and Figure 4.3c respectively. These elemental images depicts the distribution of individual element in the CMA adsorbent.

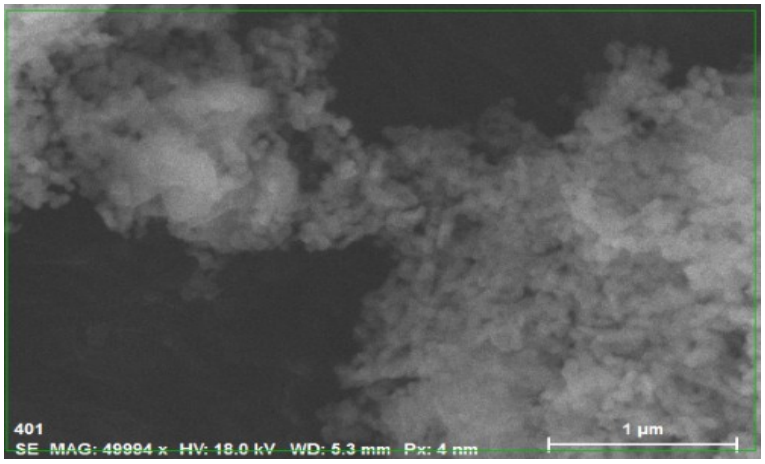

(a) SEM image of CMA

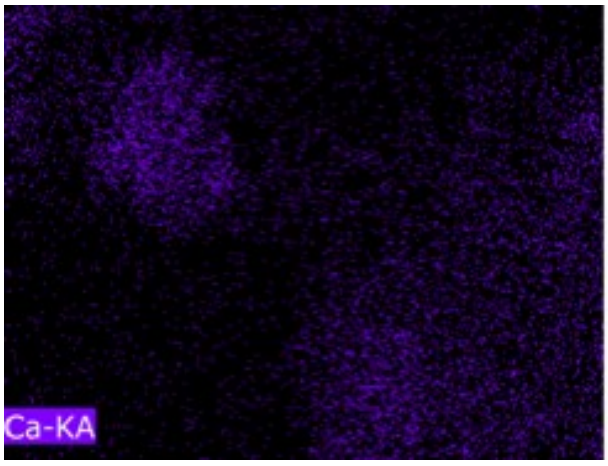

(b) Elemental mapping of CMA for Calcium

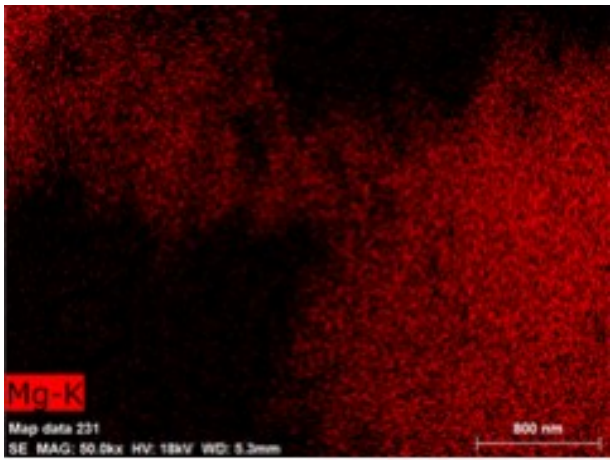

(c) Elemental mapping of CMA for magnesium

Figure 4.3: SEM image and elemental mapping of CMA adsorbent

Characterization of CMA adsorbent via FTIR studies revealed about the chemical bonds present by producing an infrared absorption spectrum. The XRD analysis showed the crystalline nature of the adsorbent and identified the phase composition of the adsorbent. The SEM study exhibited the presence of dense agglomerates and the elemental mapping gave an overview of elemental distribution present in the adsorbent.

4.2 Modification of natural Hydroxyapatite with magnesium

Natural Hydroxyapatite (aHAP) was modified by calcining it with magnesium hydroxide and named as Mg-HAP as described in section 3.2.5.1. The synthesized Mg-HAP was characterized for evaluating the functional groups, bonding patterns, crystallinity, structure, and surface morphology, and the obtained results are as follows:

4.2.1 FTIR

The FTIR was performed on Mg-HAP to evaluate the functional groups and bonding pattern present. The spectrum is presented in Figure 4.4. The peak observed around 3571.43 cm^{-1} confirmed the presence of –OH bond [153]. This peak is mainly due to O–H stretching vibration in hydroxyapatite. The peak obtained at 1043.24 cm^{-1} is associated with the stretching modes of the P–O bonds of HAP [154]. The double peak at 602.17 and 567.5 cm^{-1} is due to bending modes of P–O bonds in phosphate groups [155]. The asymmetric P–O vibration of $PO_4{}^{3-}$ observed at 961.78 cm^{-1} is distinguishable which also represents bending vibration of $PO_4{}^{3-}$ in hydroxyapatite. The FTIR spectra displayed a small broad peak at 1458.58 cm^{-1}, which is characteristic peak of $NH_4{}^{+}$ group. Presence of this peak may be attributed to the alkaline conditions required for hydroxyapatite formation. Although repeated washing was done with double distilled water, still there is a possibility of presence of small amount of ammonium ions.

4.2.2 XRD

The XRD pattern for Mg-HAP is shown in Figure 4.5. According to the results obtained by XRD analysis, Mg-HAP exhibited crystalline structure as the peaks were sharp and narrow. The highly crystalline nature of the peaks are attributed to calcination of the adsorbent. All the peaks matched the standard JCPDS pattern for hydroxyapatite and MgO with card numbers 00-024-0033 and 00-045-0946 respectively. The maximum intensity of peak was observed at a 2 θ angle of 42.83 which corresponds to magnesium oxide. Peaks of magnesium oxide (MgO) were obtained in the diffraction pattern since magnesium hydroxide used in the preparation of Mg-HAP was calcined and magnesium oxide was formed. The average crystallite size of Mg-HAP was calculated from the Scherer equation and found to be 65 nm.

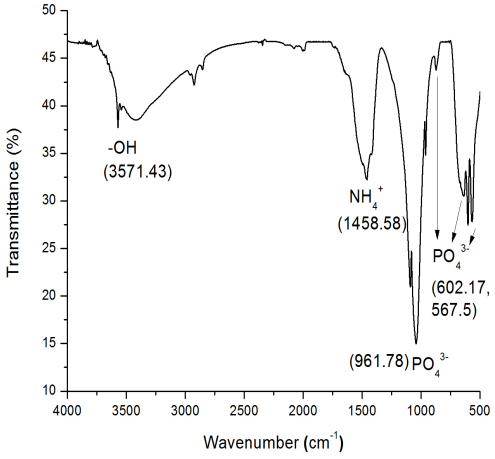

Figure 4.4: FTIR spectra for Mg-HAP adsorbent

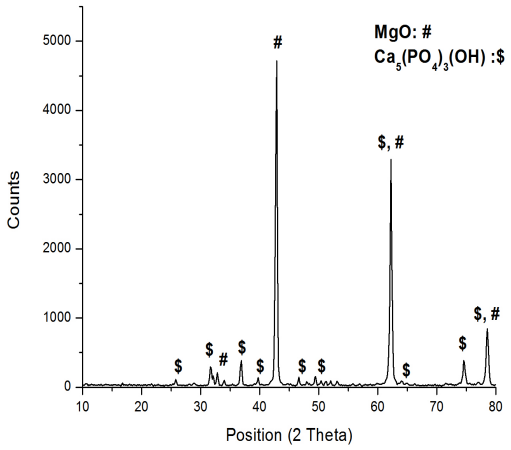

Figure 4.5: XRD pattern for Mg-HAP adsorbent

4.2.3 TEM/EDX

TEM analysis was used for investigating the crystal structures and their orientations at submicron level whereas the EDX analysis was conducted for gaining information about the elemental composition of the adsorbent. TEM micrograph of Mg-HAP at different magnifications is shown in Figure 4.6. Figure 4.6a shows TEM image of Mg-HAP adsorbent. To get a better perspective of the crystal arrangements, image at higher magnification is presented in Figure 4.6b. The TEM image at lower magnification indicate an average size of particles with 70 – 150 nm length and 30 – 40 nm width. The microstructures exhibit elongated morphology; however, it appears agglomerated at places and the crystals are arranged in different orientations. The crystalline nature of the Mg-HAP adsorbent was confirmed through dark field image of TEM presented in Figure 4.6c. The energy-dispersive X-ray spectroscopy (EDX) spectrum of Mg-HAP given in Figure 4.6d depicts the presence of magnesium, calcium, phosphorus, and oxygen in the structure. No impurities were observed in the spectrum; hence, pure Mg-HAP was obtained. A peak for copper was obtained, since the grid used for mounting the sample is made of copper.

The mean crystallite size was also calculated from Scherer formula, and it showed that the nanocrystals have an average size of 65 nm which is close to the particle size observed in TEM (70 nm approximately).

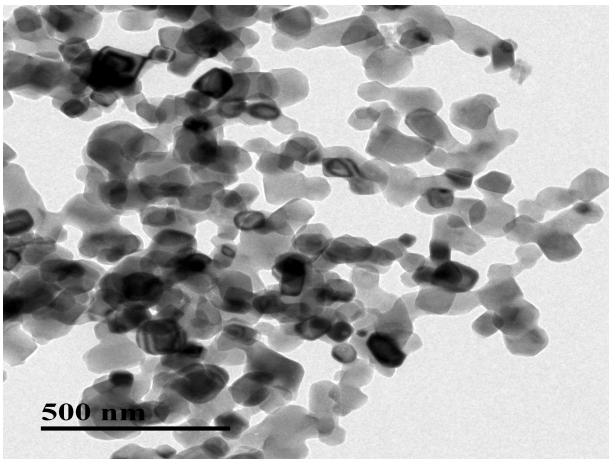

(a) TEM image of Mg-HAP at lower magnification

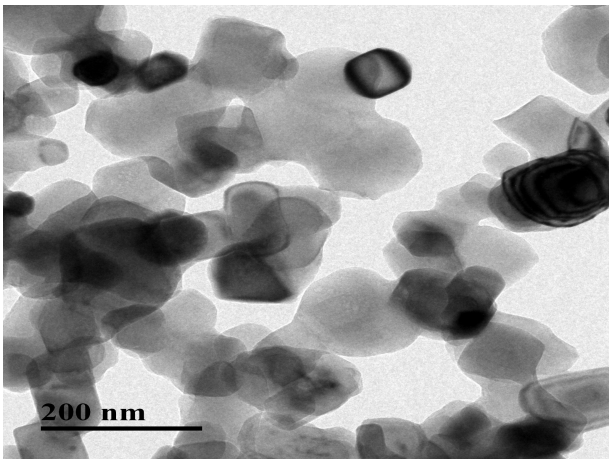

(b) TEM image of Mg-HAP at higher magnification

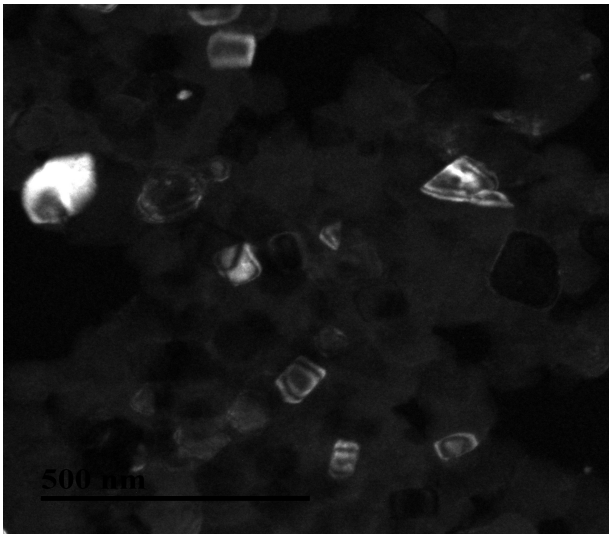

(c) Dark field image of Mg-HAP

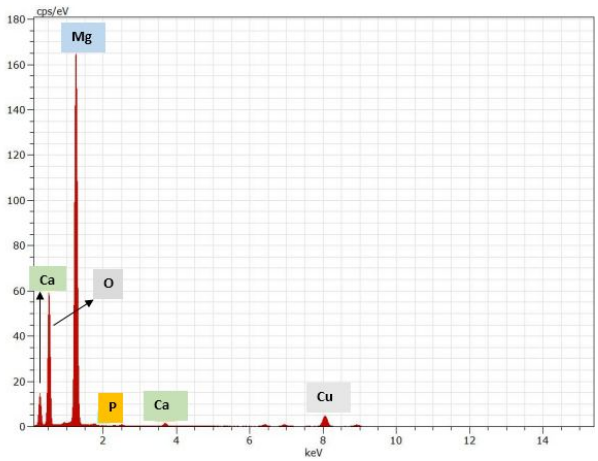

(d) EDX spectra of Mg-HAP

Figure 4.6: TEM images of Mg-HAP

4.2.4 SEM

The SEM image of prepared Mg-HAP is shown in Figure 4.7a at 20000X magnification. Figure 4.7b gives a more clear surface perspective of the adsorbent at 50000X magnification. Numerous dense agglomerations of particles were observed in the SEM image. The image clearly shows that the adsorbent is composed of porous particles which makes it feasible for the fluoride ions to be adsorbed in this type of structure. Elemental mapping images for calcium, phosphorous, and magnesium are also shown in Figure 4.8, which provides an overview of location of different elements present according to the color assigned, viz. red for phosphorous, blue for magnesium, and green for calcium.

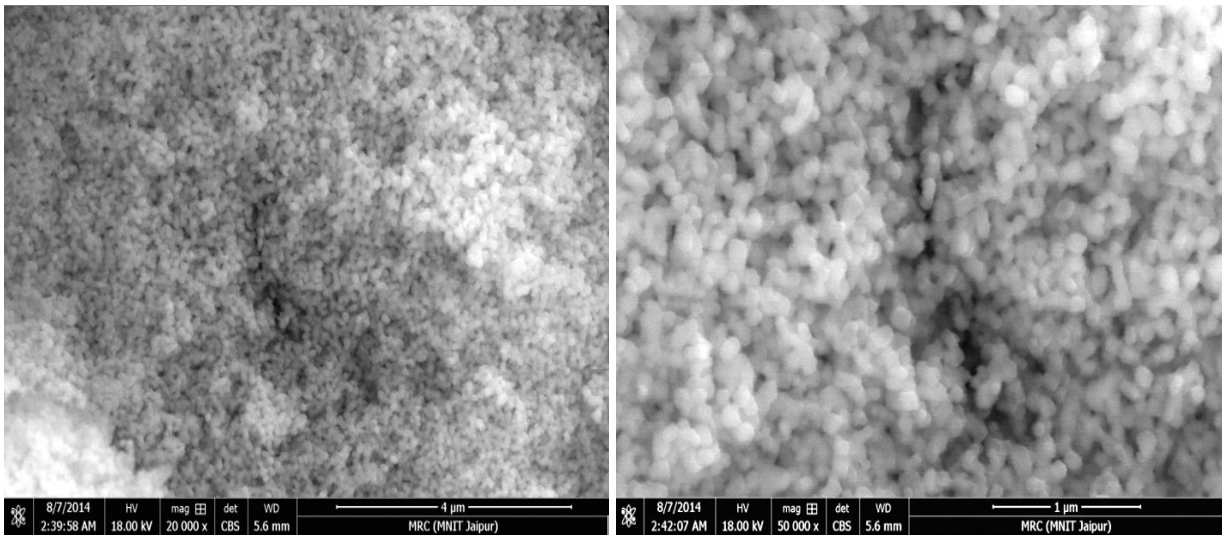

(a) Image at 20000X (b) Image at 50000X

Figure 4.7: SEM images of Mg-HAP at different magnifications

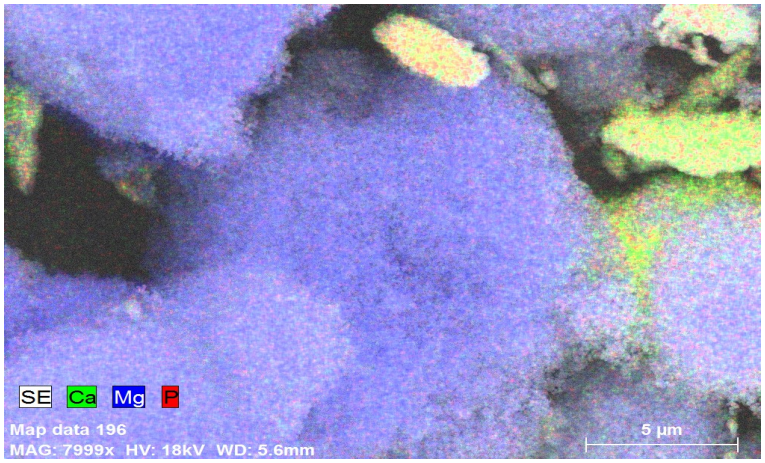

(a) Mapping image of Mg-HAP

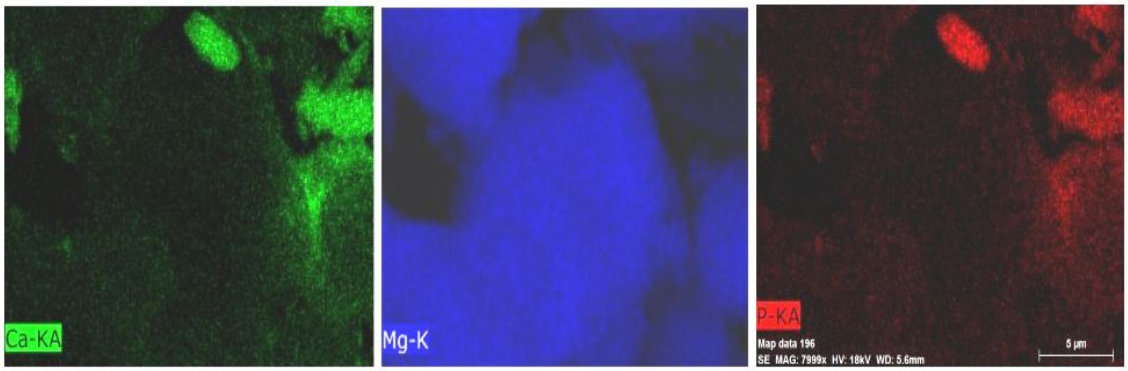

(b) Individual element distribution of Calcium, Magnesium and Phosphorus

Figure 4.8: Mapping of elements

4.3 Pure-Hydroxyapatite and Magnesium incorporated Hydroxyapatite powder

This section presents the characterization of pure-hydroxyapatite (p-HAP) and magnesium incorporated hydroxyapatite (M-i-HAP) using FTIR, XRD, TEM/EDX, SEM, BET, TGA-DTA and particle size distribution. The effect of magnesium incorporation into hydroxyapatite structure is also discussed.

4.3.1 FTIR

FTIR studies were conducted for assessing the functional groups and bonding patterns in the sample as well as to evaluate the effect of magnesium incorporation on phosphate and hydroxyl groups. As presented in Figure 4.9, bands at 3560 and 633 cm^{-1} corresponds to the stretching and vibrational mode of -OH groups respectively. The characteristic PO_4^{3-} bands related with hydroxyapatite were seen at 566, 633, 980 and 1041 cm^{-1}. Precipitated powders generally have high specific surface area, due to which adsorbed water bands were spotted at 3000 – 3300 cm^{-1}. The bands observed in the range 1470 – 1410 cm^{-1} demonstrate that the CO_3^{2-} (carbonate) groups substitute phosphate in the hydroxyapatite lattice since the experiments are performed in air. Similar observations were noted by Suchanek et al. [131] and Farzadi et al. [156]. Spectra of M-i-HAP showed broadening and splitting of the characteristic PO_4^{3-} absorption bands due to presence of magnesium.

4.3.2 XRD

The XRD pattern of different forms of M-i-HAP and p-HAP is presented in Figure 4.10 . Hydroxyapatite peaks were distinctly observed and crystallographic identification of samples was achieved by using the standards of JCPDS (Joint committee on Powder diffraction) followed by matching them with experimental patterns obtained. All the peaks matched with card no. 09-0432 for hydroxyapatite and a peak for MgO was observed at 2θ of 37.5º (045-0946) demonstrating the incorporation of Mg^{2+} in HAP structure. Due to the large size difference between Mg and Ca radius (~0.28Å according to the Pauling scale) strong distortions of the hydroxyapatite lattice is observed which in turn reduces its crystallinity. As per Scherer equation, the calculated crystallite size was found to be 31.33 nm.

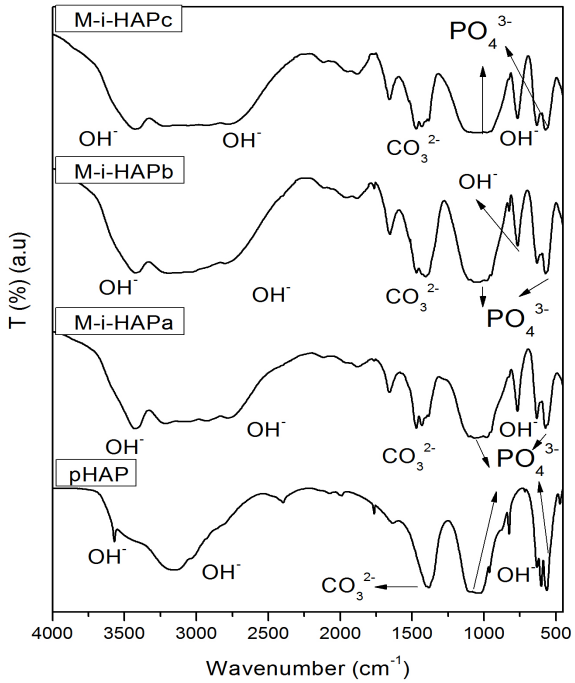

Figure 4.9: FTIR spectra for M-i-HAP and p-HAP

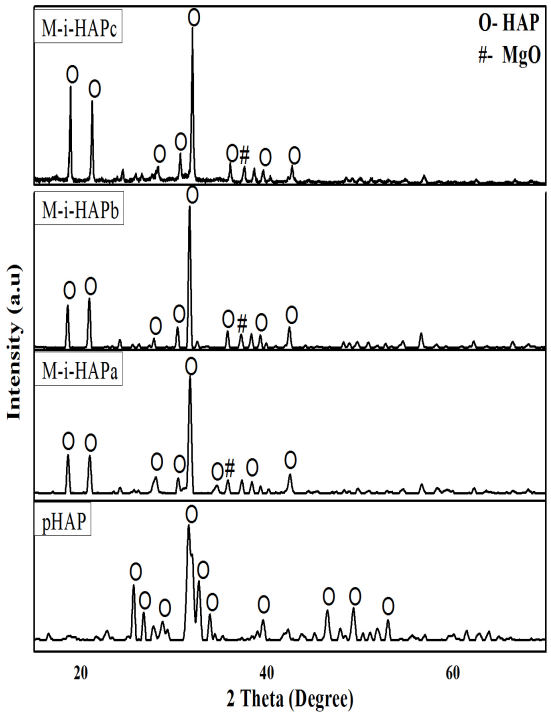

Figure 4.10: XRD pattern for M-i-HAP and p-HAP

4.3.3 SEM

SEM micrograph of pHAP (Figure 4.11a) shows distinct nano-rod morphology. It can clearly be seen in the Figure that introduction of magnesium into hydroxyapatite caused reduction in size of the rod-like structures. SEM image of pHAP was taken at 50000X magnification because below this, the nano rod structure of pHAP was not distinguishable. Large flake like structures were observed for M-i-HAPa and irregular shaped particles were found in the SEM image of M-i-HAPb. The micrograph of M-i-HAPc displayed more irregular particles clustered together. It is quite evident that M-i-HAPa (Figure 4.11b) has more porous texture to offer for adsorption of fluoride as compared to pHAP, M-i-HAPb and M-i-HAPc.

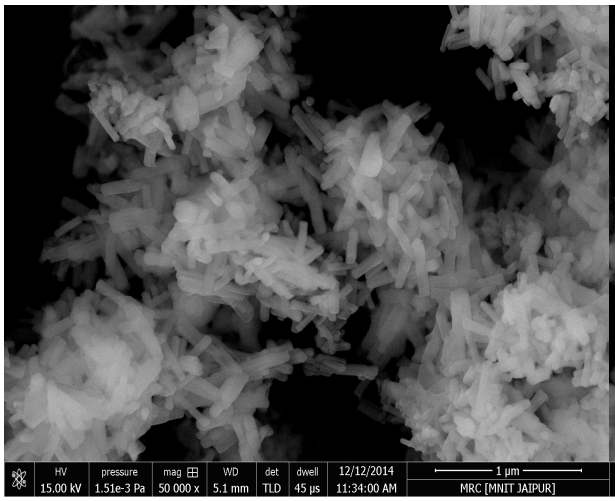

(a) SEM image of pHAP at 50000X

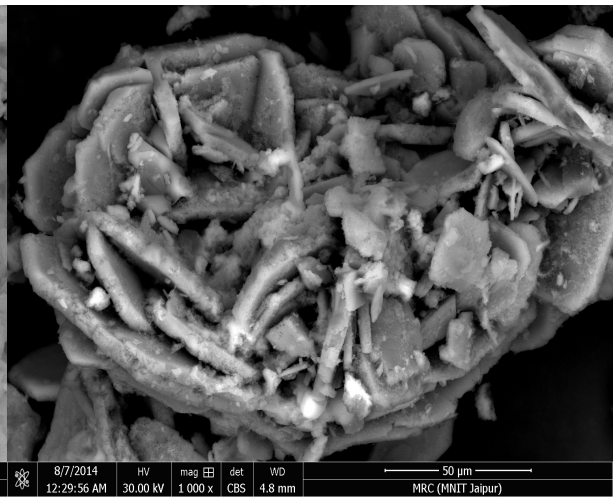

(b) SEM image of M-i-HAPa at 1000X

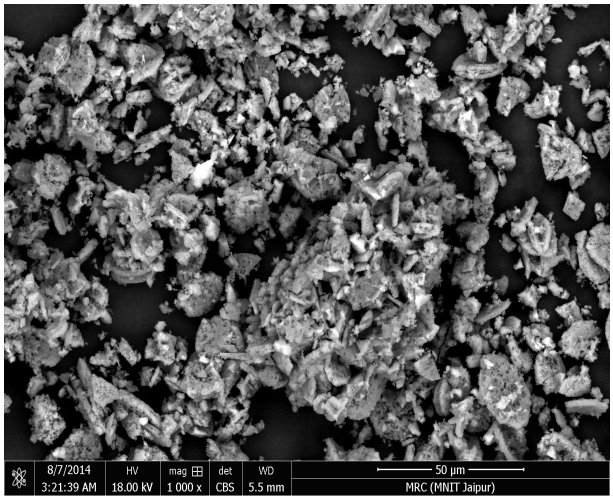

(c) SEM image of M-i-HAPb at 1000X

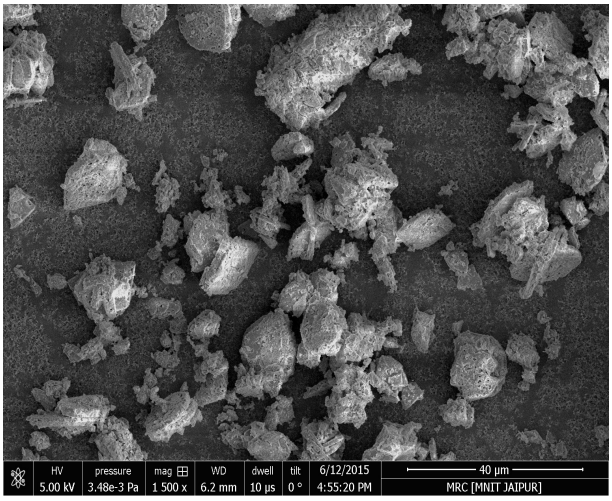

(d) SEM image of M-i-HAPc at 1000X

Figure 4.11: SEM images of pHAP and M-i-HAP

4.3.4 TEM/EDX

TEM images as shown in Figure 4.12 displayed elongated needle like nano-rod structure for pHAP and aggregated structures arranged in random orientations were observed for M-i-HAPs. Higher concentration of magnesium induces greater agglomeration and did not favor hydroxyapatite formation. Clear reduction of grain size on incorporation of magnesium into hydroxyapatite structure is observed. Particle size estimated from TEM for pHAP is 100 - 150 nm in length and 15 - 18 nm in width. The particle size was observed to be smaller after magnesium incorporation i.e 6 - 10 nm for M-iHAPa and M-i-HAPb. Owing to cluster formation particle size for M-i-HAPc could not be estimated accurately. Due to

higher agglomeration, spherical structures were noticed in TEM image of M-i-HAPa which may have attributed to its higher surface area as compared to pHAP.

The elemental composition of the adsorbents synthesized were analyzed through EDX and displayed in Figure 4.13. The EDX spectra for pHAP shows peaks of calcium, oxygen and phosphorus only (Figure 4.13a). On the other hand, in the EDX spectra for M-i-HAPa, M-i-HAPb and M-i-HAPc a peak for magnesium is also observed (Figure 4.13b,c and d). The intensity of magnesium peak is comparable for M-i-HAPa and M-i-HAPb; while for M-i-HAPc, the peak intensity was much higher. This is in accordance with the composition of the adsorbent synthesized in section 3.2.5.2, as greater amount of magnesium was introduced into M-i-HAPc.

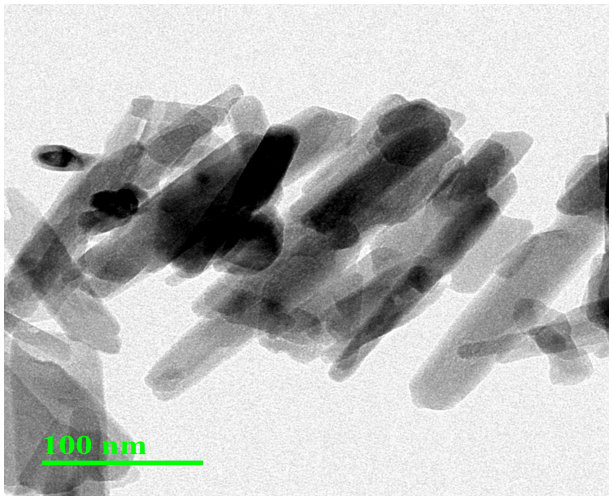

(a) TEM image of pHAP

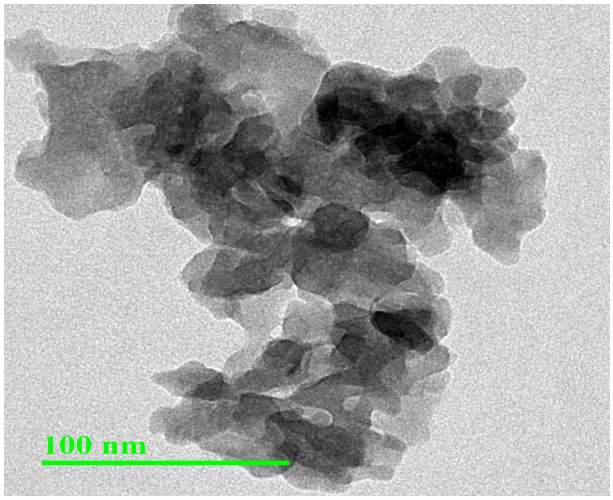

(b) TEM image of M-i-HAPa

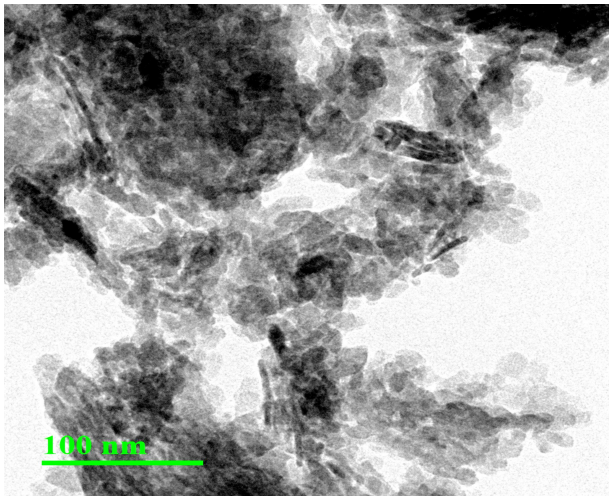

(c) TEM image of M-i-HAPb

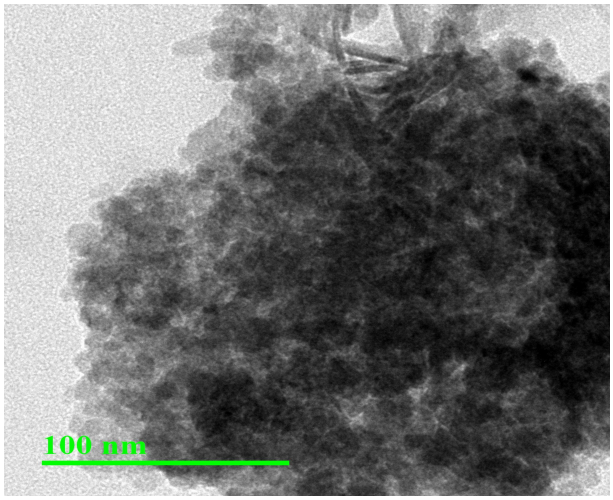

(d) TEM image of M-i-HAPc

Figure 4.12: TEM image of pHAP and M-i-HAPs at 100 nm

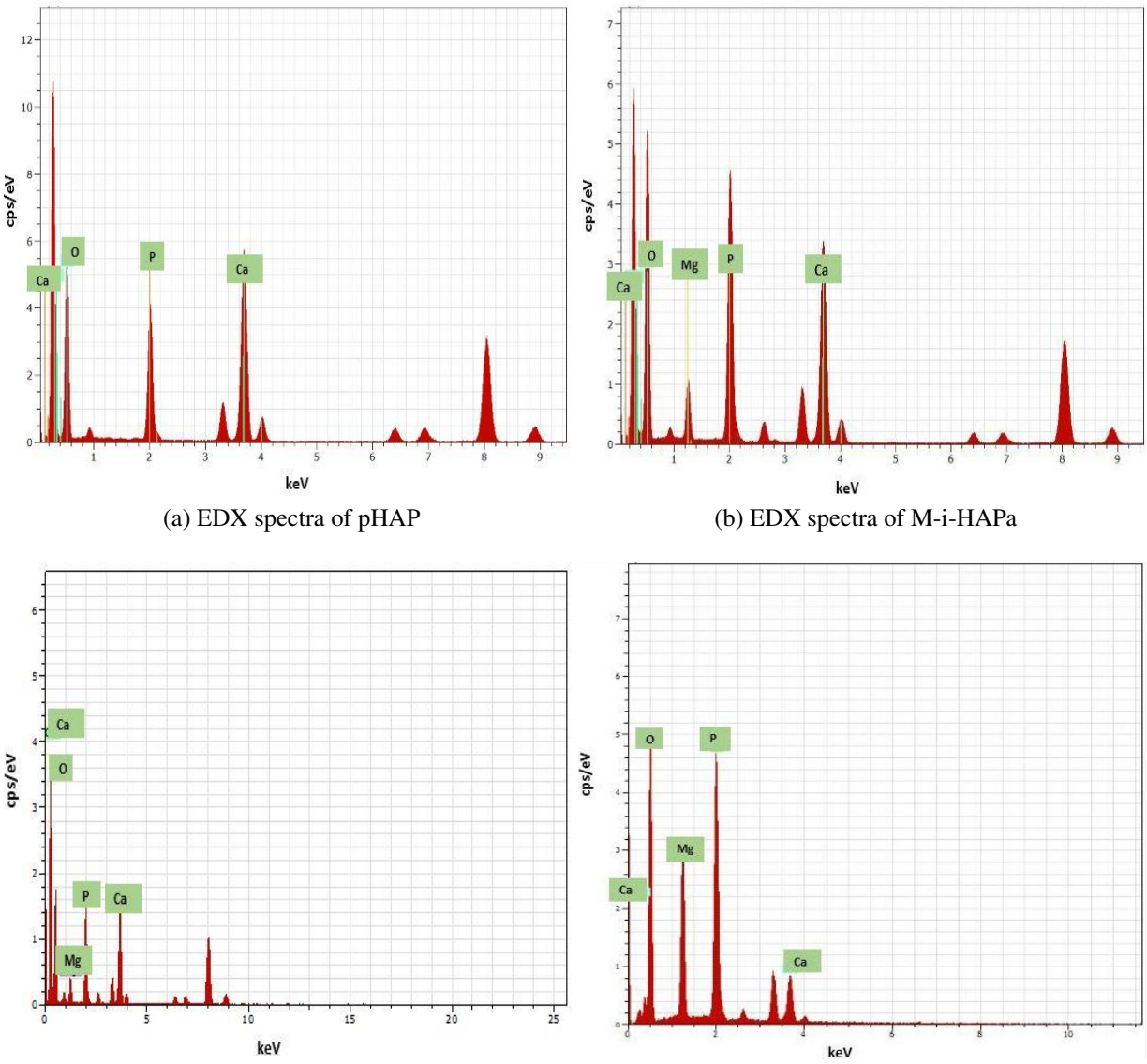

(a) EDX spectra of pHAP

(b) EDX spectra of M-i-HAPa

(c) EDX spectra of M-i-HAPb

(d) EDX spectra of M-i-HAPc

Figure 4.13: EDX spectra

The characterization results from SEM and TEM analysis clearly depicts that M-i-HAPa adsorbent has a better surface morphology and microstructure required for adsorption of fluoride. The same has been tested through a preliminary defluoridation study using pHAP, M-i-HAPa, M-i-HAPb and M-i-HAPc shown in section 5.7.1, Figure 5.22.

Therefore, characterization for surface area, particle size and thermal behaviour was carried out with M-i-HAPa adsorbent and pHAP was used for comparison of results.

4.3.5 BET

M-i-HAPa adsorbent exhibited a surface area of 46.62 m^2/g which is more than twice of pHAP (21.25 m^2/g). The increase in surface area may of M-i-HAPa may lead to higher fluoride removal capacity of the adsorbent. The pore volume and pore size of M-i-HAPa was 0.177 cm^3/g and 152.51 Å respectively while that of pHAP was 0.090 cm^3/g and 169.83 Å respectively. Figure 4.14 represents the nitrogen adsorption–desorption isotherm and the corresponding pore size and pore volume distributions of pHAP and M-i-HAPa respectively.

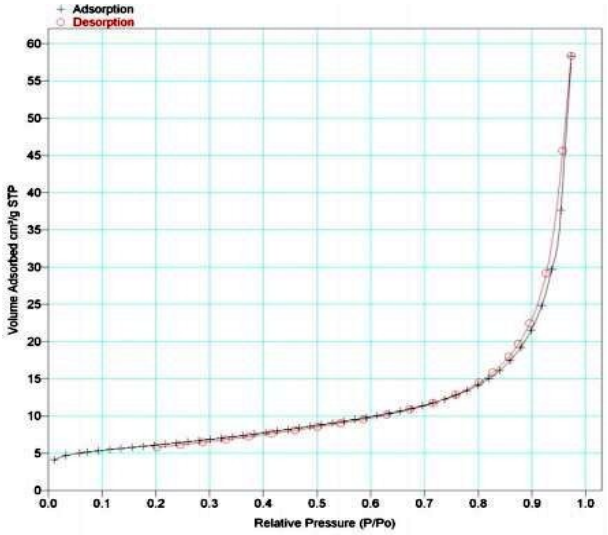

(a) BET surface area of pHAP

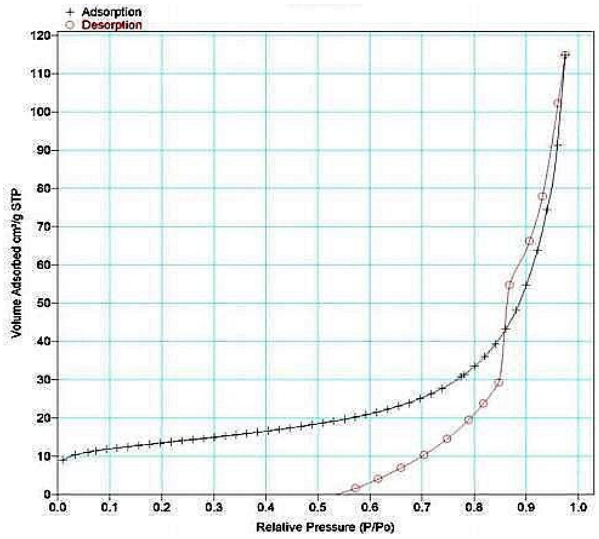

(b) BET surface area of M-i-HAPa

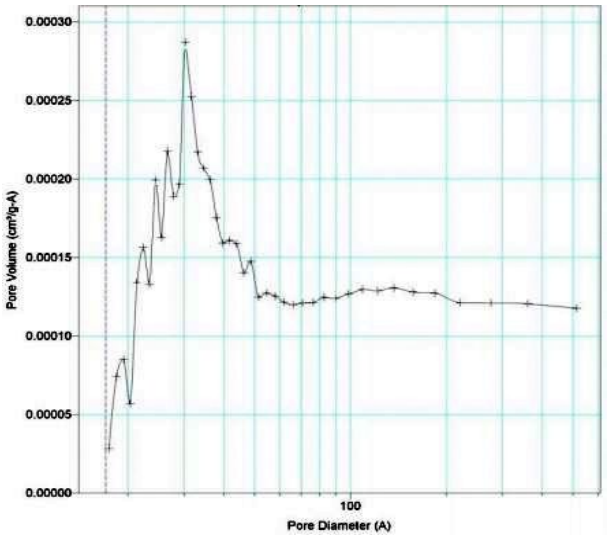

(c) Pore volume of pHAP

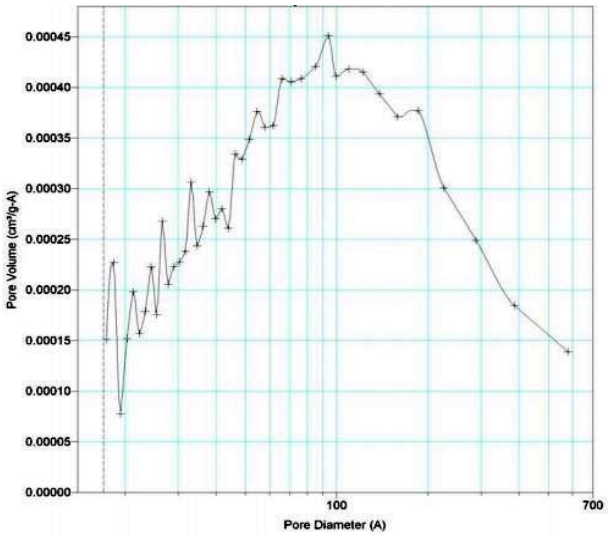

(d) Pore volume of M-i-HAPa

Figure 4.14: BET surface area and pore volume

4.3.6 Thermal analysis

The Thermogravimetric analysis and Differential thermal analysis as shown in Figure 4.15 depicted a four stage weight loss in pHAP and M-i-HAPa adsorbent with corresponding endothermic peaks. Upto 150 °C, 2% weight loss was observed in pHAP due to loss of surface water and 6.51 % weight loss was seen between temperature of 150 to 250 °C due to lattice water loss. From 250 to 500 °C, the graph shows a weight loss of 6.79 % because of conversion of hydrogen phosphates into pyrophosphates. Above 500 °C, the hydroxyapatite structure lost OH ions and converted to $\beta-$tricalcium phosphate with a weight loss of 3.7 %. Corresponding to each weight loss, the four endothermic peaks were spotted at 47 °C, 232 °C, 330°C and 442 °C.

In M-i-HAPa adsorbent, below 200 °C, loss of surface bound water (5.3 %) was seen, between 200 to 400 °C lattice water loss and carbonate loss (16.98 %) was noted. At temperature ranging from 400 to 600 °C, hydrogen phosphate (HPO_4^{2-}) coverts to pyrophosphate ($P_2O_7^{4-}$) and 2.57 % weight loss is detected while a weight loss of 1.85 % was noticed for temperature greater than 550 to 600°C due to loss of carbonate ions and OH^- ions during conversion to $\beta-$tricalcium phosphate. The four endothermic peaks observed corresponding to each stage of weight loss are at 131 °C, 256 °C, 365 °C and 563 °C respectively. It is noteworthy that the decomposition temperature decreased after incorporation of magnesium (M-i-HAPa) which confirmed that magnesium has entered the lattice structure of hydroxyapatite. If the magnesium ions had only been present on the surface , the decomposition temperature would have been unaffected. Ren et al. [157] also reported similar observations after substituting magnesium into hydroxyapatite lattice.

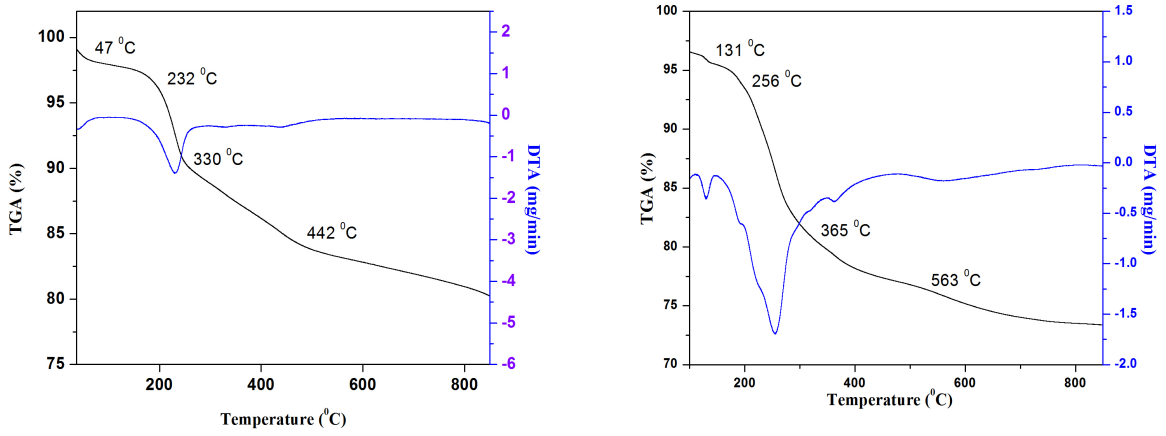

(a) TGA/DTA analysis of pHAP

(b) TGA/DTA analysis of M-i-HAPa

Figure 4.15: Thermal behavior of pHAP and M-i-HAPa

4.3.7 Particle size estimation

A particle size distribution analysis for pHAP and M-i-HAPa adsorbent are presented in Figure 4.16. The particle size analysis revealed a mean particle size of 417 nm for pHAP which was observed to decrease to 155 nm after magnesium was incorporated into pHAP (M-i-HAPa). A lower particle size supports higher removal for fluoride ions which indicate that M-i-HAPa may possess higher defluoridation capability than pHAP.

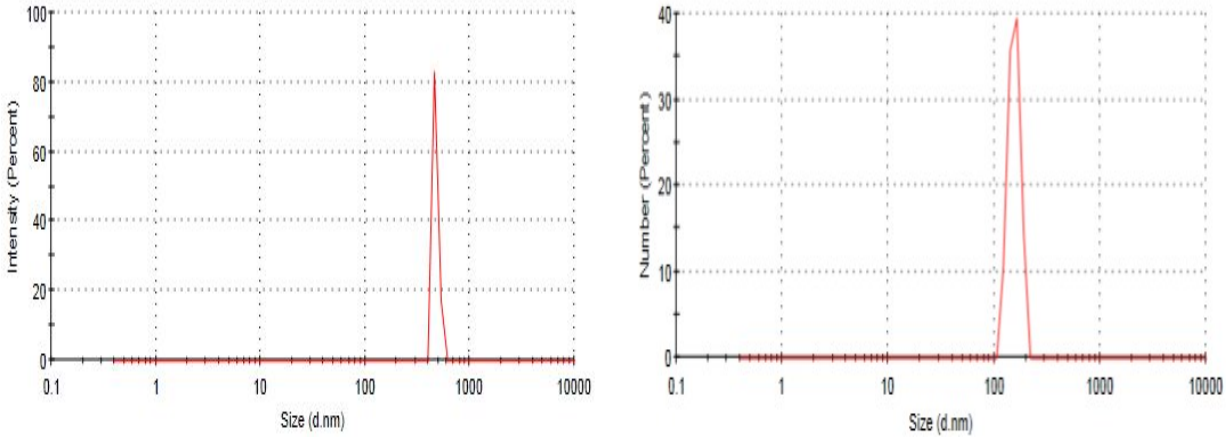

(a) pHAP (b) M-i-HAPa

Figure 4.16: Particle size distribution

4.4 Summary of the Chapter

This chapter emphasized on characterization of the adsorbents which were used in this study. A brief summary of this chapter in tabular form is presented in Table 4.1.

Table 4.1: Brief tabular summary of the Chapter

Adsorbent	Structure	Crystallite size (via XRD)	Particle size (TEM)	Surface texture	Surface area
CMA	Crystalline	43.55 nm	-	Densely agglomerated	-
Mg-HAP	Crystalline	65 nm	70 nm	Porous, agglomerated	-
M-i-HAPa	Crystalline	31.33 nm	6-10 nm	Irregular, Flake like structures, Clustered	46.62 m^2/g

The analysis of different characterization methods were done in terms of bonding pattern, mineral composition, microstructural detail, surface texture, thermal behaviour, surface area, pore volume, pore diameter and elements present. These studies assisted for selection of a suitable adsorbent i.e M-i-HAPa for further experimentation.

The next chapter is focused on the batch defluoridation studies conducted using different adsorbents and the various process parameters are discussed thoroughly.

CHAPTER 5

Chapter 5

Batch Defluoridation Studies

This chapter enlightens about the defluoridation potential of various adsorbents used in this study through batch experiments. These adsorbents are Activated calcite, Calcia-Magnesia adsorbent, Dolomite, Dicalcium phosphate, Natural Hydroxyapatite, Magnesia-Hydroxyapatite and Magnesium incorporated Hydroxyapatite. The chapter also discusses the effect of process parameters on defluoridation such as effect of pH, adsorbent dose, contact time, initial fluoride concentration, temperature and presence of interfering ions. Different adsorption isotherms and kinetic models were also studied for better understanding of mechanism of the process. Optimization studies using response surface methodology were performed for fluoride removal using only one adsorbent (Magnesium incorporated Hydroxyapatite) and a quadratic model was developed representing the fluoride removal efficiency and capacity.

Furthermore, the chapter describes the mechanism for fluoride adsorption using Magnesium incorporated Hydroxyapatite adsorbent and identifies an eluent for regeneration of the adsorbent. The findings of this chapter helped to choose a suitable adsorbent which can be converted into pellet form in order to conduct column studies.

5.1 Activated Calcite

Defluoridation experiments were conducted in batch mode for varying adsorbent dosage for determining the adsorption capacity of calcite. Different concentrations of fluoride water acidified using varying concentrations of glacial acetic acid were used to activate the calcite adsorbent for better removal of solute. The experiments were conducted at a temperature of 30 ± 0.5 ° C, contact time of 180 min and agitation rate of 200 rpm. The concentration of fluoride in all test samples was kept at 10 mg/L. The initial pH of water samples used for studying effect of calcite dose were 7.2 ± 0.1 whereas the initial pH of samples used

for testing effect of acid concentration varied from 1 to 3.39 according to variation in acid concentrations (Figure 5.4).

5.1.1 Effect of calcite dose

The effect of calcite dose on fluoride adsorption capacity of calcite was observed by varying the dose from 1 to 15 g/L as shown in Figure 5.1. The adsorption capacity was observed to decrease from 2.93 mg/g to 0.53 mg/g with corresponding increase in dose from 1 to 15 g/L. This suggests that with increase in the dose of calcite the adsorbent was not completely exhausted to its full capacity as the fluoride level was at a low concentration. The fluoride uptake capacity of calcite remained approximately constant after usage of 7 g/L of adsorbent; therefore this adsorbent dose was considered as optimum and used for conducting experiments regarding variation of acid concentration and contact time.

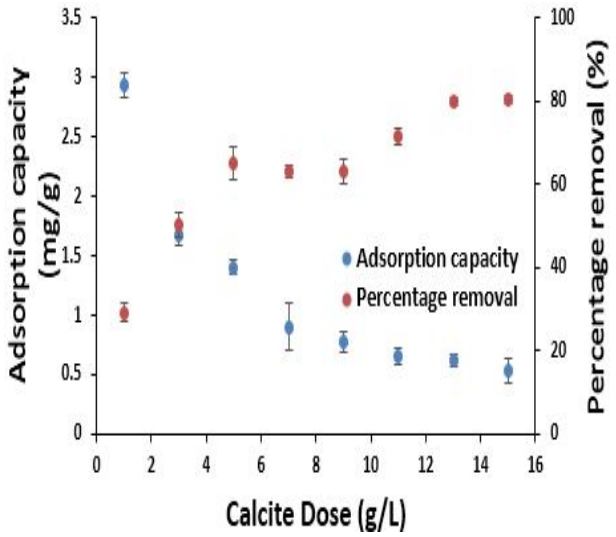

Figure 5.1: Effect of activated calcite dose on F^- adsorption capacity (contact time:180 min, initial fluoride concentration: 10 mg/L,dosage: 1-15 g/L)

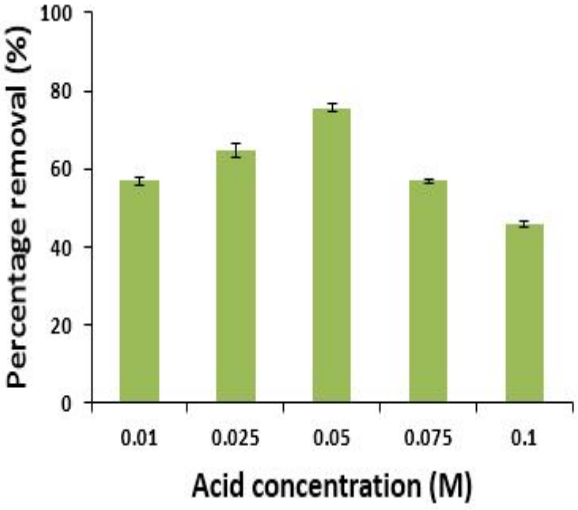

Figure 5.2: Effect of acid concentration on F^- removal efficiency of calcite (contact time:180 min, initial fluoride concentration: 10 mg/L,dosage: 7 g/L,acid concentration: 0.01-0.1 M)

5.1.2 Effect of acid concentration

To improve the capacity of calcite ions, it was activated using a weak acid (glacial acetic acid) as poor fluoride uptake capacity of calcite was reported in literature [48]. The effect of fluoride removal capacity of calcite at different concentrations of acetic acid (0.01, 0.025, 0.05, 0.075, 0.1 M) using 7 g/L dose is shown in Figure 5.2. The results depict that acetic

acid at concentrations of 0.05 M and 0.025 M was able to remove 75.6 % (1.08 mgF^-/g) and 64.9 % (0.92 mgF^-/g) of fluoride from a solution having 10 mg/L F^- concentration. Other concentrations of acetic acid viz. 0.01 M, 0.75 M and 0.1 M were less effective in removing fluoride from water than 0.05 M and 0.025 M concentrations. Therefore, these two acid concentrations were used for investigating the influence of contact time on removal capacity of activated calcite.

In acidic conditions, large amount of H^+ ions are present which dissolves the calcite surface, generates calcium ions and precipitates as CaF_2. As this occurs, new active sites form on surface of calcite and fluoride ions get adsorbed onto them [158, 159]. The following reaction shows the reaction of calcite ($CaCO_3$) and sodium fluoride:

$$CaCO_3 + 2NaF \rightarrow CaF_2 + Na_2CO_3 \tag{5.1.1}$$

The fact that adsorption phenomenon takes place instantaneously with precipitation was confirmed through change in surface morphology via SEM, as observed by Turner et al. [158]. The dissolution of calcium ions into solution continues, till calcium ions are available to replenish the dissolved Ca^{2+} ions.

5.1.3 Effect of contact time

The influence of contact time on fluoride removal using activated calcite adsorbent was determined by measuring the residual fluoride ion concentration in samples withdrawn up to 210 min. Since acetic acid concentrations of 0.025 M and 0.05 M removed the highest amount of fluoride from solution (Figure 5.2), these were used in the experiments for effect of contact time on F^- removal efficiency. As observed from Figure 5.3, the removal rate of fluoride was rapid at first, but it gradually reached equilibrium at 180 min. The graph in Figure 5.3 shows initial high rate of adsorption followed by a plateau indicating that equilibrium is attained. After 180 min, the fluoride removal reached to an equilibrium point for both 0.025 M and 0.05 M of acidified fluoride sample solutions. In case of 0.05 M acidified sample, 71 % F^- removal (1.01 mgF^-/g adsorbent) was achieved in 180 min while in case of 0.025 M acidified sample, 65 % F^- removal (0.92 mgF^-/g adsorbent) was achieved in the same time period. This shows that at higher concentration of acid the fluoride removal rate is higher and faster due to higher rate of dissolution of calcium ions.

Still, the residual fluoride concentration was found to be much higher than 1.0 mg/L (permissible limit).

5.1.4 Effect on pH of treated water

The pH of the water was checked at different concentration of acidified fluoride water before adsorption and after adsorption with activated calcite as shown in Figure 5.4. The concentration of fluoride ions in the samples were initially 10 mg/L with 7 g/L calcite dose and the samples were provided a contact time of 180 min. pH of water treated with activated calcite was observed to be 6.7 to 7.4. According to WHO and BIS, the pH of drinking water may vary but it should be in the range of 6.5 to 8.5 [13, 72]. Therefore, the pH after adsorption was under the permissible range.

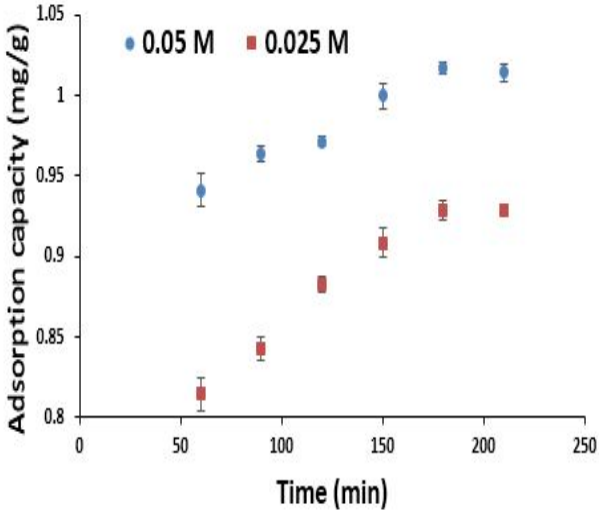

Figure 5.3: Effect of contact time on F^- removal capacity of activated calcite (contact time: 60-210 min, initial fluoride concentration: 10 mg/L,dosage: 7 g/L)

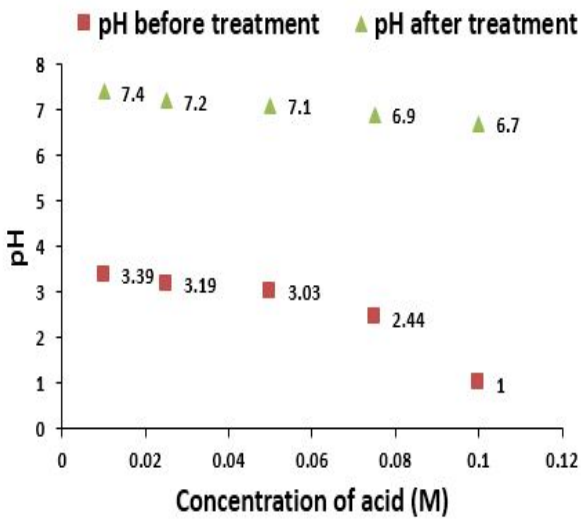

Figure 5.4: Effect on pH of water after and before treating with activated calcite (contact time:180 min, initial fluoride concentration: 10 mg/L,dosage: 7 g/L)

5.1.5 Conclusion

Calcite was used as an adsorbent for defluoridation studies. It was then activated using acetic acid for enhancing the fluoride removal efficiency. Before activating the calcite, fluoride removal efficiency and capacity were 65.03 % and 0.89 mg/g respectively; which increased to 75.6 % and 1.08 mg/g respectively after using acetic acid concentration of 0.05 M for activation procedure. The pH of treated water was observed to be in the range of 6.7 and 7.4.

However, the fluoride removal efficiency was still low even after acid treatment and activated calcite dose as high as 15 g/L also could not bring the residual fluoride

concentration to permissible limit required (1.0 mg/L). Therefore, activated calcite was not studied further for defluoridation of water.

5.2 Calcia-Magnesia Adsorbent (CMA)

Calcia-Magnesia adsorbent was synthesized in the laboratory and the effect of CMA dose, pH of solution and initial fluoride concentration on fluoride removal was studied. The results obtained are discussed in the following sections:

5.2.1 Effect of CMA dose

The effect of CMA dose on fluoride removal was studied using an adsorbent concentration of 1 to 10 g/L at fixed fluoride concentration of 10 mg/L, 200 rpm agitation rate, 30 ± 0.5 ºC temperature and 180 min of contact time. While exploring the effect of adsorbent dose it was observed that the adsorption capacity in treated water gradually decreased with increase in CMA dose and then became nearly constant. It was observed that an optimum removal can be achieved with 5 g/L of CMA (Figure 5.5). It was the minimum adsorbent dose required to keep the fluoride concentration under permissible limit (less than 1.0 mg/L), and further increase in the dose did not affect the capacity significantly. Therefore, the dose of 5 g/L of CMA was used for experiments regarding influence of pH and initial fluoride concentration.

5.2.2 Effect of pH

The effect of pH on fluoride removal was tested using 5 g/L of adsorbent dose in fluoride solutions of 10 mg/L concentration for 180 min contact time at pH of 5, 6, 7, 8 and 9 and 30 ± 0.5 º C temperature. The percentage removal of fluoride at different pH is reported in Figure 5.6. The figure shows that the fluoride removal is maximum at pH 7 and is minimum at pH 5 and 9. With increasing pH, fluoride removal percentage also increased from 56 to 84.1 %, while beyond pH 7 the removal rate decreased linearly to 64.5 %. At lower pH, hydrofluoric (HF) acid are formed which offers a competition with fluoride ions for adsorption sites while at higher pH, the competition is between OH^- ions and fluoride ions causing a decrease in fluoride removal. Raichur and Basu [160] and Das et al. [161] observed similar trend with the results for effect of pH on fluoride removal efficiency while working with mixed rare earth oxide and Zn/Al hydrotalcite-like compound adsorbent.

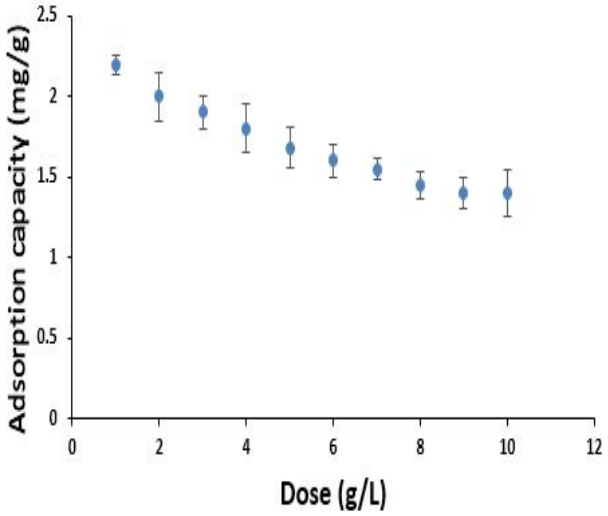

Figure 5.5: Effect of CMA dose on F^- removal capacity (contact time:180 min, initial fluoride concentration: 10 mg/L,dosage: 1-10 g/L)

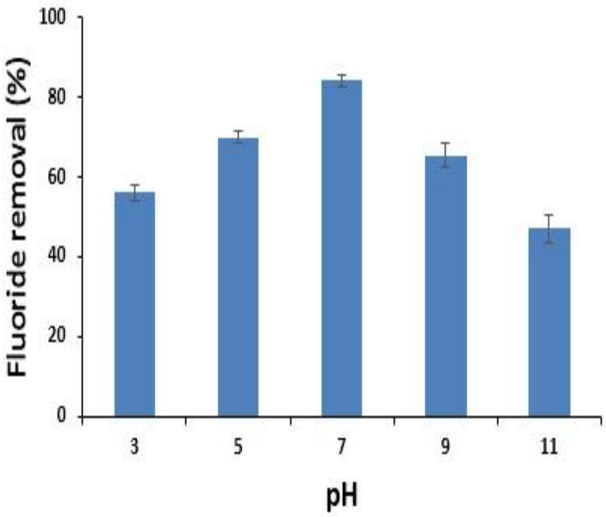

Figure 5.6: Effect of pH on F^- removal efficiency of CMA (contact time:180 min, initial fluoride concentration: 10 mg/L,dosage: 5 g/L)

5.2.3 Effect of initial fluoride concentration

CMA adsorbent dose of 5 g/L was used to examine the effect of varying initial fluoride concentrations on fluoride removal capacity of CMA at constant temperature of 30 ± 0.5 ° C and 200 rpm agitation rate (Figure 5.7). The concentration of fluoride solutions used were 2, 4, 6, 8, 10 mg/L and a contact time of 180 min was given to each test sample. As the initial fluoride concentration was increased, the fluoride removal capacity also increased, due to higher availability of fluoride ions at higher concentrations and it became nearly constant after reaching equilibrium.

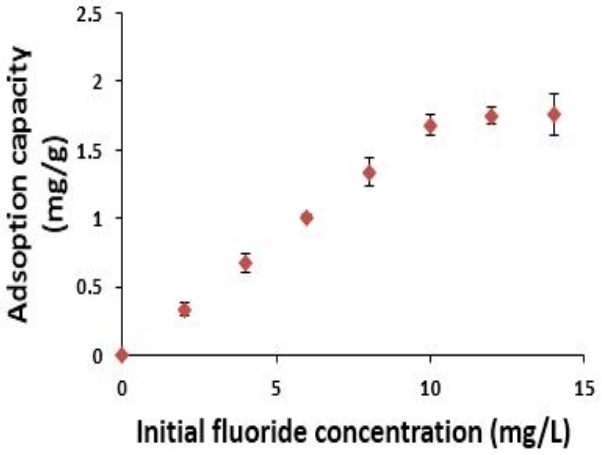

Figure 5.7: Effect of initial fluoride concentration on F^- removal capacity of CMA (contact time: 180 min, initial fluoride concentration: 2-10 mg/L,dosage: 5 g/L)

5.2.4 Adsorption isotherms

Two adsorption isotherm models Langmuir and Freundlich were fitted to the experimental data using CMA as adsorbent. The graph for Langmuir isotherm was plotted between C_e/q_e vs C_e and for Freundlich isotherm model the graph was plotted between log q_e vs log C_e as shown in Figure 5.8a and 5.8b respectively. The values of different parameters of the models were calculated using Eq. 3.4.13 and Eq. 3.4.15 for Langmuir and Freundlich isotherm respectively.

The maximum adsorption capacity deduced from Langmuir isotherm model is 0.505 mg/g, the term 'b' a constant related to energy was calculated to be 3.39 L/g and the value of R^2 was 0.979. The separation factor (R_L) was calculated to be 0.034 which is less than 1, suggesting feasibility of the process. However, it is evident from Figure 5.8 that the adsorption pattern fits best to Freundlich isotherm with a R^2 value of 0.999. Also, the experimental value for fluoride uptake capacity (1.68 mg/g) of CMA adsorbent matches more closely with the Freundlich adsorption capacity value (K_f = 1.047 mg/g). Chi-squared test was applied to these models and the value for Freundlich model was found to be 0.13 while that of Langmuir was 0.69. Clearly, Freundlich model has a smaller chi square value and hence a better isotherm fit. This means that the adsorption process is multilayed in nature. The heterogeneity factor '1/n' was found to be 0.9 which lies between 0.1 and 1 depicting a favorable adsorption process.

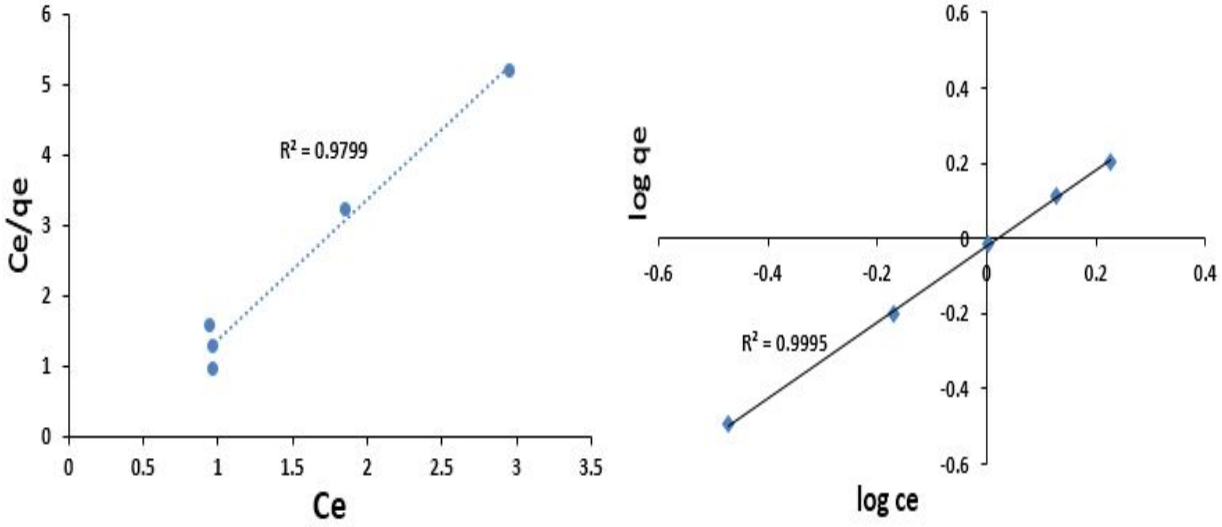

(a) Langmuir isotherm (b) Freundlich isotherm

Figure 5.8: Adsorption Isotherms for CMA adsorbent

5.2.5 Leaching of calcium and magnesium from CMA

The treated water with 5 g/L CMA dose was investigated for leaching experiments. Calcium and magnesium ions were found to be leaching into water from the adsorbent with concentrations 120 and 87 mg/L respectively. Figure 5.9 shows that calcium and magnesium leaching was beyond the permissible limits of 75 and 30 mg/L respectively. It is evident that due to leaching of magnesium and calcium into treated water, the TDS and total hardness also increased to concentrations of 420 and 480 mg/L respectively which were also close to the permissible limit of 500 mg/L. High leaching of elements from adsorbent indicate a low stability of CMA adsorbent in solution and is not desirable. Moreover, SEM studies indicated non-uniform distribution of calcium and magnesium in form of dense agglomerates. Therefore, this adsorbent was not found suitable for defluoridation and was not studied further.

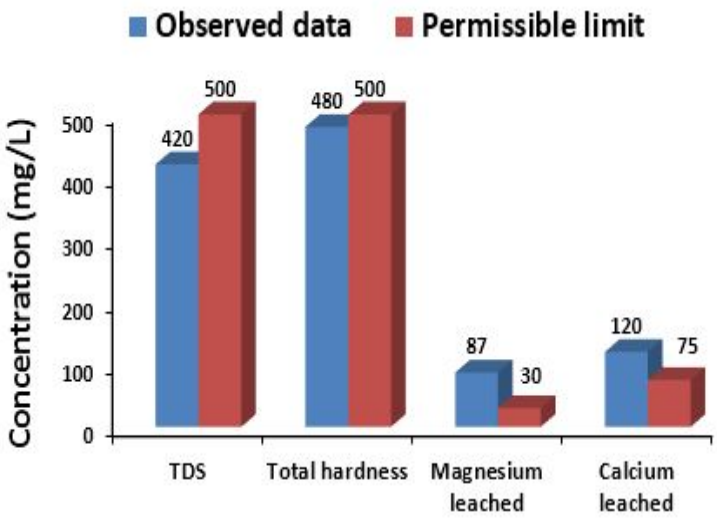

Figure 5.9: Treated water quality after F^- adsorption on CMA (Permissible limit given as per WHO and BIS [13, 72])

5.2.6 Conclusion

The defluoridation capability of CMA adsorbent has been found effective with a fluoride uptake capacity of 1.68 mg/g. Characterization of CMA had revealed formation of calcium and magnesium based compounds (section 4.1.2) which were responsible for adsorption of fluoride onto CMA. Freundlich isotherm model has been observed to be best fit to the experimental data obtained with a R^2 value of 0.999. This depicts a multilayer adsorption pattern of fluoride on Calcia-Magnesia adsorbent. The adsorbent worked very well at pH 6.5 to 7.5 range while in acidic and alkaline conditions the removal efficiency was found to decrease.

The limitation encountered with CMA adsorbent was that a large amount of calcium and magnesium leached into treated water which increased the TDS as well as total hardness of water. Due to these limitations, this adsorbent was not used for further experimentations.

5.3 Dolomite

Dolomite [$CaMg(CO_3)_2$] is a very abundantly found material and consists of calcium-magnesium carbonate compound. It is often referred as magnesium-limestone in industry due to similarity of properties with limestone [162]. Dolomite was used as procured without any modifications and batch defluoridation studies with varying adsorbent dose was performed.

5.3.1 Effect of dolomite dose

To study the effect of dolomite dose on fluoride removal capacity, a fluoride solution of 10 mg/L concentration was used with agitation rate of 200 rpm for 180 min, at neutral pH and 30 ± 0.5 ° C temperature. Dolomite dose was varied from 5 to 25 g/L and it was observed that the amount of fluoride loaded per unit weight of sorbent (adsorption capacity) gradually decreased with increase in dose from 0.552 mg/g to 0.322 mg/g. But, the residual fluoride concentration was above the permissible limit for all doses of dolomite. Since, the capacity of dolomite was very low, experiments with varying pH, contact time, initial fluoride concentration were not carried out. Therefore, it was concluded that dolomite can not be used as a potential adsorbent for defluoridation of water.

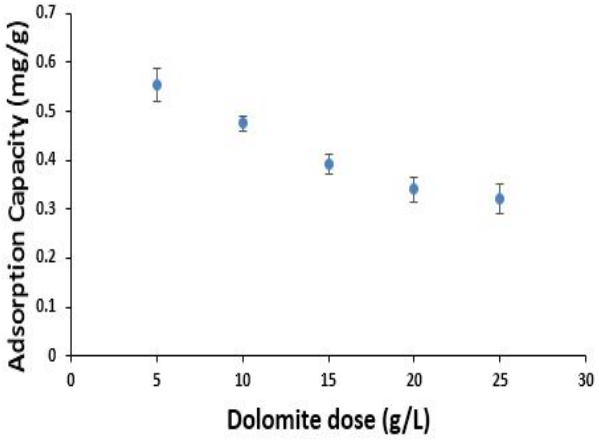

Figure 5.10: Effect of Dolomite dose on F^- removal capacity (contact time: 180 min, initial fluoride concentration: 10 mg/L,dosage: 5-25 g/L)

5.3.2 Conclusion

The capacity for fluoride adsorption by Dolomite adsorbent was found to be very low (0.322 mg/g). Even at dolomite concentration as high as 25 g/L, the residual fluoride concentration in water was 2 mg/L which was still still higher than the permissible limit required (1.0 mg/L [13]). Using concentrations higher than this was not advisable since it would cause increase the TDS and hardness of treated water. Keeping these shortcomings in mind, dolomite adsorbent was not used for further defluoridation studies.

5.4 Dicalcium phosphate ($CaHPO_4$)

Dicalcium phosphate is mostly used as a food additive, sometimes found in toothpastes as a polishing agent and is basically a biomaterial. Dicalcium phosphate was used as an adsorbent for investigating its defluoridation capacity in batch mode through varying the adsorbent dose.

5.4.1 Effect of dicalcium phosphate dose

The dose of dicalcium phosphate was varied from 2 to 12 g/L and other parameters such as F^- concentration (10 mg/L), agitation rate (200 rpm) , temperature (30 ± 0.5 ° C) and contact time (180 min) were kept constant. The adsorbent showed very good removal capacity and even with lower dose of 2 g/L the residual fluoride obtained was below 1.0 mg/L. The adsorption capacity decreased with increase in dose and became nearly constant after 8 g/L dose as shown in Figure 5.11.

However, the limitation faced with this adsorbent was the low pH of treated water. The pH of water after adsorption was found to be between 5 to 5.4 for all adsorbent doses due to formation of phosphoric acid in the solution. The reactions occurring in the solution are as follows:

$$CaHPO_4.2H_2O \rightleftharpoons Ca^{2+} + HPO_4^{2-} \tag{5.4.1}$$

$$HPO_4^{2-} + H^+ \rightleftharpoons H_2PO_4^- \tag{5.4.2}$$

$$H_2PO_4^- + H^+ \rightleftharpoons H_3PO_4\,(Phosphoric\,acid) \tag{5.4.3}$$

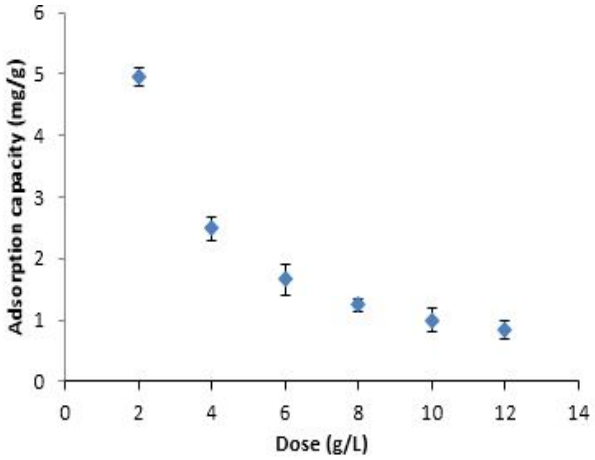

Figure 5.11: Effect of Dicalcium phosphate dose on F^- removal capacity (contact time:180 min, initial fluoride concentration: 10 mg/L,dosage: 2-12 g/L)

5.4.2 Conclusion

Dicalcium phosphate as an adsorbent showed good defluoridation capacity of 2 mg/g but due to formation of phosphoric acid in the treated water the pH was lower than permissible range for drinking water. Therefore, no further studies were conducted using dicalcium phosphate as an adsorbent.

5.5 Natural-Hydroxyapatite (aHAP)

Natural hydroxyapatite used for batch defluoridation was of animal origin (bovine bones) and therefore named as aHAP. It was used as procured from the market without any modifications and the effect of aHAP dose was studied as discussed in the following section:

5.5.1 Effect of aHAP dose

To examine the effect of aHAP dose on fluoride uptake capacity, a solution of 10 mg/L F^- concentration was used and the sample was given a contact time of 180 min at 200 rpm and 30 ± 0.5 ° C . The dose of aHAP was varied from 5 to 30 g/L as shown in Figure 5.12. The capacity of adsorption decreased with increase in adsorbent dose because at lower aHAP dose the capacity was more owing to the better use of the available adsorption sites while when the aHAP dose was higher large number of sites were available for limited quantity of fluoride ions. Using high aHAP dose even 30 g/L, was unable to bring the residual fluoride concentration in the solution below 1.0 mg/L (permissible limit).

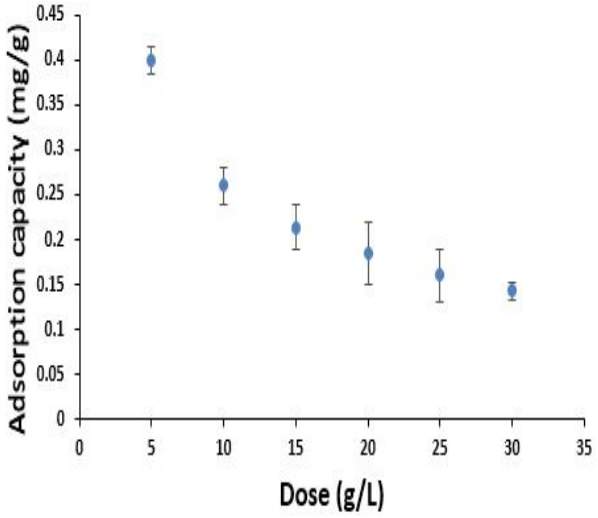

Figure 5.12: Effect of aHAP dose on F^- removal capacity (contact time:180 min, initial fluoride concentration: 10 mg/L,dosage: 5-30 g/L)

5.5.2 Conclusion

Very low fluoride removal was achieved using natural hydroxyapatite (adsorption capacity: 0.133 mg/g), therefore it was modified using magnesium hydroxide as described in the following section for further experiments.

5.6 Magnesia-Hydroxyapatite (Mg-HAP)

Mg-HAP was prepared from aHAP to increase the fluoride removal capacity of the adsorbent. Batch defluoridation studies for effect of adsorbent dose, pH of solution, contact time and interfering ions were conducted and are discussed in the following sections.

5.6.1 Effect of Mg-HAP dose

Experiments were carried out for studying the effect of adsorbent dose on removal of fluoride using Mg-HAP for initial fluoride concentration of 10 mg/L, agitation rate of 200 rpm and at 25 ± 0.5 °C for a contact time of 180 min (Figure 5.13). It was observed that percentage removal of fluoride increased with the increase in adsorbent dose gradually; however, beyond 10 g/L of adsorbent dosage, no significant removal was observed. The amount of fluoride loaded per unit weight of adsorbent gradually decreased for the same due to lower concentration of fluoride available at higher adsorbent dose. It was observed that percent fluoride removal increased from 48.7 to 92.34% with an increase in Mg-HAP

dose from 2 to 10 g/L at an initial fluoride concentration of 10 mg/L. This is due to the increase in the ratio of active sites to fluoride ions present. On further increasing the dose of adsorbent to 24 g/L, no significant removal was observed because of the very low equilibrium concentration of fluoride, in other words low driving force was responsible for adsorption. The fluoride concentration was reduced from 10 to 0.766 mg/L in aqueous solution thus attaining the permissible limit of fluoride in drinking water according to WHO (1.5 mg/L) and BIS (1.0 mg/L) at an Mg-HAP dose of 10 g/L [13, 72]. Hence, 10 g/L dose was selected for further experiments.

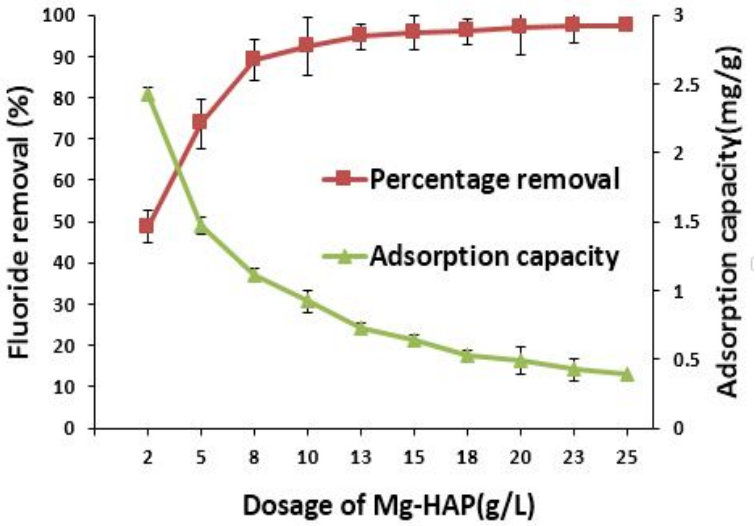

Figure 5.13: Effect of Mg-HAP dose on F^- removal capacity and efficiency (contact time:180 min, initial fluoride concentration: 10 mg/L,dosage: 2-24 g/L)

5.6.2 Effect of pH

The pH of the aqueous solution plays an important role in controlling the fluoride adsorption at the adsorbent–water interface. Therefore, the adsorption of fluoride on Mg-Hap was examined at various pH ranges from pH 3 to 11 with 10 mg/L as initial fluoride concentration at room temperature (25 ± 0.5 °C). It can be inferred from Figure 5.14a that percent fluoride removal varied from 96.02 to 94.47 % over the entire pH range of 3 to 11 for Mg-HAP. Slighly higher removal efficiency was observed in acidic pH range and there was not much significant effect of pH as compared to conventionally used adsorbents such as activated alumina which is an added advantage of the Mg-HAP over other adsorbents. Concentration of dissolved calcium ions at different pH varying from 3 to 10 is also given in Figure 5.14b. It was observed that at pH 9 and 10 (alkaline conditions), there was some release of calcium into water of 17.4 and 19.13 mg/L, respectively. Leaching of calcium in

alkaline conditions has also been reported while working with calcium aluminate adsorbent [79].

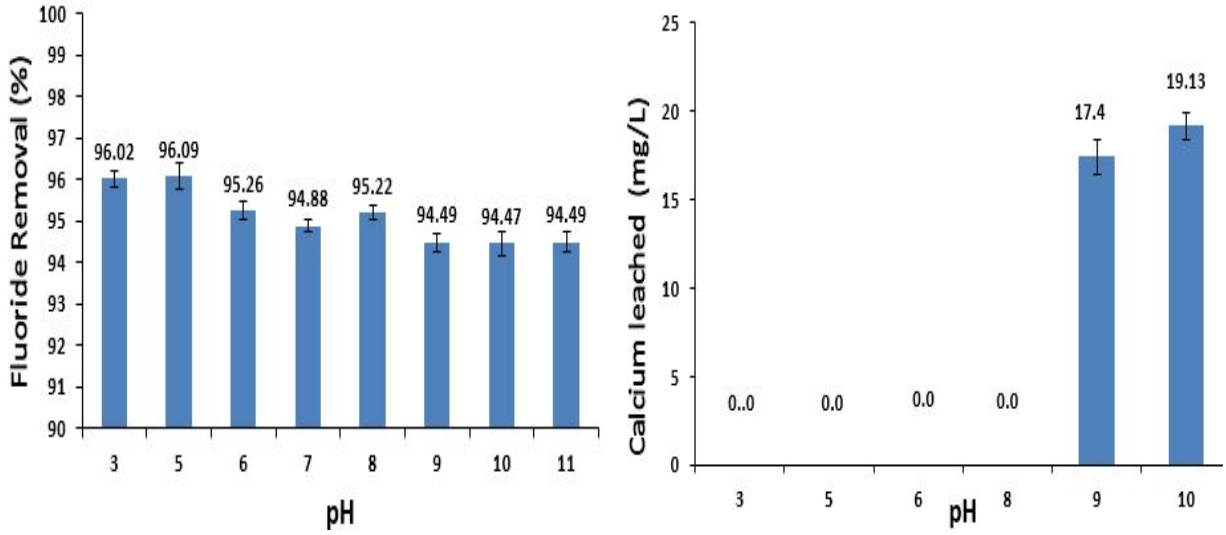

(a) Effect of pH on fluoride removal efficiency

(b) Calcium leaching from treated water

Figure 5.14: Effect of pH on F^- removal efficiency of Mg-HAP (contact time: 180 min,pH: 3-11, initial fluoride concentration: 10 mg/L,dosage: 10 g/L)

5.6.3 Effect of contact time

The adsorption capacity of fluoride as a function of contact time for Mg-HAP is shown in Figure 5.15. The study was conducted for a duration of 15 to 480 min with 10mg/L fluoride concentration and adsorbent dose of 10 g/L. As the contact time between adsorbate and adsorbent increased, it was noticed that the percentage of fluoride removal also increased up to equilibrium point (180 min) and then beceme constant and no significant removal occured thereafter.

5.6.4 Effect of initial fluoride concentration

The effect of initial fluoride concentration on fluoride adsorption by Mg-HAP was studied by keeping all other parameters constant (Mg-HAP dose 10 g/L, temperature 25 ± 0.5 °C, shaking speed 200 rpm, contact time 180 min, and pH 7.5 ± 0.1) as shown in Figure 5.16. It was observed that with an increase in fluoride concentration from 2 to 20 mg/L, the residual fluoride in treated water also increases due to more availability of fluoride ions at higher fluoride concentration for adsorption. Eventually, the binding capacity of the adsorbent reaches saturation, resulting in an increase of residual fluoride in water.

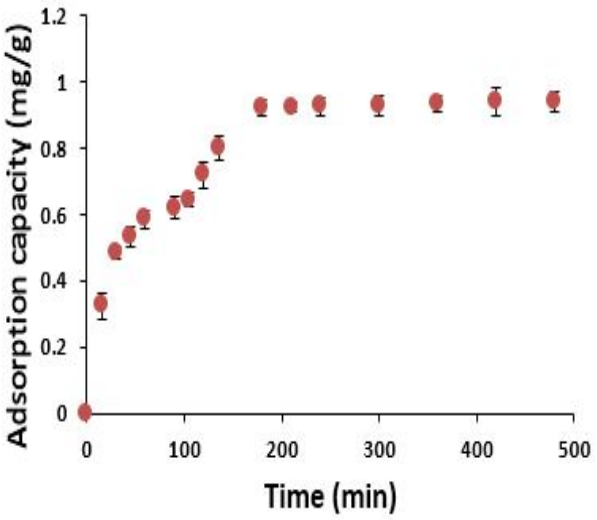

Figure 5.15: Effect of contact time on F^- removal capacity of Mg-HAP (contact time: 15-480 min, initial fluoride concentration: 10 mg/L, dosage: 10 g/L)

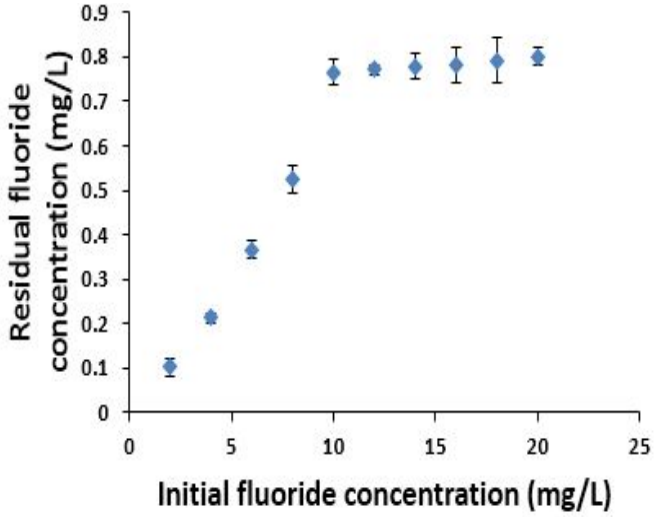

Figure 5.16: Effect of initial F^- concentration on residual F^- concentration (contact time: 180 min, initial fluoride concentration: 2-20 mg/L, dosage: 10 g/L)

5.6.5 Effect of interfering ions

Drinking water usually contains other ions such as chloride, sulfate, nitrate, phosphate, and bicarbonate, which may compete with fluoride during the adsorption process. Hence, it is necessary to study the effect of coexisting ions on the removal of fluoride. Batch adsorption studies were performed at varying initial concentrations of Cl^-, SO_4^{2-}, NO_3^{2-}, PO_4^{2-}, and HCO_3^- in the range of 100, 200, and 300 mg/L by keeping other parameters such as Mg-HAP dosage (10 g/L), fluoride concentration (10 mg/L), temperature (25 ± 0.5 °C), shaking speed (200 rpm), and contact time (180 min) constant. The effect of co-ions on the fluoride removal efficiency for Mg-HAP is depicted in Figure 5.17. It was observed that even in the presence of high concentrations of nitrate and chloride ions (300 mg/L), there was negligible effect on fluoride removal capacity. This is due to the fact that fluoride ions competed more than chloride and nitrate ions. However, the presence of phosphate ions in aqueous medium exhibited strong hindrance in fluoride adsorption capacity. The orders of interference by these competing ions from lower to higher are in the following order: nitrate < chloride < sulfate < bicarbonate < phosphate, but such high concentrations of ions are seldom present in drinking water.

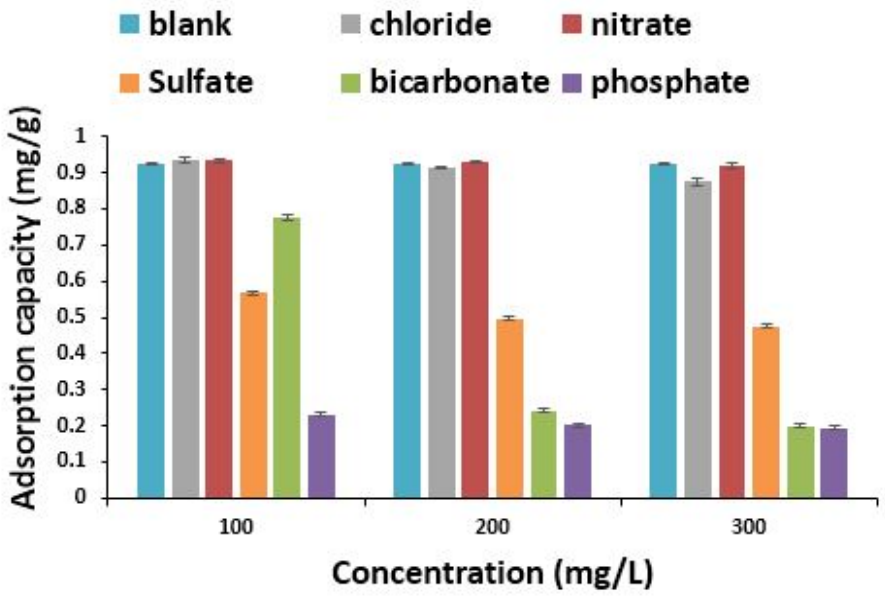

Figure 5.17: Effect of interfering ions on F^- removal capacity of Mg-HAP (contact time: 180 min, initial fluoride concentration: 10 mg/L, dosage: 10 g/L, anion concentration: 100-300 mg/L)

5.6.6 Adsorption isotherms

Adsorption of fluoride onto Mg-HAP involves the establishment of equilibrium between the fluoride adsorbed on the surface of Mg-HAP and the concentration of fluoride ions in solution.

The four isotherm models studied were Langmuir, Freundlich, Temkin and Dubinin-Radushkevich and are given in Figure 5.18. The various isotherm parameters with their values are presented in Table 5.1. The experimental data were fitted to the linearised adsorption isotherm models explained in section 3.4.6. Both R^2 and χ^2 values were considered for determining the best fitted isotherm model. The fit of the data to Langmuir isotherm model indicated that adsorption is monolayer in nature. The Langmuir adsorption capacity Q_0 was found to be 1.4 mg/g and the R_L(separation factor) value was 0.024, depicting favorable nature of the process. The K_{ap} value (product of Q_0 and constant b) was found to be 5.472 which show high affinity of Mg-HAP adsorbent towards fluoride ions.

Further, the experimental fluoride uptake capacity and the capacity predicted by different isotherms models were compared, and the results are presented in Figure 5.19 which confirmed Langmuir isotherm as the best model to describe the adsorption mechanism.

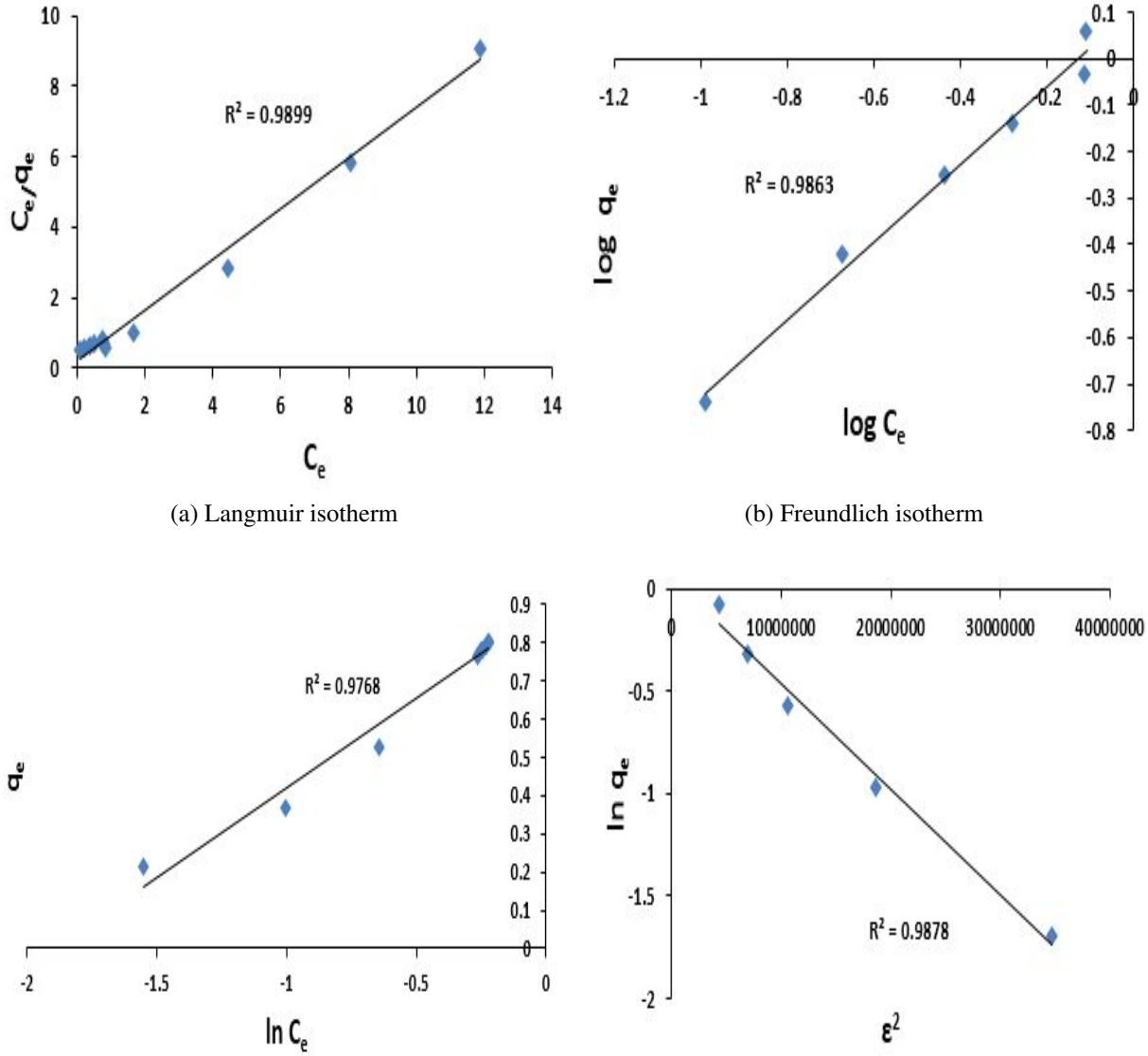

(a) Langmuir isotherm

(b) Freundlich isotherm

(c) Temkin isotherm

(d) Dubinin-Radushkevich isotherm

Figure 5.18: Adsorption isotherms for Mg-HAP

5.6.7 Adsorption kinetics

For estimating the efficiency of adsorption systems, kinetic study is considered an important aspect. Pseudo-first order, pseudo-second order and intraparticle diffusion models were studied in order to test the adsorption data.

The rate constant (k_1) and theoretical equilibrium sorption capacity, q_e, calculated from the slope and intercept of the linear plots (Figure 5.20a) of the pseudo-first order kinetic model, are given in Table 5.2. The straight line plot of t/q_t versus t for the kinetic data

Table 5.1: Isotherm parameters for Mg-HAP adsorbent

Isotherm	Parameter	Values
	q_{exp}(mg/g)	0.923
Langmuir	Q_0(mg/g)	1.4
	R^2	0.989
	b (L/g)	3.909
	K_{ap}	5.472
	R_L	0.102
	χ^2	0.025
Freundlich	K_f(mg/g)	1.280
	R^2	0.986
	n	1.19
	χ^2	0.064
Temkin	R^2	0.976
	A_T(L/g)	6.619
	B_T	0.47
	χ^2	1.31
Dubinin-Radushkevich	q_d(mg/g)	1.024
	R^2	0.987
	E_d (J/mol)	3.225
	χ^2	0.19

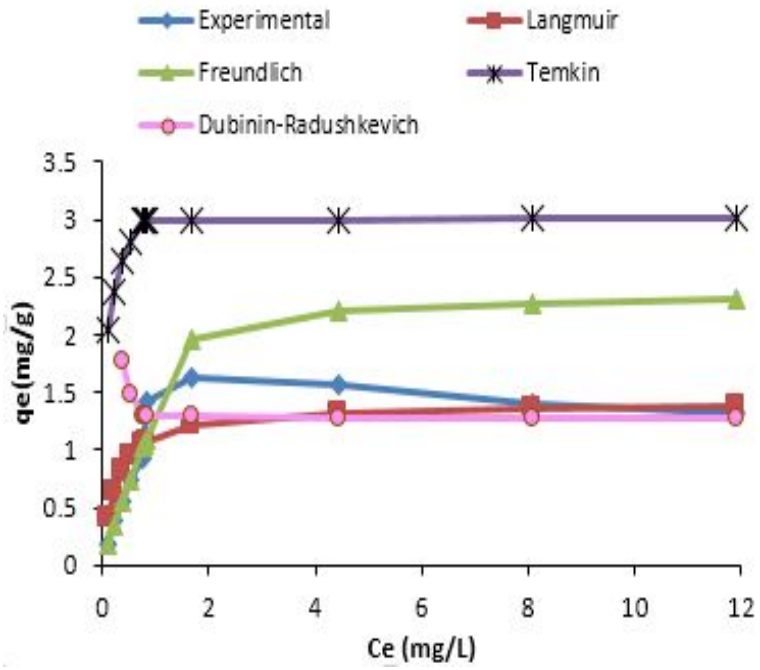

Figure 5.19: Comparative plots of isotherms with experimental data for Mg-HAP

shown in Figure 5.20b provided q_e and $k_2$values calculated from the slope and intercept.

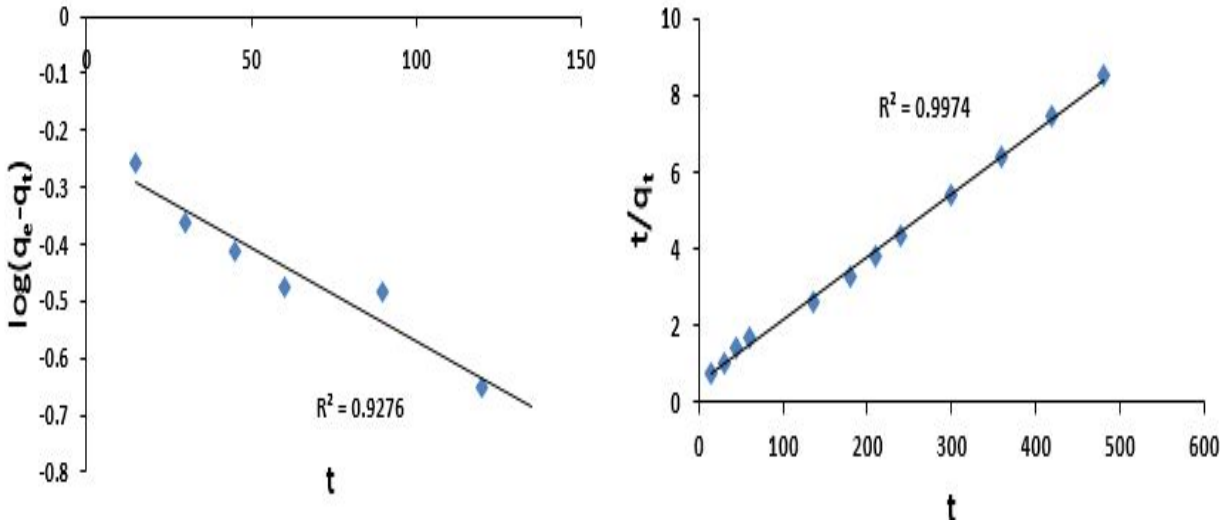

(a) Pseudo-first order kinetic model (b) Pseudo-second order kinetic model

Figure 5.20: Kinetic models for Mg-HAP

The k_i value was obtained from the slope of the linear portion of the curve (Figure 5.21). It was found that the plot was not entirely linear, but the graph reflected a two-staged nature. It is evident from the plots that there are two separate stages: first linear portion and second curved path followed by a plateau. This implied that a stage of intraparticle diffusion was continued up to 135 min followed by an equilibrium adsorption which began after 180 min. In other words, first stage is attributed to the immediate utilization of the most readily available adsorbing sites on the adsorbent surfaces. In second stage, very slow diffusion of adsorbate from surface site into the inner pores is observed. The value of "I" was observed to be 0.103 which depicts the thickness of boundary layer. A similar behavior of the intraparticle diffusion curve with an initial linear portion and then a plateau was reported by researchers who worked on $KMnO_4$ modified activated carbon derived from steam pyrolysis of rice straw [89]. The values of R^2 and SSE suggest that the sorption of fluoride by Mg- HAP follows a pseudo second-order reaction kinetic model and is also governed by intraparticle diffusion model (Table 5.2).

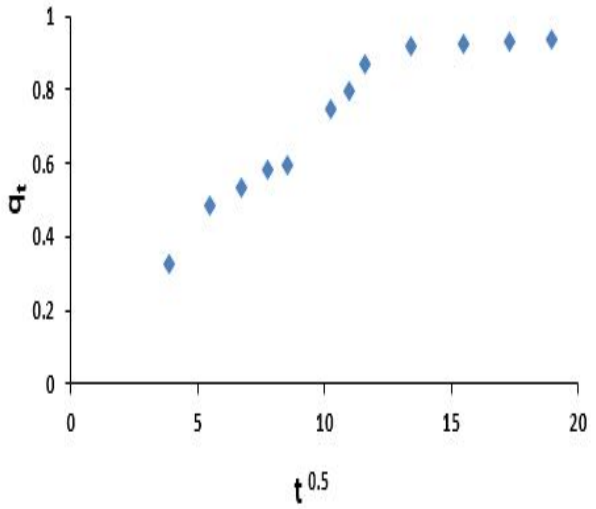

Figure 5.21: Intraparticle diffusion plot for Mg-HAP

Table 5.2: Values of parameters of Kinetic models for Mg-HAP adsorbent

Pseudo-first order model parameters	Values	Pseudo-second order model parameters	Values	Intraparticle diffusion model parameters	Values
R^2	0.927	R^2	0.997	R^2	0.979
$k_1(min^{-1})$	0.006	k_2 (g mg^{-1} min^{-1})	0.031	k_i(mg $min^{1/2}$/g)	0.039
q_e(mg/g)	0.570	q_e(mg/g)	0.980	I	0.103
SSE	0.155	SSE	1.6E-3	SSE	0.18

5.6.8 Conclusion

The Mg-HAP adsorbent developed for fluoride removal from aqueous solution has very good potential for defluoridation with a capacity of 1.4 mg/g. Fluoride removal of 92.34 % was achieved with 10 g/L, and equilibrium was reached in 180 min. It was observed that increasing the amount of adsorbent and contact time increased the percentage of removal initially; however, gradually, it attained equilibrium and became constant. SEM studies indicated porous texture and the individual elemental mapping indicate uniform distribution of calcium and magnesium in the adsorbent which explains the good fluoride removal potential. The adsorption capacity of Mg-HAP was not affected by pH of the medium. Calcium leaching in the solution was only observed at alkaline pH (9 and 10). Other anions such as nitrate and chloride do not affect the process significantly; however, the

presence of bicarbonate, sulfate, and phosphate ions lowered the defluoridation capacity. The mechanism of fluoride removal followed both adsorption and ion exchange mechanism. Adsorption pattern followed Langmuir isotherm the best and the rate of reaction follows pseudo-second order kinetics and the sorption of fluoride ion on Mg-HAP occurred through intraparticle diffusion pattern. Diffusion played a key role in the adsorption of fluoride ions onto Mg-HAP, as depicted in intraparticle diffusion model.

However, the treated water had pH value >10 and was not fit for consumption. Considering this aspect, Mg-HAP was not used for further experimentations.

5.7 Magnesium incorporated Hydroxyapatite (M-i-HAP) and pure-Hydroxyapatite

M-i-HAPa , M-i-HAPb and M-i-HAPc adsorbents were synthesized in the laboratory and a preliminary experiment was conducted to predict the fluoride removal capabilities of these adsorbents. The adsorbent which showed best defluoridation capacity was selected for batch studies by optimizing various parameters such as dose, contact time, temperature and pH. Pure-hydroxyapatite (pHAP) was used in the batch studies for comparison of results. Effect of interfering ions were also examined and a mechanism of the removal process is proposed. This section also discusses about the regeneration process of magnesium incorporated hydroxyapatite.

5.7.1 Fluoride removal studies with different M-i-HAP synthesized

A set of preliminary experiments were performed with 10 g/L of adsorbent dose, 180 min of contact time, at pH 7, 200 rpm agitation rate and 30 ± 0.5 °C using 10 mg/L of fluoride solution for perceiving the adsorbent with highest adsorption capacity. The results are presented in Figure 5.22 which shows that M-i-HAPa possessed highest fluoride removal capacity. This observation is also supported by the characterization studies shown in section 4.3 using TEM, BET, SEM and particle size estimation. The SEM studies revealed that M-i-HAPa has more porous texture to offer for adsorption of fluoride as compared to pHAP, M-i-HAPb and M-i-HAPc. Spherical shapes were noticed in TEM image of M-i-HAPa which may have attributed to its higher surface area as compared to pHAP. Thus,the characterization results from SEM and TEM analysis clearly depicted that M-i-HAPa adsorbent has a better surface morphology and microstructure required for adsorption of fluoride. Therefore, M-i-HAPa was used as an adsorbent for all the experiments further.

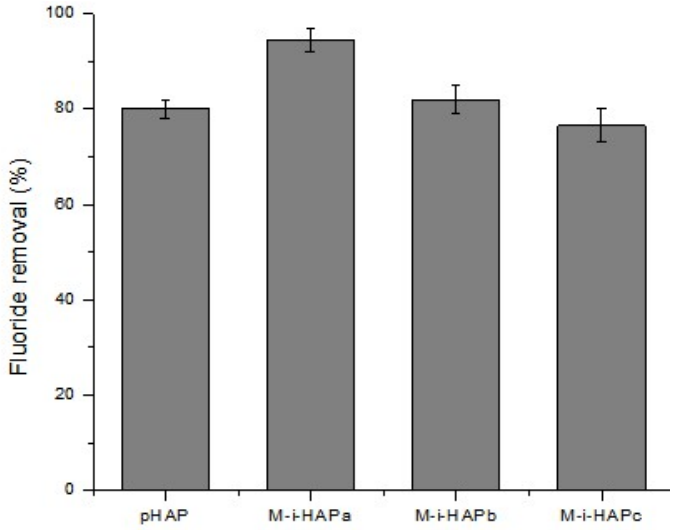

Figure 5.22: Comparison of F^- removal efficiency for different M-i-HAP synthesized (contact time: 180 min, initial fluoride concentration: 10 mg/L, dosage: 10 g/L)

5.7.2 Effect of pH

Performance of most of the adsorbents is pH dependent which makes it an important parameter to study. The effect of pH on fluoride removal efficiency of M-i-HAPa was evaluated at pH ranging between 3 and 11, keeping the adsorbent dose (10 g/L), contact time (180 min), initial fluoride concentration (10 mg/L), temperature (30 ± 0.5 °C) and agitation rate (200 rpm) constant. The pH_{PZC} was depicted to be 7.5 for both pHAP and M-i-HAPa (Figure 5.23). As it is evident from Figure 5.24, there is only a slight variation in removal efficiency with changing pH. A minor decrease in percentile adsorption of fluoride was noted at pH higher than 8 which may be due to competition by hydroxyl ions present at alkaline conditions. On the other hand, pHAP removal decreased drastically at higher pH. However, it is noteworthy that the residual fluoride concentrations using M-i-HAPa at all the pH values were below 1.0 mg/L. Thus, satisfying the permissible limits prescribed by regulatory authorities [13, 72]. Since, for pH < pH_{PZC} (7.5) the adsorbent surface is positive, higher fluoride adsorption is observed due to electrostatic attraction [151]. Defluoridation studies using M-i-HAPa were not affected by pH, which is an advantage over other adsorbents found in literature which have narrow working pH range [63, 89, 101].

5.7.3 Effect of adsorbent dose

The effect of the dose of adsorbent on fluoride removal capacity was studied at fixed conditions of 180 min contact time, 10 mg/L initial fluoride concentration, 30 ± 0.5 °C temperature and 200 rpm agitation rate. The dose of adsorbent was varied from 2 to 18 g/L

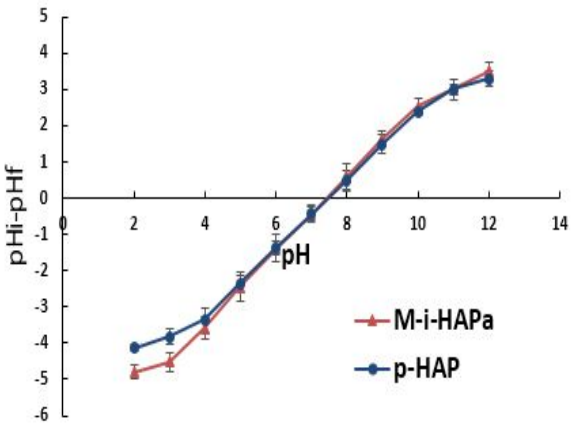

Figure 5.23: pH_{PZC} determination for M-i-HAPa and pHAP

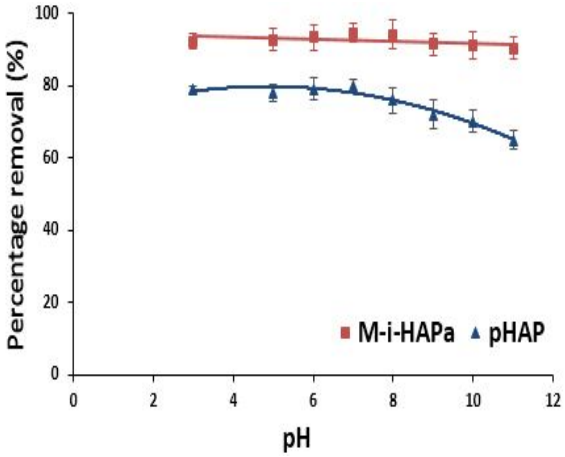

Figure 5.24: Effect of pH on F^- removal efficiency (contact time: 180 min, initial fluoride concentration: 10 mg/L, pH: 3-11, dosage: 10 g/L)

(Figure 5.25). At higher doses, availability of active sites for fluoride adsorption is higher and after certain limit the capacity becomes constant. It was found that 10 mg/L of M-i-HAPa was required for obtaining residual fluoride below permissible limit (< 1.0 mg/L) [13].

5.7.4 Effect of contact time

Batch studies were conducted varying contact time of adsorbent in fluoride solution of fixed concentration (10 mg/L), constant adsorbent dose (10 g/L), initial fluoride concentration (10 mg/L), temperature (30 ± 0.5 °C) and agitation rate (200 rpm). It was observed that more than 70 % removal was achieved in the first 30 min itself. After 135 min, the removal rate started to stabilize with negligible removal after 180 min indicating attainment of equilibrium (Figure 5.26). The driving force for mass transfer between solid and liquid phases reduces with time and after exhaustion of the mesopores, fluoride ions have to encounter higher resistances which tend to slow adsorption at later stages.

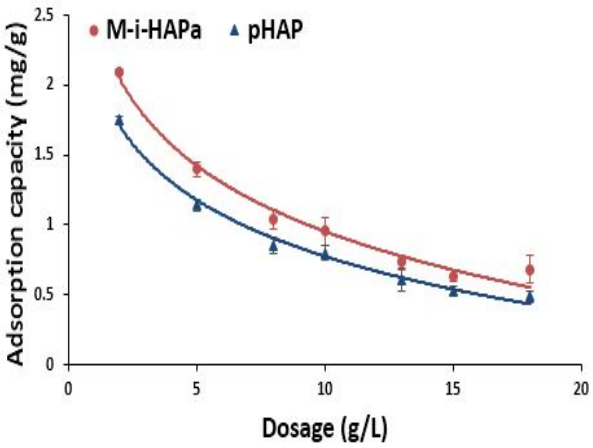

Figure 5.25: Effect of M-i-HAPa and pHAP dose on F^- removal capacity (contact time: 180 min, initial fluoride concentration: 10 mg/L, dosage: 2-18 g/L)

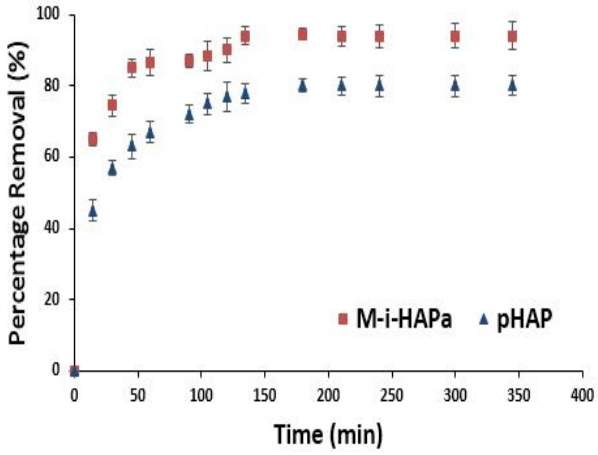

Figure 5.26: Effect on contact time on F^- removal efficiency (contact time: 15-345 min, initial fluoride concentration: 10 mg/L, dosage: 10 g/L)

5.7.5 Effect of interfering ions on adsorption capacity

Groundwater contaminated with fluoride contains many other ions which compete with fluoride during the adsorption process. To examine the effect of these coexisting ions studies were conducted with varying concentrations (100–300 mg/L) of chloride, sulfate, nitrate, phosphate, and bicarbonate anions. It is clear from Figure 5.27 that bicarbonate ions reduces the fluoride adsorption at all concentrations by approximately 12 %. Chloride, sulfate, nitrate, and phosphate ions slightly decrease the adsorbent capacity at higher anion concentration (300 mg/L). This decrease in fluoride uptake capacity of M-i-HAPa is attributed to the competition among the coexisting ions for the sites on the adsorbent surfaces which is governed by the charge, concentration, and size of the ion. The order of interference in terms of reduction in adsorption capacity posed by the coexisting ions is as follows: Chloride < Sulfate < Nitrate < Phosphate < Bicarbonate. Chloride, nitrate, and sulfate ions form outer sphere complexes, whereas phosphate and bicarbonate ions form inner sphere complexes with binding surfaces [163]. The adsorption mechanism for chloride, nitrate, and sulfate is through the formation of weak bonds with the sorption sites at the outer Helmholtz plane. Therefore, their presence in solution have less effect on adsorption of fluoride since fluoride ions interact via forming strong bonds with sorption sites at the inner Helmholtz plane. Phosphate and bicarbonate ions may also compete for active sorption site thus, reducing the fluoride uptake capacity of the adsorbent. The

adverse effect on removal capacity due to presence of bicarbonate ions in solution was also recounted by Sakhare et al. [79], Veeraputhiran and Alagumuthu [108] and Kamble et al. [114]. However, the decrease in adsorption capacity was marginal for all the co-ions studied and the concentration range considered were too high to be present in groundwater.

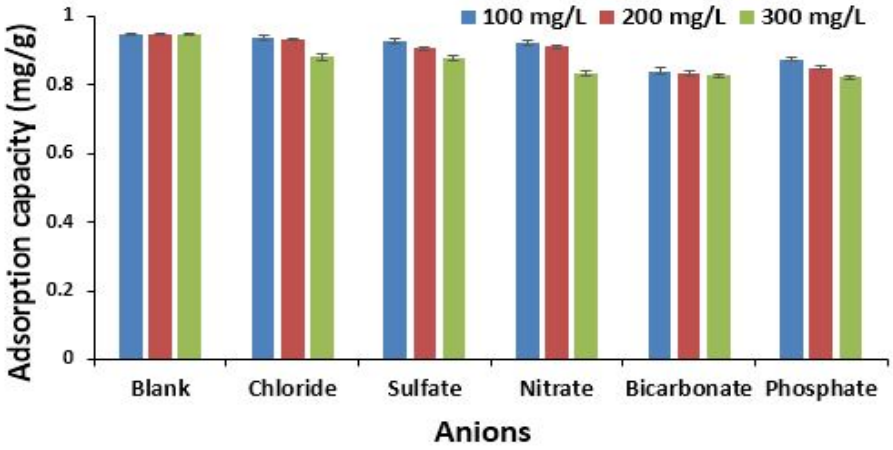

Figure 5.27: Effect of interfering ions on F^- adsorption capacity of M-i-HAPa (contact time: 180 min, initial fluoride concentration: 10 mg/L, dosage: 10 g/L, anion concentration:100-300 mg/L)

5.7.6 Effect of temperature

The feasibility of adsorption process at a given temperature and the spontaneity of the process can be known by exploring the thermodynamic parameters.

The effect of temperature on fluoride removal was studied in the solution for temperature at 30, 40 and 50 °C i.e 303, 313 and 323 K. It showed that fluoride removal capacity of the M-i-HAPa decreased with the increase in temperature (Figure 5.28). The lower removal capacity at high temperatures may attribute to the fact that at higher temperatures the thickness of the boundary layer decreases due to increased tendency of the molecules to escape from the adsorbent surface to the solution phase, which results in a decrease in the adsorption capacity as temperature is increased [151, 164].

The values of Gibbs free energy at 303, 313, and 323 K were found to be – 7.15, – 6.16, and – 5.10 kJ/mol, respectively. The negative values of ΔG° confirm the spontaneous nature of adsorption of the fluoride ion by M-i-HAPa, while the negative value of ΔH° (– 38.13 kJ/mol) shows that the process is exothermic. The negative values of ΔS° (– 0.102 kJ mol^{-1} K^{-1}) imply increased randomness at the solid-solution interface during the adsorption process [151]. Various other researchers also reported exothermic sorption process while studying removal of lead, strontium and nitrobenzene using hydroxyapatite

[165, 166, 167]

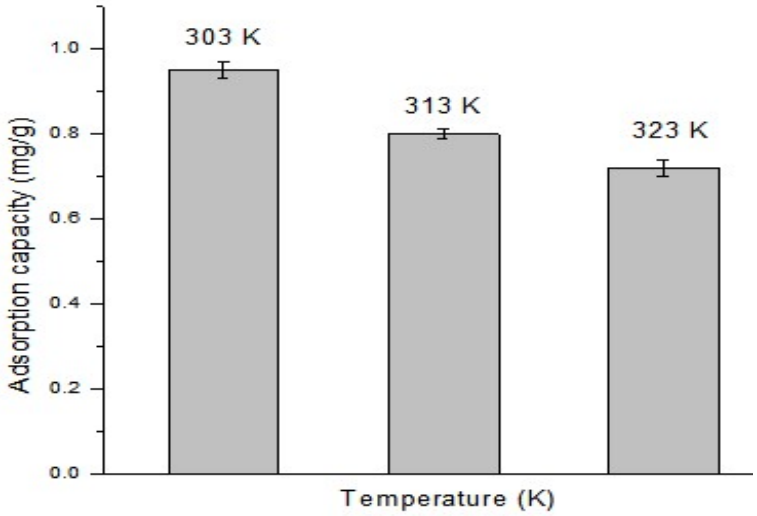

Figure 5.28: Effect of temperature on F^- adsorption capacity of M-i-HAPa (contact time: 180 min, initial fluoride concentration: 10 mg/L, dosage: 10 g/L, temperature: 303-323 K)

5.7.7 Experimental design and quadratic model fitting using RSM approach

Conventional methods of studying adsorption process includes studying of one parameter at a time while other parameters are kept constant at pre-determined values. This approach fail to depict the interactive effect of all the factors influencing the process. Response surface methodology using Central composite design was employed for fluoride removal using M-i-HAPa adsorbent and its process parameters were optimized. The relevance of this approach is based on an empirical relationship between input parameters and response generated which is stated by a quadratic model. The result obtained through each experimental run is presented in Table 5.3.

After conducting different runs for design and statistical analysis, the final equation in terms of coded factors are shown in Eq. (I) and (II):

Fluoride removal (%) = 90.12 + 19.44A - 4.12B + 10.83C - 1.36D + 0.88AB + 6.15625AC + 0.86AD - 1.88BC - 0.84BD + 0.30CD - 33.73 A^2 + 0.35B^2 - 7.58C^2 + 2.66D^2 (I)

Adsorption capacity (mg/g) = 0.96 - 0.60A - 0.12B + 0.16C - 0.058D + 0.11AB - 0.071AC + 0.05AD - 0.06BC - 0.04B - 0.006CD (II)

where A, B, C, and D are four independent variables. A positive sign for terms signify synergistic effect whereas a negative sign signifies antagonistic effects [168].

The outcome of the quadratic model for fluoride removal (%) and adsorption capacity (mg/g) in the form of analysis of variance (ANOVA) is presented in Table 5.4 and Table 5.4, respectively. It is observed that the value of correlation coefficient was 0.99 and 0.97, respectively for fluoride removal percentage and adsorption capacity with the respective standard deviation of 1.81 and 0.12. Additionally, the model F^{-} value is also significant, while the model depicts extremely low value of pure error of 0.053 and 8.333 E-005 for fluoride removal percentage and adsorption capacity, respectively. This implies that the regression model provides a very good elucidation of the relationship between the independent variables (chosen factors) and the response. The plot of predicted values vs. experimental values for fluoride removal (%) and adsorption capacity (mg/g) is illustrated in Figure 5.29 indicating that the models developed were successful in estimating the correlation.

Table 5.3: Experimental design matrix and responses for fluoride sorption using M-i-HAPa

Run	Factor 1	Factor 2	Factor 3	Factor 4	Response 1: Fluoride removal		Response 2: Adsorption capacity	
	A: Adsorbent dose (g/L)	**B: Temperature (K)**	**C: Time (min)**	**D: pH**	**Experimental value (%)**	**Predicted value (%)**	**Experimental value (mg/g)**	**Predicted value (mg/g)**
1	2	323	345	11	25	27.4	1.25	1.33
2	10	313	180	9	90	90.1	0.9	0.93
3	2	303	345	3	45	45.02	2.25	2.17
4	2	323	15	3	28	27.95	1.4	1.3
5	18	323	345	3	82	84.16	0.45	0.44
6	18	323	15	11	50	51.16	0.27	0.28
7	10	313	180	7	91.5	90.12	0.91	0.96
8	2	323	15	11	22	21.19	1.1	1.00
9	10	313	100	7	83	83.09	0.83	0.88
10	18	323	345	11	85	82.09	0.472	0.32
11	10	313	180	5	90	91.47	0.9	0.99
12	18	303	15	11	55	55.67	0.3	0.26
13	10	313	180	7	91	90.12	0.91	0.96
14	10	318	180	7	87	88.15	0.87	0.90
15	18	323	15	3	55	54.55	0.33	0.36
16	2	303	345	11	43.8	42.85	2.19	2.03
17	10	313	260	7	92	93.59	0.92	1.04
18	18	303	345	11	92.7	94.03	0.52	0.55
19	2	303	15	11	30	29.12	1.5	1.4
20	10	313	180	7	91	90.12	0.91	0.96
21	2	303	15	3	31	32.51	1.55	1.57
22	10	313	180	7	91	90.12	0.91	0.96
23	2	323	345	3	35	32.94	1.75	1.66
24	6	313	180	7	70	71.97	1.16	1.26
25	10	303	180	7	94.5	94.6	0.95	1.09
26	10	313	180	7	91	90.12	0.91	0.96
27	18	303	345	3	93.3	92.72	0.52	0.49
28	14	313	180	7	91.8	91.41	0.918	0.66
29	18	303	15	3	56.7	55.58	0.32	0.17
30	10	313	180	7	91	90.1	0.9	0.96

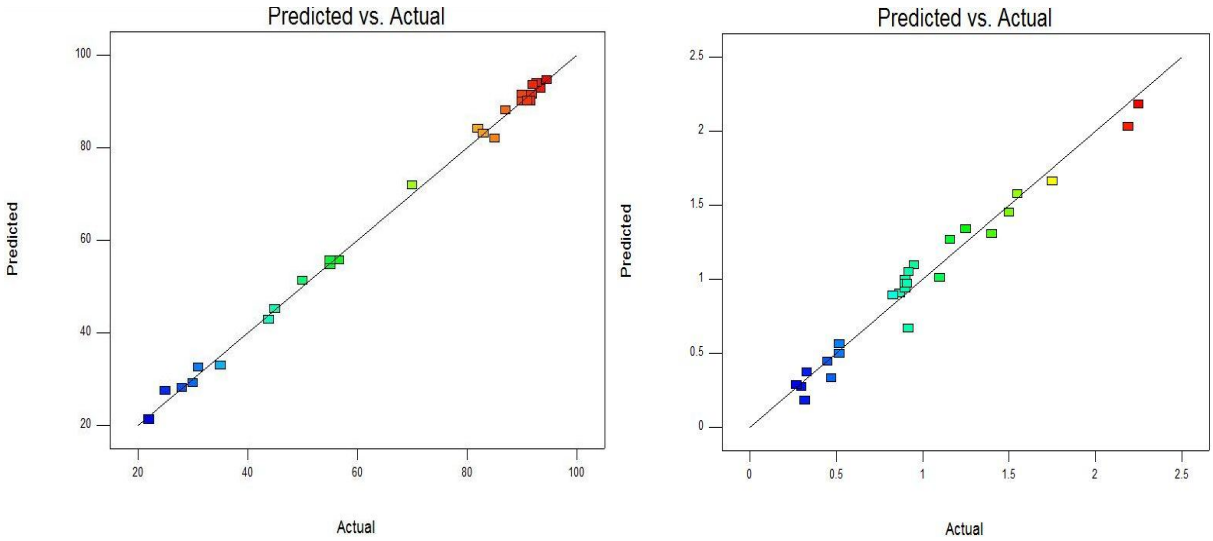

(a) Actual and predictive fluoride removal percentage (b) Actual and predictive fluoride removal capacity

Figure 5.29: Actual and predictive fluoride removal

5.7.7.1 Effects of experimental factors on adsorption

For the graphical interpretation of the interactions, the use of three-dimensional plots of the regression model is vastly suggested [39]. Analysis of variance for percentage fluoride removal using M-i-HAPa and fluoride removal capacity is presented in Table 5.4 and Table 5.5. The F-value in the tables confirmed that all the four chosen factors have significant effect on the removal efficiency of fluoride. In Table 5.4 and Table 5.5, p-value is the probability value which determines the statistically significant effects in the model. Parameters with p-value < 0.05 are considered to be statistically significant. Sum of squares of each parameter quantifies its significance in the adsorption process and with increase in the value of sum of squares, the importance of respective parameters in the process also increases.

In order to assess the relationship between the experimental factors and responses, three-dimensional (3D) response surface plots were generated and presented in Figure 5.30 and Figure 5.31 as graphical representations of the regression equation. Figure 5.30a and Figure 5.31a shows the combined effect of temperature and adsorbent dose on fluoride removal efficiency and capacity respectively. With increase in temperature, the fluoride removal efficiency was noticed to decrease while increase in adsorbent dose increases the efficiency due to more availability of adsorption sites. Figure 5.30b and Figure 5.31b correspond to the combined effect of contact time and adsorbent dose on fluoride removal efficiency and capacity. Increase in contact time led to increased removal efficiency and capacity upto 180 min and then the response was constant. This indicates to the fact

Table 5.4: Analysis of variance for percentage fluoride removal using M-i-HAPa

Source	Sum of Squares	df	Mean square	F value	p-value (Prob > F)
Model	20649.65	14	1474.98	174.26	< 0.0001
A-Adsorbent dose	6175.07	1	6175.07	729.55	< 0.0001
B-Temperature	2223.58	1	2223.58	262.70	< 0.0001
C-Time	2133.71	1	2133.71	252.09	< 0.0001
D-pH	14.09	1	14.09	1.67	0.2164
AB	7.70	1	7.70	0.91	0.3553
AC	839.55	1	839.55	99.19	< 0.0001
AD	1.05	1	1.05	0.12	0.7295
BC	32.21	1	32.21	3.80	0.0700
BD	2.98	1	2.98	0.35	0.5621
CD	4.31	1	4.31	0.51	0.4867
A^2	451.52	1	451.52	53.34	< 0.0001
B^2	44.74	1	44.74	5.29	0.0363
C^2	2.62	1	2.62	0.31	0.5862
D^2	30.18	1	30.18	3.57	0.0785
Residual	126.96	15	8.46		
Lack of fit	126.91	10	12.69	1189.78	< 0.0001
Pure error	0.053	5	0.011		
Cor Total	20776.61	29			

that higher removal efficiency and capacity can be achieved by simultaneous increase in adsorbent dose and contact time upto certain point. The combined effect of pH of solution and M-i-HAPa dose are presented in the form of 3D plots in Figure 5.30c and Figure 5.31c in terms of fluoride removal efficiency and capacity respectively. It was observed that fluoride removal efficiency increased with increasing the amount of adsorbent and the removal capacity decreased with increase in M-i-HAPa dose but pH of the solution didn't have any effect on the adsorption process. Hence, the adsorbent worked considerably well over a wide range of pH.

The study of interactive effect of contact time and temperature revealed that higher fluoride removal can be achieved with increase in contact time till equilibrium and increasing the temperature will lead to lower fluoride removal capacity of M-i-HAPa (Figure 5.30d and Figure 5.31d). Combined effect of pH and temperature is shown in 3D graph in Figure 5.30e and Figure 5.31e which clearly predicts that pH has no effect on the process and the reaction is exothermic. The interactive effect of pH of solution and contact time is illustrated in Figure 5.30f and Figure 5.31f which convey that with increase in contact time the adsorption is rapid initially then gradually approaches towards saturation.

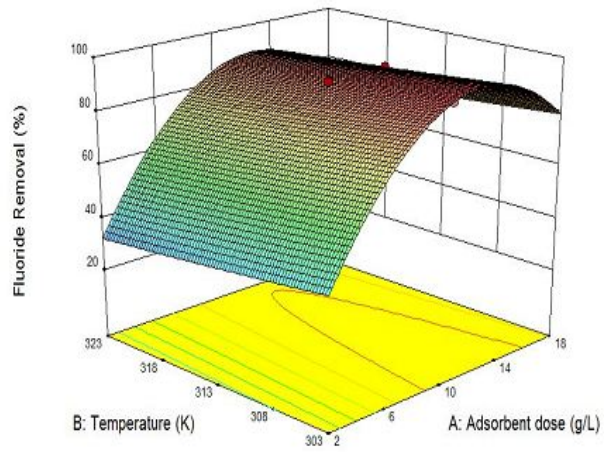

(a) Combined effect of temperature and adsorbent dose

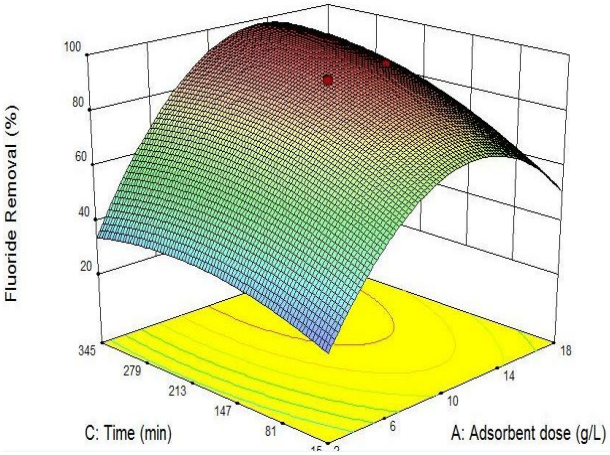

(b) Combined effect of contact time and adsorbent dose

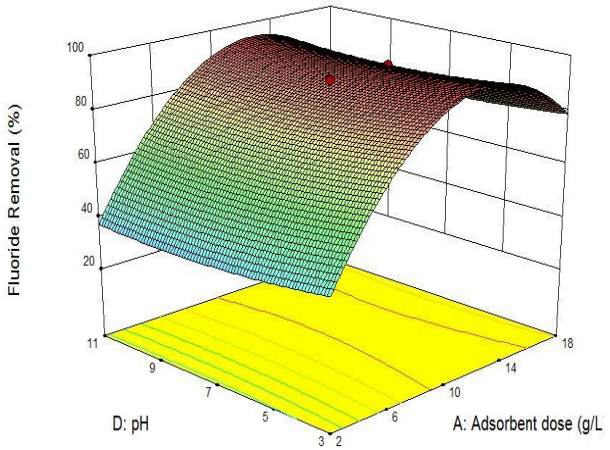

(c) Combined effect of pH and adsorbent dose

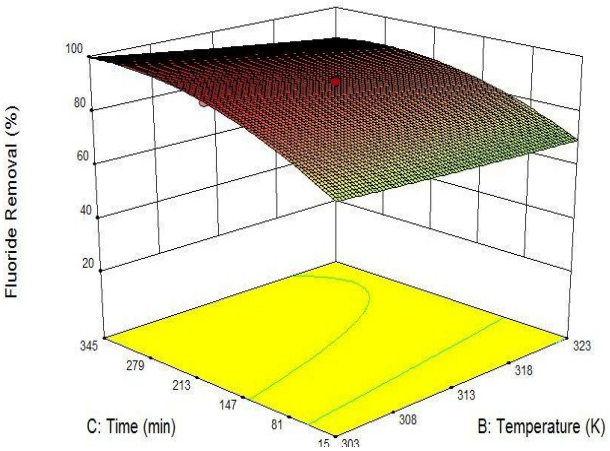

(d) Combined effect of contact time and temperature

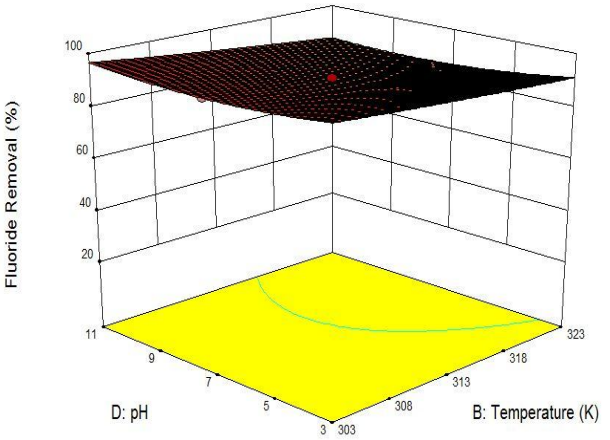

(e) Combined effect of pH and temperature

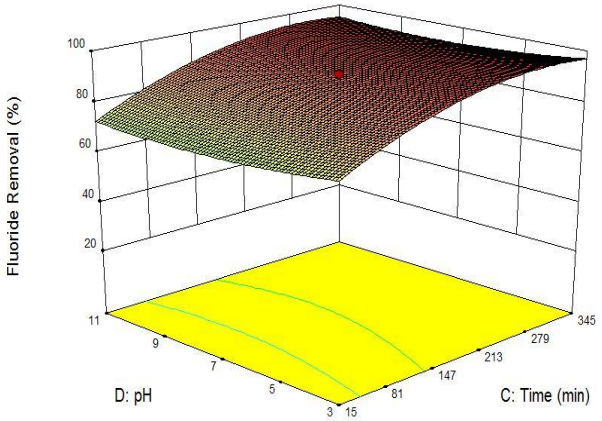

(f) Combined effect of pH and contact time

Figure 5.30: Response surface plots for M-i-HAPa varying parameters for fluoride removal efficiency (%) (contact time: 15-345 min, initial fluoride concentration: 10 mg/L, dosage: 2-18 g/L, pH: 3-11,temperature 303-323K)

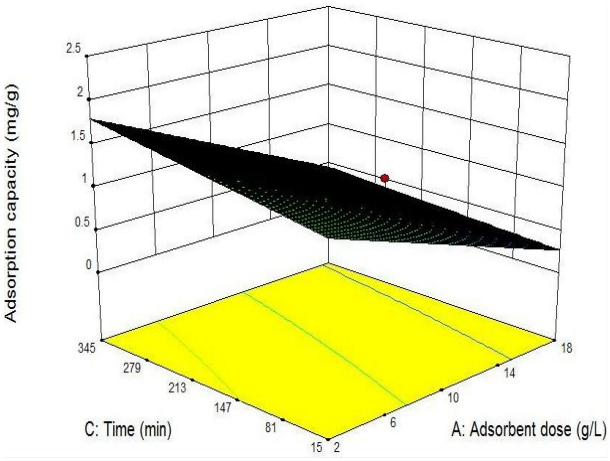

(a) Combined effect of temperature and adsorbent dose

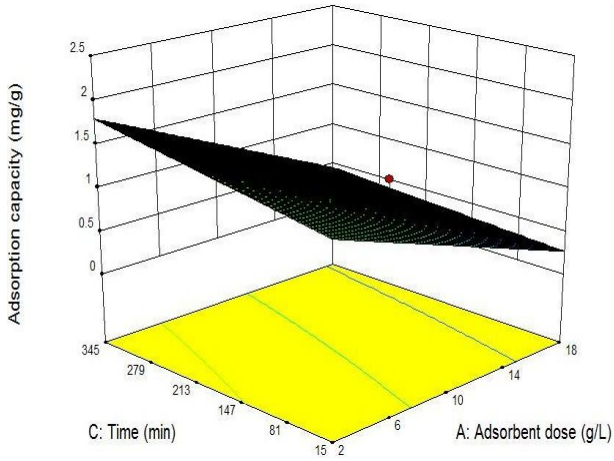

(b) Combined effect of contact time and adsorbent dose

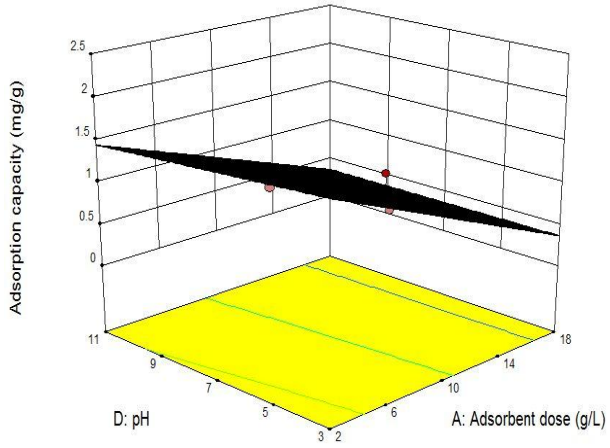

(c) Combined effect of pH and adsorbent dose

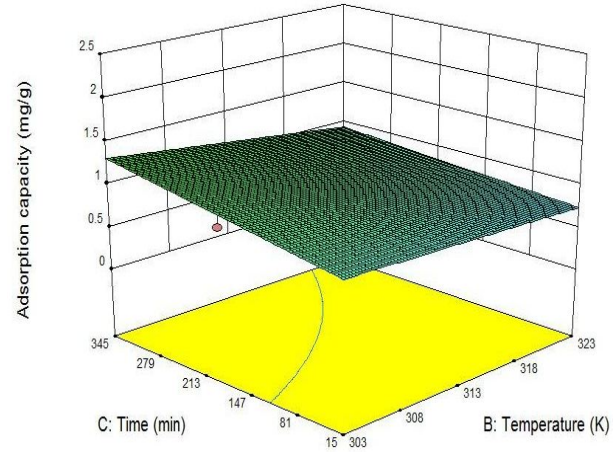

(d) Combined effect of contact time and temperature

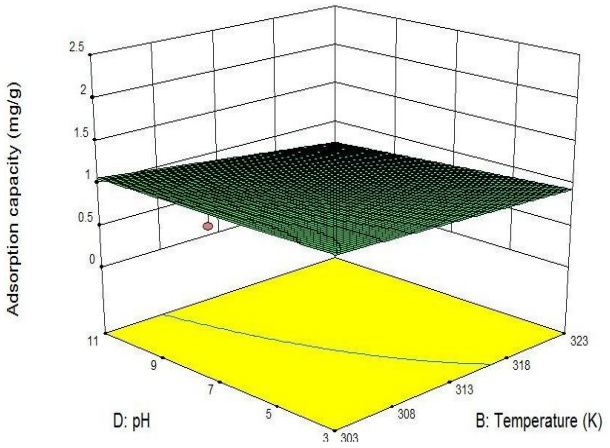

(e) Combined effect of pH and temperature

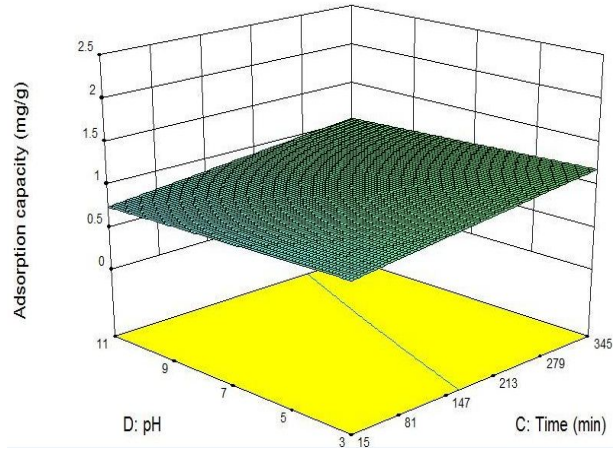

(f) Combined effect of pH and contact time

Figure 5.31: Response surface plots for M-i-HAPa varying parameters for fluoride removal capacity (mg/g) (contact time: 15-345 min, initial fluoride concentration: 10 mg/L, dosage: 2-18 g/L, pH: 3-11,temperature 303-323K)

Table 5.5: Analysis of variance for fluoride removal capacity using M-i-HAPa

Source	Sum of Squares	df	Mean square	F value	p-value (Prob > F)
Model	7.17	10	0.72	52.54	< 0.0001
A-Adsorbent dose	5.97	1	5.97	437.68	< 0.0001
B-Temperature	0.27	1	0.27	19.79	0.0003
C-Time	0.43	1	0.43	31.84	< 0.0001
D-pH	0.057	1	0.057	4.16	0.0555
AB	0.21	1	0.21	15.70	0.0008
AC	0.082	1	0.082	6.03	0.0238
AD	0.045	1	0.045	3.32	0.0841
BC	0.061	1	0.061	4.47	0.0480
BD	0.031	1	0.031	2.29	0.1463
CD	7.290E-004	1	7.290E-004	0.053	0.8197
Residual	0.26	19	0.014		
Lack of fit	0.26	14	0.019	1111.24	< 0.0001
Pure error	8.333E-005	5	1.667E-005		
Cor Total	7.43	29			

5.7.7.2 Verification of the model and confirmatory experiments

The desired goal for each factor and response was selected in numerical optimization. Figure 5.32 shows desirability ramp for numerical optimization.

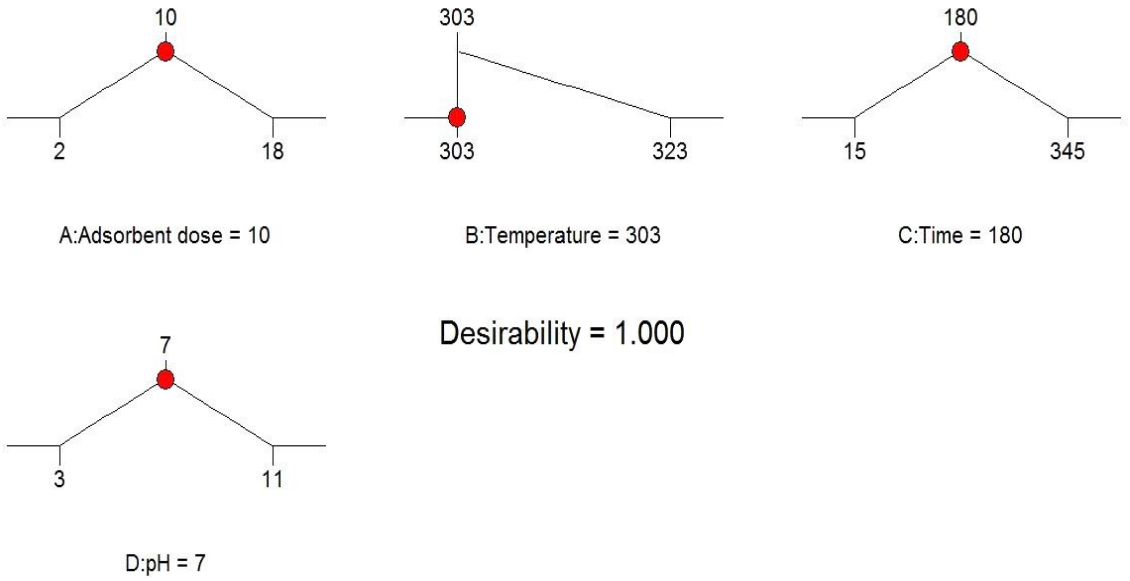

Figure 5.32: Desirability ramp for numerical optimization

The variables were set within the studied range and goals were targeted to achieve maximum possible adsorption capacity and removal percentage by the software. The obtained value of desirability (1.000) showed that the estimated function may represent the experimental model and desired condition. For confirming the data as given by numerical modeling under optimized condition, the confirmatory experiments were conducted with the parameters as suggested by the model (pH 7, adsorbent dose 10 g/L, temperature 303 K, and contact time 180 min). The efficiency of fluoride removal was found to be 94.5 % and adsorption capacity was estimated to be 0.95 mg/g experimentally, while the model predicted it to be 94.6 % and 1.09 mg/g, respectively. A good agreement was observed evidently between experimental and predicted values.

5.7.8 Adsorption isotherms

The data acquired during equilibrium study has been fitted to various adsorption isotherm equations such as Langmuir, Freundlich, Temkin, and Dubinin– Radushkevich isotherms to gain insight of the equilibrium characteristics of the adsorption process. The isotherm constants were calculated for all temperatures studied and are summarized in Table 5.6

Table 5.6: Isotherm parameters for M-i-HAPa adsorbent

Isotherm	Parameter	303K	313K	323K
	q_{exp}(mg/g)	0.95	0.80	0.72
Langmuir	Q_0(mg/g)	1.16	1.17	0.79
	R^2	0.99	0.93	0.98
	b (L/g)	5.9	1.16	2.21
	R_L	8.3E-3	0.041	0.022
	K_{ap}	6.89	1.75	1.36
	χ^2	2.1E-3	0.024	0.153
Freundlich	K_f(mg/g)	0.857	0.572	0.519
	R^2	0.988	0.974	0.948
	n	4.14	2.65	2.25
	χ^2	0.017	0.10	0.025
Temkin	R^2	0.918	0.964	0.946
	A_T(L/g)	81.45	6.56	24.9
	B_T	0.21	0.306	0.170
	χ^2	0.10	0.25	0.31
Dubinin-Radushkevich	q_d(mg/g)	0.98	0.72	0.76
	R^2	0.806	0.748	0.741
	B	9E-06	9E-06	2E-05
	E_d (J/mol)	235.7	235.7	158.11
	χ^2	0.017	0.10	0.025

The analysis of adsorption data for Langmuir isotherm was performed after plotting a graph between C_e/q_e versus C_e as shown in Figure 5.33a. The experimental data fitted well with high R^2 values which is given in Table 5.6 along with other Langmuir isotherm constants. The value of separation factor (R_L), a dimensionless number lied between 0 and 1 which indicated towards the process feasibility. The adsorption intensity (mg/g) and heterogeneity factor in terms of Freundlich isotherm corresponding to 'K_f' and n were obtained from the intercept and slope of the curve between log q_e against log C_e (Figure 5.33b). The magnitude of the hetrogeneity factor was higher than 1 for all conditions, depicting favorability of adsorption process.

The parameters for Temkin isotherm were acquired by plotting q_e versus ln C_e shown in Figure 5.33c. The positive values obtained for 'B_T' (Table 5.6) signifying adsorption energy shows that the process is exothermic, which is in agreement with the thermodynamic data. The R^2 values of Temkin isotherm for all temperatures were higher than Dubinin-Radushkevich isotherm. For Dubinin-Radushkevich isotherm, a plot between ln qe against ε^2 is presented in Figure 5.33d. The value of 'E_d' in Dubinin-Radushkevich isotherm suggests about the type of adsorption process. If the value of E_d is less than 8 kJ/mol, the process is physiadsorption while if E_d is greater than 50, the process is chemical reaction controlled [89, 169]. However, for fluoride adsorption using M-i-HAPa adsorbent, the Dubinin-Radushkevich isotherm data fitted very poorly thus the value of E_d is not applicable.

It is evident from Table 5.6 that the adsorption mechanism can be best described using Langmuir isotherm attributing to highest R^2 value and low χ^2 at all temperatures studied. Also, the experimental adsorption capacity (q_{exp}) was very close to the langmuir adsorption capacity. This indicates uniform distribution of active sites on M-i-HAPa surface and a monolayer adsorption mechanism.

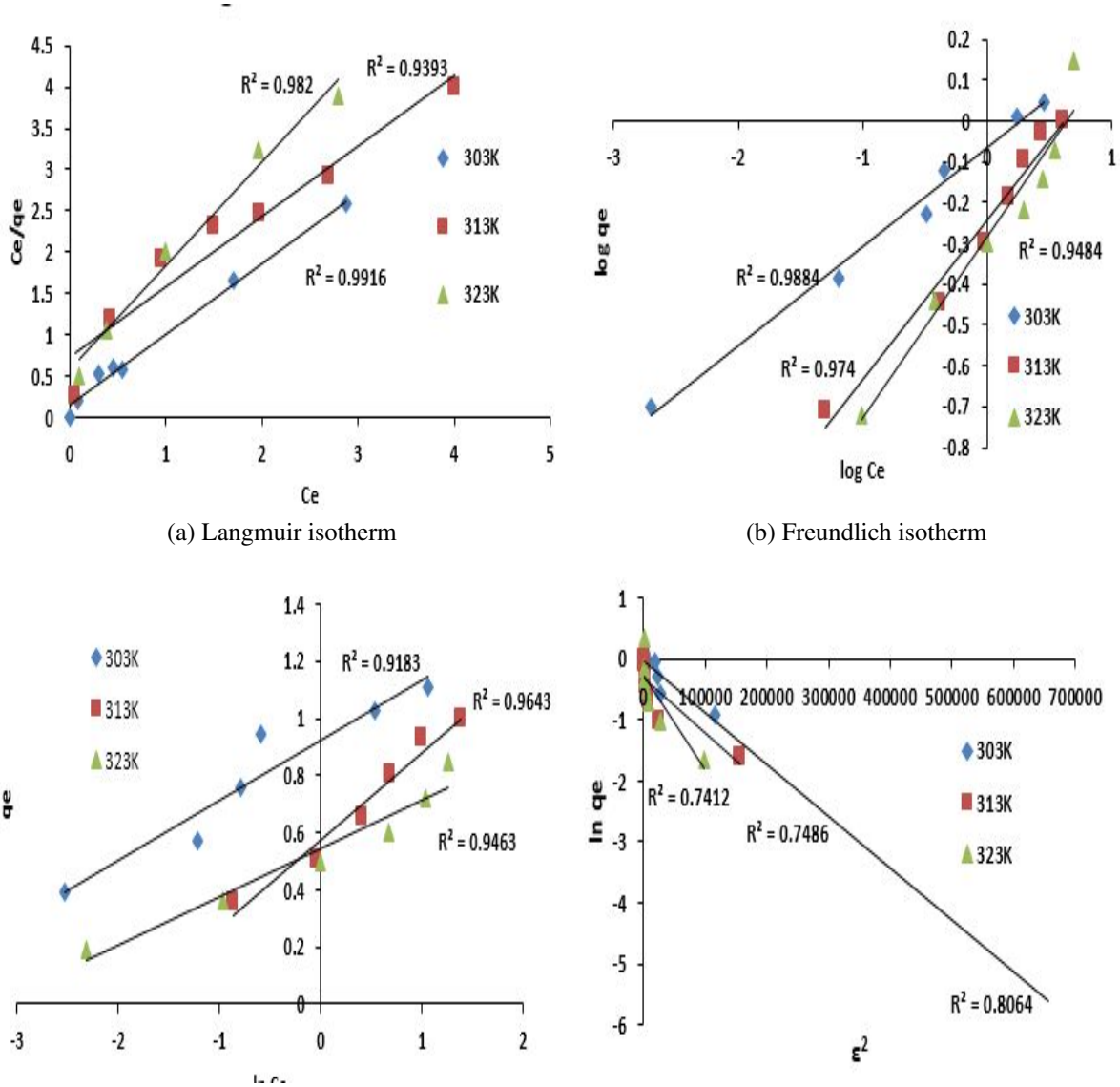

(a) Langmuir isotherm

(b) Freundlich isotherm

(c) Temkin isotherm

(d) Dubinin-Radushkevich isotherm

Figure 5.33: Adsorption isotherms for M-i-HAPa

5.7.9 Adsorption kinetics

Kinetic models recurrently used to determine various kinetic parameters of the adsorption system are reaction-based and diffusion-based models. For analyzing the reaction kinetics, pseudo-first-order and pseudo-second-order models have been used. Diffusion model used for the adsorption of a liquid adsorbate on porous solid was the intraparticle diffusion model by Weber-Morris.

The slope deduced from the plot of $\log(q_e - q_t)$ against t of pseudo first-order equation at varying experimental conditions (Figure 5.34a) provided the values of the rate constant

(k_1), given in Table 5.7. The lower correlation coefficient (R^2) value of pseudo-first order model suggested its lack of fit to the adsorption data.

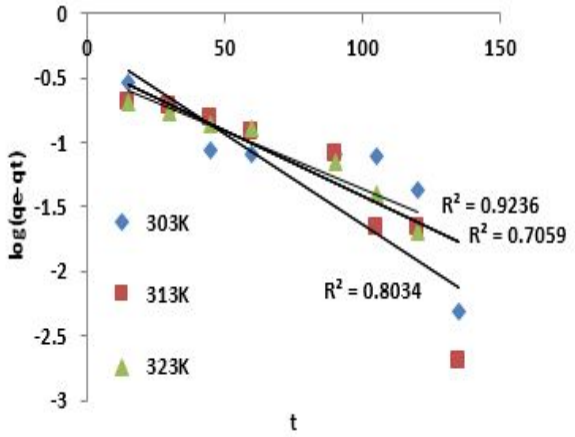

(a) Pseudo-first order kinetic model

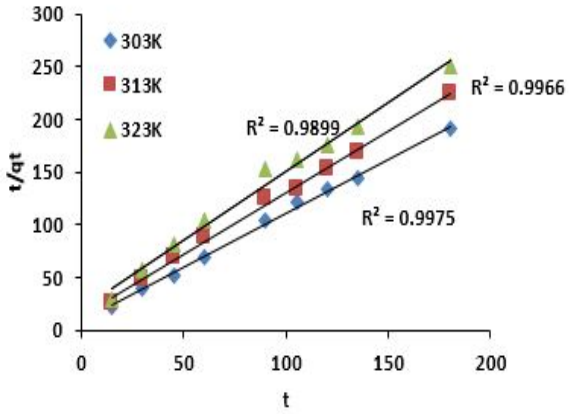

(b) Pseudo-second order kinetic model

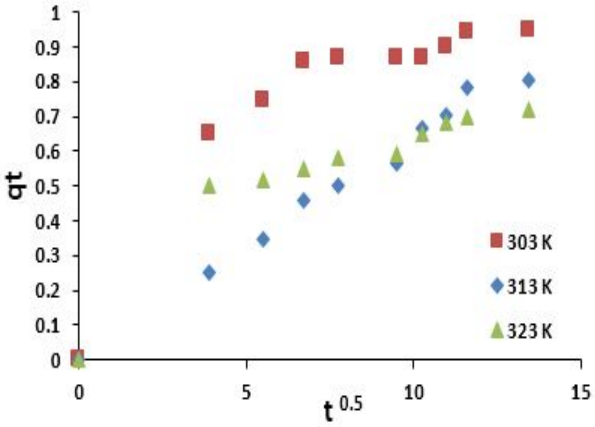

(c) Intraparticle diffusion model

Figure 5.34: Kinetic models for M-i-HAPa

For estimating the rate constant for pseudo-second order model, t/q_t was plotted against t as shown in Figure 5.34b. The R^2 value for all experimental conditions for pseudo-second order model was close to unity which confirms the suitability of this model. It is apparent from Table 5.7 that pseudo-second-order kinetic model fits the experimental data best with high R^2 value and extremely low SSE value for all experimental conditions. The initial adsorption rate ($k_2 q_e^2$) was highest for 303 K followed by 323 K and 323 K which indicated that at lower temperature, fluoride adsorption was more rapid, which is in agreement with the thermodynamic studies (section 5.7.6).

To determine the rate controlling step, the intra-particle diffusion model was used and plots of q_t vs $t^{0.5}$ at different temperatures revealed involvement of two stages in the process

of adsorption (Figure 5.7c). In first stage, rapid adsorption on the external surface occurs due to large availability of active sites whereas the second stage is slower where intraparticle diffusion is rate controlling and fluoride ions diffuse into the micropores of M-i-HAPa. The value for intraparticle diffusion constant (k_i) and thickness of boundary layer (I) is also given in Table 5.7. The comparatively low R^2 and high SSE values indicate that there is less possibility of contribution of intraparticle diffusion in the process.

Table 5.7: Kinetic model parameters for M-i-HAPa adsorbent

Kinetic models	Parameter	303K	313K	323K
Pseudo-first order	k_1	0.23	0.032	0.020
	R^2	0.705	0.803	0.923
	$q_{e\ calc}$(mg/g)	0.406	0.595	2.92
	SSE	0.32	0.072	0.136
Pseudo-second order	k_2	0.113	0.1	0.03
	R^2	0.997	0.966	0.986
	$q_{e\ calc}$(mg/g)	0.981	0.853	0.766
	SSE	1.38E-3	2.76E-3	2.70E-3
Intraparticle diffusion	k_i	0.060	0.062	0.046
	R^2	0.743	0.988	0.812
	I	0.284	0.112	0.181
	SSE	0.4	0.13	0.53

5.7.10 Mechanism of fluoride adsorption

The adsorption mechanism of M-i-HAPa in aqueous fluoride solution was examined through XRD pattern obtained (Figure 5.35) which illustrated the formation of hydroxyfluoropatite (JCPDS: 034-0010) and fluorapatite (JCPDS: 00-034- 0011) as expected. The mechanism is further described through the following reactions in Eq. (5.7.1) and (5.7.2) which illustrates the formation of Magnesium incorporated hydroxyfluoroapatite and Magnesium incorporated fluoroapatite respectively. :

$$Ca_{(10-n)}Mg_n(PO_4)_6(OH)_2 + F^- \rightarrow Ca_{(10-n)}Mg_n(PO_4)_6(OH)(F) + OH^- \quad (5.7.1)$$

$$Ca_{(10-n)}Mg_n(PO_4)_6(OH)(F) + F^- \rightarrow Ca_{(10-n)}Mg_n(PO_4)_6(F_2) \quad (5.7.2)$$

In Figure 5.35, a peak for MgF_2(JCPDS: 00-006-0290) was also observed due to reaction of fluoride ions with magnesium ions. Some fluoride ions may have reacted with magnesium ions due to which hydroxyfluoroapatite and hydroxyapatite were found in the XRD pattern indicating that all the M-i-HAPa was not converted to fluoroapatite and some adsorption sites were still available. In other words, the higher capacity of M-i-HAPa as compared to pHAP may be attributed to the presence of magnesium ions.

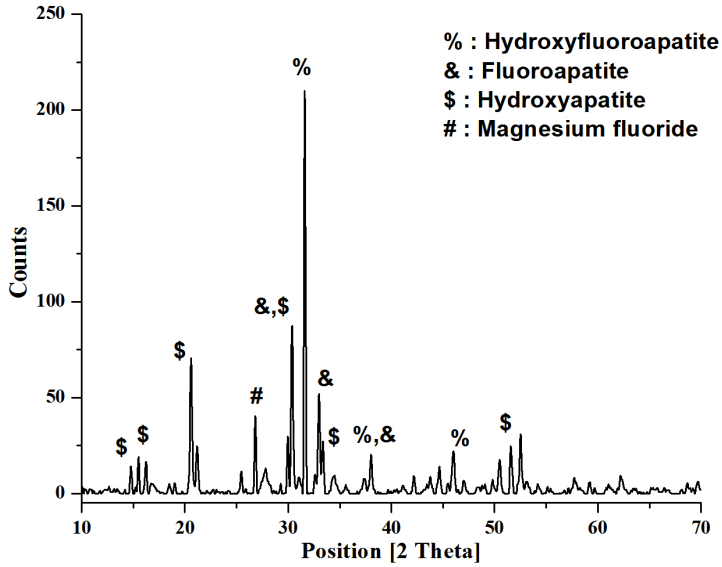

Figure 5.35: XRD pattern of M-i-HAPa after fluoride adsorption

Fluoride and hydroxyl ions are of similar size and comparable ionic radii, therefore, they may undergo iso-electronic substitution as reported by Maliyekkal and Shukla [66]. Fluoride adsorption onto M-i-HAPa was accelerated at first then reached a stationary phase with increased contact time. Thus, the mechanism of fluoride adsorption involves diffusion of F^- ions on adsorbent surface then adsorption at active sites followed by exchange of OH^- and F^- ions. Fitness of the adsorption data to pseudo-second-order kinetics indicated that the process is governed by chemisorption**.** In addition, the adsorption isotherm studies showed Langmuir isotherm to be best fitted to represent the experimental data. Since, Langmuir isotherm also supports the chemisorption theory, it is apparent that the adsorption mechanism is chemical in nature.

5.7.11 Regeneration studies of M-i-HAPa

It is immensely essential to regenerate the saturated adsorbent to make the process efficient as well as to prevail over the disposal problem. The adsorbent was first saturated with fluoride solution of 10 g/L for 180 min and this cycle was repeated till M-i-HAPa got saturated (Figure 5.36a). Approximately 20 % decrease in removal efficiency was observed in the second and third cycle each followed by ~30 % and ~20 % in fourth and fifth cycles respectively. The regeneration of adsorbent was studied using different solutions of sodium hydroxide, sulfuric acid, hydrochloric acid, and potassium hydroxide. The saturated adsorbent (10 g/L) was shaken with different regeneration solutions for 90 min after which it was filtered, washed, and dried at 95 °C for 60 min. The results obtained are illustrated in Figure 5.36b. About 91% regeneration was achieved with 0.1 M NaOH confirming to the ion exchange mechanism of adsorption.

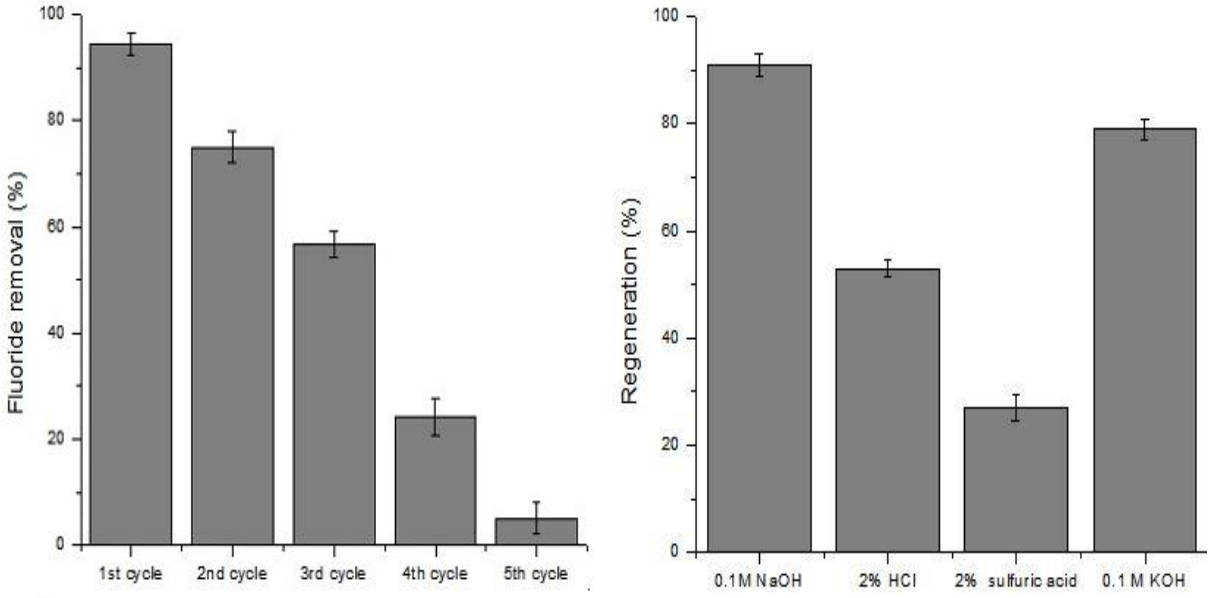

(a) Number of usable cycles (b) Identification of eluents

Figure 5.36: Regeneration studies with M-i-HAPa adsorbent

5.7.12 Water quality after adsorption

The quality of water treated with M-i-HAPa adsorbent was studied for various parameters. This study was carried out to predict the feasibility of M-i-HAPa as an adsorbent for defluoridation of drinking water. The adsorbent dose in the sample tested was 10 g/L, with 10 mg/L fluoride concentration, agitation rate of 200 rpm, 180 min of contact time at pH 7 and temperature 30 ± 0.5 ° C. Table 5.8 presents the value of concerned parameters

before and after adsorption along with the permissible limit determined by WHO and BIS [13, 72]. It is apparent from Table 5.8 that the water treated with magnesium incorporated hydroxyapatite is fit for treating potable water and all the parameters are within acceptable limit.

Table 5.8: Water quality after adsorption with M-i-HAPa

Parameters	**Before adsorption**	**After adsorption**	**Permissible limit [72, 13]**
pH	7.54	7.32	6.5-7.5
EC (µS/cm)	67	508	2000
TDS (ppm)	33	248	500
Alkalinity (CaCO3 eqv., mg/L)	0	15	600
Total Hardness (CaCO3 eqv.,mg/L)	0	135	500
Ca^{2+} (mg/L)	0	20	75-200
Mg^{2+} (mg/L)	0	27	30-100
Phosphate (mg/L)	0	Below detection limit	Not mentioned
F^- (mg/L)	10	0.552	1-1.5
Turbidity (NTU)	0	0	10

5.7.13 Conclusion

In this work, the adsorbent magnesium-incorporated hydroxyapatite was synthesized and investigated for fluoride removal. Characterization with XRD, FTIR, and TEM confirmed the incorporation of magnesium into the apatite lattice. BET surface area of the synthesized adsorbent was 46.62 m^2/g which is more than twice as compared to hydroxyapatite (21.25 m^2/g), due to this higher adsorption rate was attained. The influence of experimental factors (initial fluoride concentration, contact time, pH of the aqueous solution, dose of M-i-HAPa, and temperature) on fluoride removal percentage was explored. RSM by CCD was used to investigate the chosen factors on fluoride removal and adsorption capacity. A second order polynomial regression model interpreted the experimental data with coefficient of determination value of 0.99 and 0.97, respectively for fluoride removal percentage and adsorption capacity. The numerical optimization achieved with the desirability function specified the probable fluoride removal to be 94.60 % and adsorption capacity to be 1.09 mg/g. The optimum values for experimental parameters were found to be pH 7, 303 K temperature, 10 mg/L fluoride concentration, and 180 min contact period with a dose of 10 mg/L.

The mechanism of adsorption was governed by Langmuir model with maximum fluoride uptake of 1.16 mg/g. Pseudo-second-order kinetic model was followed by the process along with some contribution of intraparticle diffusion. Thermodynamic studies clearly show the spontaneity of the process and a better removal at lower temperatures. The adsorbent could be regenerated to 91 % making the reusability of the adsorbent possible. Thus, the adsorbent M-i-HAPa is found to be surely a promising defluoridation agent.

5.8 Summary of the Chapter

This chapter was dedicated to explore the defluoridation capacities of different calcium based adsorbents and selecting the most suitable adsorbent for column studies which will state the practical feasibility of the process.

Preliminary experiments using various calcium based adsorbents were carried out. On the basis of their fluoride removal capacity and quality of treated water, adsorbents were screened. The characterization studies carried out in Chapter 4 also helped in selection of suitable adsorbent for further experimentation. The screening process for calcium based adsorbents is summarized in Figure 5.37. The study of M-i-HAPa pellets in column mode is discussed in the next chapter. The adsorbents studied were Activated Calcite (ACal), Synthesized Calcia-Magnesia Adsorbent (CMA), Dicalcium phosphate ($CaHPO_4$), Dolomite [$CaMg(CO_3)_2$] and Natural Hydroxyapatite (aHAP). Each of these adsorbents were not studied beyond preliminary experiments due to their lower fluoride removal capacity and quality of treated water such as high/low pH or leaching of calcium-magnesium ions. Activated calcite and dolomite possessed low fluoride removal capacity (0.78 mg/g and 0.322 mg/g respectively) while the treated water obtained from CMA adsorbent and dicalcium phosphate adsorbents were not suitable for consumption due to high amount of calcium-magnesium dissolution (Ca^{2+}: 120mg/L; Mg^{2+}: 87 mg/L) and low pH (~ 5) respectively. Such high leaching of elements from adsorbent indicate a low stability of CMA adsorbent in solution and is not desirable. Moreover, SEM studies indicated non-uniform distribution of calcium and magnesium in form of dense agglomerates. Therefore, this adsorbent was not found suitable for defluoridation and was not studied further.

Mg-HAP adsorbent derived from natural HAP was studied by varying adsorbent dose, contact time, pH and co-existing ions. The Mg-HAP adsorbent had an adsorption capacity of 1.4 mg/g with initial fluoride concentration of 10 mg/L in 180 min. The adsorption capacity of Mg-HAP was slightly affected by pH of the medium but calcium leaching in the solution was observed at alkaline pH (9 and 10). Also, the treated water had

pH value greater than 10 and therefore it was not found fit for drinking purposes. SEM studies indicated porous texture of Mg-HAP and the individual elemental mapping indicate uniform distribution of calcium and magnesium in the adsorbent which explains the good fluoride removal potential.

Optimization of fluoride removal on M-i-HAPa was carried out with Design Expert Version 9.0.4.1 software by choosing four independent process variables (pH,dose, contact time, temperature) and their interactive effects were discussed. The numerical optimization achieved with the desirability function specified the probable fluoride removal to be 94.60 % and adsorption capacity to be 1.09 mg/g which was very close to the experimental values of 94.5 % and 0.95 mg/g respectively. The characterization results from SEM and TEM analysis clearly depicted that M-i-HAPa adsorbent has a better surface morphology and microstructure required for adsorption of fluoride. One of the most important factor in an adsorption process is the pH as it governs the entire process chemistry of defluoridation. In our studies with M-i-HAP adsorbent, negligible effect of pH was found which makes this adsorbent more suitable for practical purposes. While studying the effect of interfering ions M-i-HAPa showed a selective adsorption process towards fluoride ions. Moreover, the water quality parameters after adsorption were satisfactory as per WHO and BIS norms.

The adsorbent M-i-HAPa was chosen for converting into pellets for continuous column operation which is discussed in the next chapter. The criteria for choosing this adsorbent was its novelty, adsorption capacity, negligible effects of solution pH and interfering ions, ability for regeneration and water quality after adsorption. The characterization studies also supported that the adsorbent M-i-HAPa has better surface area, morphology required for fluoride adsorption.

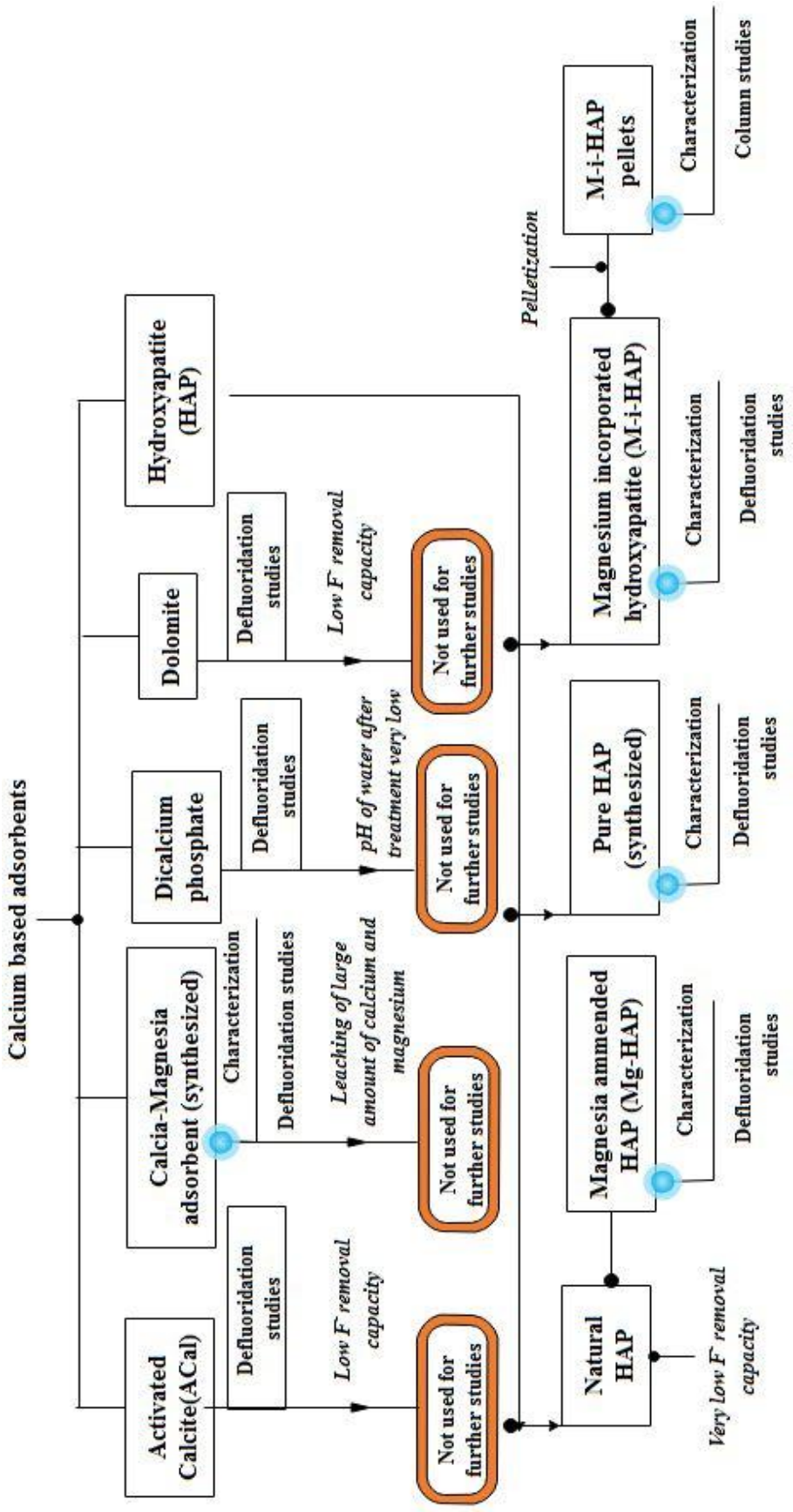

Figure 5.37: Screening of Calcium based adsorbents

CHAPTER 6

Chapter 6

Column Defluoridation Experiments

This chapter is focused on exploring the practical feasibility of defluoridation using M-i-HAPa adsorbent. It was concluded in the previous chapter that M-i-HAPa adsorbent was highly effective for water defluoridation and the treated water quality was also acceptable as per WHO and BIS norms. For column studies, the powder form of M-i-HAPa adsorbent was converted into pellets through extrusion-spheronization method (section 3.2.6).

Breakthrough curves were obtained from experimental studies as described in section 3.4.2 and the performance of continuous adsorption processes were estimated by varying parameters such as shape of particles, size of particles, flow rate, feed fluoride concentration and bed height. Three kinetic models (Thomas model, Hutchins BDST model and Yoon Nelson model) were used to fit the adsorption data. The experimental results obtained by varying flow rate and size of particles were compared with simulated data obtained from an adsorption simulator "ADSORB" developed in MATLAB software. In addition, the regeneration of saturated M-i-HAPa adsorbent was also studied.

6.1 Parameters influencing column adsorption behaviour

The batch defluoridation studies using M-i-HAPa powder revealed that the defluoridation capacity is not affected by pH of the solution. Therefore, no alteration in the pH of solution was done while studying the column system. The performance of the column adsorption system was predicted in terms of the breakthrough curve. The breakthrough curve was obtained by plotting the fluoride concentration (C_e/C_0) against time (t). The breakthrough concentration (C_b) in this study was 1 mg/L i.e. the permissible limit for fluoride in water determined by BIS [13] and the breakthrough point or time (t_b) is the time at which the effluent concentration (C_e) from the column is equal to C_b.

6.1.1 Experimental studies

Column adsorption experiments were carried out in a column of 50 cm height, 5 cm inner diameter and area of cross-section 19.62 cm^2. Experimental studies were conducted to observe the effect of shape of particles (cylindrical and spherical), effect of size of particles (< 1 mm, 1 - 1.5 mm and 1.5 - 2 mm), effect of bed height (5, 10 and 30 cm), effect of flow rates (1, 1.5 and 2 L/h) and effect of feed fluoride concentration (5 and 10 mg/L). Breakthrough curves were plotted for determining the effect of these parameters. The breakthrough point and the shape of the breakthrough curve are salient characteristics for predicting the operation and dynamic response of the adsorption column. The mass for 5, 10 and 30 cm bed heights were 14, 27 and 80 g respectively and the density of the adsorbent was 280 kg/m^3.

6.1.1.1 Effect of shape of particles

Cylindrical shaped pellets of 0.5 - 1 mm in length, 0.5 to 1 mm in diameter (mean equivalent diameter = 1.12 mm) and spherical shaped pellets of 1 - 1.5 mm in diameter were obtained through the pelletization procedure and both types of pellets were tested for fluoride removal in the continuous column adsorption system. The flow rate, bed height and feed fluoride concentration were kept constant at 1 L/h, 30 cm and 10 mg/L respectively. The breakthrough curves were obtained which showed that spherical pellets were more efficient of removing fluoride ions from the solution as compared to cylindrical shaped pellets. The breakthrough time (t_b) and exhaustion time (t_{EX}) of cylindrical shaped pellets were 3 h and 6.5 h respectively while that for spherical pellets were 13 h and 16 h respectively. As seen in Figure 6.1a, faster breakpoint was achieved with cylindrical pellets and the adsorption capacities were also less than spherical pellets. The equivalent diameter of cylindrical particles (1.12 mm) being lower than the spherical partcles (1.25 mm) offered lower adsorption capacity. There might also be some discrepancies in flow patterns like channeling within the cylindrical pellet bed which may be responsible for decrease in adsorption capacity. The adsorption capacity upto breakthrough (q_b) and exhaustion (q_{EX}) for spherical pellets were 1.46 mg/g and 1.8 mg/g respectively while the same corresponding to cylindrical pellets were 0.34 mg/g and 0.73 mg/g. The delayed breakthrough observed for spherical pellets is because of the higher surface area offered due to their structure which led to higher adsorption capacity. Therefore, spherical particles were used for further experimentations.

6.1.1.2 Effect of size of particles

Three different particle size of pellets were studied viz. < 1 mm, 1 - 1.5 mm and 1.5 - 2 mm for obtaining the breakthrough curves and estimating the adsorption capacity (Figure 6.1b). Other operational parameters such as bed height, flow rate and feed fluoride concentration were kept constant at 30 cm, 1 L/h and 10 mg/L respectively. The breakthrough time (t_b) and throughput volume upto exhaustion (V_{EX}) increases with decreasing particle size as listed in Table 6.1. The fluoride uptake capacity upto breakpoint (q_b) at < 1 mm, 1 - 1.5 mm and 1.5 - 2 mm particle sizes were evaluated as 1.57, 1.46 and 0.9 mg/g, respectively. Clearly, smaller particle size of pellets delayed the breakpoint and caused increase in adsorption. Better adsorption with smaller particle sizes may be attributed to their large surface areas which reduces the equilibrium time. In large particle sizes, some of the interior pores are not accessible whereas more pores are accessible in small size particles and diffusion is faster. The particles having size < 1 mm showed best fluoride removal capacity but due to extremely small size, they were observed to clog the mesh present at the bottom of the column and some of the adsorbent was leached into treated water. On analyzing these results, 1-1.5 mm particle size was chosen for further experiments.

6.1.1.3 Effect of flow rate

Column adsorption experiments with varied flow rate were conducted at 16, 25 and 33 mL/min i.e at 1, 1.5 and 2 L/h. The process was carried out with the initial fluoride concentrations of 10 mg/L and bed height of 30 cm. Figure 6.1c presents the effect of flow rate on the breakthrough curve at these operating conditions. Results showed that the uptake of fluoride ions onto M-i-HAPa pellets decreased when the flow rate across the bed increased. This can be explained by the fact that the residence time of the fluoride ions in the column was not enough for the adsorption equilibrium to be reached at that particular flow rate and therefore the solute in the solution left the column early i.e before equilibrium occurred. The adsorption capacity for flow rate of 1, 1.5 and 2 L/h was found to be 1.46, 1.01 and 0.56 mg/g respectively. As shown in Figure 6.1c, the M-i-HAPa pellets were found to be exhausted at 16, 10 and 4.5 h when the flow rates were 1, 1.5 and 2 L/h respectively. At these flow rates, the respective empty bed contact time (EBCT) were observed to be 0.588 ,0.392 and 0.294 h i.e 35.28 , 23.62 and 17.64 min (Table 6.1). It was noted that the throughput volume also increased with a higher EBCT which means with increase in EBCT, the fluoride ions had more time to contact with the adsorbent resulting in higher removal of fluoride ions in the adsorption column. The same trend was also observed by other researchers while working with zinc ion adsorption in continuous mode [170].

6.1.1.4 Effect of bed height

Feed fluoride solution with 10 mg/L concentration was introduced into the adsorption column with 1 L/h flow rate in order to observe the effect of bed height on breakthrough curves. The breakthrough curves for fluoride adsorption on M-i-HAPa pellets at different bed heights of 5, 10 and 30 cm are shown in Figure 6.1d.

It is evident from the Table 6.1 that the exhaustion time and volume of treated fluoride solution increased with increasing the bed height due to more contact time available for adsorption. On the contrary, the breakthrough curve appeared steeper when the bed height was less indicating the faster exhaustion of the adsorbent bed due to lower contact time available between adsorbate and adsorbent. When the bed height was increased from 5 to 30 cm, the throughput volume of water upto breakthrough point (V_b) and exhaustion point (V_{EX}) varied between 1.5 to 13 L and 4 to 16 L respectively (Table 6.1). The fluoride uptake capacity (q_b) at 5, 10 and 30 cm bed height were observed to be 0.96, 1.16 and 1.46 mg/g. The higher fluoride uptake capacity with increase in bed depth is because of increase in the surface area of the adsorbent providing more number of binding sites to fluoride ions in solution. From Table 6.1, the increase in breakthrough time (t_b) is evident with increase in bed height, which shows that a delayed 't_b' points towards higher bed adsorption capacity. The results for column performance of fluoride adsorption by Kanuma mud studied by Chen et al. [171] also showed similar trend.

6.1.1.5 Effect of feed fluoride concentration

Experiments were conducted in column mode with two feed fluoride concentration viz, 5 and 10 mg/L to determine the effect of solute concentration on the behaviour of the breakthrough curve. Parameters such as bed height and flow rate were kept 30 cm and 1 L/h respectively during the experimental runs. It can be seen from Figure 6.1e that with increase in fluoride concentration the breakthrough time decreased as the binding sites became more quickly exhausted. The breakthrough time was 13 h at 10 mg/L feed fluoride concentration while it was 16 h at 5 mg/L. The fluoride adsorption capacity (q_b) and the total fluoride adsorbed upto exhaustion point (q_{EX}) were also found to increase with increase in feed fluoride concentration. The adsorption capacity of M-i-HAPa pellets at breakpoint and at exhaustion point were observed to increase from 0.8 to 1.46 mg/g and 1 to 1.8 mg/g respectively, with increase in fluoride concentration from 5 to 10 mg/L (Table 6.1). High feed fluoride concentration contributed to a higher driving force to overcome the mass transfer resistance. Also, the increase in inlet fluoride concentration increased the driving force for mass transfer, which in turn decreased the length of the adsorption zone

(δ). It was also noticed that a rise in the feed fluoride concentration decreases the volume treated before the bed in the column got exhausted as shown in Table 6.1. It means lower the feed fluoride concentrations, latter will be exhaustion of the adsorbent pellets. The exhaustion time for the M-i-HAPa pellets reduced from 20 to 16 h when the fluoride ion concentration was increased from 5 to 10 mg/L (Figure 6.1e, Table 6.1). Similar results were reported by Baral et al. [146] and Paudyal et al. [170] while working on chromium and zinc adsorption respectively.

Table 6.1: Experimental F^- adsorption data on M-i-HAPa pellets in column system for different process conditions

	Z (cm)			F (L/h)			C_0 (mg/L)		Particle size (mm)		
Parameters	5	10	30	1	1.5	2	5	10	<1	1-1.5	1.5-2
t_b(h)	1.5	3.5	13	13	6	2.5	16	13	14	13	8
t_{EX}(h)	4	6	16	16	8.5	4.5	20	16	17	16	12
V_b(L)	1.5	3.5	13	13	9	5	20	13	14	13	8
V_{EX}(L)	4	6	16	16	12.75	9	20	16	17	16	12
q_b (mg/g)	0.96	1.16	1.46	1.46	1.01	0.56	0.8	1.46	1.57	1.46	0.9
q_{EX}(mg/g)	2.5	2	1.8	1.8	1.43	1.01	1.00	1.8	1.91	1.8	1.35
EBCT (h)	0.098	0.196	0.588	0.588	0.392	0.294	0.588	0.588	0.588	0.588	0.588

After studying the effect of various parameters on column adsorption behaviour, it can be concluded that an efficient column performance can be achieved using spherical shaped pellets, slower flow rate, greater bed height and smaller particle size are desirable. Increase in feed fluoride concentration increase the adsorption capacity, however the column reached saturation faster and the breakthrough time was also shortened. On analyzing the breakthrough curves (Figure 6.1) and the experimental F^- adsorption data for different process conditions (Table 6.1); it is clear that bed height of 30 cm with 1-1.5 mm pellet particle size, flow rate of 1 L/h and feed fluoride concentration of 10 mg/L were optimum for efficient column performance.

Adsorption capacity from experimental curves is estimated to be 1.46 mg/g for 30 cm bed height, 1 L/h flow rate and 10 mg/L initial fluoride concentration. The adsorption capacities of the columns were slightly higher than their respective batch capacities (1.09 mg/g) for the same initial fluoride concentration (10 mg/L).

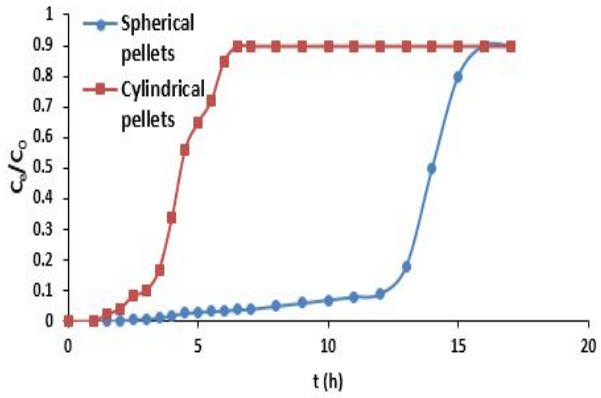

(a) Effect of different shapes of pellets (initial fluoride concentration: 10 mg/L, flow rate: 1 L/h, bed height: 30 cm)

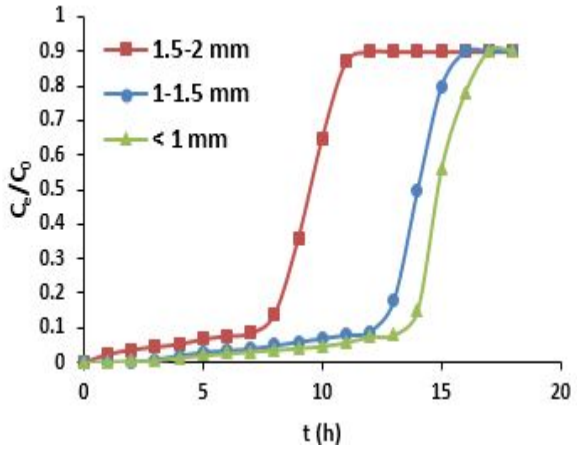

(b) Effect of varying particle size (initial fluoride concentration: 10 mg/L, flow rate: 1 L/h, bed height: 30 cm)

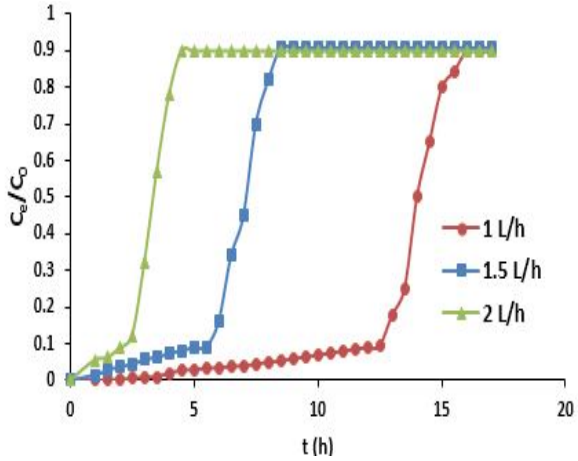

(c) Effect of varying flow rate (initial fluoride concentration: 10 mg/L, flow rate: 1-2 L/h, bed height: 30 cm)

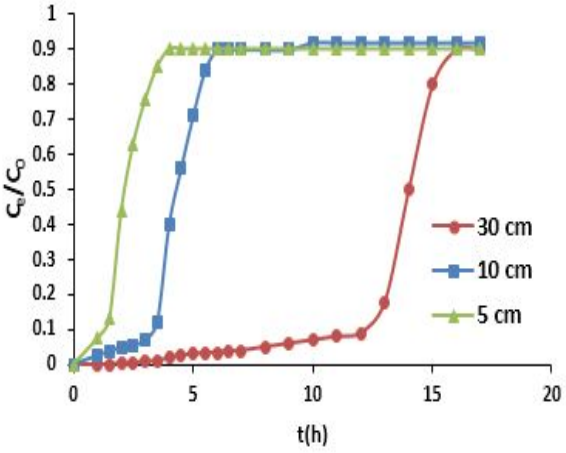

(d) Effect of bed height (initial fluoride concentration: 10 mg/L, flow rate: 1 L/h, bed height: 5-30 cm)

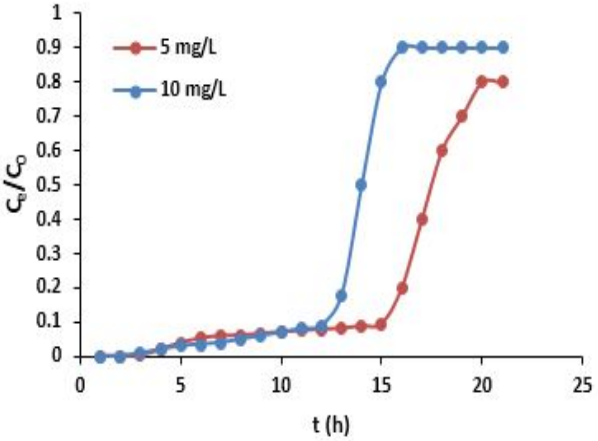

(e) Effect of varying feed fluoride concentration (initial fluoride concentration: 5-10 mg/L, flow rate: 1 L/h, bed height: 30 cm)

Figure 6.1: Effect of varying parameters influencing column adsorption behaviour

6.2 Simulation studies

The breakthrough curves for varying particle size and flow rates were generated through the simulator (ADSORB) to study the effect of these parameters. The concentration profiles with respect to time with varying flow rates and particles sizes were obtained from the MATLAB programme and validated with the experimental data. The input parameters for the programme are given in Table 6.2 and the programme code is given in the Appendix. The results in form of breakthrough curves are shown in Figure 6.2 and Figure 6.3. The theoretical breakthrough concentration curve obtained by numerical solution of the model in section 6.1.1.2 and section 6.1.1.3 were checked for convergence with the experimental profiles. From the simulated results, the data points corresponding to the experimental data obtained were taken and comparative graph were plotted.

The mathematical model was validated with the experimental data of this study as seen in Figure 6.2 and Figure 6.3. It was observed that initial part of breakthrough curve fitted extremely well with the simulated data and a little deviation was seen in latter part of curve. Experimentally, C_e/C_0 was obtained upto 0.9, but through the simulated data this ratio was 0.8. The breakthrough time as per simulated curve for 1, 1.5 and 2 L/h was 13.5, 6 and 3 h respectively while the same values corresponding to experimental curve was 13, 6 and 2.5 h.

Table 6.2: Input parameters for MATLAB program

Parameters	Values
Radius of adsorbent, m	Varied
Bed porosity	0.63
Particle porosity	0.37
Flow rate, m/s	Varied
Depth of bed, m	0.3
Diameter of bed, m	0.05
Initial concentration, mg/L	10
Solid phase adsorbate concentration, mg/g	1.1
Mass transfer coefficient, m/s	9.5×10^{-11}
Heat of adsorption, J/mol	38.13×10^{3}
Density of adsorbent, kg/m^3	280
Specific heat of liquid, J/kg.K	4200
Inlet temperature, K	298
Axial mass dispersion coefficient, m^2/s	10^{-5}
Axial heat dispersion coefficient, m.K	0.688

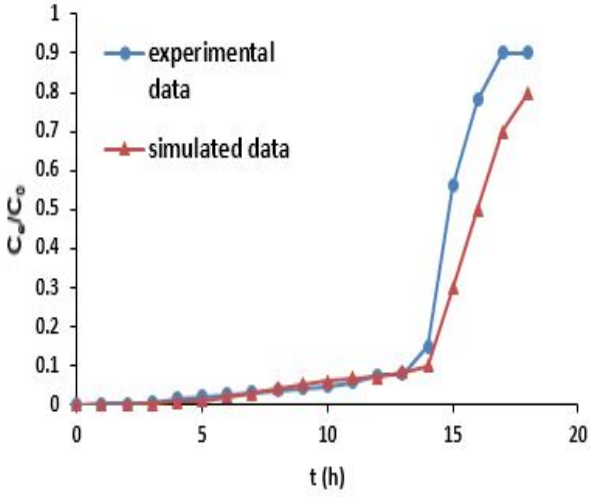

(a) Breakthrough curve at < 1 mm particle size

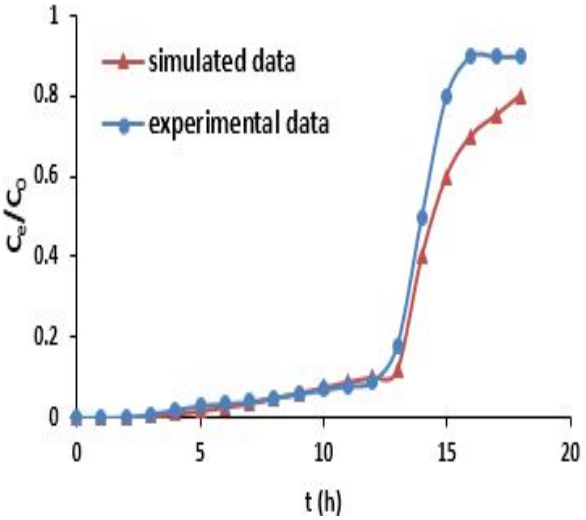

(b) Breakthrough curve at 1-1.5 mm particle size

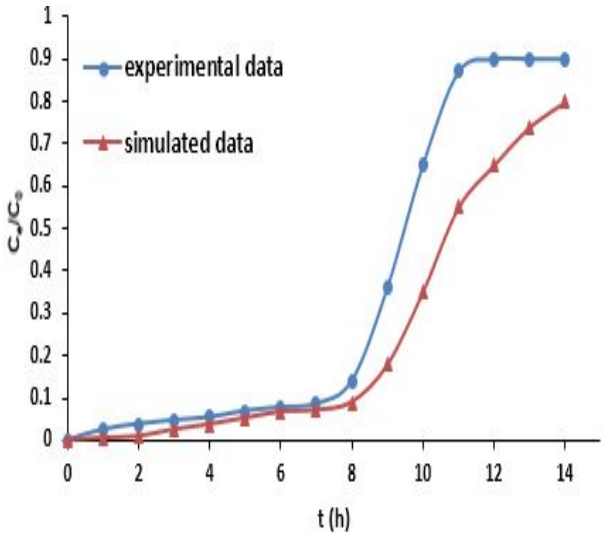

(c) Breakthrough curve at 1.5-2 mm particle size

Figure 6.2: Comparison of experimental and simulated breakthrough curves for varying particle sizes (initial fluoride concentration: 10 mg/L, flow rate: 1 L/h, bed height: 30 cm)

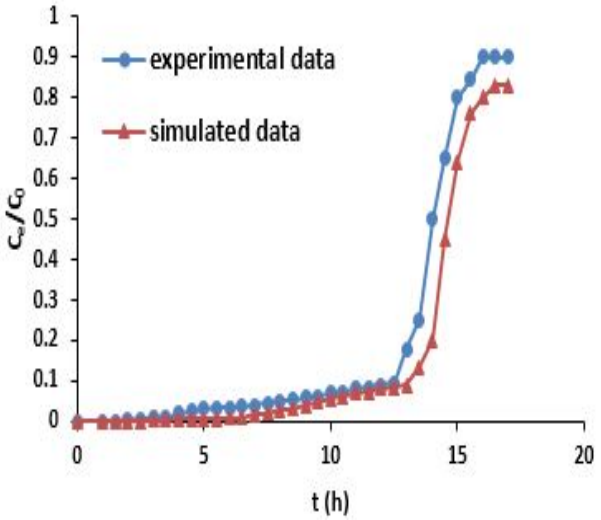

(a) Breakthrough curve at 1 L/h flow rate

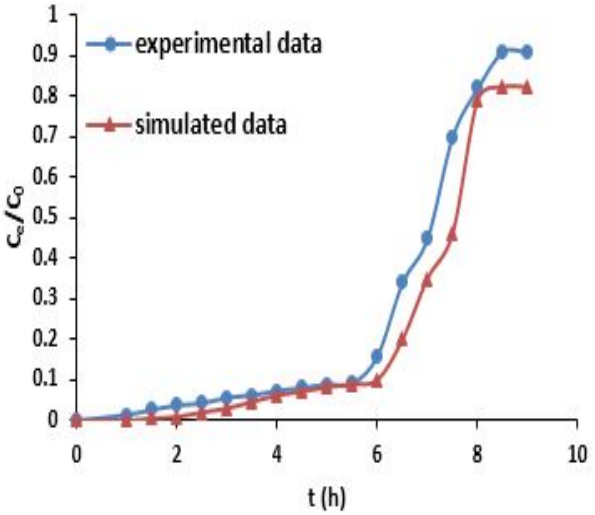

(b) Breakthrough curve at 1.5 L/h flow rate

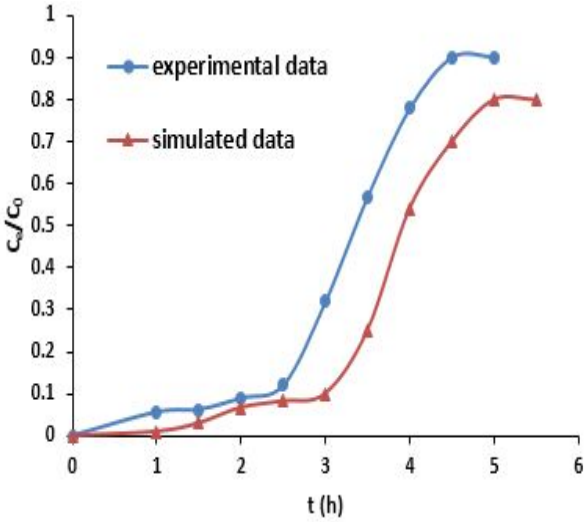

(c) Breakthrough curve at 2 L/h flow rate

Figure 6.3: Comparison of experimental and simulated breakthrough curves for varying flow rates (initial fluoride concentration: 10 mg/L, flow rate: 1-2 L/h, bed height: 30 cm)

6.3 Estimation of column design parameters

Breakthrough curves were obtained for varying operational conditions in the previous section. These curves were used to calculate the values of column design parameters such as t_x (time to establish primary adsorption zone), t_f (time for formation of primary adsorption zone), t_z (time for movement of primary adsorption zone down the column), δ (length of primary adsorption zone), f (fractional capacity of M-i-HAPa pellets in the adsorption

zone), % S (percentage saturation in column), and H_{UNB} (height of unused bed). The part of the adsorbent bed between C_{EX} (exhaustion concentration) and C_b(breakthrough concentration) is termed as the primary adsorption zone or PAZ. An illustration of movement of adsorption zone which results in breakthrough and finally exhaustion of the column is presented in Figure 6.4. The time required for the PAZ to establish and move out of the column was calculated from the following equation [172, 173]:

$$t_x = \frac{V_{EX}}{F} \tag{6.3.1}$$

The time needed for the movement of adsorption zone down its own length in the column may be computed by the equation given below [172, 173]:

$$t_z = \frac{(V_{EX} - V_b)}{F} \tag{6.3.2}$$

For a bed depth "Z" of M-i-HAPa pellets, the depth and time ratios can be calculated as follows [172, 173]:

$$\frac{\delta}{Z} = \frac{t_z}{(t_x - t_f)} \tag{6.3.3}$$

The time for the formation of PAZ is given by the following equation [172, 173]:

$$t_f = (1-f)\delta \tag{6.3.4}$$

The fractional capacity of the pellets in the adsorption zone may be computed as [172, 173]:

$$f = \frac{\int_{V_b}^{V_{EX}} (C_0 - C_t)dv}{C_0(V_{EX} - V_b)} \tag{6.3.5}$$

The percentage saturation of the column may be given by the following mathematical expression [172, 173]:

$$\%S = \left[1 + \frac{\delta(f-1)}{Z}\right] X\ 100 \tag{6.3.6}$$

The length of unused bed in a column system can be calculated from the following equation:

$$H_{UNB} = \frac{Z}{t_{EX}}(t_{EX} - t_b) \tag{6.3.7}$$

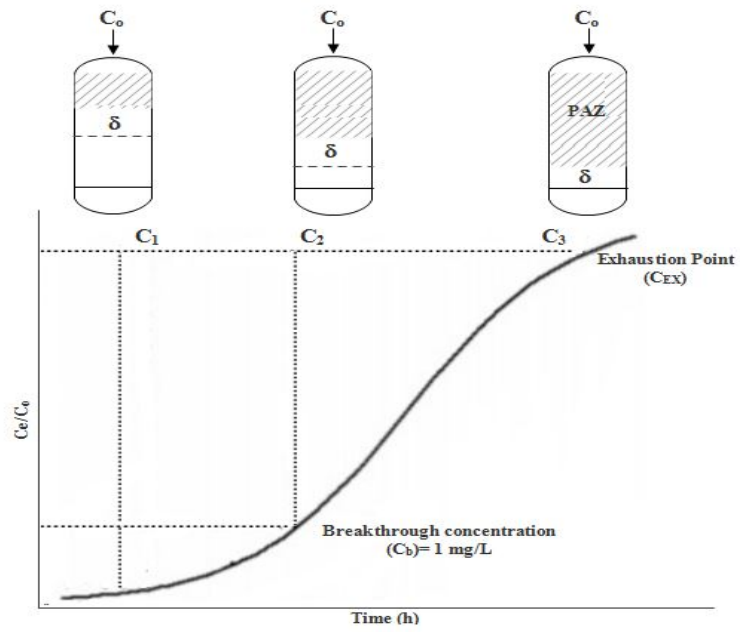

Figure 6.4: Illustration of movement of adsorption zone

The values of column design parameters as calculated using equations 6.3.1 to 6.3.7 is given in Table 6.3. The time required for the formation of the PAZ was noticed to decrease with decrease in bed height, increase in flow rate and feed fluoride concentration as expected. The higher the bed length, the more time it will take to form the primary adsorption zone. Similarly, with decrease in flow rate, the contact time necessary for formation of the zone also reduces. It was observed that the length of the adsorption zone of column increased as the flow rate and bed height increased. However, the percent saturation for column increased with increasing bed height and decreased with increasing flow rate. On the other hand, value of fractional capacity of column at breakthrough point decreased in general with rise in flow rate, feed fluoride concentration and increase in bed height. Similar trends were found by Ghosh et al. [174] while studying column performance of Ce(IV)-Zr(IV) mixed oxide nanoparticles. Reduction in the "f" value was due to the less number of fluoride ions available ion per active adsorption site with increase in bed height. As the flow rate was elevated, the value of δ increased and the % S decreased since the adsorption zone travelled faster. However, for bed height of 5 cm, 10 cm and fluoride concentration of 5 mg/L, 10 mg/L, the "f" value was approximately same in this study. Furthermore, owing to the greater degree of freedom of the fluoride ions over the adsorbent pellet surface, the adsorption zone was found to decrease slightly with increase in fluoride concentration in the feed water. It can be seen from the Table 6.3 that more amount of adsorbent bed remains unused when the flow rate is high since at higher flow rates the fluoride solution leaves the

column early.

Table 6.3: Column design parameters

	Z (cm)			F (L/h)			C_0 (mg/L)	
Parameters	5	10	30	1	1.5	2	5	10
t_x(h)	4	6	16	16	8.5	4.5	20	16
t_z(h)	2.5	2.5	3	3	2.5	2	4	3
t_f(h)	1.37	1.4	1.6	1.6	1.52	1.25	1.8	1.6
δ (cm)	4.77	5.43	6.24	6.24	10.71	18.46	6.59	6.24
f	0.45	0.44	0.467	0.467	0.391	0.375	0.5	0.467
% S	48.3	69.59	88.91	88.91	78.25	61.54	90.1	88.91
H_{UNB}(cm)	3.12	4.16	5.62	5.62	8.82	13.32	6	5.62

6.4 Application of the breakthrough curve

Time for attaining breakthrough and the shape of the curve are essential characteristics for predicting the operation and dynamic response of the fluoride adsorption column. In this study, three mathematical models viz. Hutchins Bed depth service time model (BDST model), the Thomas model and the Yoon-Nelson model were applied to predict the adsorption behaviour of fluoride ions in the column packed with M-i-HAPa pellets.

6.4.1 Application of the Hutchins Bed Depth Service Time (BDST) model

Hutchins Bed Depth Service Time (BDST) model can be used to predict column performance of any height from some existing experimental data on the same. Therefore, this model holds its significance in scaling up of the column system. The BDST model was used to describe the linear relationship between the breakthrough time (t_b) and bed depth (Z) as given in Eq. 3.4.19. Application of the BDST model with variations in the flow rate at constant feed fluoride concentration (10 mg/L) is presented in Figure 6.5a and variations in feed fluoride concentration at constant flow rate (1 L/h) is presented in Figure 6.5b. The results show that the slope tend to increase when the feed fluoride concentration and flow rate decreases, allowing to treat more volume of solution. The BDST adsorption potential (N_0) and rate constant of the adsorption reaction (K_A) were calculated from the slope and intercept of the graph for different flow rates and fluoride concentrations and are given in Table 6.4. The BDST adsorption potential represented by N_0 increased about 68 % when the fluoride concentration was increased from 5 to 10 mg/L and the N_0 was observed to

decrease gradually from 236.7 mg/L to 94.79 mg/L when the flow rate increased 1 L/h to 2 L/h. . The high value of N_0 along with high correlation coefficient (R^2) suggests the high efficiency of M-i-HAPa pellets and ensures the validity of Hutchins BDST model for the column adsorption system.

The critical bed depth "Z_0" was calculated from Eq. 3.4.20 and is listed in Table 6.4. The critical bed depth is defined as the theoretical bed height essential to prevent the adsorbate concentration to exceed the breakthrough concentration (C_b). As seen from the Table 6.4, the value of critical bed depth increases for higher flow rates as the contact time between adsorbate and pellets decrease and more adsorbent is needed to prevent the effluent concentration to be less than C_b . Similarly, for a high fluoride feed solution the critical bed depth needs to be higher as compared to a low fluoride feed solution since more number of fluoride ions are available which requires more adsorbent surfaces for adsorption.

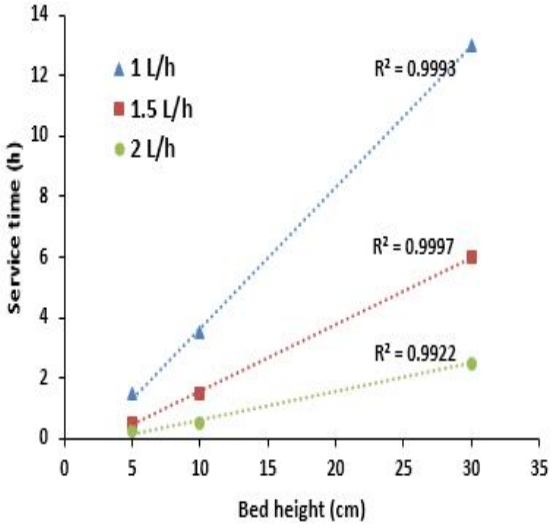

(a) BDST plot for varying flow rates

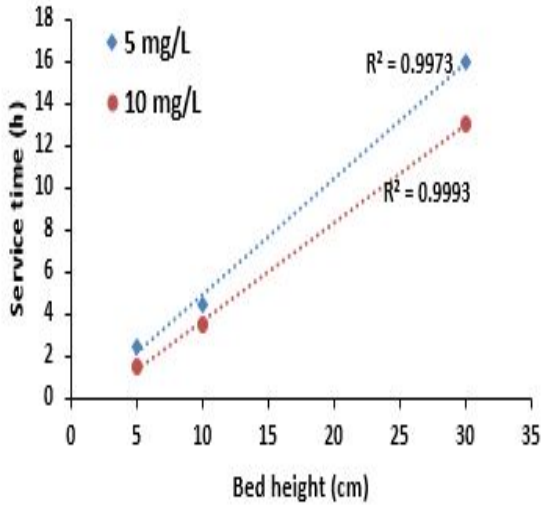

(b) BDST plot for varying feed fluoride concentration

Figure 6.5: BDST plot showing relationship between service time and bed height

Table 6.4: Kinetics parameters for Hutchins BDST model

	F (L/h)			C_0 (mg/L)	
Parameters	1	1.5	2	5	10
N_0(mg/L)	236.7	169.13	94.79	140.3	236.7
K_A(L/mgh)	0.227	0.334	0.708	0.548	0.227
R^2	0.9993	0.9997	0.9922	0.9973	0.9993
Z_0(cm)	2.07	2.96	3.33	1.06	2.08

6.4.2 Application of Thomas Model

Thomas model was used for predicting the dynamic behavior of the adsorption bed in the column system. The Thomas model constants "k_{th}" and "q_0" were determined from the plot of ln (C_0/C_e-1) against t at predetermined flow rates, bed heights and feed fluoride concentrations. The model parameters thus obtained are listed in Table 6.5. It was noted that the value of "k_{th}" decreased with increase in bed depth while the value of "q_0" increased. The Thomas constant (k_{th}) decreased due to increased mass transport resistance since the mass transport resistance is proportional to axial dispersion and thickness of the liquid film on particle surface [123, 174]. The Thomas adsorption capacity (q_0) increased because of higher contact time of fluoride ions with M-i-HAPa pellets.

As the flow rates were increased, the values of k_{th} increased while the values of q_0 reduced due to lower mass transport resistance and faster exhaustion of adsorbent bed. With increasing feed fluoride concentration (C_0) the values of k_{th} decreased, as with increase in $C_0$the solute acquired greater degree of freedom over the adsorbent surface. The q_0 value was higher at higher fluoride concentration since more fluoride ions were loaded per active adsorption site on the pellets which in turn caused faster saturation of adsorbent bed and lower throughput volume. With increase in particle size the q_0 values decreased from 2.59 to 1.09 mg/g while the k_{th} values showed a reverse trend. Lower particle size have greater surface area for adsorption and hence the magnitude of thomas adsorption capacity was more. A high correlation value (R^2) was observed for all the operating conditions as seen in Table 6.5 which suggested than the experimental data fitted well to the Thomas model.

Table 6.5: Kinetics parameters for Thomas model

	Z (cm)			F (L/h)			C_0 (mg/L)		Particle size (mm)		
Parameters	5	10	30	1	1.5	2	5	10	<1	1-1.5	1.5-2
k_{th} (L/mg h)	0.162	0.122	0.0501	0.0501	0.0784	0.31	0.060	0.050	0.027	0.050	0.054
q_0(mg/g)	1.61	1.65	1.58	1.58	1.22	0.43	1.00	1.58	2.59	1.58	1.09
R^2	0.961	0.955	0.971	0.971	0.974	0.98	0.952	0.971	0.935	0.971	0.953

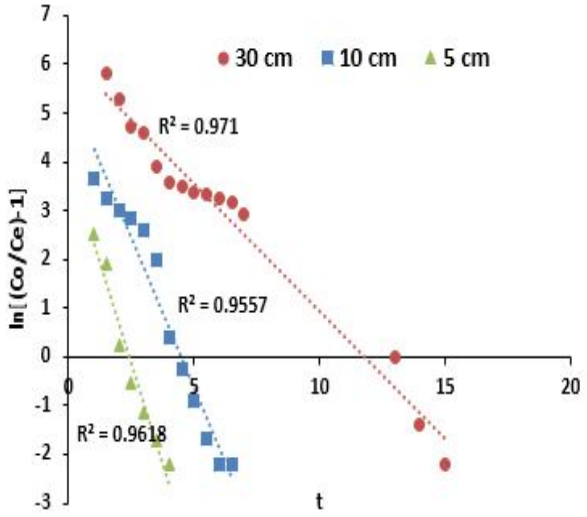

(a) Thomas model plots at varying bed heights

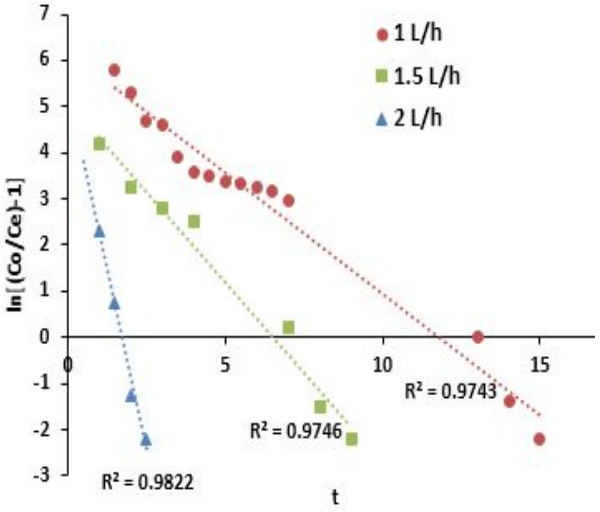

(b) Thomas model plots at varying flow rates

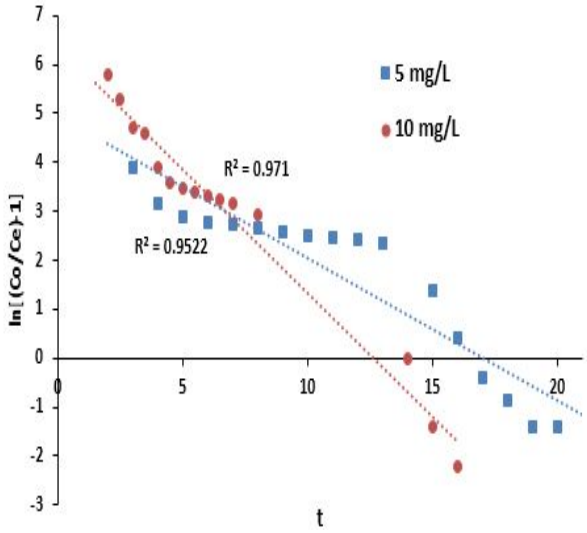

(c) Thomas model plots at varying feed fluoride concentrations

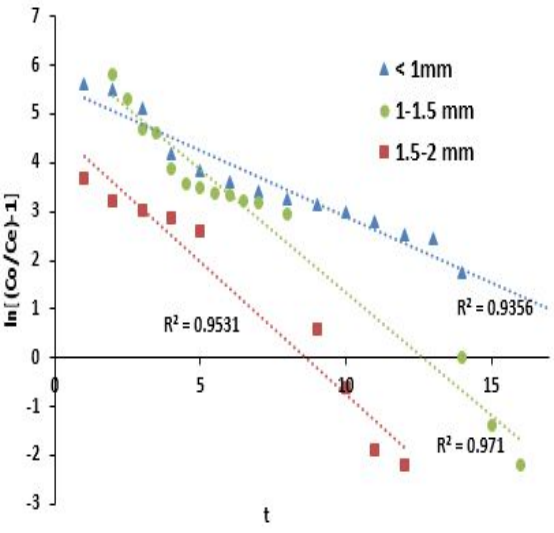

(d) Thomas model plots at varying particle sizes

Figure 6.6: Thomas model plots

6.4.3 Application of Yoon-Nelson model

Yoon and Nelson model was proposed for a single-component system and is described by the equation in Eq 3.4.22. The values of K_Y(Yoon - Nelson rate constant) and τ (time required for 50 % adsorbate breakthrough) were determined from the graph between ln $(C_e/C_0 - C_e)$ vs "t" at varying flow rates, bed heights, particle sizes and feed fluoride concentrations. It was noted from Table 6.6 that values of "τ" i.e the time required for 50% adsorbate breakthrough increased with increase in bed height whereas it decreased

with corresponding increase in flow rate, fluoride concentration and particle size. Similar trends were reported by Baral et al. [146] and Malkoc et al. [175] Yoon-Nelson model showed poor fitting with the experimental data with correlation coefficients less than 0.96 as shown in Figure 6.7 and Table 6.6.

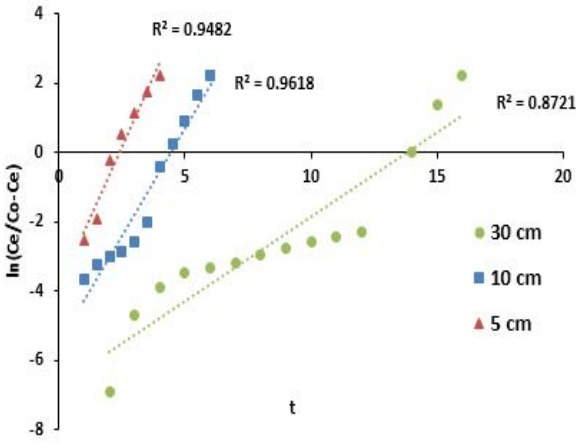

(a) Yoon-Nelson model plots at varying bed heights

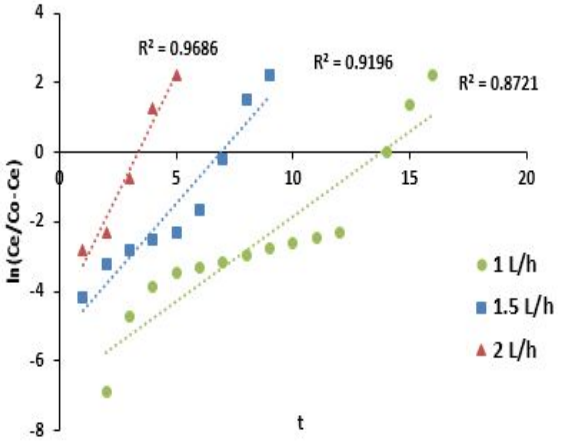

(b) Yoon-Nelson model plots at varying flow rates

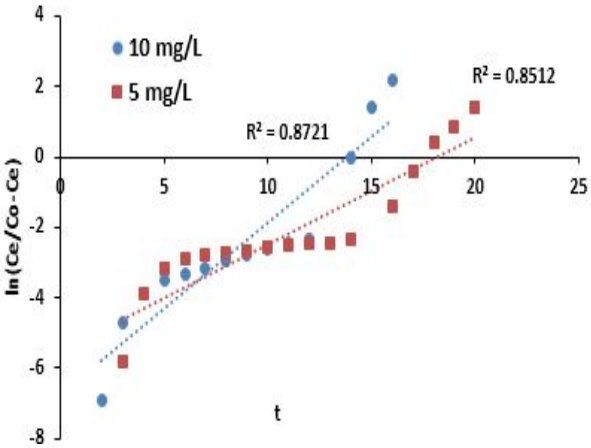

(c) Yoon-Nelson model plots at varying feed fluoride concentration

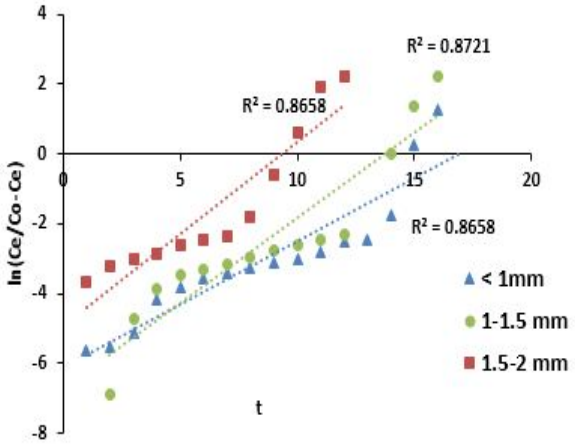

(d) Yoon-Nelson model plots at varying particle sizes

Figure 6.7: Yoon-Nelson model plots

Table 6.6: Kinetics parameters for Yoon-Nelson model

	Z (cm)			F (L/h)			C_0(mg/L)		Particle size (mm)		
Parameters	5	10	30	1	1.5	2	5	10	<1	1-1.5	1.5-2
$K_Y(h^{-1})$	1.62	1.254	0.488	0.488	0.764	1.36	0.303	0.488	0.361	0.488	0.524
τ (h)	2.4	4.42	13.83	13.83	6.92	3.36	18.18	13.83	16.89	13.83	9.33
R^2	0.961	0.948	0.872	0.872	0.919	0.968	0.851	0.872	0.865	0.872	0.865

6.5 Column performance evaluation

The performances of column systems are predicted by the number of bed volumes (BV) treated before the breakthrough point and the adsorbent exhaustion rate (AER). The number of bed volumes is calculated from the following expression [146, 174, 175]:

$$BV = \frac{Volume\,of\,water\,treated\,at\,breakpoint\,(L)}{Volume\,of\,adsorbent\,bed\,(L)} \tag{6.5.1}$$

It is assumed that higher number of bed volumes prior to the breakpoint depicts a better adsorption in the column system.

The AER can be defined as mass of adsorbent used per volume of solution treated at breakthrough point. The AER is an indicator of the column performance efficiency and the value of the adsorbent exhaustion rate reflects the goodness of the adsorbent bed performance. It can be estimated from the following equation [146, 174, 175]:

$$AER = \frac{Mass\,of\,M-i-HAPa\,pellets\,(g)}{Volume\,of\,water\,treated\,(L)} \tag{6.5.2}$$

The calculated values of BV and AER are given in Table 6.7. It was noted that the number of bed volumes processed before the breakpoint increased as the bed height increased whereas it decreased when the flow rate, feed fluoride concentration and particle size increased. The adsorbent exhaustion rate was faster at higher flow rates, bed heights, particle sizes and higher fluoride concentration as expected. Several other researchers also noted the same trend for BV and AER [146, 174, 175].

Table 6.7: Column performance indicators at different operating conditions

	Z (cm)			F (L/h)			C_0(mg/L)		Particle size (mm)		
Parameters	5	10	30	1	1.5	2	5	10	<1	1-1.5	1.5-2
Processed BVs	15.30	17.85	22.1	22.1	15.30	8.50	27.21	22.1	23.8	22.1	13.6
AER (g/L)	9.33	7.71	6.15	6.15	8.88	16	5	6.15	5.71	6.15	10

6.6 Regeneration

Regeneration studies provide an insight about the mechanism of adsorption as well as the stability of the adsorbent before further use. As per literature, adsorption of fluoride

on adsorbents are either chemical, physical or ion exchange or a combination. Physical adsorption would mean that the fluoride ions are loosely bound to the adsorbent surface and can easily be desorbed. But, if the nature of adsorption is chemical or ion exchange or both, then strong acidic or alkaline solutions needed to be used. Thus, the desorption behaviour helps in confirming the mechanism of adsorption. M-i-HAPa pellets saturated with fluoride were washed with double distilled water and only 2 % desorption was found. Dilute alkali (0.1 M NaOH) solution was found to be an effective regenerant in the batch system (section 5.7.11), therefore it was also used for regeneration of M-i-HAPa pellets in the column mode.

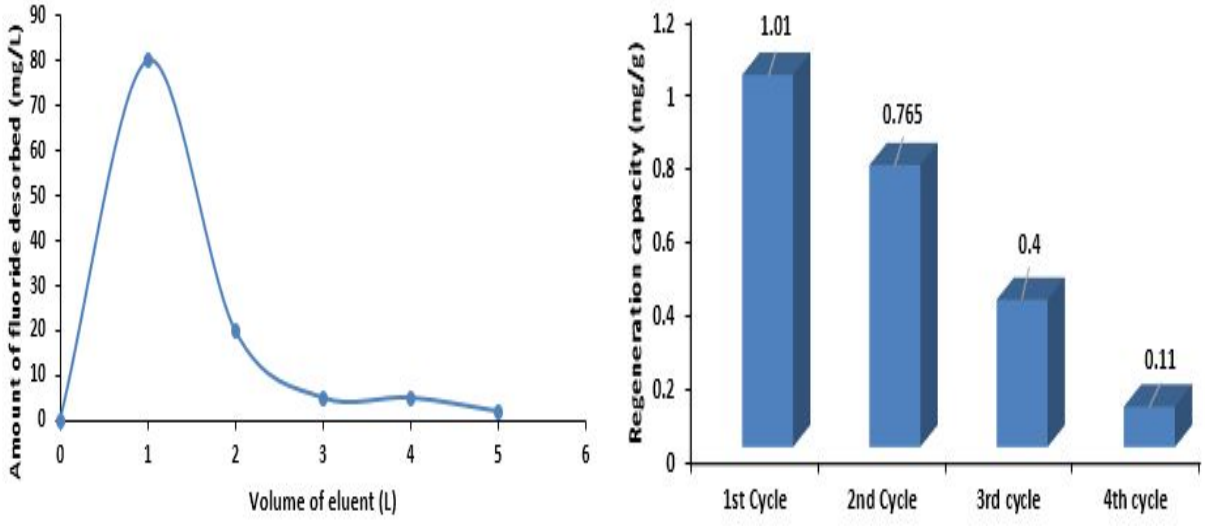

(a) Desorption of fluoride from M-i-HAPa pellets (b) Regeneration capacity

Figure 6.8: Desorption-Regeneration Process

After M-i-HAPa pellets were exhausted using 10 mg/L fluoride solution at 1 L/h, they were regenerated using 0.1 M NaOH solution in an upflow mode at a flow rate of 1 L/h for 5 h. The intent was to use minimum eluent solution to remove the fluoride ions from the adsorbent bed.

For verifying the performance stability of the M-i-HAPa pellets column, three cycles of adsorption and regeneration process were conducted. In each cycle, similar results were found and average results are reported. The volume of eluent collected versus the amount of fluoride desorbed showed that major amount of fluoride (~ 69%) was desorbed in first 1 h and the remaining fluoride was collected in the next 4 h with a total of 5 L of NaOH solution used as shown in Figure 6.8a. The regenerated adsorbent was then utilized again in the column system for defluoridation and the adsorption capacity was observed to be reduced. The adsorbent pellets were then subjected to the elution-retention process for

four cycles, after which its capacity to adsorb fluoride diminished significantly as shown in Figure 6.8b. This indicates that for complete use of the synthesized pellets, regeneration is required after every defluoridation cycle.

The higher percentage of desorption signify towards an ion exchange mechanism for adsorption process. Similar adsorption mechanism was noticed in the batch regeneration experiments shown in section 5.7.11. Regeneration of M-i-HAPa pellets through alkaline solution supported the fact that adsorption mechanism is chemical in nature.

6.7 Characterization of M-i-HAPa pellets

In order to study fluoride removal in column mode, M-i-HAPa adsorbent was pelletized into spherical shape using polyvinyl alcohol (PVA) and malonic acid as a binder. In this section, FTIR, XRD, SEM and XPS techniques are used for characterizing the M-i-HAPa pellets before adsorption, after adsorption and after regeneration. BET surface area, pore volume and pore diameter has been determined for M-i-HAPa pellets.

6.7.1 FTIR

The FTIR spectra of the M-i-HAPa pellets before fluoride adsorption, after fluoride adsorption and after regeneration are presented in Figure 6.9. The bands present at 3420 $cm^{-1}$and 633 cm^{-1} represent the characteristic stretching vibration modes of the -OH group. The peaks observed around 1465 cm^{-1}indicate the incorporation of CO_3^{2-} ions in the OH– sites, because when the reaction conditions are alkaline some OH^- ions from the solution may react with the atmospheric CO_2 present. The bands for PO_4^{3-} appeared around 1045 $cm^{-1}$and 565 cm^{-1}corresponding to the characteristic phosphate peaks in apatite. The adsorption capacity of an adsorbent depends on chemical reactivity of functional groups at the adsorbent surface [176].

The FTIR spectra obtained after adsorption of fluoride display a significant decrease in intensity of OH^- peaks due to formation of OH–F bonds. This confirmed that hydroxyl ions in the adsorbent are replaced by fluoride ions in the adsorption process.

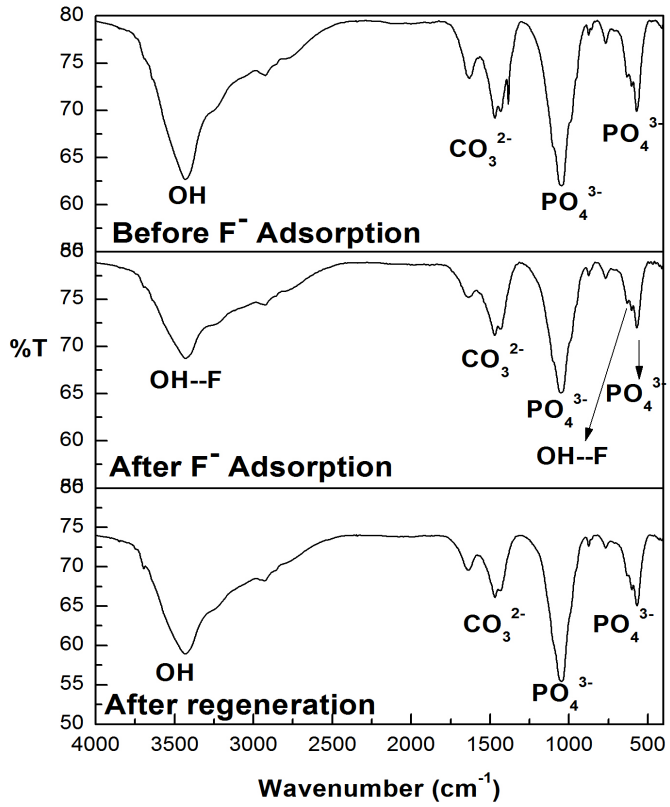

Figure 6.9: FTIR of M-i-HAPa pellets

6.7.2 XRD

The XRD pattern of M-i-HAPa pellets before fluoride adsorption (M-i-HAPa pellets), after fluoride adsorption (M-i-HAPF pellets) and after regeneration (M-i-HAPR pellets) are shown in Figure 6.10. The peaks obtained before fluoride adsorption can be indexed to hydroxyapatite and magnesium oxide with JCPDS card number 09-0432 and 89-4248 respectively. The pattern obtained after fluoride adsorption revealed the formation of hydroxyfluoroapatite, fluoroapatite and magnesium fluoride corresponding to JCPDS card numbers 034-0010, 034-0011 and 01-1196. This showed that the hydroxyapatite peaks are replaced by hydroxyfluoroapatite and fluoroapatite while the magnesium oxide peak was replaced by magnesium fluoride. After regeneration of M-i-HAPa pellets, XRD pattern obtained was similar to the one before adsorption of fluoride. The crystallite size calculated as per Scherer equation is 48.7 nm.

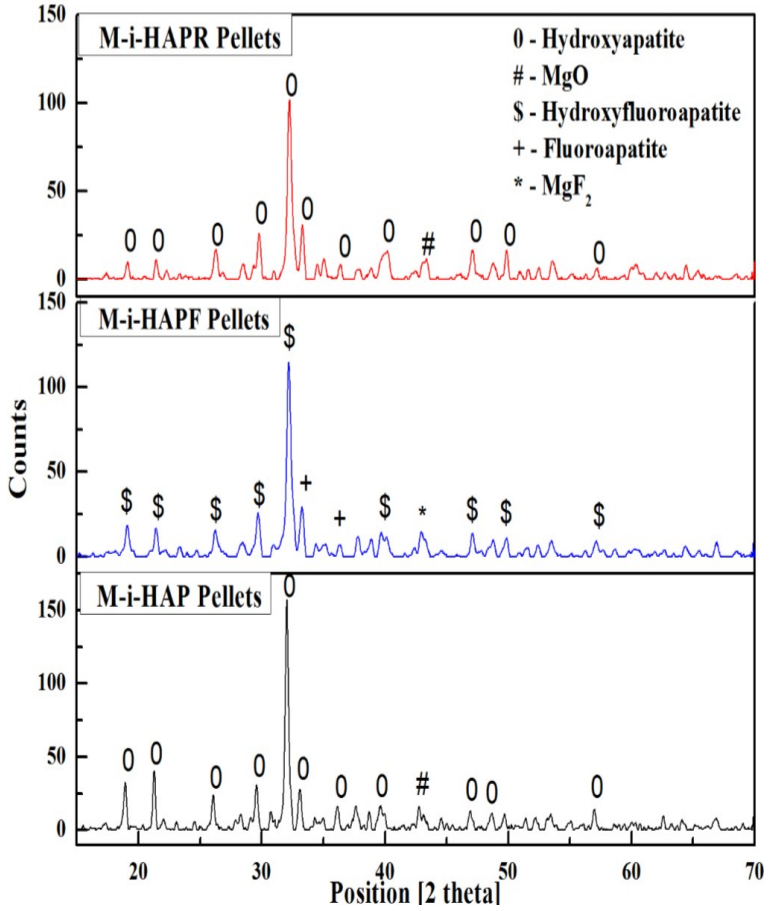

Figure 6.10: XRD pattern of M-i-HAPa pellets

6.7.3 SEM

Scanning electron micrograph for M-i-HAPa pellets before fluoride adsorption, after fluoride adsorption and after regeneration taken at 2000X magnification are given in Figure 6.11. The fresh pellets show extremely rough surface with a number of pores on the surface which may be used for capturing fluoride ions from the solution. For a better glimpse on the surface morphology of the unused adsorbent SEM image at 100000X magnification is presented in Figure 6.11b which exhibit the porous nature of the adsorbent. Micrographs of the fluoride loaded M-i-HAPa pellets showed a distinct change in the morphology as compared to micrograph obtained before adsorption. In Figure 6.11c fluoride ions appeared adhering to the surface of the pellets and most of the pores were occupied by fluoride ions. Post regeneration, the surface of the pellets again display a porous texture signifying the removal of fluoride from pores as given in Figure 6.11d. It means that the regenerated adsorbent can again be used for defluoridation experiments. However, the pellet surface showed reduced number of pores as compared to the unsused adsorbent which point to the

fact that after each cycle of regeneration, the adsorbent would loose some of its adsorption capacity.

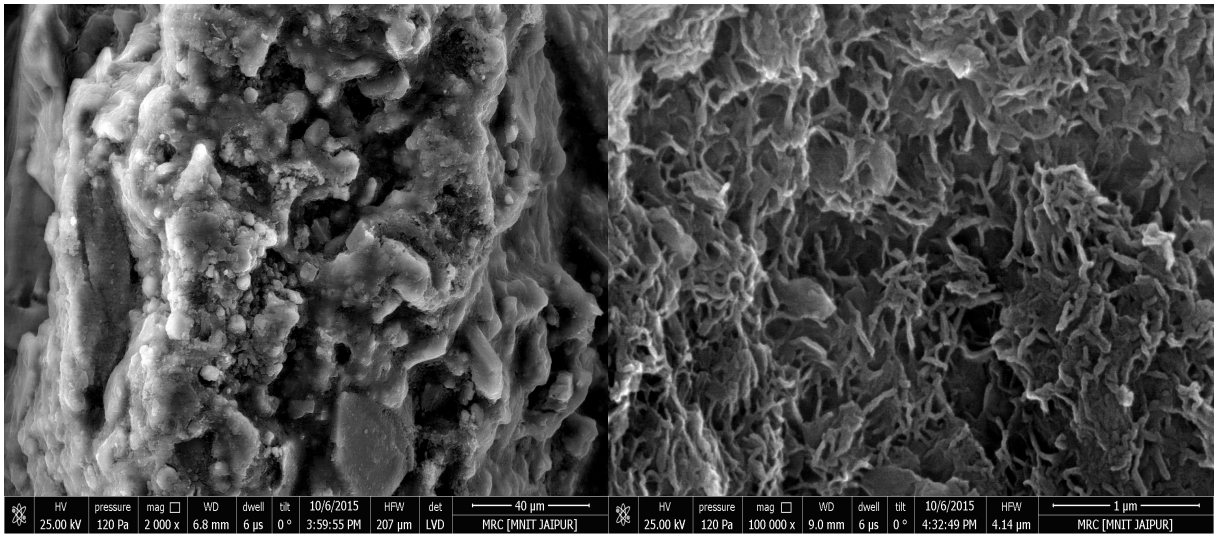

(a) SEM image of M-i-HAPa pellets before adsorption at 2000X magnification

(b) SEM image of M-i-HAPa pellets before adsorption at 100000X magnification

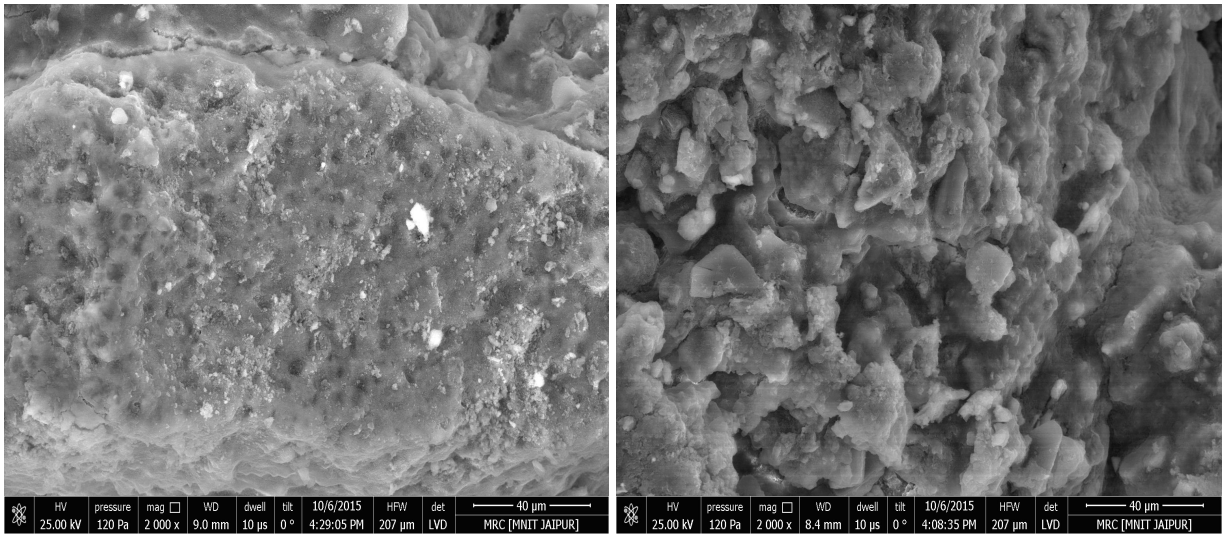

(c) SEM image of M-i-HAPa pellets after adsorption at 2000X magnification

(d) SEM image of M-i-HAPa pellets after regeneration at 2000X magnification

Figure 6.11: SEM image of M-i-HAPa pellets

6.7.4 BET surface area, pore volume and pore diameter

After pelletizing the powdered form of M-i-HAPa adsorbent using PVA and malonic acid as binders, the pellets were characterized for estimating the changes in surface area, pore volume and pore diameter. The specific surface area of M-i-HAPa pellets was found to

be 21.22 m^2/g while the pore volume and pore diameter was observed to be 0.096 cm^3/g and 181.59 Å respectively. Due to pelletization, 54.48 % reduction in surface area was observed. It was noticed that the specific surface area after pelletizing decreased from 46.62 m^2/g to 21.22 m^2/g, which may be due to modification during the extrusion-spheronization procedure. Maliyekkal et al. [66] and Tripathy and Raichur [67] also reported decrease in surface area after modification of activated alumina spherical balls with magnesia and manganese dioxide respectively. It is is interesting to note that the specific surface area and pore volume of M-i-HAPa pellets was approximately same as that of pHAP (21.25 m^2/g, 0.09 cm^3/g). However, the pore diameter of M-i-HAPa pellets was higher than both pHAP (169 Å) and M-i-HAPa powder (153 Å).

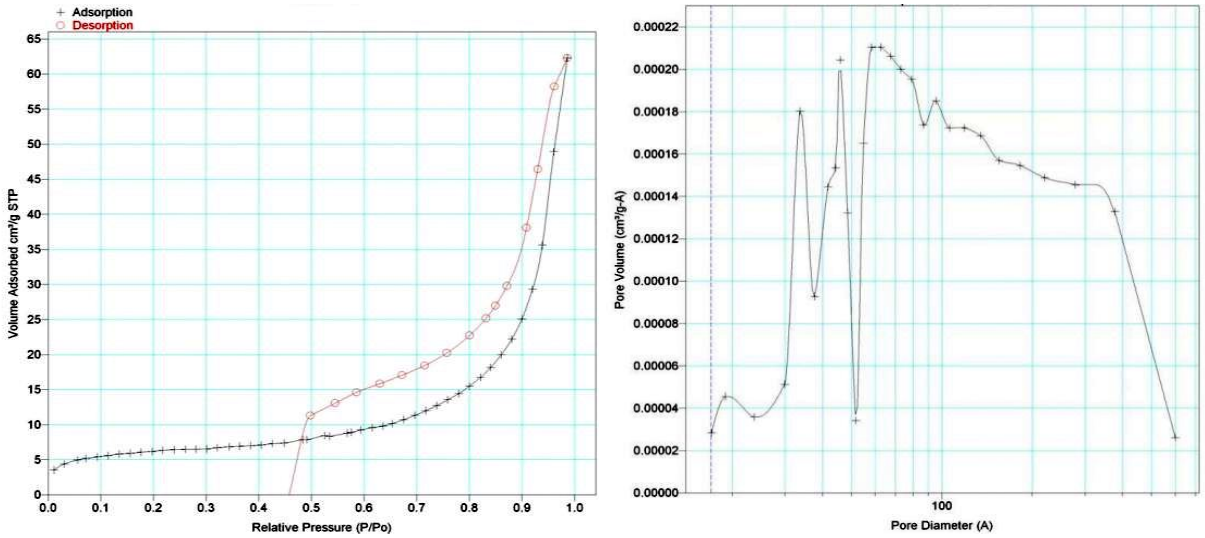

(a) BET surface area of M-i-HAPa pellets

(b) Pore volume of M-i-HAPa pellets

Figure 6.12: BET surface area and pore volume of M-i-HAPa pellets

6.7.5 XPS

XPS analysis was carried out with M-i-HAPa adsorbent before fluoride adsorption, after fluoride adsorption and after regeneration (Figure 6.13). The wide scan XPS spectra is given in Figure 6.13a which indicates that Ca, Mg, O and P are present in the adsorbent before adsorption. A fluoride characteristic peak at 685 eV is spotted for M-i-HAPa pellets after fluoride adsorption, which confirmed that fluoride is being adsorbed (Figure 6.13b). The intensity of this peak is smaller since the adsorbent was not totally saturated with fluoride and 10 mg/L fluoride solution was used in the adsorption process. A decrease in intensity of peaks for magnesium and calcium was observed in fluoride loaded sample as compared to fresh adsorbent sample. However, the intensity of these peaks again increased

in regenerated sample. The XPS spectra obtained in Figure 6.13c after regeneration of the pellets is similar to the spectra before fluoride adsorption. This showed that the adsorbent pellets were regenerated successfully.

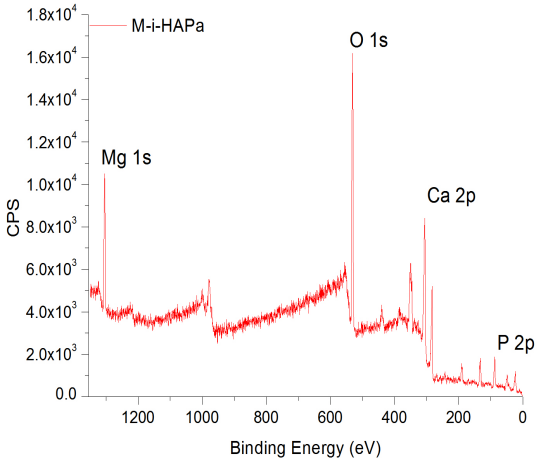

(a) XPS spectra for M-i-HAPa pellets before adsorption

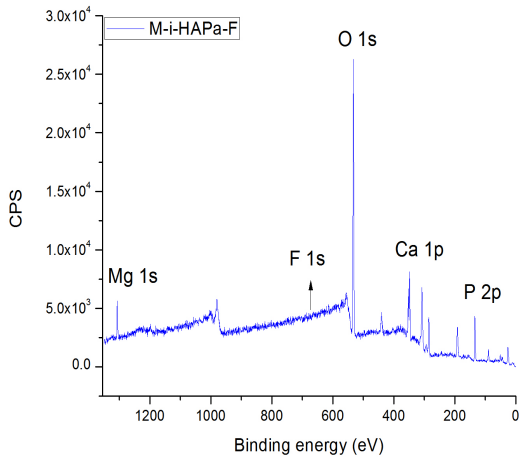

(b) XPS spectra for M-i-HAPa pellets after adsorption

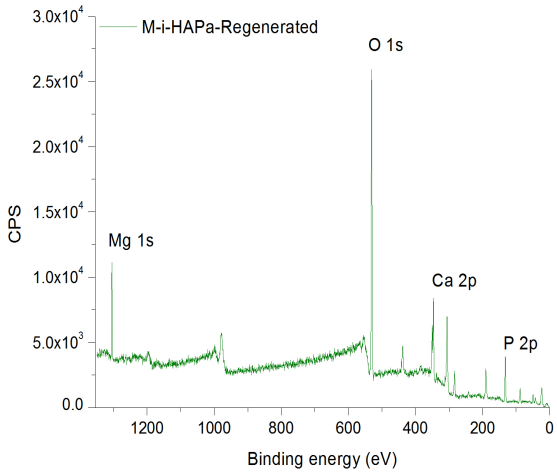

(c) XPS spectra for M-i-HAPa pellets after regeneration

Figure 6.13: Wide scan XPS spectra for M-i-HAPa pellets

6.8 Summary of the Chapter

The M-i-HAPa pellets synthesized in the laboratory were found to be an effective defluoridation agent in column adsorption system. The adsorption capacity was observed to be 1.46 mg/g at feed fluoride concentration of 10 mg/L, flow rate of 1 L/h and bed

height of 30 cm. The effect of varying adsorption parameters such as flow rate, fluoride concentration, particle size, particle shape and bed height on the removal of fluoride was studied. Adsorption column dynamics was also studied through simulation to optimize the column configuration for fluoride removal.

The performance of the column system was evaluated in terms of number of bed volume and adsorbent exhaustion rate. It was noticed that for 30 cm bed height, 22.1 bed volumes can be processed and the AER for the same was 6.15 g/L. Experimental data were fitted to Hutchins BDST model, Thomas model and Yoon-Nelson model to obtain characteristic parameters from each model. Thomas and Hutchins BDST model fitted well with the data with very high correlation coefficient value. The adsorption capacity calculated from Thomas model was very close to the experimentally obtained values at all operating conditions. Regeneration studies were conducted to confirm the mechanism of adsorption and study the stability of the adsorbent during defluoridation. The results showed that the pellets were stable for repeated use upto four times. The desorption experiments also confirmed the ion exchange mechanism dominating the process of adsorption. The adsorption capacities of the columns were slightly higher than their respective batch capacities (qe = 1.09 mg/g) for the same initial fluoride concentration (10 mg/L). The reason for the observed differences between the batch and column systems may be that the pores in M-i-HAPa pellets were utilized more in column mode relative to the batch test.

Characterization of M-i-HAPa pellets assisted in getting a much clear view of the defluoridation process and regeneration. The FTIR results obtained after adsorption of fluoride confirmed that hydroxyl ions in the adsorbent are replaced by fluoride ions and formation of hydroxyfluoroapatite, fluoroapatite and magnesium fluoride was observed through XRD pattern. Further through SEM micrographs fluoride ions appeared adhering to the surface of the pellets and most of the pores were occupied by fluoride ions. Post regeneration, the surface of the pellets again display a porous texture signifying the removal of fluoride from pores. It means that the regenerated adsorbent can again be used for defluoridation experiments.

CHAPTER 7

Chapter 7

Studies with Field Water Samples and Assessment of Treated Water Quality

This chapter is accentuates the field application of M-i-HAPa adsorbent via studies with field water samples and assesment of treated water quality. In order to make the M-i-HAPa adsorbent feasible for field water applications, samples were collected from fluorosis prone areas and treated with the adsorbent for their water quality assessment. Physico-chemical properties of groundwater are the chief tool to determine the water quality and its suitability for drinking [177, 178]. The water quality standards help to identify the problems associated as well as support the efforts to achieve and maintain protective water quality conditions [179].

Water quality parameters for M-i-HAPa powder with distilled water was discussed in section 5.7.12 in order to confirm the suitability of the adsorbent to explore further. This chapter presents analysis of field water samples with M-i-HAPa powder adsorbent and M-i-HAPa pellets. Physico-chemical parameters such as TDS, EC, pH, total hardness, total alkalinity were studied along with leaching tests for calcium, magnesium and phosphate ions. Finally, a domestic defluoridation unit was designed for M-i-HAPa pellets and its performance was assessed.

7.1 Field sample collection

Rajasthan is a classic case of falling water tables and increasing incidence of fluoride in water. The state has extreme climatic and geographical condition with low water resources. There being no perennial surface source for drinking water, the state is dependent chiefly on groundwater and its level is deeper year-by-year due to over exploitation. Considering the high fluoride concentration in groundwater and severity of fluorosis cases in the state

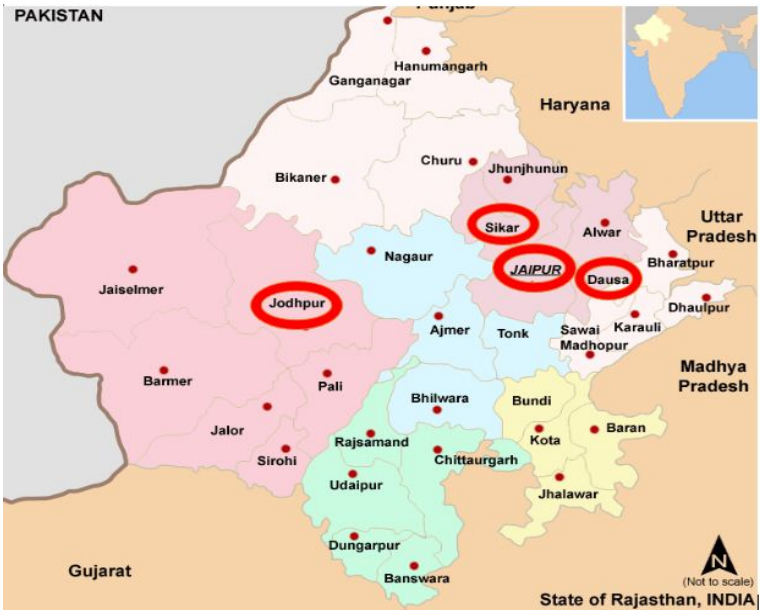

Figure 7.1: Different districts of Rajasthan (Samples collected from the marked districts)

of Rajasthan, it was selected for conducting field studies. Being the largest state of the country Rajasthan covers 10.4 % of total geographical area of the country with only 1 % of water resources accessible to the state for 5.5 % population [177]. There are a total of thirty three districts in Rajasthan and all the 33 districts are reported to be contaminated with fluoride in groundwater. Among them, four districts were chosen where 20 - 40% villages are reported to be affected with excess fluoride in water [180]. Field water samples were collected from four different districts of Rajasthan viz. Sikar, Jodhpur, Jaipur and Dausa as shown in Figure 7.1. While visiting different places for collecting water samples, some cases of fluoride affected health issues were identified. Some pictures of common people suffering from dental and skeletal fluorosis are presented in Figure 7.3.

Ground water samples were collected from seven villages in plastic containers during April 2015 from hand pumps located in respective villages and the samples were analyzed in Department of Chemical Engineering, MNIT, Jaipur. The fluoride concentration in these villages is shown in Figure 7.2. Water quality parameters such as pH, EC, TDS, salinity, alkalinity, total hardness, turbidity, Cl^-, Ca^{2+}, Mg^{2+} and F^- for different places are enlisted in Table 7.1. It is evident that the villages with less fluoride concentration has higher concentration of calcium and vice versa. This is attributed to the fact that higher concentration calcium ions decrease the solubility of fluoride as calcium ions binds with F^- ions to form CaF_2. High alkalinity in groundwater favoured higher fluoride concentration in water while the pH varied between 6.8 to 8.5 for the samples tested. Turbidity in water is caused by suspended particles or colloidal matter that obstructs light transmission

through the water. However, the turbidity value was very low for in all the field water samples. When water moves through soil and rock, it tends to dissolve small amounts of minerals and holds them in solution. Two most prominent minerals that cause hardness in water are calcium and magnesium and the extent of hardness becomes more as the calcium and magnesium concentration increases and is also associated to the concentration of multivalent cations already dissolved in the water.

Among the samples collected, water from Kanteva village and Bhoomchota village in Sikar district; Basni village in Jodhpur district and Bandikui in Dausa district showed fluoride concentration higher than permissible limit (1.0 mg/L) (Figure 7.2). Therefore, defluoridation studies were conducted with these samples only.

Table 7.1: Water quality parameters for different places

	District: Sikar		District: Jodhpur		District: Jaipur		District: Dausa
Parameters	Kanteva village	Bhoomachota village	Basni	Ratanada	Pratap nagar	Malaviya Nagar	Bandikui
F^-(mg/L)	2.76	5.22	12.6	0.685	0.460	0.8	2.53
Ca^{2+} (mg/L)	69	46	58	256	432	297	80
Mg^{2+} (mg/L)	17	23	57	62	29	28	66
Hardness (mg/L)	139	142	295	512	555	415	352
Alkalinity (mg/L)	300	395	200	197	200	84	220
pH	8.13	8.4	8.08	6.8	7.89	8.06	8.5
Turbidity (NTU)	0	0.11	0	0	0.26	0	0.41
Cl^- (mg/L)	165	310	1520	500	117	248	220
TDS (mg/L)	770	1419	3752	678	251	375	1271
Conductivity (µs/cm)	1572	2882	7660	1389	512	754	2545
Salinity (psu)	0.874	1.654	4.685	0.798	0.274	0.431	2.34

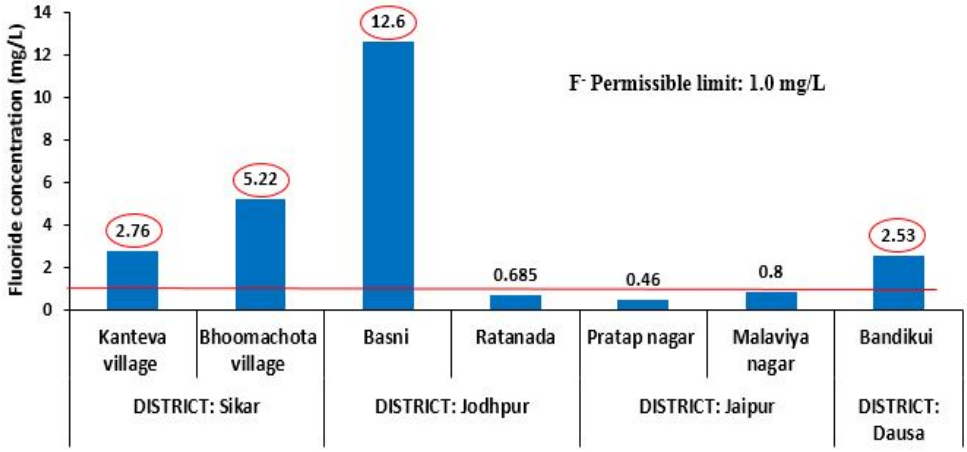

Figure 7.2: Fluoride concentration at different places

7.1.1 Quality assessment of water samples treated through batch mode

7.1.1.1 Analysis of residual fluoride ions

Fluoride removal studies with field water samples were conducted using M-i-HAPa powder adsorbent in batch mode. For this study, 10 g/L of adsorbent dose was taken, 3 h agitation time was given at 200 rpm and the results are shown in Figure 7.4. The synthesized adsorbent (M-i-HAPa powder) was able to bring down fluoride under permissible limit (< 1.0 mg/L) in all the field water samples tested. Fluoride ion concentration was highest in groundwater of Basni village of Jodhpur district i.e 12.6 mg/L. After treatment with adsorbent, the residual fluoride ion was found to be 0.9 mg/L in the sample water. After adsorption, the concentration of fluoride ions in the samples reduced from 2.76, 5.22, and 2.53 mg/L to 0.34, 0.656 and 0.371 mg/L respectively for Kanteva, Bhoomkota and Bandikui villages.

(a) People suffering from dental fluorosis in Kanteva village (Left) and Boomchota village (Right) , Rajasthan

(b) A person suffering from skeletal fluorosis in Kanteva village, Rajasthan

Figure 7.3: People suffering from Fluorosis

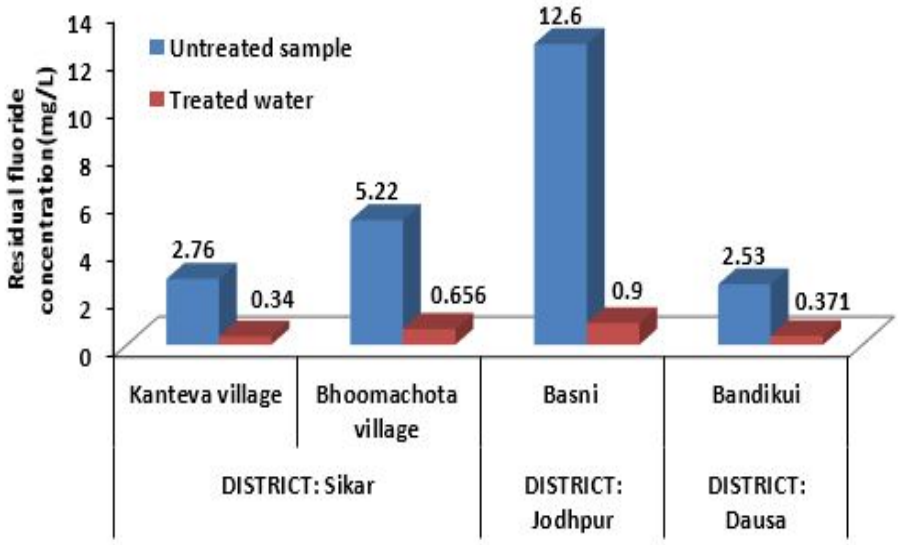

Figure 7.4: Batch Defluoridation study on field water samples

7.1.1.2 Analysis of pH

In most natural waters, pH is a measure of the acid–base equilibrium and is governed by the carbon dioxide - bicarbonate - carbonate equilibrium system. Hence, increase in concentration of CO_2 will lower pH and vice versa. According to WHO, temperature is an important factor affecting the equilibria and the pH of water. For instance, in pure water a decrease in pH of about 0.45 occurs with 25 ° C rise in temperature [72]. However, pH of most raw water lies between 6.5 to 8.5 [137]. The mild alkalinity in pH i.e around 8 implies the presence of weak basic salts in the soil [181] and it indicates that approximately 95% of carbon dioxide in water is in the form of bicarbonate [182]. During the field studies also the pH of water was found to be the range of 6.5 to 8.5. After adsorption treatment with M-i-HAPa powder through batch experiments the pH of water varied 8 to 8.4 as illustrated in Figure 7.5. Since, pH is one of the crucial operational parameters for water quality, it is necessary control or maintain pH at all stages of water treatment to ensure delivery of safe water.

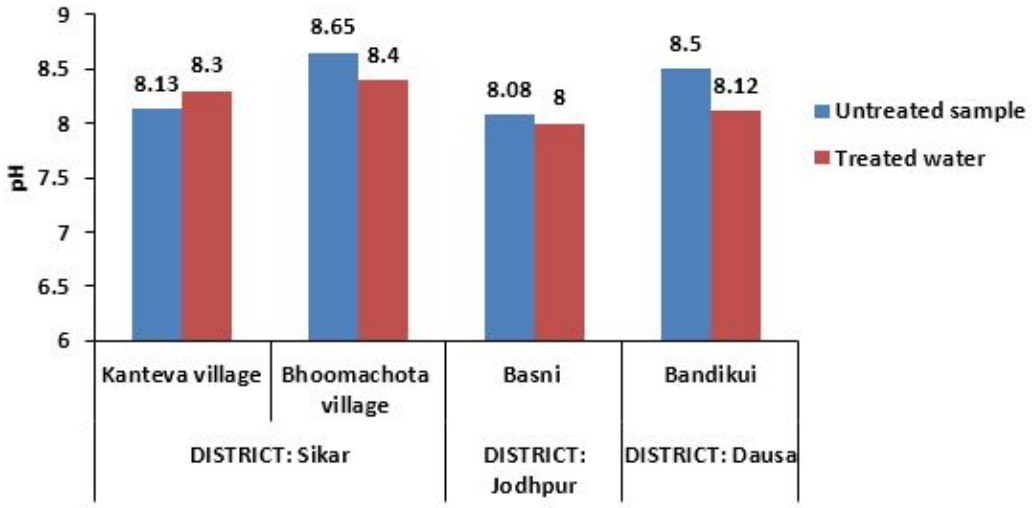

Figure 7.5: Analysis of pH in water samples

7.1.1.3 Analysis of TDS

Total dissolved solids or TDS is the inorganic salts (mainly calcium, magnesium, potassium, sodium, bicarbonates, chlorides, and sulfates) and small amounts of organic matter present in solution in water. The permissible limit for TDS in water is 500 mg/L. The TDS concentration is a secondary drinking water standard and it should be controlled because of its aesthetic value not a health hazard. The amount of TDS can be related to the electrical conductivity (EC) in water, however this relationship is not a constant rather is a function of the type and nature of the dissolved cations and anions in the water. EC observed in the field samples tested was between from 512 to 7660 µS/cm. EC can be defined as the measure of ability of the water to conduct electric current. Most of the salts in water are available in their respective ionic forms, so groundwater normally possess high electrical conductivity.

Very high TDS amount was observed in all the field samples examined ranging from 770 to 3752 mg/L, which were higher than the permissible limit for drinking water. Figure 7.6 gives a detailed information of TDS of water samples before and after adsorption onto M-i-HAPa powder. It was found that TDS value in treated samples were under the permissible limit of 500 mg/L. This may indicate that M-i-HAPa powder was able to adsorb some of the dissolved ions also, which reduced the TDS level in treated water.

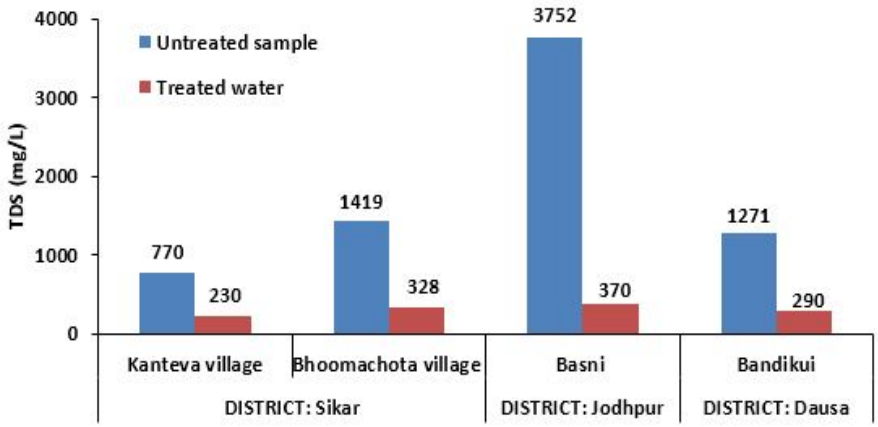

Figure 7.6: Analysis of TDS in water samples

7.1.1.4 Analysis of Total hardness

Hardness in water is a measure of the concentration of calcium and magnesium ions expressed in equivalent of calcium carbonate. Groundwater from Sikar district had low hardness value ranging from 139 to 142 mg/L while the permissible limit is 500 mg/L as $CaCO_3$ equivalent. Total hardness found in water samples from Jodhpur and Dausa district were 295 and 352 mg/L respectively as shown in Figure 7.7. After treatment with M-i-HAPa powder adsorbent, the total hardness for Kanteva, Bhoomchota, Basni and Bandikui village were found to be 148, 74, 75 and 185 mg/L respectively. Hence, it may be said that hardness of all the test samples were below permissible limit after treatment. The reason behind the reduction in hardness in two samples from Basni and Bandikui may be attributed due to precipitation of calcium in the form of CaF_2 due to the high fluoride present in water.

7.1.1.5 Analysis of Alkalinity

Alkalinity of water is measure of its capacity to neutralize acids and hence the sum of all the titratable bases. It is measure of an aggregate property of water and for interpretation of specific substances in it, chemical composition of the sample must be known [137]. However, alkalinity is basically a function of carbonate, bicarbonate, and hydroxide content in water, so its value is considered as an indication of the concentration of these constituents. The alkalinity of the test samples varied from 185 to 395 mg/L. High alkalinity in some areas may be attributed to the presence of minerals dissolved in water from mineral rich soil. Different ionic species that contribute to alkalinity includes bicarbonates, carbonates, hydroxides, phosphates, borates, silicates and organic acids [177]. After adsorption treatment with M-i-HAPa adsorbent all the samples were found to be in the permissible

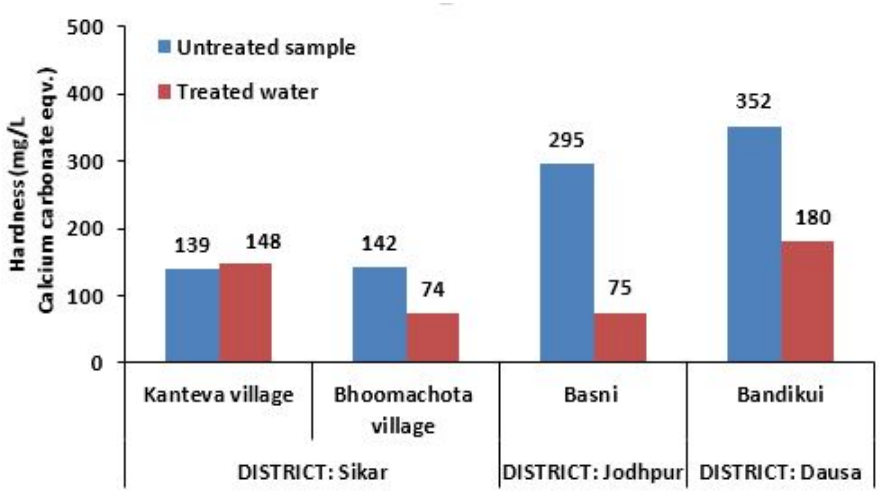

Figure 7.7: Analysis of Total hardness in water samples

limit of 300 mg/L as $CaCO_3$ equivalent as shown in Figure 7.8.

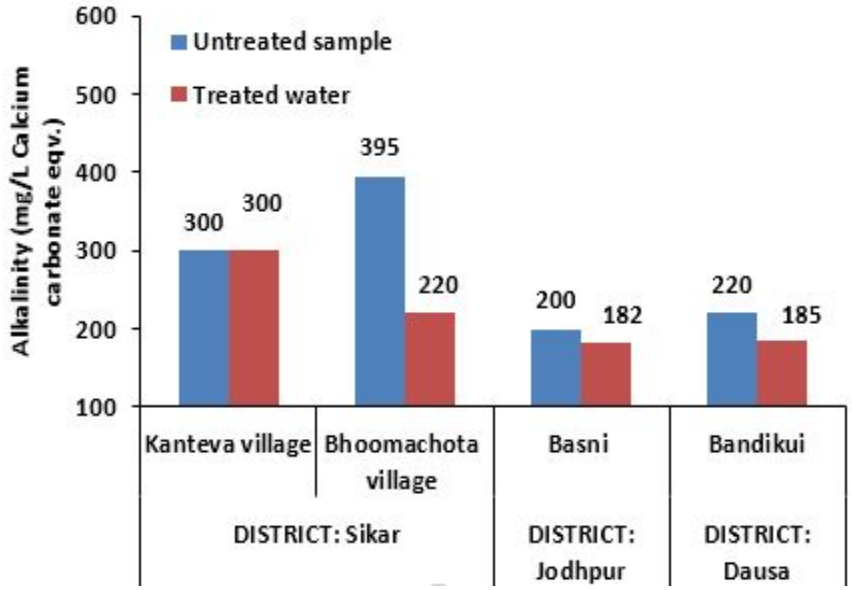

Figure 7.8: Analysis of alkalinity in water samples

7.1.1.6 Analysis of Calcium ions

Calcium is naturally present in water. It dissolves from limestone, marble, calcite, dolomite, gypsum, fluorite and apatite. The concentration of calcium ions may vary significantly in water according to the source. Figure 7.9 shows the concentration of calcium in the field samples (untreated sample) and concentration after treatment with M-i-HAPa adsorbent. In

the field samples examined, the concentration was found to be 46 to 69 mg/L which post treatment with M-i-HAPa adsorbent was noted to be between 29 to 45 mg/L for all samples. The permissible limit for calcium ions in drinking water is 75 mg/L.

7.1.1.7 Analysis of Magnesium ions

A large number of minerals contain magnesium, such as dolomite, magnesite and magnesium is washed from rocks and subsequently may end up in groundwater. Our body contains about 25 g of magnesium, of which 60 % is present in the bones and 40 % is present in muscles and other tissue. Since, it is a dietary mineral for humans, presence of magnesium doesn't pose any threat to health.

Figure 7.10 shows the concentration of magnesium in the field samples (untreated sample) and concentration after treatment with M-i-HAPa adsorbent. The permissible value for magnesium ions as per IS:10500 in drinking water is 30 mg/L, however it may be extended to 100 mg/L. The value of magnesium ion concentration detected after treatment with M-i-HAPa adsorbent were 28, 11 and 65 for Kanteva, Bhoomkota and Basni village respectively.

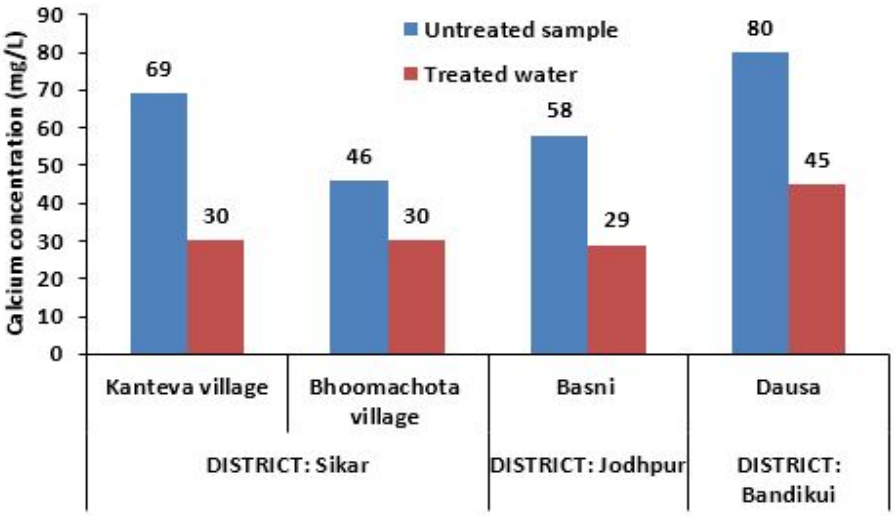

Figure 7.9: Analysis of calcium ions in water samples

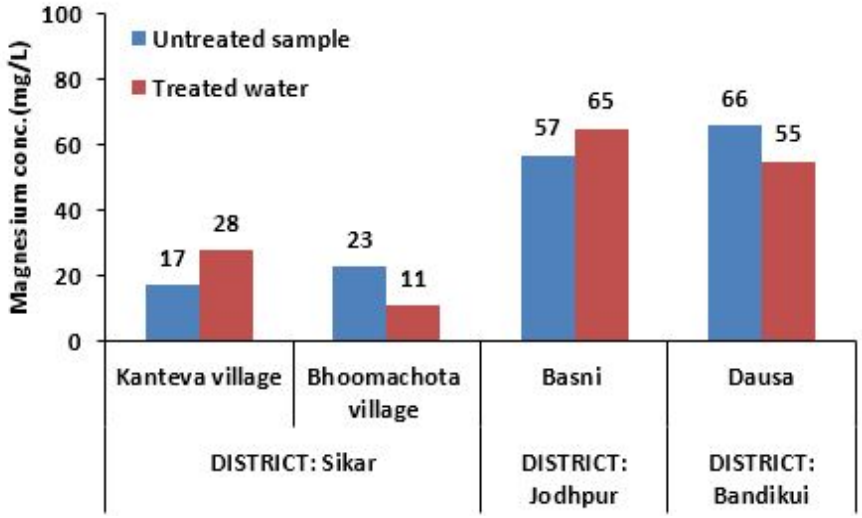

Figure 7.10: Analysis of Magnesium ions in water samples

7.1.2 Quality assessment of water samples treated through column mode

The physico-chemical properties of water were examined after running the column system with fluoridated water. The bed height was 30 cm, a flow rate of 1 L/h was maintained and feed fluoride concentration was 10 mg/L. The treated water was collected after 13 h (breakthrough point) and thereafter the water quality parameters were checked as shown in Figure 7.11a. The TDS, total hardness, alkalinity in treated water were 230, 118, 115 mg/L respectively while the residual concentration of calcium and magnesium were 23 and 23 mg/L respectively. pH of treated water was found to be 7.5. It is apparent from the figure that all the physico-chemical parameters were under the permissible limit according to BIS (IS:10500) as well as WHO [13, 72].

Studies were also conducted using the field water from Basni village, Jodhpur district where the highest fluoride concentration was highest among the field samples. Figure 7.11b shows the quality of water after treatment with the pellets in the column adsorption system. After treating the water sample with M-i-HAPa pellets, the TDS, total hardness and alkalinity were observed to be 255, 160 and 200 respectively. The concentration of calcium and magnesium in the treated sample were 23 and 25 respectively. The pH of water after treatment was 7.82. Reduction in concentration of magnesium and calcium ions may be due to adsorption of fluoride with them. The suitability of M-i-HAPa pellets as adsorbent is clearly depicted from quality of water obtained.

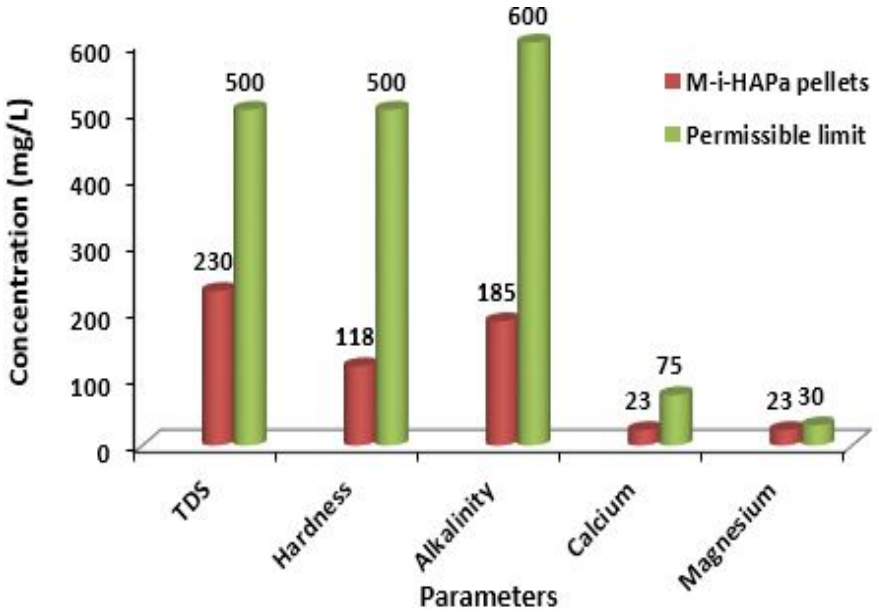

(a) Water quality parameters after treatment (fluoridated water)

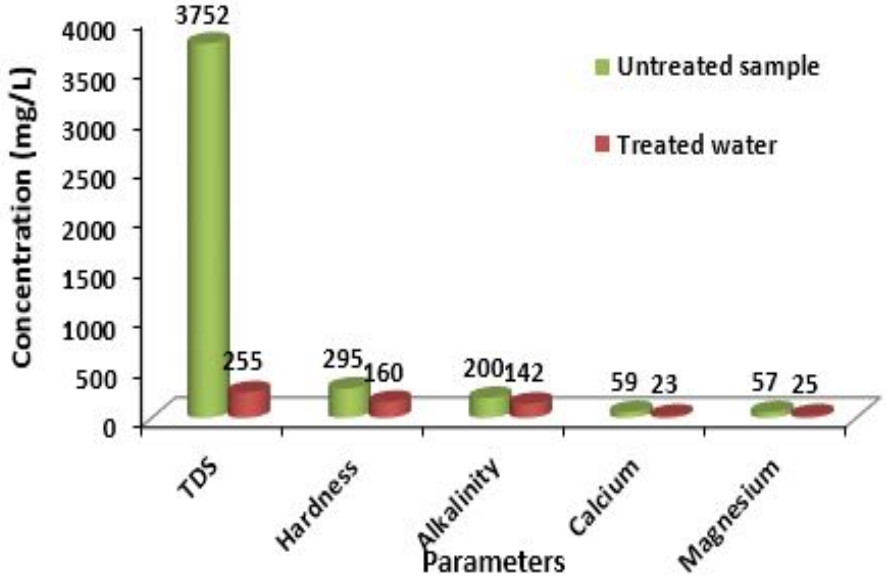

(b) Water quality parameters after treatment (Basni village water sample)

Figure 7.11: Water quality parameters examined after column studies with (M-i-HAPa pellets)

7.2 Domestic Defluoridation Unit (DDU)

Considering the domestic needs of people, a domestic defluoridation unit was designed assuming that approximately 5 L of water will fulfill the daily requirement for cooking and drinking per person.

In this study, domestic defluoridation unit was designed for M-i-HAPa pellets as shown in Figure 7.12. The performance of the DDU designed for M-i-HAPa pellets was compared with that of activated alumina DDU at IIT Kanpur (reported by Chauhan et al. [183] and Iyengar [184]). The characteristics of activated alumina used in the study [183] and corresponding characteristics of M-i-HAPa pellet is listed in Table 7.2. The fluoride uptake capacity (FUC) was found to be 1788 mg/kg AA when 3 kg of AA was used in the DDU and the concentration of fluoride in water was 10 ± 0.5 mg/L [183]. The flow rate of the slot opening between the two chambers was 9 to 10 L for AA DDU unit. It was reported that with 3 kg of activated alumina, the volume of water treated (F^- $\leq$1.5 mg/L) was 550 L. The domestic defluoridation unit used was in the following dimension: 22 cm diameter and 23 cm height.

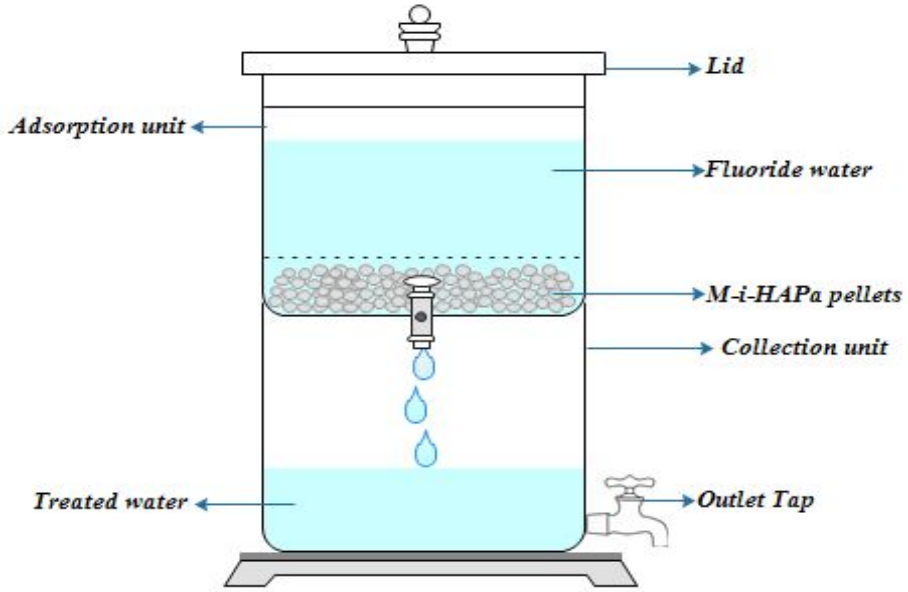

Figure 7.12: Domestic defluoridation unit

Table 7.2: Characteristics of activated alumina and M-i-HAPa pellets

S.no	Characteristics	Value of AA	Value of M-i-HAPa
1.	Particle form	Spheres	Spheres
2.	Particle size (mm)	0.4-1.2	1-1.5
3.	Surface area (m^2/g)	310	21.22
4.	Pore volume (cm^3/g)	0.41	0.096

The capacity of M-i-HAPa adsorbent was found to be 1.16 mg/g using initial fluoride concentration of 10 mg/g. Therefore, the fluoride uptake capacity will be 1160 mg/kg M-i-HAPa adsorbent and approximately 348 L of water could be treated with 3 kg of the

adsorbent in the DDU. The slot opening between the adsorption and collection chamber had a flow rate of 5 to 6 L/h. The dimensions for each chamber of the DDU was 30 cm height and 25/23 (top/bottom) diameter. The specifications of the DDU designed and the DDU reported by Chauhan et al. [183] are given in Table 7.3. The fluoride solution and adsorbent should be given a contact time of 3 h (equilibrium time) before collecting the treated water, so that the treated water is below the permissible limit of 1 mg/L. The studies conducted in section 5.7.2 and 5.7.5 showed no effect of pH and negligible interference from co-existing ions on the adsorption process respectively. Hence, for treating field water sample from Basni village where fluoride concentration was 12.6 mg/L (highest among the field data obtained), the fluoride uptake capacity will be 1086 mg/kg M-i-HAPa adsorbent and approximately 259 L of water will be treated with 3 kg of adsorbent. Further, the exhausted activated alumina was regenerated using 1 % NaOH followed by acid treatment and the adsorbent was used for five cycles. In this study, M-i-HAPa adsorbent was regenerated using only 0.1 M NaOH for 90 min, thereafter the adsorbent was dried at 95° ± C for 60 min. Ninety one percent regeneration was achieved and after using for five consequent cycles the removal efficiency lost (section 5.7.11).

Table 7.3: Specifications of the domestic defluoridation units

	DDU (AA)	DDU (M-i-HAPa)
Diameter (cm) (top/bottom)	22/22	25/23
Height (cm)	23	30
Flow rate of slot in between chambers (L/h)	9-10	5-6
Regeneration	1 % NaOH followed by acid treatment	0.1 M NaOH

On comparing the values of FUC for AA and M-i-HAPa (1788 and 1160 mg/kg adsorbent respectively), it can be seen that AA has slightly higher fluoride uptake capacity. However, usage of AA defluoridation units have led to leaching of aluminum in ionic and complex form (alumino-fluro complexes) [47]. The residual aluminum in treated water if consumed can cause severe health issues. On the other hand, the M-i-HAPa adsorbent consist of calcium and magnesium compounds and are completely safe to use for defluoridation of drinking water (as leaching of Ca^{2+} and Mg^{2+} are under permissible limits).

7.3 Summary of the Chapter

Studies with field water samples and the assessment of water quality after treatment with both M-i-HAPa powder in batch mode and M-i-HAPa pellets in column mode. This study was conducted to determine the suitability of usage of the adsorbent synthesized for drinking water purposes. Physico-chemical parameters of water were tested in terms of pH, EC, TDS, salinity, alkalinity, total hardness, turbidity, Cl^-, Ca^{2+}, Mg^{2+} and F^- for different places. The values of these parameter after adsorption with M-i-HAPa adsorbent was observed to be under permissible limits as per WHO and BIS guidelines.

Finally, a domestic defluoridation unit was designed and its fluoride uptake capacity (FUC) was compared with DDU designed for AA at IIT Kanpur. It was estimated that for 10 mg/L of fluoride in water, 3 kg of M-i-HAPa could treat 348 L of water. The spent adsorbent that is rich in fluoride can become a raw material for making cement, refractory bricks or for direct use in road construction purposes.

CONCLUSION

Conclusion

This chapter summarizes the the whole work of this thesis. The major findings and significant contribution to the existing knowledge are also mentioned.

Availability of safe water for consumption is the one of the most important gifts to mankind. But, unfortunately, the increase in concentration of contaminants such as fluoride above the permissible limit in groundwater resources over the years has become a serious matter of concern in many countries. In the present work experimental studies were conducted to remove fluoride from drinking water using adsorption process to bring it below the permissible limit prescribed by BIS (IS: 10500). Conventionally, aluminum based adsorbents are used for defluoridation due to their high affinity towards fluoride ions. However, recent literature shows leaching of aluminum ions into treated water causing adverse health issues since the permissible limit of aluminum ions is very low (0.2 mg/L). Therefore, the focus of this study was to use non-toxic compounds for fluoride removal such as calcium and magnesium which have higher permissible limit in water (75 and 30 mg/L respectively)**.** The following set of conclusions were drawn on basis of this research work:

Adsorbents used and Characterization studies

- Various calcium based adsorbents were used to explore their defluoridation potential and feasibility for usage in drinking water treatment. These adsorbents were Activated Calcite (ACal), Synthesized Calcia-Magnesia Adsorbent (CMA), Dicalcium phosphate, Dolomite, Hydroxyapatite of animal origin (aHAP), Magnesia-Hydroxyapatite (Mg-HAP), pure Hydroxyapatite (pHAP) and Magnesium incorporated hydroxyapatite (M-i-HAPa). Some of these adsorbents were synthesized in the laboratory (CMA, Mg-HAP, pHAP, M-i-HAP) and some were procured from the market (Calcite, Dolomite, Dicalcium phosphate, aHAP). Pure Hydroxyapatite (p-HAP) was synthesized via chemical precipitation technique and to increase the adsorption capacity magnesium ions were incorporated into p-HAP structure forming Magnesium incorporated hydroxyapatite. The synthesis of magnesium incorporated hydroxyapatite was carried out with variation in magnesium content in the adsorbent and named as M-i-HAPa, M-i-HAPb and M-i-HAPc. Based on characterization studies and preliminary fluoride removal experiments M-i-HAPa adsorbent was selected for further studies. The adsorbent M-i-HAPa was further pelletized using the extrusion-spheronisation method in order to perform column

studies.

- The synthesized adsorbents were characterized using FTIR, XRD, SEM, TEM/EDX, TGA-DTA, BET, XPS and particle size distribution techniques which gave an insight into the functional groups, bonding patterns, crystallinity, structure, composition, particle size, surface area, pore diameter, pore volume, thermal behavior and surface morphology of the adsorbent.

- XRD studies revealed that all the synthesized adsorbents were crystalline in nature with crystallite size varying from 31.33 nm to 65 nm. The SEM results showed densely agglomerated particles on the surface of CMA adsorbent while the surface texture of Mg-HAP showed a porous and agglomerated surface. The TEM micrograph for Mg-HAP depicted the average size of particles to be 70 – 150 nm in length and 30 – 40 nm in width which was very close to the crystal size estimated (65 nm) from XRD data using Scherer equation.

- The surface morphology of magnesium incorporated hydroxyapatite adsorbent showed a distinct nano-rod morphology. The SEM results for magnesium incorporated hydroxyapatite adsorbent were compared with pHAP and it was observed that introduction of magnesium into hydroxyapatite structure caused reduction in size of the rod-like structures. These results were further confirmed through TEM studies which exhibited elongated needle like nano-rod structure for pure hydroxyapatite and aggregated structures arranged in random orientations were observed for magnesium incorporated hydroxyapatite. The aggregated structutes were obtained due to reduction in particle size. Particle size estimated from TEM for pHAP is 100 - 150 nm in length and 15 - 18 nm in width whereas the particle size was observed to be smaller after magnesium incorporation i.e 6 - 10 nm.

- Through BET surface area measurements, it was found that M-i-HAPa adsorbent had a surface area of 46.62 m^2/g which is more than twice of pHAP (21.25 m^2/g). The increase in surface area may of M-i-HAPa may lead to higher fluoride removal capacity of the adsorbent. The pore volume and pore size of M-i-HAPa was 0.177 cm^3/g and 152.51 Å respectively while that of pHAP was 0.090 cm^3/g and 169.83 Å respectively. The particle size analysis revealed a mean particle size of 417 nm for pHAP which was observed to decrease to 155 nm after magnesium was incorporated into pHAP. A lower particle size supports higher removal for fluoride ions which indicated that M-i-HAPa adsorbent may possess higher defluoridation capability than pHAP.

- Characterization studies with M-i-HAPa pellets were carried out before fluoride adsorption, after fluoride adsorption and after regeneration using FTIR, XRD, SEM and XPS. The FTIR spectra obtained after adsorption of fluoride display a significant decrease in intensity of OH^- peak due to formation of OH–F bond. This confirmed that hydroxyl ions in the adsorbent are replaced by fluoride ions in the adsorption process. The XRD pattern obtained after fluoride adsorption revealed the formation of hydroxyfluoroapatite, fluoroapatite and magnesium fluoride whereas fluoride after regeneration of M-i-HAPa pellets was similar to the one before adsorption of fluoride. The SEM images showed that fresh pellets possessed extremely rough surface with a number of pores on the surface which may be used for capturing fluoride ions from the solution. SEM micrographs of the fluoride loaded M-i-HAPa pellets showed a distinct change in the morphology and fluoride ions appeared adhering to the surface of the pellets and most of the pores were occupied by fluoride ions. Post regeneration, the surface of the pellets again display a porous texture however with reduced number of pores as compared to the unused adsorbent which indicated that after each cycle of regeneration, the adsorbent would lose some of its adsorption capacity.

Batch defluoridation studies

- On the basis of fluoride removal capacity and quality of treated water, the adsorbents were screened and a suitable adsorbent was chosen for further experiments. The fluoride adsorption capacity of natural Hydroxyapatite (aHAP) derived from bovine bones was found to be extremely low (0.133 mg/g) and therefore aHAP was modified with magnesium and Magnesia-Hydroxyapatite (Mg-HAP) was prepared for enhanced fluoride removal from aqueous solutions. Activated calcite and dolomite possessed low fluoride removal capacity (0.78 mg/g and 0.322 mg/g respectively) while the treated water obtained from calcia-magnesia adsorbent and dicalcium phosphate adsorbents were not suitable for consumption due to high amount of calcium-magnesium dissolution (Ca^{2+}: 120 mg/L; Mg^{2+}: 87 mg/L) and low pH (~ 5) respectively.

- Mg-HAP adsorbent derived from natural HAP was studied by varying adsorbent dose, contact time, pH and co-existing ions. The Mg-HAP adsorbent had an adsorption capacity of 1.4 mg/g with initial fluoride concentration of 10 mg/L in 180 min at pH 7.5 ± 0.1. Investigations with varying interfering ion concentrations (phosphate, bicarbonate, sulfate, chloride and nitrate ; 100 – 300 mg/L) were carried

out with 10g/L of Mg-HAP and the orders of interference by these competing ions from lower to higher are in the following order: Nitrate < Chloride < Sulfate < Bicarbonate < Phosphate. The adsorption capacity of Mg-HAP was not affected significantly by pH of the medium but calcium leaching in the solution was observed at alkaline pH (9 and 10). However, the treated water had pH value greater than 10 and therefore it was not found fit for drinking purposes.

- The process parameters of M-i-HAPa adsorbent were optimized using RSM and a comparison of its defluoridation capacity with pHAP was carried out through batch studies.

Optimization of process parameters for M-i-HAPa adsorbent

- The optimization of fluoride removal on M-i-HAPa was carried out by choosing four independent process variables viz. adsorbent dose (2 - 18 g/L), pH (3 - 11), contact time (15 - 345 min) and temperature (303 - 323K) and the response was observed in terms of fluoride removal (%) and adsorption capacity (mg/g). Response surface methodology by Central composite design (CCD) was used to investigate the chosen parameters on fluoride removal and adsorption capacity. CCD consists of a 2n factorial runs with 2n axial runs and nc center runs (six replicates) which indicated that thirty experiments were required. A set of thirty experimental runs were conducted for design and statistical analysis. The numerical optimization achieved with the desirability function specified the probable fluoride removal to be 94.60% and adsorption capacity to be 1.09 mg/g which was very close to the experimental values of 94.5 % and 0.95 mg/g respectively. The optimum values for experimental parameters were found to be at pH 7, 303 K temperature, 10 mg/L fluoride concentration, 180 min contact period with a dose of 10 g/L. Furthermore, thermodynamic studies revealed the exothermic nature of the process.

Mechanism of fluoride adsorption on M-i-HAPa

- A mechanism for fluoride adsorption on M-i-HAPa was also proposed and explained with the help of XRD data obtained after fluoride adsorption. It was observed that the mechanism involves diffusion of F^- ions on adsorbent surface then adsorption at active sites followed by exchange of OH^- and F^- ions. Fitness of the adsorption data to pseudo-second-order kinetics indicated that the process is governed by chemisorption. In addition, the adsorption isotherm studies showed Langmuir isotherm to be best fitted to represent the experimental data. Since, langmuir isotherm

also supports the chemisorption theory, it is apparent that the adsorption mechanism is chemical in nature.

Significant features of M-i-HAPa adsorbent:

- One of the most important factor in an adsorption process is the pH as it governs the entire process chemistry of defluoridation. In our studies with M-i-HAP adsorbent, negligible effect of pH was found which makes this adsorbent more suitable for practical purposes. Groundwater contaminated with fluoride contains several other ions that can compete with fluoride during the adsorption process. Therefore, studies of effect of coexisting ions at different concentrations were conducted with 10 g/L of M-i-HAP adsorbent, 10mg/L of fluoride solution for 180 min. The results showed that there was a slight reduction in fluoride adsorption capacity due to bicarbonate ions while the other ions (chloride, nitrate, phosphate and sulfate) didn't affect the capacity significantly. These results indicate that M-i-HAP follows a selective adsorption process towards fluoride ions.

Adsorption isotherms and kinetic studies

- Experimental isotherm data for M-i-HAP was collected at different temperatures to fit in Langmuir, Freundlich, Temkin and Dubinin-Raduskevich adsorption isotherms. However, isotherm data for Mg-HAP was collected only at room temperature (25 ± 0.5 ºC). Better fitting of the Langmuir isotherm for both Mg-HAP and M-i-HAP adsorbent suggested monolayer coverage of fluoride at the surface of the adsorbent. Contribution of intraparticle diffusion in the adsorption process was also notable. To investigate the mechanism of fluoride adsorption by adsorbent materials, four kinetic models (Pseudo first order, Pseudo second order, Intraparticle diffusion) were studied. The rates of adsorption were found to follow the pseudo-second-order kinetics indicating towards a chemical sorption mechanism.

Column defluoridation studies

- The M-i-HAPa pellets synthesized in the laboratory were found to be an effective defluoridation agent in column adsorption system. The effect of varying adsorption parameters such as flow rate, fluoride concentration, particle size, particle shape and bed height on the removal of fluoride was studied. The adsorption capacity was observed to be 1.46 mg/g at feed fluoride concentration of 10 mg/L, flow rate of 1

L/h and bed height of 30 cm. It was noticed that for 30 cm bed height, 22.1 bed volumes can be processed and the AER for the same was 6.15 g/L.

- Experimental data were fitted to Hutchins BDST model, Thomas model and Yoon-Nelson model to obtain characteristic parameters from each model. Thomas and Hutchins BDST model fitted well with the data with very high corelation coefficient value. The adsorption capacity calculated from Thomas model was very close to the experimentally obtained values at all operating conditions.

- Regeneration studies were conducted to confirm the mechanism of adsorption and study the stability of the adsorbent during defluoridation. The results showed that the pellets were stable for repeated use upto four times. The desorption experiments also confirmed the ion exchange mechanism dominating the process of adsorption. Morever, the chemical regeneration of the adsorbent also indicated the process to be chemisorption. Adsorption column dynamics was also studied through simulation to optimize the column configuration for fluoride removal.

- The experimental results obtained by varying flow rate and size of particles were compared with simulated data obtained from an adsorption simulator "ADSORB" developed in MATLAB software. The concentration profiles with respect to time with varying flow rates and particles sizes were obtained from the MATLAB program and validated with the experimental data.

Field water studies and Assessment of treated water quality

- Studies with field water samples and the assesment of water quality after treatment with both M-i-HAPa powder in batch mode and M-i-HAPa pellets in column mode. This study was conducted to determine the suitability of usage of the adsorbent synthesized for drinking water purposes. Physico-chemical parameters of water were tested in terms of pH, EC, TDS, salinity, alkalinity, total hardness, turbidity, Cl^-, Ca^{2+}, Mg^{2+} and F^- for different places. The values of these parameter after adsorption with M-i-HAPa adsorbent was observed to be under permissible limits as per WHO and BIS guidelines.

- Finally, a domestic defluoridation unit was designed and its fluoride uptake capacity (FUC) was compared with DDU designed for AA at IIT Kanpur. It was estimated that for 10 mg/L of fluoride in water, 3 kg of M-i-HAPa could treat 348 L of water.

Significant contributions towards the scientific community

- A novel calcium based adsorbent M-i-HAPa was synthesized in the laboratory for defluoridation of drinking water and it was able to successfully remove excess fluoride ions from water. Hydroxyapatite has widely been used in the medical field as bone and teeth implants, while magnesium substituted hydroxyapatite has recently been used in bone tissue engineering as artificial bone substitutes in view of the fact that magnesium stimulates osteoblast proliferation. However, hydroxyapatite incorporated with magnesium has never been used as an adsorbent to solve water contamination issues such as defluoridation.

- Most of the adsorbents found in literature with high capacities are metal based due to which presence of residual metal ions in treated water is a major area of concern. Therefore, use of magnesium-incorporated hydroxyapatite for fluoride removal will provide an added advantage of the absence of any toxic metal leaching. The leaching tests for calcium and magnesium ions showed that these ions are present below their permissible limits in the treated water. Literature studies showed that calcium rich water is a good supplement to calcium-deficient people who are more susceptible to fluorosis. Consequently, the small amount of residual calcium ions present in treated water could help the people suffering from dental and skeletal fluorosis.

- The most common issue with adsorbents used for defluoridation is the working pH range and reduction in adsorption capacity in presence of competing ions. However, the M-i-HAPa adsorbent works well over a broad pH range (3 to11) and the in presence of ionic competition also negligible reduction in adsorption capacity was observed. Groundwater generally contains many ions interfering in the removal of fluoride but M-i-HAPa adsorbent acted as an efficient defluoridation agent as observed through field studies.

- Column studies depict the practical feasibility of the adsorbent. Therefore, the M-i-HAPa powdered adsorbent was converted into spherical pellets. The column defluoridation studies conducted using M-i-HAPa pellets showed that this adsorbent can be used as a promising material for defluoridation of drinking water.

- Moreover, the M-i-HAPa adsorbent can be regenerated with 0.1 M NaOH for reuse which is a necessity for its practical application and the water quality parameters of treated water indicated that the all physico chemical properties at par with the BIS and WHO guidelines.

Recommendations for Future Work

A vast literature is available on various adsorbents and their applications, still researchers have always continued to explore further possibilities with adsorbents and attempted to make the process more efficient. Some recommendations regarding scope for future work in this area are given below:

- The adsorbent "Magnesium incorporated hydroxyapatite" may be synthesized using some other method such as sol-gel, hydrothermal, multiple emulsion technique, biomimetic deposition technique and electrodeposition technique. This may enhance the properties of the adsorbent.
- Magnesium incorporated hydroxyapatite adsorbent may be studied for treating other toxic ions such as arsenic, nitrate etc. Arsenic and nitrate are also potent contaminants present in water, this adsorbent may reduce their concentration in treated water.
- The capacity of the adsorbent may be increased by incorporation of other ionic entities which may contribute to remove fluoride from water.
- Column studies may be conducted with lower flow rates for attaining higher adsorption capacity. Studies can be conducted using fluidized bed column system to achieve even better column performance.
- Other predictive models and mathematical algorithms may be developed for adsorption studies.
- Other regeneration methods may be investigated such as thermal regeneration and steam regeneration. This may increase the efficiency of the adsorbent and it might be used for higher number of cycles.
- The process may be scaled up for community level applications which may serve more number of people. However, careful analysis of a number of factors should be done before adapting the process to a certain community.
- Research activity is required to utilize the solid waste generated after adsorption to convert it into a useful product such as the usage in brick, cement and other construction materials.
- Cost analysis was not part of this study. Detailed cost estimations for the process can be done for evaluating the potential application of the adsorbent.

BIBLIOGRAPHY

Bibliography

[1] WHO/UNICEF Joint Water Supply, Sanitation Monitoring Programme, and World Health Organization. *Progress on drinking water and sanitation: 2014 Update*. World Health Organization, 2014.

[2] M Vithanage and P Bhattacharya. Fluoride in the environment: sources, distribution and defluoridation. *Environmental Chemistry Letters*, 13(2):131–147, 2015.

[3] S Ohgaki and K Fukushi. *Southeast Asian Water Environment 1: Selected Papers from the First International Symposium on Southeast Asian Water Environment (biodiversity and Water Environment), Bangkok, Thailand, October 2003*, volume 1. IWA Publishing, 2005.

[4] R Singh and RC Maheshwari. Defluoridation of drinking water: A review. *Indian Journal of Environmental Protection*, 21(11):983–991, 2001.

[5] M Mohapatra, S Anand, BK Mishra, DE Giles, and P Singh. Review of fluoride removal from drinking water. *Journal of Environmental Management*, 91(1):67–77, 2009.

[6] WM Edmunds and PL Smedley. Fluoride in natural waters. In *Essentials of Medical Geology*, pages 311–336. Springer, 2013.

[7] KK Majumdar. Health impact of supplying safe drinking water containing fluoride below permissible level on flourosis patients in a fluoride-endemic rural area of West Bengal. *Indian Journal of Public Health*, 55(4):303, 2011.

[8] BK Handa. Geochemistry and genesis of Fluoride-Containing ground waters in India. *Ground water*, 13(3):275–281, 1975.

[9] AK Susheela and HC Moolenburghb. Treatise on fluorosis. *Fluoride*, 34(3):181–183, 2001.

[10] UNICEF. States of the art report on the extent of fluoride in drinking water and the resulting endemicity in india. *Report by Fluorosis and Rural Development Foundation for UNICEF, New Delhi*, 1999.

[11] AK Susheela. Fluorosis in developing countries: remedial measures and approaches. *Proceedings-Indian National Science Academy Part B*, 68(5):389–400, 2002.

[12] L Feenstra, L Vasak, and J Griffioen. Fluoride in groundwater: Overview and evaluation of removal methods. *International Groundwater Resources Assessment Centre Report no. SP*, 1, 2007.

[13] Indian Standard Drinking Water Specification. Bureau of Indian Standards, IS10500. *World Health Organization,New Delhi*, 2012.

[14] H Long, Y Jin, M Lin, Y Sun, L Zhang, and C Clinch. Fluoride toxicity in the male reproductive system. *Fluoride*, 42(4):260–276, 2009.

[15] SL Choubisa. Endemic fluorosis in southern Rajasthan, India. *Fluoride*, 34(1):61–70, 2001.

[16] T Aoba and O Fejerskov. Dental fluorosis: chemistry and biology. *Critical Reviews in Oral Biology & Medicine*, 13(2):155–170, 2002.

[17] M Trivedi, N Sangai, R Patel, M Payak, and SJ Vyasa. Assessment of groundwater quality with special reference to fluoride and its impact on IQ of schoolchildren in six villages of the Mundra region, Kachchh, Gujarat, India. *Fluoride*, 45(4):377–383, 2012.

[18] B Spittle. Dyspepsia associated with fluoridated water. *Fluoride*, 41(1):89, 2008.

[19] JD Sharma, D Sohu, and P Jain. Prevalence of neurological manifestations in a human population exposed to fluoride in drinking water. *Fluoride*, 42(2):127, 2009.

[20] GM Whitford. Determinants and mechanisms of enamel fluorosis. *Dental Enamel*, 785:226, 2008.

[21] SK Gupta. *Environmental Health Perspective of Fluorosis in Children*. PhD thesis, 1999.

[22] ALJJ Bronckers, DM Lyaruu, and PK DenBesten. The impact of fluoride on ameloblasts and the mechanisms of enamel fluorosis. *Journal of Dental Research*, 88(10):877–893, 2009.

[23] JM Pettifor. Vitamin D &/or calcium deficiency rickets in infants & children: a global perspective. *Indian Journal of Medical Research*, 127(3):245, 2008.

[24] E Czerwinski, J Nowak, D Dabrowska, A Skolarczyk, B Kita, and M Ksiezyk. Bone and joint pathology in fluoride-exposed workers. *Archives of Environmental Health: An International Journal*, 43(5):340–343, 1988.

[25] O Barbier, L Arreola-Mendoza, and L Del Razo. Molecular mechanisms of fluoride toxicity. *Chemico-biological Interactions*, 188(2):319–333, 2010.

[26] IA Pretty, M McGrady, C Zakian, RP Ellwood, A Taylor, MO Sharif, T Iafolla, EA Martinez-Mier, P Srisilapanan, and N Korwanich. Quantitative Light Fluorescence (QLF) and Polarized White Light (PWL) assessments of dental fluorosis in an epidemiological setting. *BMC Public Health*, 12(1):366, 2012.

[27] H Limeback, APGF Vieira, and H Lawrence. Improving esthetically objectionable human enamel fluorosis with a simple microabrasion technique. *European Journal of Oral Sciences*, 114(s1):123–126, 2006.

[28] N Trivedi, A Mithal, SK Gupta, and MM Godbole. Reversible impairment of glucose tolerance in patients with endemic fluorosis. *Diabetologia*, 36(9):826–828, 1993.

[29] K Lund, M Refsnes, I Ramis, C Dunster, J Boe, PE Schwarze, E Skovlund, FJ Kelly, and J Kongerud. Human exposure to hydrogen fluoride induces acute neutrophilic, eicosanoid, and antioxidant changes in nasal lavage fluid. *Inhalation Toxicology*, 14(2):119–132, 2002.

[30] EA García-Montalvo, H Reyes-Pérez, and LM Del Razo. Fluoride exposure impairs glucose tolerance via decreased insulin expression and oxidative stress. *Toxicology*, 263(2):75–83, 2009.

[31] CD Anuradha, S Kanno, and S Hirano. Oxidative damage to mitochondria is a preliminary step to caspase-3 activation in fluoride-induced apoptosis in hl-60 cells. *Free Radical Biology and Medicine*, 31(3):367–373, 2001.

[32] P Sehn. Fluoride removal with extra low energy reverse osmosis membranes: three years of large scale field experience in Finland. *Desalination*, 223(1):73–84, 2008.

[33] K Hu and JM Dickson. Nanofiltration membrane performance on fluoride removal from water. *Journal of Membrane Science*, 279(1):529–538, 2006.

[34] S Jagtap, MK Yenkie, N Labhsetwar, and S Rayalu. Fluoride in drinking water and defluoridation of water. *Chemical Reviews*, 112(4):2454–2466, 2012.

[35] AH Essadki, B Gourich, C Vial, H Delmas, and M Bennajah. Defluoridation of drinking water by electrocoagulation/electroflotation in a stirred tank reactor with a comparative performance to an external-loop airlift reactor. *Journal of Hazardous Materials*, 168(2):1325–1333, 2009.

[36] R Sinha, A Singh, and S Mathur. Multiobjective optimization for minimum residual fluoride and specific energy in electrocoagulation process. *Desalination and Water Treatment*, pages 1–11, 2014.

[37] S Vasudevan, J Lakshmi, and G Sozhan. Studies on a Mg-Al-Zn alloy as an anode for the removal of fluoride from drinking water in an electrocoagulation process. *Clean-Soil, Air, Water*, 37(4):372, 2009.

[38] M Behbahani, MRA Moghaddam, and M Arami. Techno-economical evaluation of fluoride removal by electrocoagulation process: Optimization through response surface methodology. *Desalination*, 271(1):209–218, 2011.

[39] J Zhu, H Zhao, and J Ni. Fluoride distribution in electrocoagulation defluoridation process. *Separation and Purification Technology*, 56(2):184–191, 2007.

[40] CY Hu, SL Lo, and WH Kuan. Simulation the kinetics of fluoride removal by electrocoagulation (EC) process using aluminum electrodes. *Journal of Hazardous Materials*, 145(1):180–185, 2007.

[41] P Loganathan, S Vigneswaran, J Kandasamy, and Ri Naidu. Defluoridation of drinking water using adsorption processes. *Journal of Hazardous Materials*, 248:1–19, 2013.

[42] S Meenakshi and N Viswanathan. Identification of selective ion-exchange resin for fluoride sorption. *Journal of Colloid and Interface Science*, 308(2):438–450, 2007.

[43] N Viswanathan and S Meenakshi. Role of metal ion incorporation in ion exchange resin on the selectivity of fluoride. *Journal of Hazardous Materials*, 162(2):920–930, 2009.

[44] F Luo and K Inoue. The removal of fluoride ion by using metal (III)-loaded Amberlite resins. *Solvent Extraction and Ion Exchange*, 22(2):305–322, 2004.

[45] IB Solangi, S Memon, and MI Bhanger. Removal of fluoride from aqueous environment by modified Amberlite resin. *Journal of Hazardous Materials*, 171(1):815–819, 2009.

[46] E Dahi. The state of art of small community defluoridation of drinking water. *Eli Dahi Sunsanee Rajchagool & Nipaphan Osiriphan*, 141.

[47] S George, P Pandit, and AB Gupta. Residual aluminium in water defluoridated using activated alumina adsorption– [modeling] and simulation studies. *Water Research*, 44(10):3055–3064, 2010.

[48] X Fan, DJ Parker, and MD Smith. Adsorption kinetics of fluoride on low cost materials. *Water Research*, 37(20):4929–4937, 2003.

[49] SS Tripathy, JL Bersillon, and K Gopal. Removal of fluoride from drinking water by adsorption onto alum-impregnated activated alumina. *Separation and Purification Technology*, 50(3):310–317, 2006.

[50] RC Maheshwari. Fluoride in drinking water and its removal. *Journal of Hazardous Materials*, 137(1):456–463, 2006.

[51] JD Hem. *Study and interpretation of the chemical characteristics of natural water*, volume 2254. Department of the Interior, US Geological Survey, 1985.

[52] S Chandra, R Sharma, V Parshuram Thergaonkar, and SK Chaturvedi. Determination of optimal fluoride concentration in drinking water in an area in India with dental fluorosis. *Community Dentistry and Oral Epidemiology*, 8(2):92–96, 1980.

[53] A Mithal, N Trivedi, SK Gupta, S Kumar, and RK Gupta. Radiological spectrum of endemic fluorosis: relationship with calcium intake. *Skeletal Radiology*, 22(4):257–261, 1993.

[54] B Dawson-Hughes. Vitamin d and calcium: recommended intake for bone health. *Osteoporosis international*, 8(8):S030–S034, 1998.

[55] S Morr, E Cuartas, B Alwattar, and JM Lane. How much calcium is in your drinking water? a survey of calcium concentrations in bottled and tap water and their significance for medical treatment and drug administration. *HSS Journal*, 2(2):130–135, 2006.

[56] H Böhmer, H Müller, and KL Resch. Calcium supplementation with calcium-rich mineral waters: a systematic review and meta-analysis of its bioavailability. *Osteoporosis International*, 11(11):938–943, 2000.

[57] NA Medellin-Castillo, R Leyva-Ramos, R Ocampo-Perez, RF Garcia de la Cruz, A Aragon-Pina, JM Martinez-Rosales, RM Guerrero-Coronado, and L Fuentes-Rubio. Adsorption of fluoride from water solution on bone char. *Industrial & Engineering Chemistry Research*, 46(26):9205–9212, 2007.

[58] GL He and SR Cao. Assessment of fluoride removal from drinking water by calcium phosphate systems. *Fluoride*, 29(4):212–216, 1996.

[59] M Islam and RK Patel. Evaluation of removal efficiency of fluoride from aqueous solution using quick lime. *Journal of Hazardous Materials*, 143(1):303–310, 2007.

[60] S George, P Pandit, AB Gupta, and M Agarwal. Modeling and Simulation studies for Aluminium-Fluoride Interactions in Nalgonda Defluoridation Process. *Chemical Product and Process Modeling*, 4(1), 2009.

[61] C Banuchandra and P Selvapathy. A household defluorodation technique. *TWAD Technical Newsletter*, pages 81–90, 2005.

[62] KC Agarwal, SK Gupta, and AB Gupta. Development of new low cost defluoridation technology (KRASS). *Water Science and Technology*, 40(2):167–173, 1999.

[63] A Goswami and MK Purkait. The defluoridation of water by acidic alumina. *Chemical Engineering Research and Design*, 90(12):2316–2324, 2012.

[64] SP Kamble, G Deshpande, PP Barve, S Rayalu, NK Labhsetwar, A Malyshew, and BD Kulkarni. Adsorption of fluoride from aqueous solution by alumina of alkoxide nature: Batch and continuous operation. *Desalination*, 264(1):15–23, 2010.

[65] A Rafique, MA Awan, A Wasti, IA Qazi, and M Arshad. Removal of fluoride from drinking water using modified immobilized activated alumina. *Journal of Chemistry*, 2013, 2012.

[66] SM Maliyekkal, S Shukla, L Philip, and IM Nambi. Enhanced fluoride removal from drinking water by magnesia-amended activated alumina granules. *Chemical Engineering Journal*, 140(1):183–192, 2008.

[67] SS Tripathy and AM Raichur. Abatement of fluoride from water using manganese dioxide-coated activated alumina. *Journal of Hazardous Materials*, 153(3):1043–1051, 2008.

[68] SM Maliyekkal, AK Sharma, and L Philip. Manganese-oxide-coated alumina: a promising sorbent for defluoridation of water. *Water Research*, 40(19):3497–3506, 2006.

[69] H Liu, S Deng, Z Li, G Yu, and J Huang. Preparation of Al–Ce hybrid adsorbent and its application for defluoridation of drinking water. *Journal of Hazardous Materials*, 179(1):424–430, 2010.

[70] D Thakre, S Jagtap, N Sakhare, N Labhsetwar, S Meshram, and S Rayalu. Chitosan based mesoporous Ti–Al binary metal oxide supported beads for defluoridation of water. *Chemical Engineering Journal*, 158(2):315–324, 2010.

[71] E Kumar, A Bhatnagar, U Kumar, and M Sillanpaa. Defluoridation from aqueous solutions by nano-alumina: characterization and sorption studies. *Journal of Hazardous Materials*, 186(2):1042–1049, 2011.

[72] WHO. Guidelines for drinking-water quality. *World Health Organization,Geneva*, 2011.

[73] E Gauthier, I Fortier, F Courchesne, Pl Pepin, J Mortimer, and D Gauvreau. Aluminum forms in drinking water and risk of Alzheimer's disease. *Environmental Research*, 84(3):234–246, 2000.

[74] D Krewski, RA Yokel, E Nieboer, D Borchelt, J Cohen, J Harry, S Kacew, J Lindsay, AM Mahfouz, and V Rondeau. Human health risk assessment for aluminium, aluminium oxide, and aluminium hydroxide. *Journal of Toxicology and Environmental Health, Part B*, 10(S1):1–269, 2007.

[75] T Wajima and JF Rakovan. Removal behavior of phosphate from aqueous solution by calcined paper sludge. *Colloids and Surfaces A: Physicochemical and Engineering Aspects*, 435:132–138, 2013.

[76] SL Bhagat. Fluoride removal from water using edible oil and crushed limestone. *Science Reviews Chemical Communications*, 1(1):49–62, 2011.

[77] E Tchomgui-Kamga, E Ngameni, and A Darchen. Evaluation of removal efficiency of fluoride from aqueous solution using new charcoals that contain calcium compounds. *Journal of Colloid and Interface Science*, 346(2):494–499, 2010.

[78] S Jain and RV Jayaram. Removal of fluoride from contaminated drinking water using unmodified and aluminium hydroxide impregnated blue lime stone waste. *Separation Science and Technology*, 44(6):1436–1451, 2009.

[79] N Sakhare, S Lunge, S Rayalu, S Bakardjiva, J Subrt, S Devotta, and N Labhsetwar. Defluoridation of water using calcium aluminate material. *Chemical Engineering Journal*, 203:406–414, 2012.

[80] S Lunge, D Thakre, S Kamble, N Labhsetwar, and S Rayalu. Alumina supported carbon composite material with exceptionally high defluoridation property from eggshell waste. *Journal of Hazardous Materials*, 237:161–169, 2012.

[81] M Jimnez-Reyes and M Solache-Rios. Sorption behavior of fluoride ions from aqueous solutions by hydroxyapatite. *Journal of Hazardous Materials*, 180(1):297–302, 2010.

[82] S Gao, R Sun, Z Wei, H Zhao, H Li, and F Hu. Size-dependent defluoridation properties of synthetic hydroxyapatite. *Journal of Fluorine Chemistry*, 130(6):550–556, 2009.

[83] K Pandi and N Viswanathan. Enhanced defluoridation and facile separation of magnetic nano-hydroxyapatite/alginate composite. *International Journal of Biological Macromolecules*, 80:341–349, 2015.

[84] W Liang, L Zhan, L Piao, and C Russel. Fluoride removal performance of glass derived hydroxyapatite. *Materials Research Bulletin*, 46(2):205–209, 2011.

[85] SM Prabhu and S Meenakshi. Synthesis of surface coated hydroxyapatite powders for fluoride removal from aqueous solution. *Powder Technology*, 268:306–315, 2014.

[86] ZZ Ismail and HN AbdelKareem. Sustainable approach for recycling waste lamb and chicken bones for fluoride removal from water followed by reusing fluoride-bearing waste in concrete. *Waste Management*, 2015.

[87] Y Nie, C Hu, and C Kong. Enhanced fluoride adsorption using Al (III) modified calcium hydroxyapatite. *Journal of Hazardous Materials*, 233:194–199, 2012.

[88] SK Jha, AK Nayak, and YK Sharma. Fluoride occurrence and assessment of exposure dose of fluoride in shallow aquifers of Makur, Unnao district Uttar Pradesh, India. *Environmental Monitoring and Assessment*, 156(1-4):561–566, 2009.

[89] AAM Daifullah, SM Yakout, and SA Elreefy. Adsorption of fluoride in aqueous solutions using $KMnO_4$ $^-$ modified activated carbon derived from steam pyrolysis of rice straw. *Journal of Hazardous Materials*, 147(1):633–643, 2007.

[90] S Marquez-Mendoza, M Jimenez-Reyes, M Solache-Rios, and E Gutierrez-Segura. Fluoride removal from aqueous solutions by a carbonaceous material from pyrolysis of sewage sludge. *Water, Air, & Soil Pollution*, 223(5):1959–1971, 2012.

[91] M Karthikeyan and KP Elango. Removal of fluoride from aqueous solution using graphite: A kinetic and thermo-dynamic study. *Indian Journal of Chemical Technology*, 15(6):525, 2008.

[92] M Pekar. Fluoride anion binding by natural lignite (South Moravian Deposit of Vienna Basin). *Water, Air, and Soil pollution*, 197(1-4):303–312, 2009.

[93] V Sivasankar, S Murugesh, S Rajkumar, and A Darchen. Cerium dispersed in carbon (CeDC) and its adsorption behavior: A first example of tailored adsorbent for fluoride removal from drinking water. *Chemical Engineering Journal*, 214:45–54, 2013.

[94] VK Gupta, I Ali, and VK Saini. Defluoridation of wastewaters using waste carbon slurry. *Water Research*, 41(15):3307–3316, 2007.

[95] AK Gupta, D Deva, A Sharma, and N Verma. Adsorptive removal of fluoride by micro-nanohierarchal web of activated carbon fibers. *Industrial and Engineering Chemistry Research*, 48(21):9697–9707, 2009.

[96] YH Li, S Wang, X Zhang, J Wei, C Xu, Z Luan, and D Wu. Adsorption of fluoride from water by aligned carbon nanotubes. *Materials Research Bulletin*, 38(3):469–476, 2003.

[97] E Kumar, A Bhatnagar, M Ji, W Jung, SH Lee, SJ Kim, G Lee, H Song, JY Choi, and JS Yang. Defluoridation from aqueous solutions by granular ferric hydroxide(GFH). *Water Research*, 43(2):490–498, 2009.

[98] X Dou, Y Zhang, H Wang, T Wang, and Y Wang. Performance of granular zirconium–iron oxide in the removal of fluoride from drinking water. *Water Research*, 45(12):3571–3578, 2011.

[99] CRN Rao and J Karthikeyan. Removal of fluoride from water by adsorption onto lanthanum oxide. *Water, Air, & Soil Pollution*, 223(3):1101–1114, 2012.

[100] L Stoica, C Constantin, and C Calin. Fluoride removal from aqueous solutions by sorbtion-flotation. *Univ Politeh Buchar Sci Bull Ser B Chem Mater Sci*, 74(4):87–102, 2012.

[101] M Islam, PC Mishra, and R Patel. Fluoride adsorption from aqueous solution by a hybrid thorium phosphate composite. *Chemical Engineering Journal*, 166(3):978–985, 2011.

[102] SS Dash, MK Sahu, E Sahu, and RK Patel. Fluoride removal from aqueous solutions using cerium loaded mesoporous zirconium phosphate. *New Journal of Chemistry*, 39(9):7300–7308, 2015.

[103] J Wang, D Kang, X Yu, M Ge, and Y Chen. Synthesis and characterization of Mg–Fe–La trimetal composite as an adsorbent for fluoride removal. *Chemical Engineering Journal*, 264:506–513, 2015.

[104] S Chidambaram, AL Ramanathan, and S Vasudevan. Fluoride removal studies in water using natural materials: technical note. *Water SA*, 29(3):339–344, 2004.

[105] BM Mamilwar, AG Bhole, and AM Sudame. Removal of fluoride from ground water by using adsorbent. *International Journal of Engineering Research and Applications*, 2(4):334–338, 2012.

[106] SP Kamble, S Jagtap, NK Labhsetwar, D Thakare, Sl Godfrey, S Devotta, and SS R. Defluoridation of drinking water using chitin, chitosan and lanthanum-modified chitosan. *Chemical Engineering Journal*, 129(1):173–180, 2007.

[107] G Jayapriya, R Ramya, XR Rathinam, and PN Sudha. Equilibrium and kinetic studies of fluoride adsorption by chitin/cellulose composite. *Archives of Applied Science Research*, 3(3):415–423, 2011.

[108] V Veeraputhiran and G Alagumuthu. Sorption equilibrium of fluoride onto *Phyllanthus emblica* activated carbon. *Int. J. Res. Chem. Environ*, 1:42–47, 2011.

[109] G Alagumuthu, V Veeraputhiran, and R Venkataraman. Fluoride sorption using *Cynodon dactylon* based activated carbon. *Hemijska Industrija*, 65(1):23–35, 2011.

[110] S Chakrabarty and HP Sarma. Defluoridation of contaminated drinking water using neem charcoal adsorbent: kinetics and equilibrium studies. *International Journal of ChemTech Research*, 4(2):511–516, 2012.

[111] G Asgari, B Roshani, and G Ghanizadeh. The investigation of kinetic and isotherm of fluoride adsorption onto functionalize pumice stone. *Journal of Hazardous Materials*, 217:123–132, 2012.

[112] PK Gogoi and R Baruah. Fluoride removal from water by adsorption on acid activated kaolinite clay. *Indian Journal of Chemical Technology*, 15(5):500, 2008.

[113] A Tor and Y Cengeloglu. Removal of congo red from aqueous solution by adsorption onto acid activated red mud. *Journal of Hazardous Materials*, 138(2):409–415, 2006.

[114] SP Kamble, P Dixit, SS Rayalu, and NK Labhsetwar. Defluoridation of drinking water using chemically modified bentonite clay. *Desalination*, 249(2):687–693, 2009.

[115] D Thakre, S Rayalu, R Kawade, S Meshram, J Subrt, and N Labhsetwar. Magnesium incorporated bentonite clay for defluoridation of drinking water. *Journal of Hazardous Materialls*, 180(1):122–130, 2010.

[116] P Miretzky and AF Cirelli. Fluoride removal from water by chitosan derivatives and composites: a review. *Journal of Fluorine Chemistry*, 132(4):231–240, 2011.

[117] M Teotia, SPS Teotia, and KP Singh. Endemic chronic fluoride toxicity and dietary calcium deficiency interaction syndromes of metabolic bone diease and deformities in India: Year 2000. *Indian Journal of Pediatrics*, 65(3):371–381, 1998.

[118] MM Dubinin and LV Radushkevich. Equation of the characteristic curve of activated charcoal. *Chem. Zentr*, 1(1):875, 1947.

[119] A Kilislioglu and B Bilgin. Thermodynamic and kinetic investigations of uranium adsorption on amberliteIR-118H resin. *Applied Radiation and Isotopes*, 58(2):155–160, 2003.

[120] WJ Weber and JC Morris. Kinetics of adsorption on carbon from solution. *Journal of the Sanitary Engineering Division*, 89(2):31–60, 1963.

[121] A Gucek, S Şener, S Bilgen, and MA Mazmancı. Adsorption and kinetic studies of cationic and anionic dyes on pyrophyllite from aqueous solutions. *Journal of colloid and interface science*, 286(1):53–60, 2005.

[122] M Streat, K Hellgardt, and NLR Newton. Hydrous ferric oxide as an adsorbent in water treatment: Part 2. adsorption studies. *Process Safety and Environmental Protection*, 86(1):11–20, 2008.

[123] A Tor, N Danaoglu, Gn Arslan, and Y Cengeloglu. Removal of fluoride from water by using granular red mud: batch and column studies. *Journal of Hazardous Materials*, 164(1):271–278, 2009.

[124] SC Bondy. The neurotoxicity of environmental aluminum is still an issue. *Neurotoxicology*, 31(5):575–581, 2010.

[125] W Yongxing, W Xiaorong, and H Zichun. Genotoxicity of Lanthanum III and Gadolinium III in human peripheral blood lymphocytes. *Bulletin of Environmental Contamination and Toxicology*, 64(4):611–616, 2000.

[126] M Auffan, J Rose, T Orsiere, De MM, A Thill, O Zeyons, O Proux, A Masion, P Chaurand, and O Spalla. CeO2 nanoparticles induce DNA damage towards human dermal fibroblasts in vitro. *Nanotoxicology*, 3(2):161–171, 2009.

[127] Z Chen, Y Wang, T Ba, Y Li, J Pu, T Chen, Y Song, Y Gu, Q Qian, and J Yang. Genotoxic evaluation of titanium dioxide nanoparticles in vivo and in vitro. *Toxicology Letters*, 226(3):314–319, 2014.

[128] Z Chen, Y Wang, L Zhuo, S Chen, L Zhao, X Luan, H Wang, and G Jia. Effect of titanium dioxide nanoparticles on the cardiovascular system after oral administration. *Toxicology Letters*, 2015.

[129] QZ Chen, CT Wong, WW Lu, KMC Cheung, JCY Leong, and KDK Luk. Strengthening mechanisms of bone bonding to crystalline hydroxyapatite in vivo. *Biomaterials*, 25(18):4243–4254, 2004.

[130] VP Orlovskii, VS Komlev, and SM Barinov. Hydroxyapatite and hydroxyapatite-based ceramics. *Inorganic Materials*, 38(10):973–984, 2002.

[131] WL Suchanek, K Byrappa, P Shuk, RE Riman, VF Janas, and KS TenHuisen. Preparation of magnesium-substituted hydroxyapatite powders by the mechanochemical–hydrothermal method. *Biomaterials*, 25(19):4647–4657, 2004.

[132] CR Young, JJ Koleng, and JW McGinity. Production of spherical pellets by a hot-melt extrusion and spheronization process. *International Journal of Pharmaceutics*, 242(1):87–92, 2002.

[133] DI Wilson and SL Rough. Extrusion - spheronisation. *Handbook of Powder Technology*, 11:189–217, 2007.

[134] B Zhao, Y Zhang, X Dou, X Wu, and M Yang. Granulation of Fe–Al–Ce trimetal hydroxide as a fluoride adsorbent using the extrusion method. *Chemical Engineering Journal*, 185:211–218, 2012.

[135] K Ravindra and VK Garg. Hydro-chemical survey of groundwater of Hisar city and assessment of defluoridation methods used in India. *Environmental Monitoring and Assessment*, 132(1-3):33–43, 2007.

[136] RK Tatawat and CPS Chandel. A hydrochemical profile for assessing the groundwater quality of Jaipur city. *Environmental Monitoring and Assessment*, 143(1-3):337–343, 2008.

[137] AWWA APHA. WPCF, 1992. *Standard methods for the examination of water and wastewater*, 18:518–523, 1800.

[138] YS Ho and G McKay. Pseudo-second order model for sorption processes. *Process Biochemistry*, 34(5):451–465, 1999.

[139] G Yan and T Viraraghavan. Heavy-metal removal from aqueous solution by fungus *Mucor rouxii*. *Water Research*, 37(18):4486–4496, 2003.

[140] H Qiu, L Lv, B Pan, Q Zhang, W Zhang, and Q Zhang. Critical review in adsorption kinetic models. *Journal of Zhejiang University Science A*, 10(5):716–724, 2009.

[141] E Guibal, C Milot, and JM Tobin. Metal-anion sorption by chitosan beads: equilibrium and kinetic studies. *Industrial & Engineering Chemistry Research*, 37(4):1454–1463, 1998.

[142] KY Foo and BH Hameed. Insights into the modeling of adsorption isotherm systems. *Chemical Engineering Journal*, 156(1):2–10, 2010.

[143] KKH Choy, G McKay, and JF Porter. Sorption of acid dyes from effluents using activated carbon. *Resources, Conservation and Recycling*, 27(1):57–71, 1999.

[144] GM Walker and LR Weatherley. Adsorption of acid dyes on to granular activated carbon in fixed beds. *Water Research*, 31(8):2093–2101, 1997.

[145] HC Thomas. Heterogeneous ion exchange in a flowing system. *Journal of the American Chemical Society*, 66(10):1664–1666, 1944.

[146] SS Baral, N Das, TS Ramulu, SK Sahoo, SN Das, and GR Chaudhury. Removal of Cr (VI) by thermally activated weed *Salvinia cucullata* in a fixed-bed column. *Journal of Hazardous Materials*, 161(2):1427–1435, 2009.

[147] YH Yoon and JH Nelson. Application of gas adsorption kinetics I. A theoretical model for respirator cartridge service life. *The American Industrial Hygiene Association Journal*, 45(8):509–516, 1984.

[148] M Elibol. Response surface methodological approach for inclusion of perfluorocarbon in actinorhodin fermentation medium. *Process Biochemistry*, 38(5):667–673, 2002.

[149] M Tanyildizi. Modeling of adsorption isotherms and kinetics of reactive dye from aqueous solution by peanut hull. *Chemical Engineering Journal*, 168(3):1234–1240, 2011.

[150] P Ricou, I Lecuyer, and P Le Cloirec. Influence of ph on removal of heavy metallic cations by fly ash in aqueous solution. *Environmental Technology*, 19(10):1005–1016, 1998.

[151] R Bhaumik and NK Mondal. Optimizing adsorption of fluoride from water by modified banana peel dust using response surface modelling approach. *Applied Water Science*, pages 1–21, 2014.

[152] IAW Tan, AL Ahmad, and BH Hameed. Adsorption of basic dye using activated carbon prepared from oil palm shell: batch and fixed bed studies. *Desalination*, 225(1):13–28, 2008.

[153] SW Russell, KA Luptak, CTA Suchicital, TL Alford, and VB Pizziconi. Chemical and Structural Evolution of Sol-Gel-Derived Hydroxyapatite Thin Films under Rapid Thermal Processing. *Journal of the American Ceramic Society*, 79(4):837–842, 1996.

[154] Y Sargin, M Kizilyalli, C Telli, and H Güler. A new method for the solid-state synthesis of tetracalcium phosphate, a dental cement: X-ray powder diffraction and IR studies. *Journal of the European Ceramic Society*, 17(7):963–970, 1997.

[155] SR Ramanan and R Venkatesh. A study of hydroxyapatite fibers prepared via sol–gel route. *Materials Letters*, 58(26):3320–3323, 2004.

[156] A Farzadi, F Bakhshi, M Solati-Hashjin, M Asadi-Eydivand, and NA abu Osman. Magnesium incorporated hydroxyapatite: Synthesis and structural properties characterization. *Ceramics International*, 40(4):6021–6029, 2014.

[157] F Ren, Y Leng, R Xin, and X Ge. Synthesis, characterization and ab initio simulation of magnesium-substituted hydroxyapatite. *Acta Biomaterialia*, 6(7):2787–2796, 2010.

[158] BD Turner, P Binning, and SLS Stipp. Fluoride removal by calcite: evidence for fluorite precipitation and surface adsorption. *Environmental Science & Technology*, 39(24):9561–9568, 2005.

[159] SK Nath and RK Dutta. Acid-enhanced limestone defluoridation in column reactor using oxalic acid. *Process Safety and Environmental Protection*, 90(1):65–75, 2012.

[160] AM Raichur and M Jyoti Basu. Adsorption of fluoride onto mixed rare earth oxides. *Separation and Purification Technology*, 24(1):121–127, 2001.

[161] DP Das, J Das, and K Parida. Physicochemical characterization and adsorption behavior of calcined Zn/Al hydrotalcite-like compound (HTlc) towards removal of fluoride from aqueous solution. *Journal of Colloid and Interface Science*, 261(2):213–220, 2003.

[162] A Duffy, GM Walker, and SJ Allen. Investigations on the adsorption of acidic gases using activated dolomite. *Chemical Engineering Journal*, 117(3):239–244, 2006.

[163] A Eskandarpour, MS Onyango, A Ochieng, and S Asai. Removal of fluoride ions from aqueous solution at low pH using schwertmannite. *Journal of Hazardous Materials*, 152(2):571–579, 2008.

[164] MG Sujana and S Anand. Iron and aluminium based mixed hydroxides: A novel sorbent for fluoride removal from aqueous solutions. *Applied Surface Science*, 256(23):6956–6962, 2010.

[165] S Meski, S Ziani, and H Khireddine. Removal of lead ions by hydroxyapatite prepared from the egg shell. *Journal of Chemical & Engineering Data*, 55(9):3923–3928, 2010.

[166] B Ma, WS Shin, S Oh, YJ Park, and SJ Choi. Adsorptive removal of co and sr ions from aqueous solution by synthetic hydroxyapatite nanoparticles. *Separation Science and Technology*, 45(4):453–462, 2010.

[167] W Wei, R Sun, J Cui, and Z Wei. Removal of nitrobenzene from aqueous solution by adsorption on nanocrystalline hydroxyapatite. *Desalination*, 263(1):89–96, 2010.

[168] DC Montgomery. *Design and analysis of experiments*. John Wiley & Sons, 2008.

[169] N Swami and DB Dreisinger. Kinetics of zinc removal from cobalt electrolytes by ion exchange. *Solvent Extraction and Ion Exchange*, 13(6):1037–1062, 1995.

[170] H Paudyal, B Pangeni, K Inoue, H Kawakita, K Ohto, and S Alam. Adsorptive removal of fluoride from aqueous medium using a fixed bed column packed with Zr (IV) loaded dried orange juice residue. *Bioresource technology*, 146:713–720, 2013.

[171] N Chen, Z Zhang, C Feng, M Li, R Chen, and N Sugiura. Investigations on the batch and fixed-bed column performance of fluoride adsorption by Kanuma mud. *Desalination*, 268(1):76–82, 2011.

[172] FW Sousa, AG Oliveira, JP Ribeiro, MF Rosa, D Keukeleire, and RF Nascimento. Green coconut shells applied as adsorbent for removal of toxic metal ions using fixed-bed column technology. *Journal of Environmental Management*, 91(8):1634–1640, 2010.

[173] S Kundu and AK Gupta. Analysis and modeling of fixed bed column operations on As (V) removal by adsorption onto iron oxide-coated cement (IOCC). *Journal of Colloid and Interface Science*, 290(1):52–60, 2005.

[174] A Ghosh, S Chakrabarti, K Biswas, and UC Ghosh. Column performances on fluoride removal by agglomerated Ce (IV)–Zr (IV) mixed oxide nanoparticles packed fixed-beds. *Journal of Environmental Chemical Engineering*, 3(2):653–661, 2015.

[175] E Malkoc, Y Nuhoglu, and Y Abali. Cr (VI) adsorption by waste acorn of *Quercus ithaburensis* in fixed beds:prediction of breakthrough curves. *Chemical Engineering Journal*, 119(1):61–68, 2006.

[176] PS Kumar, S Ramalingam, C Senthamarai, M Niranjanaa, P Vijayalakshmi, and S Sivanesan. Adsorption of dye from aqueous solution by cashew nut shell: Studies on equilibrium isotherm, kinetics and thermodynamics of interactions. *Desalination*, 261(1):52–60, 2010.

[177] PL Meena, PK Jain, and KS Meena. Assessment of Ground Water Quality and its Suitability for Drinking and Domestic Uses by Using WQI and Statistical Analysis in River Basin Area in Jahzpur Tehsil, Bhilwara District (Rajasthan, India). *International Journal of Current Microbiology and Applied Sciences*, 5(3):415–427, 2016.

[178] NS Rao. Seasonal variation of groundwater quality in a part of Guntur District, Andhra Pradesh, India. *Environmental Geology*, 49(3):413–429, 2006.

[179] C Gajendra and P Thamarai. Study on statistical relationship between ground water quality parameters in Namibiyar river basin, Tamil Nadu, India. *Pollution. Research*, 27(4):679–683, 2008.

[180] AK Yadav, P Khan, and U Saxena. Geochemical observation of fluoride in ground water of tonk (Rajasthan). *Rasayanj J. Chem*, 2:994–1000, 2009.

[181] M Kumar and R Kumar. Assessment of Physico-Chemical Properties of Ground Water in Granite Mining Areas in Goramachia, Jhansi, UP, India. *International Research Journal of Environment Sciences*, 2(1):19–24, 2013.

[182] PA Azeez, NR Nadarajan, and DD Mittal. The impact of a monsoonal wetland on ground water chemistry. *Pollution Research*, 19(2):249–255, 2000.

[183] VS Chauhan, PK Dwivedi, and L Iyengar. Investigations on activated alumina based domestic defluoridation units. *Journal of Hazardous materials*, 139(1):103–107, 2007.

[184] L Iyenger. Defluoridation of water using activated alumina technology: Studies at IIT kanpur. *A Report for UNICEF, New Delhi*, 2005.

APPENDIX

Appendix

FINITE DIFFERENCE APPROXIMATIONS

1) $\frac{\partial^2 U}{\partial x^2} = \frac{1}{2h^2}\left[\left(U_{n+1,i+1} - 2U_{n+1,i} + U_{n+1,i-1}\right) + \left(U_{n,i+1} - 2U_{n,i} + U_{n,i-1}\right)\right]$

2) $\frac{\partial U}{\partial x} = \frac{1}{4h}\left[\left(U_{n+1,i+1} - U_{n+1,i-1}\right) + \left(U_{n,i+1} - U_{n,i-1}\right)\right]$

3) $U = \frac{1}{2}\left[U_{n+1,i} + U_{n,i}\right]$

4) $U_p = \frac{1}{2}\left[U_{p_{n+1,i}} + U_{p_{n,i}}\right]$

5) $\frac{\partial U}{\partial \tau} = \frac{1}{k}\left[U_{n+1,i} - U_{n,i}\right]$

6) $\frac{\partial U_p}{\partial \tau} = \frac{1}{k}\left[U_{p_{n+1,i,m}} - U_{p_{n,i,m}}\right]$

7) $\frac{\partial^2 U_p}{\partial \eta^2} = \frac{1}{2p^2}\left[\left(U_{p_{n+1,i,m+1}} - 2U_{p_{n+1,i,m}} + U_{p_{n+1,i,m-1}}\right) + \left(U_{p_{n,i,m+1}} - 2U_{p_{n,i,m}} + U_{p_{n,i,m-1}}\right)\right]$

8) $\frac{\partial U_p}{\partial \eta} = \frac{1}{4p}\left[\left(U_{p_{n+1,i,m+1}} - U_{p_{n+1,i,m-1}}\right) + \left(U_{p_{n,i,m+1}} - U_{p_{n,i,m-1}}\right)\right]$

9) $\frac{\partial^2 V}{\partial x^2} = \frac{1}{2h^2}\left[\left(V_{n+1,i+1} - 2V_{n+1,i} + V_{n+1,i-1}\right) + \left(V_{n,i+1} - 2V_{n,i} + V_{n,i-1}\right)\right]$

10) $\frac{\partial V}{\partial x} = \frac{1}{4h}\left[\left(V_{n+1,i+1} - V_{n+1,i-1}\right) + \left(V_{n,i+1} - V_{n,i-1}\right)\right]$

11) $V = \frac{1}{2}\left[V_{n+1,i} + V_{n,i}\right]$

12) $V_p = \frac{1}{2}\left[V_{p_{n+1,i}} + V_{p_{n,i}}\right]$

13) $\frac{\partial V}{\partial \tau} = \frac{1}{k}\left[V_{n+1,i} - V_{n,i}\right]$

14) $\frac{\partial V_p}{\partial \tau} = \frac{1}{k}\left[V_{p_{n+1,i,m}} - V_{p_{n,i,m}}\right]$

LIST OF DIMENSIONLESS CONSTANTS

1) $Q = \frac{q}{c_o}$ where c_o is initial concentration of the adsorbate, q is average adsorbed phase adsorbate concentration

2) $Q_o = \frac{q_o}{c_o}$ where q_o is solid phase adsorbate concentration

3) $V = \frac{T}{T_o}$ where T_o is inlet temperature, T is temperature at any time

4) $V_s = \frac{T_s}{T_o}$ where T_s is temperature of particle surface

5) $U = \frac{c}{c_o}$ where c is concentration of solute

6) $U_p = \frac{c_p}{c_o}$ where c_p is the concentration at the particle surface

7) $x = \frac{z}{L}$; where L is the characteristic length, z is axial coordinate

8) $\eta = \frac{r}{R}$; where R is the particle radius and r is the radial coordinate

9) $\tau = \frac{tD_p}{R^2}$;where D_p is the pore diffusivity, t is the time

10) $W = \frac{R^2 u}{D_p L}$;where u the fluid velocity

11) $Pe_m = \frac{uL}{D_L}$;where Pe_m is the Peclet number for mass transfer, D_L the axial mass dispersion coefficient

12) $\beta = \frac{(-\Delta H)c_o}{\rho_l c_{pl} T_0}$ where ρ_l is solution density, c_{pl} is specific heat of liquid, ΔH is standard enthalpy change

13) $\delta = \frac{(-\Delta H)}{R_g T_o}$ where R_g is the gas constant

14) $\lambda_o = \frac{b_o c_o}{1+b_0 c_0}$ where b_o is a Langmuir constant

15) $\psi = \frac{k_l R}{D_p}$ where k_l is the mass transfer coefficient

16) $\phi = \frac{\rho_l c_{pl}}{\rho_s c_{ps}}$where c_{ps} is specific heat of solid adsorbent, ρ_s is density of the adsorbent

17) $Pe_h = \frac{\rho_l c_{pl} u L}{K_L}$where Pe_h is the Peclet number for heat transfer and K_L is heat conductivity

LIST OF COEFFICIENTS

1) $A = \frac{W}{Pe_m h^2}$
2) $B = \frac{W}{Pe_m h^2} + \frac{3\Psi(1-\epsilon)}{2\epsilon} + \frac{W}{h} + \frac{WPe_m}{2}$
3) $C = \frac{1}{k}$
4) $D = 2hPe_m \left[\frac{W}{Pe_m h^2} + \frac{W}{2h}\right]$
5) $E = -3\Psi(\frac{1-\epsilon}{\epsilon})$
6) $Z = \frac{W}{4h}$
7) $B1 = \left[\frac{W}{h^2 Pe_m}\right] + \left[3\Psi\frac{1-\epsilon}{\epsilon}\right]$
8) $A2 = \frac{W}{Pe_h h^2}$
9) $B2 = \frac{W}{Pe_h h^2} - 3\Psi(\frac{1-\epsilon}{\epsilon})$
10) $J = \frac{2p\Psi}{\epsilon_p}$
11) $G = \frac{1}{2p^2}$
12) $H = \frac{-Q_c}{k}$
13) $I = \frac{-Q_t}{k}$
14) $Y_A = \left(\frac{1}{k}\right) + \left(\frac{3\Psi\Phi}{2}\right)$
15) $Y_B = \left(\frac{-3\Psi\Phi}{2}\right)$
16) $Y_C = \left(\frac{-3\Psi\Phi\beta}{2}\right)$
17) $Y_D = \left(\frac{1}{k}\right) + \left(\frac{-3\Psi\Phi}{2}\right)$

MATLAB programme

```
%taking input from user for various paramerers and conditions
e=input('enter the bed porosity,e=');
ep=input('enter the particle porosity,ep=');
R=input('enter the particle radius,R(m)=');
Dp=input('enter the pore diffusivity,Dp=');
Co=input('enter the initial concentration of the adsorbate,Co(gm/m3)=');
qo=input('enter the solid phase adsorbate concentration,qo(gm/m3)=');
To=input('enter the inlet  temperature,To(K)=');
lo=input('enter the dimensionless non lineraity paramter,lo=');
delta=input('enter the time increment,delta=');
L=input('enter the bed length,L(m)=');
ul=input('enter the fluid velocity,u(m/s)=');
DL=input('enter the axial mass dispersion coefficient,DL(m2/sec)=');
pl=input('enter the liquid density,kg/m3');
cpl=input('enter the specific heat of liquid,J/kg K');
K=input('enter the heat conducitvity,W/m K');
Dt=input('enter the bed diameter,m');
H=input('enter the heat of adsorption,J/mol');
kg=input('enter the mass transfer coefficient,m/s');
ps=input('enter the density of the adsorbent,kg/m3');
cps=input('enter the specific heat of solid adsorbent,W/m k');

Rg=8.314;
p=0.2;
h=0.2;
%calculate the dimensionless constants

Pem=ul*L/DL;
Peh=pl*cpl*ul*L/K;
Nre=D*ul*pl/ul;
del=H/(Rg*To);
Beta=H*Co/(pl*cpl*To*40);
Sh=kg*R/Dp;
fyi=pl*cpl/(ps*cps);
W=u*R^2/Dp*L;

%guess values of Y
for j=1:42;
   Y(j)=0;
end
for j=43:54;
   Y(j)=1;
end

kop=0;
for s=1:150;
   ko=s*delta;

%calculating the values of the coefficients
Qo=qo/Co;
ET0=0;
```

```
ET1=(0.2^2)*2;
ET2=(0.4^2)*2;
ET3=(0.6^2)*2;
ET4=(0.8^2)*2;
ET5=1*2;
ET=3*h/2;
bl=lo/((1-lo)*Co);
Up0=((Y(8)*ET1)+(Y(9)*ET2)+(Y(10)*ET3)+(Y(11)*ET4)+(Y(12)*ET5))*ET;
Up1=((Y(14)*ET1)+(Y(15)*ET2)+(Y(16)*ET3)+(Y(17)*ET4)+(Y(18)*ET5))*ET;
Up2=((Y(20)*ET1)+(Y(21)*ET2)+(Y(22)*ET3)+(Y(23)*ET4)+(Y(24)*ET5))*ET;
Up3=((Y(26)*ET1)+(Y(27)*ET2)+(Y(28)*ET3)+(Y(29)*ET4)+(Y(30)*ET5))*ET;
Up4=((Y(32)*ET1)+(Y(33)*ET2)+(Y(34)*ET3)+(Y(35)*ET4)+(Y(36)*ET5))*ET;
Up5=((Y(38)*ET1)+(Y(39)*ET2)+(Y(40)*ET3)+(Y(41)*ET4)+(Y(42)*ET5))*ET;
y0=del*((1/Y(54))-1);
y1=del*((1/Y(53))-1);
y2=del*((1/Y(52))-1);
y3=del*((1/Y(51))-1);
y4=del*((1/Y(50))-1);
y5=del*((1/Y(49))-1);
b0=bl*exp(y0);
b1=bl*exp(y1);
b2=bl*exp(y2);
b3=bl*exp(y3);
b4=bl*exp(y4);
b5=bl*exp(y5);
Qc0=1+((b0*Qo*Co)/lo*ep*(1+b0*Co*Up0)^2);
Qc1=1+((b1*Qo*Co)/lo*ep*(1+b1*Co*Up1)^2);
Qc2=1+((b2*Qo*Co)/lo*ep*(1+b2*Co*Up2)^2);
Qc3=1+((b3*Qo*Co)/lo*ep*(1+b3*Co*Up3)^2);
Qc4=1+((b4*Qo*Co)/lo*ep*(1+b4*Co*Up4)^2);
Qc5=1+((b5*Qo*Co)/lo*ep*(1+b5*Co*Up5)^2);
Qt0=(-b0*Qo*Co*Up0*del)/(lo*ep*(Y(54))^2*(1+b0*Co*Up0)^2);
Qt1=(-b1*Qo*Co*Up1*del)/(lo*ep*(Y(53))^2*(1+b1*Co*Up1)^2);
Qt2=(-b2*Qo*Co*Up2*del)/(lo*ep*(Y(52))^2*(1+b2*Co*Up2)^2);
Qt3=(-b3*Qo*Co*Up3*del)/(lo*ep*(Y(51))^2*(1+b3*Co*Up3)^2);
Qt4=(-b4*Qo*Co*Up4*del)/(lo*ep*(Y(50))^2*(1+b4*Co*Up4)^2);
Qt5=(-b5*Qo*Co*Up5*del)/(lo*ep*(Y(49))^2*(1+b5*Co*Up5)^2);

A=W/(Pem*h^2);
A2=W/(Peh*h^2);
B2=[W/(Peh*h^2)+(1.5*Sh*(1-e)/e)];
B=[W/(Pem*h^2)]+ [1.5*Sh*(1-e)/e]+[W/h]+[0.5*W*Pem];
C=1/ko;
D=(2*h*Pem)*((W/(Pem*h^2))+(0.5*W/h));
E=-1.5*Sh*(1-e)/e;
Z=W/(4*h);
B1=[W/(Pem*h^2)]+[1.5*Sh*(1-e)/e];
Ya=(1/ko)+(1.5*Sh*fyi);
Yb=(-1.5*Sh*fyi);
Yc=(-1.5*Sh*fyi*Beta);
Yd=(1/ko)+(-1.5*Sh*fyi);
J=2*p*Sh/ep;
G=1/(2*p^2);

H0=-Qc0/ko;
```

```
H1=-Qc1/ko;
H2=-Qc2/ko;
H3=-Qc3/ko;
H4=-Qc4/ko;
H5=-Qc5/ko;
I0=-Qt0/ko;
I1=-Qt1/ko;
I2=-Qt2/ko;
I3=-Qt3/ko;
I4=-Qt4/ko;
I5=-Qt5/ko;

AA=A;
A2A=A2;
CC=-E;
BB=-(B+C);
CB=B-C;
AZ=A/2+Z;
ZA=-A/2+Z;
ZZA=A/2-Z;
BC=-(B1+C);
B1C=B1-C;
AE=-(A/2)-Z-C+E;
AZE=(A/2)+Z-C-E;
A2ZE=(A2/2)+Z-C-E;
A2E=-(A2/2)-Z-C+E;
A2Z=A2/2+Z;
Z2A=-A2/2+Z;
ZZ2A=A2/A-Z;
B2C=-(B2+C);
C2B=B2-C;
DD=D;

GH0=6*G+H0;
GH1=6*G+H1;
GH2=6*G+H2;
GH3=6*G+H3;
GH4=6*G+H4;
GH5=6*G+H5;
FH0=2*G+H0;
FH1=2*G+H1;
FH2=2*G+H2;
FH3=2*G+H3;
FH4=2*G+H4;
FH5=2*G+H5;
QQ0=2*G+H0+(6/5)*J*G;
QQ1=2*G+H1+(6/5)*J*G;
QQ2=2*G+H2+(6/5)*J*G;
QQ3=2*G+H3+(6/5)*J*G;
QQ4=2*G+H4+(6/5)*J*G;
QQ5=2*G+H5+(6/5)*J*G;

DD0=-6*G+H0;
EE0=6*G;
FF0=-2*G+H0;
```

```
GG0=2*G;
NG0=2*G;
HH0=0.5*G;
II0=1.5*G;
JJ0=(2/3)*G;
KK0=(4/3)*G;
LL0=0.75*G;
MM0=1.25*G;
NN0=(6/5)*J*G;
AAA0=-2*G+H0-(6/5)*J*G;
DD1=-6*G+H1;
EE1=6*G;
FF1=-2*G+H1;
GG1=2*G;
NG1=2*G;
HH1=0.5*G;
II1=1.5*G;
JJ1=(2/3)*G;
KK1=(4/3)*G;
LL1=0.75*G;
MM1=1.25*G;
NN1=(6/5)*J*G;
AAA1=-2*G+H1-(6/5)*J*G;
DD2=-6*G+H2;
EE2=6*G;
FF2=-2*G+H2;
GG2=2*G;
NG2=2*G;
HH2=0.5*G;
II2=1.5*G;
JJ2=(2/3)*G;
KK2=(4/3)*G;
LL2=0.75*G;
MM2=1.25*G;
NN2=(6/5)*J*G;
AAA2=-2*G+H2-(6/5)*J*G;
DD3=-6*G+H3;
EE3=6*G;
FF3=-2*G+H3;
GG3=2*G;
NG3=2*G;
HH3=0.5*G;
II3=1.5*G;
JJ3=(2/3)*G;
KK3=(4/3)*G;
LL3=0.75*G;
MM3=1.25*G;
NN3=(6/5)*J*G;
AAA3=-2*G+H3-(6/5)*J*G;
DD4=-6*G+H4;
EE4=6*G;
FF4=-2*G+H4;
GG4=2*G;
NG4=2*G;
HH4=0.5*G;
II4=1.5*G;
```

```
JJ4=(2/3)*G;
KK4=(4/3)*G;
LL4=0.75*G;
MM4=1.25*G;
NN4=(6/5)*J*G;
AAA4=-2*G+H4-(6/5)*J*G;
DD5=-6*G+H5;
EE5=6*G;
FF5=-2*G+H5;
GG5=2*G;
NG5=2*G;
HH5=0.5*G;
II5=1.5*G;
JJ5=(2/3)*G;
KK5=(4/3)*G;
LL5=0.75*G;
MM5=1.25*G;
NN5=(6/5)*J*G;
AAA5=-2*G+H5-(6/5)*J*G;
WX0=I0;
VX0=I0;
YX0=I0;
WX1=I1;
VX1=I1;
YX1=I1;
WX2=I2;
VX2=I2;
YX2=I2;
WX3=I3;
VX3=I3;
YX3=I3;
WX4=I4;
VX4=I4;
YX4=I4;
WX5=I5;
VX5=I5;
YX5=I5;

%first iterations

AA=AA/CC;
BB=BB/CC;
CB=CB/CC;
DD=DD/CC;
BC=BC/CC;
AZE=AZE/CC;
AE=AE/CC;
B1C=B1C/CC;
AZ=AZ/CC;
ZA=ZA/CC;
ZZA=ZZA/CC;
CC=CC/CC;
A2E=A2E/CC;
A2Z=A2Z/CC;
Z2A=Z2A/CC;
```

```
ZZ2A=ZZ2A/CC;
B2C=B2C/CC;
A2ZE=A2ZE/CC;
C2B=C2B/CC;
A2A=A2A/CC;

NN0=NN0/AAA0;
NG0=NG0/AAA0;
QQ0=QQ0/AAA0;
WX0=WX0/AAA0;
AAA0=AAA0/AAA0;

MM0=MM0/FF0;
LL0=LL0/FF0;
KK0=KK0/FF0;
JJ0=JJ0/FF0;
II0=II0/FF0;
HH0=HH0/FF0;
GG0=GG0/FF0;
FH0=FH0/FF0;
VX0=VX0/FF0;
FF0=FF0/FF0;

EE0=EE0/DD0;
GH0=GH0/DD0;
YX0=YX0/DD0;
DD0=DD0/DD0;

Yb=Yb/Ya;
Yc=Yc/Ya;
Yd=Yd/Ya;
Ya=Ya/Ya;

NN1=NN1/AAA1;
NG1=NG1/AAA1;
QQ1=QQ1/AAA1;
WX1=WX1/AAA1;
AAA1=AAA1/AAA1;

MM1=MM1/FF1;
LL1=LL1/FF1;
KK1=KK1/FF1;
JJ1=JJ1/FF1;
II1=II1/FF1;
HH1=HH1/FF1;
GG1=GG1/FF1;
FH1=FH1/FF1;
VX1=VX1/FF1;
FF1=FF1/FF1;

EE1=EE1/DD1;
GH1=GH1/DD1;
YX1=YX1/DD1;
DD1=DD1/DD1;
```

```
NN2=NN2/AAA2;
NG2=NG2/AAA2;
QQ2=QQ2/AAA2;
WX2=WX2/AAA2;
AAA2=AAA2/AAA2;

MM2=MM2/FF2;
LL2=LL2/FF2;
KK2=KK2/FF2;
JJ2=JJ2/FF2;
II2=II2/FF2;
HH2=HH2/FF2;
GG2=GG2/FF2;
FH2=FH2/FF2;
VX2=VX2/FF2;
FF2=FF2/FF2;

EE2=EE2/DD2;
GH2=GH2/DD2;
YX2=YX2/DD2;
DD2=DD2/DD2;

NN3=NN3/AAA3;
GG3=GG3/AAA3;
QQ3=QQ3/AAA3;
WX3=WX3/AAA3;
AAA3=AAA3/AAA3;

MM3=MM3/FF3;
LL3=LL3/FF3;
KK3=KK3/FF3;
JJ3=JJ3/FF3;
II3=II3/FF3;
HH3=HH3/FF3;
GG3=GG3/FF3;
FH3=FH3/FF3;
VX3=VX3/FF3;
FF3=FF3/FF3;

EE3=EE3/DD3;
GH3=GH3/DD3;
YX3=YX3/DD3;
DD3=DD3/DD3;

NN4=NN4/AAA4;
NG4=NG4/AAA4;
QQ4=QQ4/AAA4;
WX4=WX4/AAA4;
AAA4=AAA4/AAA4;

MM4=MM4/FF4;
LL4=LL4/FF4;
KK4=KK4/FF4;
```

```
JJ4=JJ4/FF4;
II4=II4/FF4;
HH4=HH4/FF4;
GG4=GG4/FF4;
FH4=FH4/FF4;
VX4=VX4/FF4;
FF4=FF4/FF4;
EE4=EE4/DD4;
GH4=GH4/DD4;
YX4=YX4/DD4;
DD4=DD4/DD4;

NN5=NN5/AAA5;
NG5=NG5/AAA5;
QQ5=QQ5/AAA5;
WX5=WX5/AAA5;
AAA5=AAA5/AAA5;

MM5=MM5/FF5;
LL5=LL5/FF5;
KK5=KK5/FF5;
JJ5=JJ5/FF5;
II5=II5/FF5;
HH5=HH5/FF5;
GG5=GG5/FF5;
FH5=FH5/FF5;
VX5=VX5/FF5;
FF5=FF5/FF5;

EE5=EE5/DD5;
GH5=GH5/DD5;
YX5=YX5/DD5;
DD5=DD5/DD5;

%input coefficient matrix

for b=1;
   for a=3:17;19:54;
      m(b,a)=0;
   end
     m(b,1)=BB;
     m(b,2)=AA;
     m(b,12)=CC;
end
for b=2;
   for a=1:6;9:53;
      m(b,a)=0;
   end
      m(b,54)=YX0;
      m(b,7)=DD0;
      m(b,8)=EE0;
end
for b=3;
   for a=1:7;10:53;
      m(b,a)=0;
```

```
    end
        m(b,8)=FF0;
        m(b,9)=GG0;
        m(b,54)=VX0;
end
for b=4;
    for a =1:7;11:53;
        m(b,a)=0;
    end
        m(b,8)=HH0;
        m(b,9)= FF0;
        m(b,10)= II0;
        m(b,54)=VX0;
end
for b=5;
    for a=1:8;12:53;
        m(b,a)=0;
    end
        m(b,9)= JJ0;
        m(b,10)=FF0;
        m(b,11)=KK0;
        m(b,54)=VX0;
end
for b=6;
    for a=1:9;13:53;
        m(b,a)=0;
    end
        m(b,10)=LL0;
        m(b,11)=FF0;
        m(b,12)=MM0;
        m(b,54)=VX0;
end
for b=7;
        m(b,1)=NN0;
   for a=2:10;13:53;
        m(b,a)=0;
   end
        m(b,11)=NG0;
        m(b,12)=AAA0;
        m(b,54)=WX0;
end
for b=8;
        m(b,1)=AZ;
        m(b,2)=BC;
        m(b,3)=ZZA;
    for a=4:17;19:54;
        m(b,a)=0;
    end
        m(b,18)=CC;
end
for b=9;
   for a=1:12;15:52;54;
        m(b,a)=0;
   end
        m(b,13)=DD1;
        m(b,14)=EE1;
```

```
        m(b,53)=YX1;
end
for b=10;
   for a=1:13;16:52;54;
        m(b,a)=0;
   end
        m(b,14)=FF1;
        m(b,15)=GG1;
        m(b,53)=VX1;
end
for b=11;
   for a=1:13;17:52;54;
        m(b,a)=0;
   end
        m(b,14)=HH1;
        m(b,15)=FF1;
        m(b,16)=II1;
        m(b,53)=VX1;
end
for b=12;
   for a =1:14;18:52;54;
        m(b,a)=0;
   end
        m(b,15)=JJ1;
        m(b,16)=FF1;
        m(b,17)=KK1;
        m(b,53)=VX1;
end
for b=13;
   for a=1:15;19:52;54;
        m(b,a)=0;
   end
        m(b,16)=LL1;
        m(b,17)=FF1;
        m(b,18)=MM1;
        m(b,53)=VX1;
end
for b=14;
   for a=1;3:16;19:52;54;
        m(b,a)=0;
   end
        m(b,2)=NN1;
        m(b,17)=NG1;
        m(b,18)=AAA1;
        m(b,53)=WX1;
end
for b=15;
   for a=1;5:23;25:54;
        m(b,a)=0;
   end
        m(b,2)=AZ;
        m(b,3)=BC;
        m(b,4)=ZZA;
        m(b,24)=CC;
end
for b=16;
```

```
    for a=1:18;21:51;53;54;
        m(b,a)=0;
    end
        m(b,19)=DD2;
        m(b,20)=EE2;
        m(b,52)=YX2;
end
for b=17;
    for a=1:19;22:51;53;54;
        m(b,a)=0;
    end
        m(b,20)=FF2;
        m(b,21)=GG2;
        m(b,52)=VX2;
end
for b=18;
    for a=1:19;23:51;53;54;
        m(b,a)=0;
    end
        m(b,20)=HH2;
        m(b,21)=FF2;
        m(b,22)=II2;
        m(b,52)=VX2;
end
for b=19;
    for a=1:20;24:51;53;54;
        m(b,a)=0;
    end
        m(b,21)=JJ2;
        m(b,22)=FF2;
        m(b,23)=KK2;
        m(b,52)=VX2;
end
for b=20;
    for a =1:21;25:51;53;54;
        m(b,a)=0;
    end
        m(b,22)=LL2;
        m(b,23)=FF2;
        m(b,24)=MM2;
        m(b,52)=VX2;
end
for b=21;
    for a=1;2;4:22;25:51;53;54;
        m(b,a)=0;
    end
        m(b,3)=NN2;
        m(b,23)=NG2;
        m(b,24)=AAA2;
        m(b,52)=WX2;
end
for b=22;
    for a=1;2;6:29;31:54;
        m(b,a)=0;
    end
        m(b,3)=AZ;
```

```
        m(b,4)=BC;
        m(b,5)=ZZA;
        m(b,30)=CC;
end
for b=23;
    for a=1:24;27:50;52:54;
        m(b,a)=0;
    end
        m(b,25)=DD3;
        m(b,26)=EE3;
        m(b,51)=YX3;
end
for b=24;
    for a =1:25;28:50;52:54;
        m(b,a)=0;
    end
        m(b,26)=FF3;
        m(b,27)=GG3;
        m(b,51)=VX3;
end
for b=25;
    for a=1:25;29:50;52:54;
        m(b,a)=0;
    end
        m(b,26)=HH3;
        m(b,27)=FF3;
        m(b,28)=II3;
        m(b,51)=VX3;
end
for b=26;
    for a=1:26;30:50;52:54;
        m(b,a)=0;
    end
        m(b,27)=JJ3;
        m(b,28)=FF3;
        m(b,29)=KK3;
        m(b,51)=VX3;
end
for b=27;
    for a=1:27;31:50;52:54;
        m(b,a)=0;
    end
        m(b,28)=LL3;
        m(b,29)=FF3;
        m(b,30)=MM3;
        m(b,51)=VX3;
end
for b=28;
    for a=1:3;5:28;31:50;52:54;
        m(b,a)=0;
    end
        m(b,4)=NN3;
        m(b,29)=NG3;
        m(b,30)=AAA3;
        m(b,51)=WX3;
end
```

```
for b=29;
   for a=1:3;7:35;37:54;
      m(b,a)=0;
   end
      m(b,4)=AZ;
      m(b,5)=BC;
      m(b,6)=ZZA;
      m(b,36)=CC;
end
for b=30;
   for a=1:30;33:49;51:54;
      m(b,a)=0;
   end
      m(b,31)=DD4;
      m(b,32)=EE4;
      m(b,50)=YX4;
end
for b=31;
   for a =1:31;34:49;51:54;
      m(b,a)=0;
   end
      m(b,32)=FF4;
      m(b,33)=GG4;
      m(b,50)=VX4;
end
for b=32;
   for a=1:31;35:49;51:54;
      m(b,a)=0;
   end
      m(b,32)=HH4;
      m(b,33)=FF4;
      m(b,34)=II4;
      m(b,50)=VX4;
end
for b=33;
   for a=1:32;36:49;51:54;
      m(b,a)=0;
   end
      m(b,33)=JJ4;
      m(b,34)=FF4;
      m(b,35)=KK4;
      m(b,50)=VX4;
end
for b=34;
   for a=1:33;37:49;51:54;
      m(b,a)=0;
   end
      m(b,34)=LL4;
      m(b,35)=FF4;
      m(b,36)=MM4;
      m(b,50)=VX4;
end
for b=35;
   for a=1:4;6:34;37:49;51:54;
      m(b,a)=0;
   end
```

```
        m(b,5)=NN4;
        m(b,35)=NG4;
        m(b,36)=AAA4;
        m(b,50)=WX4;
end
for b=36;
    for a=1:4;7:41;43:54;
        m(b,a)=0;
    end
        m(b,5)=AZ;
        m(b,6)=AE;
        m(b,42)=CC;
end
for b=37;
    for a=1:36;39:48;50:54;
        m(b,a)=0;
    end
        m(b,37)=DD5;
        m(b,38)=EE5;
        m(b,49)=YX5;
end
for b=38;
    for a=1:37;40:48;50:54;
        m(b,a)=0;
    end
        m(b,38)=FF5;
        m(b,39)=GG5;
        m(b,49)=VX5;
end
for b=39;
    for a=1:37;41:48;50:54;
        m(b,a)=0;
    end
        m(b,38)=HH5;
        m(b,39)=FF5;
        m(b,40)=II5;
        m(b,49)=VX5;
end
for b=40;
    for a=1:38;42:48;50:54;
        m(b,a)=0;
    end
        m(b,39)=JJ5;
        m(b,40)=FF5;
        m(b,41)=KK5;
        m(b,49)=VX5;
end
for b=41;
    for a=1:39;43:48;50:54;
        m(b,a)=0;
    end
        m(b,40)=LL5;
        m(b,41)=FF5;
        m(b,42)=MM5;
        m(b,49)=VX5;
end
```

```
for b=42;
   for a=1:5;7:40;43:48;50:54;
      m(b,a)=0;
   end
      m(b,6)=NN5;
      m(b,41)=NG5;
      m(b,42)=AAA5;
      m(b,49)=WX5;
end
for b=43;
   for a=1:42;45:53;
      m(b,a)=0;
   end
      m(b,43)=BB;
      m(b,44)=A2A;
      m(b,54)=CC;
end
for b=44;
   for a=2:11;13:42;44:53;
      m(b,a)=0;
   end
      m(b,1)=Yc;
      m(b,12)=-Yc;
      m(b,43)=Yb;
      m(b,54)=Ya;
end
for b=45;
   for a=1:42;46:52;54;
      m(b,a)=0;
   end
      m(b,43)=A2Z;
      m(b,44)=B2C;
      m(b,45)=ZZ2A;
      m(b,53)=CC;
end
for b=46;
   for a=1;3:17;19:43;45:52;54;
      m(b,a)=0;
   end
      m(b,2)=Yc;
      m(b,18)=-Yc;
      m(b,44)=Yb;
      m(b,53)=Ya;
end
for b=47;
   for a =1:43;47:51;53;54;
      m(b,a)=0;
   end
      m(b,44)=A2Z;
      m(b,45)=B2C;
      m(b,46)=ZZ2A;
      m(b,52)=CC;
end
for b=48;
   for a=1;2;4:23;25:44;46:51;53;54;
      m(b,a)=0;
```

```
    end
        m(b,3)=Yc;
        m(b,24)=-Yc;
        m(b,45)=Yb;
        m(b,52)=Ya;
end
for b=49;
    for a=1:44;48:50;52:54;
        m(b,a)=0;
    end
        m(b,45)=A2Z;
        m(b,46)=B2C;
        m(b,47)=ZZ2A;
        m(b,51)=CC;
end
for b=50;
    for a=1:3;5:29;31:45;47:50;52:54;
        m(b,a)=0;
    end
        m(b,4)=Yc;
        m(b,30)=-Yc;
        m(b,46)=Yb;
        m(b,51)=Ya;
end
for b=51;
    for a=1:45;49;51:54;
        m(b,a)=0;
    end
        m(b,46)=A2Z;
        m(b,47)=B2C;
        m(b,48)=ZZ2A;
        m(b,50)=CC;
end
for b=52;
    for a=1:4;6:35;37:46;48;49;51:54;
        m(b,a)=0;
    end
        m(b,5)=Yc;
        m(b,36)=-Yc;
        m(b,47)=Yb;
        m(b,50)=Ya;
end
for b=53;
    for a=1:46;50:54;
        m(b,a)=0;
    end
        m(b,47)=A2Z;
        m(b,48)=A2E;
        m(b,49)=CC;
end
for b=54;
    for a=1:5;7:41;43:47;50:54;
        m(b,a)=0;
    end
        m(b,6)=Yc;
        m(b,42)=-Yc;
```

```
        m(b,48)=Yb;
        m(b,49)=Ya;
end

%forming matrix P

P(1,1)=-DD-AA*Y(2)+CB*Y(1)-CC*Y(12);
P(2,1)=-EE0*Y(8)+GH0*Y(7)+YX0*Y(54);
P(3,1)=-GG0*Y(9)+FH0*Y(8)+VX0*Y(54);
P(4,1)=-II0*Y(10)+FH0*Y(9)-HH0*Y(8)+VX0*Y(54);
P(5,1)=-KK0*Y(11)+FH0*Y(10)-JJ0*Y(9)+VX0*Y(54);
P(6,1)=-MM0*Y(12)+FH0*Y(11)-LL0*Y(10)+VX0*Y(54);
P(7,1)=QQ0*Y(12)-NG0*Y(11)-NN0*Y(1)+WX0*Y(54);

P(8,1)=ZA*Y(3)+B1C*Y(2)-AZ*Y(1)-CC*Y(18);
P(9,1)=-EE1*Y(14)+GH1*Y(13)+YX1*Y(53);
P(10,1)=-GG1*Y(15)+FH1*Y(14)+VX1*Y(53);
P(11,1)=-II1*Y(16)+FH1*Y(15)-HH1*Y(14)+VX1*Y(53);
P(12,1)=-KK1*Y(17)+FH1*Y(16)-JJ1*Y(15)+VX1*Y(53);
P(13,1)=-MM1*Y(18)+FH1*Y(17)-LL1*Y(16)+VX1*Y(53);
P(14,1)=QQ1*Y(18)-NG1*Y(17)-NN1*Y(2)+WX1*Y(53);

P(15,1)=ZA*Y(4)+B1C*Y(3)-AZ*Y(2)-CC*Y(24);
P(16,1)=-EE2*Y(20)+GH2*Y(19)+YX2*Y(52);
P(17,1)=-GG2*Y(21)+FH2*Y(20)+VX2*Y(52);
P(18,1)=-II2*Y(22)+FH2*Y(21)-HH2*(20)+VX2*Y(52);
P(19,1)=-KK2*Y(23)+FH2*Y(22)-JJ2*Y(21)+VX2*Y(52);
P(20,1)=-MM2*Y(24)+FH2*Y(23)-LL2*Y(22)+VX2*Y(52);
P(21,1)=QQ2*Y(24)-NG2*Y(23)-NN2*Y(3)+WX2*Y(52);

P(22,1)=ZA*Y(5)+B1C*Y(4)-AZ*Y(3)-CC*Y(30);
P(23,1)=-EE3*Y(26)+GH3*Y(25)+YX3*Y(51);
P(24,1)=-GG3*Y(27)+FH3*Y(26)+VX3*Y(51);
P(25,1)=-II3*Y(28)+FH3*Y(27)-HH3*Y(26)+VX3*Y(51);
P(26,1)=-KK3*Y(29)+FH3*Y(28)-JJ3*Y(27)+VX3*Y(51);
P(27,1)=-MM3*Y(30)+FH3*Y(29)-LL3*Y(28)+VX3*Y(51);
P(28,1)=QQ3*Y(30)-NG3*Y(29)-NN3*Y(4)+WX3*Y(51);

P(29,1)=ZA*Y(6)+B1C*Y(5)-AZ*Y(4)-CC*Y(36);
P(30,1)=-EE4*Y(32)+GH4*Y(31)+YX4*Y(50);
P(31,1)=-GG4*Y(33)+FH4*Y(32)+VX4*Y(50);
P(32,1)=-II4*Y(34)+FH4*Y(33)-HH4*Y(32)+VX4*Y(50);
P(33,1)=-KK4*Y(35)+FH4*Y(34)-JJ4*Y(33)+VX4*Y(50);
P(34,1)=-MM4*Y(36)+FH4*Y(35)-LL4*Y(34)+VX4*Y(50);
P(35,1)=QQ4*Y(36)-NG4*Y(35)-NN4*Y(5)+WX4*Y(50);

P(36,1)=AZE*Y(6)-AZ*Y(5)-CC*Y(42);
P(37,1)=-EE5*Y(38)+GH5*Y(37)+YX5*Y(49);
P(38,1)=-GG5*Y(39)+FH5*Y(38)+VX5*Y(49);
P(39,1)=-II5*Y(40)+FH5*Y(39)-HH5*Y(38)+VX5*Y(49);
P(40,1)=-KK5*Y(41)+FH5*Y(40)-JJ5*Y(39)+VX5*Y(49);
P(41,1)=-MM5*Y(42)+FH5*Y(41)-LL5*Y(40)+VX5*Y(49);
P(42,1)=QQ5*Y(42)-NG5*Y(41)-NN5*Y(6)+WX5*Y(49);
```

```
P(43,1)=-DD-A2A*Y(44)+CB*Y(43)-CC*Y(54);
P(44,1)=Yd*Y(54)-Yb*Y(43)-Yc*Y(1)+Yc*Y(12);
P(45,1)=Z2A*Y(45)+C2B*Y(44)-A2Z*Y(43)-CC*Y(53);
P(46,1)=Yd*Y(53)-Yb*Y(44)-Yc*Y(2)+Yc*Y(18);
P(47,1)=Z2A*Y(46)+C2B*Y(45)-A2Z*Y(44)-CC*Y(52);
P(48,1)=Yd*Y(52)-Yb*Y(45)-Yc*Y(3)+Yc*Y(24);
P(49,1)=Z2A*Y(47)+C2B*Y(46)-A2Z*Y(45)-CC*Y(51);
P(50,1)=Yd*Y(51)-Yb*Y(46)-Yc*Y(4)+Yc*Y(30);
P(51,1)=Z2A*Y(48)+C2B*Y(47)-A2Z*Y(46)-CC*Y(50);
P(52,1)=Yd*Y(50)-Yb*Y(47)-Yc*Y(5)+Yc*Y(36);
P(53,1)=A2ZE*Y(48)-A2Z*Y(47)-CC*Y(49);
P(54,1)=Yd*Y(49)-Yb*Y(48)-Yc*Y(6)+Yc*Y(42);

%gauss jordan elimination method
X=Jordan(m,P);

for j=1:54;
   Y(j)=X(j);
end

kop=kop+ko;

conc(s,1)=Y(6);
temp(s,1)=Y(48);
tempdiff(s,1)=To*Y(48)-To;
time(s,1)=kop*(R^2/Dp);

end


function x = Jordan (A ,c)
% JORDAN(A,C): A is the matrix of coefficients and C is the
% vector of constants.
c = (c(:).')'; % Make sure it's a column vector
n = length(c);
[nr nc] = size(A);
% Check coefficient matrix and vector of constants
if nr ~= nc
error('coefficient matrix is not square.')
end
if nr ~= n
error('C0efficient matrix and vector of constants do not have the same length.')
end
% Check if the coefficient matrix is singular
if det(A) == 0
fprintf ( ' \n Rank = %7.3g\n', rank( A))
error('The coefficient matrix is singular.')
end

unit = eye(n); % Unit matrix
order = [1 : n]; % Order of unknowns
aug = [A c]; % Augmented matrix

% Gauss - Jordan algorithm
```

```
for k=1:n;
pivot = abs (aug(k , k) ) ;
prow = k;
pcol = k;

% Locating the maximum pivot element
for row = k : n;
for col = k : n;
if abs(aug(row , col)) > pivot
pivot = abs(aug(row , col) ) ;
prow = row;
pcol = col;
end
end
end

% Interchanging the rows
pr = unit;
tmp = pr(k , : ) ;
pr(k , : ) = pr(prow , : ) ;
pr(prow , : ) = tmp;
aug = pr * aug;

% Interchanging the columns
pc = unit;
tmp = pc(k , : ) ;
pc(k ,:) = pc(pcol , :);
pc(pcol , : ) = tmp;
aug(1 : n , 1 : n) = aug(1 : n , 1 : n) * pc;
order = order * pc; % Keep track of the column interchanges
% Reducing the elements above and below diagonal to zero
lk = unit;
for m = 1 : n
if m == k
lk(m , k) = 1 / aug(k , k);
else
   lk(m,k)=-aug(m,k)/aug(k,k);
end
end
aug = lk * aug;
end
x = zeros (n , 1) ;
% Solution
for k = 1: n
x(order(k)) = aug(k , n + 1);
end
```

Brief Biodata

Ms. Poonam Mondal is a Research scholar in Department of Chemical Engineering, Malaviya National Institute of Technology (MNIT), Jaipur. She has received her B.Tech and M.Tech degree in Biotechnology from Department of Biotechnology, Lovely Professional University, Punjab, India in 2012. She had joined Ph.D. in 2012 under the supervision of Dr. Suja George, Department of Chemical Engineering, MNIT, Jaipur. Her research interests are mainly in the areas Defluoridation, Water treatment & Analysis, Material characterization, Biomaterials. During her research work she has published six research papers in International Journals. She has also attended various National and International Conferences & Workshops. She has been awarded MHRD scholarship from Government of India, qualified GATE (Biotechnology) in 2012 and UGC-NET (Environmental Sciences) in 2011.

Contact no.: +91-9887097782
Email id: poonam.mbiotech@gmail.com